CERN-Proceedings-2011-001
10-06-2011

ORGANISATION EUROPÉENNE POUR LA RECHERCHE NUCLÉAIRE
CERN EUROPEAN ORGANIZATION FOR NUCLEAR RESEARCH

LHC "LUMI DAYS"

LHC WORKSHOP ON LHC LUMINOSITY CALIBRATION

CERN, Geneva, Switzerland
13–14 January 2011

Edited by
H. Burkhardt, M. Ferro-Luzzi, A. Macpherson, M. Mangano

GENEVA
2011

Workshop Website

http://indico.cern.ch/conferenceDisplay.py?confId=109784

ISBN 978–92–9083–361-1 ISSN 2078-8835 Copyright © CERN, 2011
Creative Commons Attribution 3.0
Knowledge transfer is an integral part of CERN's mission.
CERN publishes this report Open Access under the Creative Commons Attribution 3.0 license (http://creativecommons.org/licenses/by/3.0/) in order to permit its wide dissemination and use.

These proceedings should be cited as:
Proceedings of the LHC Lumi Days, Geneva, Switzerland, 13-14 January 2011, edited by H. Burkhardt, M. Ferro-Luzzi, A. Macpherson, M. Mangano, CERN-Proceedings-2011-001

A contribution in these proceedings should be cited as:
[Author name(s)], in Proceedings of the LHC Lumi Days, Geneva, Switzerland, 13-14 January 2011, edited by H. Burkhardt, M. Ferro-Luzzi, A. Macpherson, M. Mangano, CERN-Proceedings-2011-001, pp. [first page]–[lastpage]

Abstract

This report contains the proceedings of the LHC "Lumi Days" Workshop held at CERN from 13 to 14 January 2011. The meeting was organized as a joint LHC machine and experiments workshop.

The main aims were to review the results of the first luminosity calibration measurements at the LHC and to stimulate a discussion on future measurements. A total accuracy of around 5% seems achievable with the current instrumentation, on relatively short term, and both the need and challenges associated with a more precise determination have been debated. Further, the importance of knowing the cross section scale to a given precision is reviewed. Direct luminosity calibration methods are compared to indirect methods, and include recent experience at other colliders. Physics motivations, systematic uncertainties, proposals for optimal running conditions for future luminosity calibration experiments, etc., are also discussed.

Contents

Motivations and precision targets for an accurate luminosity determination at the LHC

M.L. Mangano, CERN, PH-TH, Geneva, Switzerland

Abstract

We present a pedagogical introduction to the physics implications of a precise knowledge of the LHC luminosity, defining the goals and some benchmark accuracy targets.

INTRODUCTION

The cross section for the production of a general final state O at the LHC is given by the following formula:

$$\sigma(pp \to O + X) = \int dx_1\, dx_2 \times \sum_{i,j} f_i(x_1, Q) f_j(x_2, Q) \hat{\sigma}_{(ij\to O)}(M_O, g_{ijO}, \ldots)\,. \qquad (1)$$

Here, $f_i(x, Q)$ is the density of partons (PDF) of type i (quarks of different flavours or gluons) inside the proton, carrying a fraction x of the proton momentum at a resolution scale Q. Theory predicts the PDFs to be independent of O. $\hat{\sigma}_{(ij\to O)}$ is the *partonic* cross section to produce the final state O in the collisions of partons i and j. It depends on properties of the final state (e.g. the mass of O, M_O, the momenta of the various particles involved, etc), and on the the nature of the interactions involved in the process (for example the strength, g_{ijO}, of the coupling between i, j and O). Parameters like M_O and g_{ijO} are therefore what defines the underlying theory, and extracting their value as accurately as possible is the ultimate goal of an experimental measurement. For example, M_Z and the weak-force mixing angle $\sin^2\theta_W$ were determined at LEP/SLC by measuring the shape and normalization of the e^+e^- cross sections as a function of $\sqrt{S}$.

The precision of the extraction of these parameters is determined by:

- The precision of the calculation of $\hat{\sigma}_{ij\to O}$, as a function of M_O, g_{ijO}, etc.. This is a theoretical issue. Inclusion of higher and higher orders of perturbation theory makes the prediction more accurate.

- The precision of the knowledge of the PDFs. This touches on both theory and experiment. For example, experimental data from measurements such as deep inelastic scattering (DIS) are necessary to extract the PDFs, by fitting these data to the DIS equivalent of an equation like (1). Likewise, one expects to use the LHC data themselves to improve our knowledge of the PDFs, by including the functions f_i to the list of parameters in eq. (1) that are allowed to float in order to fit the data.

- The precision of the measured cross section, $\sigma_{exp}(O)$, determined by the quantities on the right-hand-side of the following relation: $\sigma_{exp}(O) = N_{events}(O)/Luminosity$. Here N_{events} depends on the accurate knowledge of signal and background acceptances and efficiencies, and *Luminosity* is what we are discussing at this Workshop.

The target of the programme of precision measurements is therefore to bring to the same level the accuracy all elements in the following relation:

$$\sigma(pp \to O) = \frac{N_{events}(O)}{Luminosity}\,. \qquad (2)$$

The target is driven by the level of accuracy of the available, required, inputs. At LEP/SLC, the theoretical precision in the cross section calculations was very high, setting tough requirements on the determination of the luminosity and of the experimental accuracy, in order to allow a precise extraction of the fundamental theory parameters. At the LHC, the theoretical calculations for hadronic processes are less precise than at LEP/SLC. On one side the calculations are harder, since perturbation theory for strong interactions is less effective. On the other, the limited knowledge of PDFs introduces a new uncertainty. The possibility to have a very accurate absolute luminosity determination, and therefore very accurate experimental cross section measurements, allows to develop a physics programme in which this precise information can help improve, at the same time, the theoretical calculations, the PDF knowledge, and ultimately the measurement of the theory parameters such as masses and couplings. In this review we shall now provide a few examples of the interplay between these different ingredients.

EXAMPLES

Indirect luminosity measurement

When a certain process is known with great theoretical precision, the relation (2) can be used in its inverted form, as a means of determining the luminosity:

$$\text{Luminosity} = \frac{N_{events}(O)}{\sigma(pp \to O)}\,. \qquad (3)$$

This is what we refer to as "indirect" luminosity measurement. By using these measurements to set the scale of the luminosity we typically give up the possibility of using them for physics. The assumption is that we know them well enough already that we have nothing to gain from a comparison of the calculated cross section to an absolute cross sections measurement. This was the approach used at

LEP, where elastic ("Bhabha") e^+e^- scattering was the reference process. The only input parameters for the Bhabha rates are the electron mass and α_{em}, which are known well enough that no realistic effort towards a direct luminosity measurement could possibly help improving their knowledge.

At the LHC, examples of this type include some processes of electromagnetic nature, which are expected to be calculable from first principles with precision better than 1%, on the basis of the knowledge of the EM proton form factor. Since, for these processes, we do not anticipate to learn new physics from a possible precise comparison of data and theory, we can afford using them as a luminosity-setting standard candle. The simplest example is the mesurement of the elastic pp cross section at very small angle, where the impact parameter is so large that only the well known Coulomb interaction between protons is relevant [1]. This is the programme of ATLAS's ALFA spectrometer [2]. Other examples that have been considered include the reactions $pp \to pp\mu^+\mu^-$ (pair production via $\gamma\gamma$ collisions) and $pp \to pp\gamma$, and have been discussed in the presentation by V. Khoze at this Workshop [1]. The main challenge in these cases is of experimental nature. In the case of the $\mu^+\mu^-$ final states, which are discussed in the LHCb presentation [3], the measured cross section varies very strongly with the p_T detection threshold of muons, introducing a potentially large systematics. In the case the $pp\gamma$ reactions, dedicated photon detectors at large rapidities are required [4]. In both cases, the requirement that no other particles are produced (which is a precondition to the validity of the calculations for these purely semi-elastic processes) sets a further source of uncertainty, since no detector is fully hermetic, and the real precision of the MC modeling of the final states is still not known [1]. It is however expected that the current MCs will be improved and validated using LHC data, particularly from the detectors with acceptance in the forward regions.

Another concrete example, which forms the basis of the programme of the TOTEM experiment [5], is the use of the optical theorem, together with the measurement of the elastic and inelastic rates. This allows a simultaneous determination of the luminosity and of the total pp cross section [1]:

$$\sigma_{tot}^{pp} = \frac{16\pi}{1+\rho^2} \frac{\frac{dN_{el}}{dt}|_{t=0}}{N_{el}+N_{inel}} \quad (4)$$

$$L = \frac{1+\rho^2}{16\pi} \frac{(N_{el}+N_{inel})^2}{\frac{dN_{el}}{dt}|_{t=0}} \quad (5)$$

where N_{el} and N_{inel} are the number of elastic and inelastic events in a given data sample, $dN_{el}/dt|_{t=0}$ is the differential elastic rate extrapolated at zero scattering angle, and ρ is the ratio of real and imaginary part of the forward elastic scattering amplitude. The uncertainty on $\rho \sim 0.12 \pm 0.03$ leads to a 1% uncertainty in eqs. (4) and (5). A detailed account of the systematics due to the modeling of the extrapolation of the elastic and inelastic rates to uninstrumented detector regions, was given in [1, 5].

The W and Z cross sections can also be calculated with good precision, and in the past have been proposed as possible channels for indirect luminosity measurements. We discuss these prospects in more detail in the following.

Indirect mass measurements

The mass of a particle can be reconstructed *directly* from the full reconstruction of its decay particles, using $M_O^2 = (\sum_{decays} p_i)^2$. Alternatively, one can use the mass-dependence of the production cross section. This *indirect* measurement is the technique used, for example, in the Z mass measurement at LEP/SLC [6], where M_Z is one of the parameters in the fit of the Z line shape, namely the energy dependence of the e^+e^- cross section. The knowledge of the absolute luminosity, and thus of the absolute cross section, has a small impact on the systematics, since it is mostly the shape that counts. The leading systematics here is therefore the theoretical knowledge of the mass-dependence of the cross setion, and the absolute scale of the beam energy. In hadron collisions the beam energy is practically unknown, since the relevant initial state is made of quarks or gluons, and the energy determination from the reconstructed final states has limited precision. The precision of the indirect mass measurement is therefore limited by the theoretical knowledge of the cross section, and of the experimental determination of the absolute cross section, which includes both the experimental systematics (acceptance and reconstruction efficiency) and the beam luminosity.

A concrete example is given by the top quark mass, m_t. The relative m_t dependence of the production cross section for top quark pairs is known very accurately, and is given by the relation $\delta m_t/m_t = 0.21\delta\sigma/\sigma$. The measurement and theoretical determination of the cross section with a total precision of 5% will therefore lead to an indirect determination of m_t with a 1% precision, or about 1.5 GeV. This would provide a significant measurement of m_t, with a systematics totally independent of that botained in the direct reconstruction of the top mass form its decay products, whose ultimate accuracy at the Tevatron and LHC is expected to reach 1 GeV.

At this time, the theoretical calculations have, for a fixed m_t value, an uncertainty of $\pm 8\%$(NLL)$\pm 3\%$(PDF) (see e.g. [7]). The first uncertainty is due to the incomplete knowledge of higher-order perturbative corrections beyond the fixed next-to-leading-order (NLO) and the next-to-leading logarithms (NLL) which dominate at all orders of pertubation theory. The second uncertainty comes from the uncertainties in the quark and gluon PDFs. It is expected that, within a couple of years, the combined theoretical uncertainty will be reduced to an overall $\pm 3-5\%$. The experimental systematics could be reduced to the percent level. A luminosity uncertainty at the level of 3% would therefore provide a firm ground on which to stimulate further progress on the theoretical side, to achieve the desired

± 1.5 GeV precision on m_t.

W and Z production cross sections

The production of W and Z gauge bosons is the process with the best theoretical precision. For a fixed PDF choice, the cross sections $\sigma_{W,Z}$ are known to within $1-2\%$ [8, 9]. A larger uncertainty comes from the knowledge of the PDFs. As of today, the envelope of the predictions for the W and Z cross sections, obtained by using the various PDF fits in the literature [10], is at the level of $\pm 5\%$, as shown in Fig. 1. The ultimate experimental accuracy on

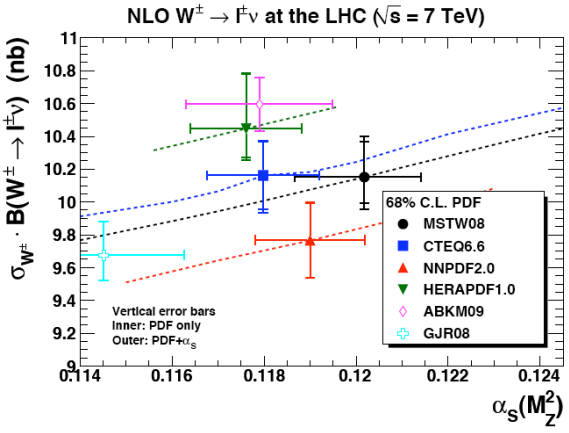

Figure 1: Predictions of the W cross section, at the LHC, as obtained with different sets of PDFs [10].

this observable is at the level of percent, or below, as documented in the current analyses of LHC data [11, 12] and as discussed at this Workshop [13, 14]. The systematics will therefore soon be dominated by the luminosity. When this will be known to 5%, the first compelling tests of the theoretical predictions for $\sigma_{W,Z}$ will be possible. Below the 5% threshold one will start gaining new information, capable of selecting among different sets of PDFs. The ultimate precision is set, today, by the theoretical uncertainty on the partonic cross section $\hat{\sigma}_W$, namely 2%.

Of course one could anticipate an improvement in the knowledge of the protons PDFs, using input from the LHC, as discussed in the next Section, and use the prediction of $\sigma_{W,Z}$ to obtain an indirect determination of the LHC luminosity, at a level of the order of few percent. For example, the ratio of W and Z cross sections, a quantity which is not subject to luminosity uncertainty, shows some degree of correlation with the PDFs, and a potential to improve the PDF knowledge. This is shown in Fig. 2 [17], where the correlation coefficients between the prediction for σ_W/σ_Z with various parton distributions is shown. Notice, however, that the correlation is much stronger with the absolute determination of σ_W (Fig. 3). Therefore, given the physics interest in the comparison of the data and theory for the absolute rates, and the possibility of using the measurement

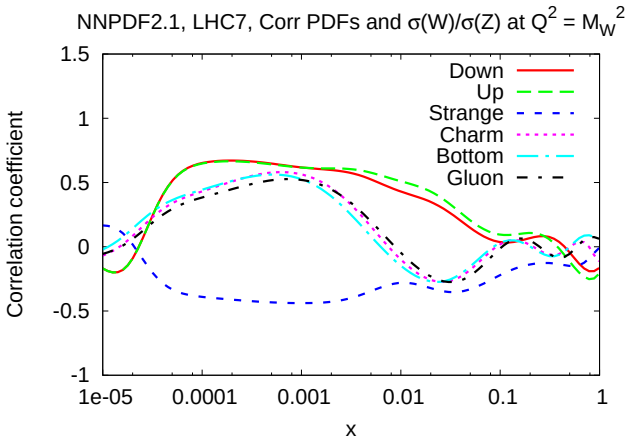

Figure 2: Correlation between various PDFs and ratio of W and Z cross sections [17].

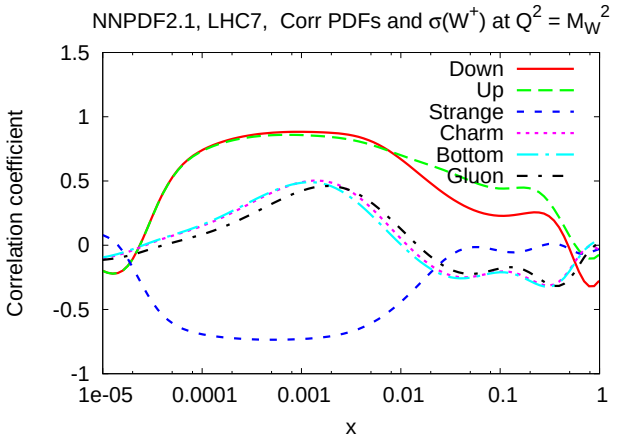

Figure 3: Correlation between various PDFs and σ_W [17].

as a way of pinning down with the greatest possible accuracy the PDFs, it would be a loss to sacrifice this physics channel for an indirect luminosity measurement.

W and Z distributions

In addition to the measurement of the total W and Z cross sections, input on the proton PDFs will also arise from their rapidity distributions. These, in fact, probe the spectrum of quarks and gluons at different values of x, providing important constraints on the PDFs. For example, the forward acceptance of the LHCb detector selects initial states where one of the two partons has large $x \sim 0.1$, and the other has $x \ll 1$. Furthermore, at the LHC the difference between up-quark (u) and down-quark (d) distributions is directly reflected in the production asymmetry between W^+ and W^-. The convolution of the $W^\pm$ production spectra and of their decay angular distributions, leads to a characteristic shape of the ratio of the positive and negative lepton rapidity spectra, which is larger than one for lepton rapidity $y \lesssim 3$, and smaller than one

for $y \gtrsim 3$. These asymmetries are already being measuremed, with increasing precision, by the LHC experiments [3, 13, 14, 15, 16].

The precise interplay of the measurement of the absolute production rates and of the shapes of rapidity spectra in improving our knowledge of PDFs, is the subject of ongoing work [10, 17]. I present here some preliminary results, as an illustration of some possible outcomes of these analyses.

The correlation between $\sigma_{W,Z}$ and the W rapidity distribution is shown in Fig. 4. The continuous (red) curve, in

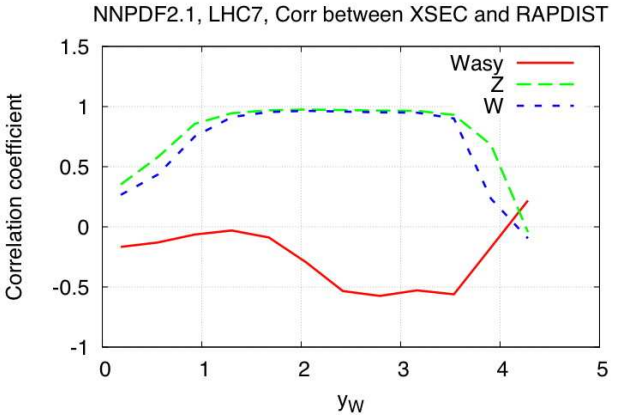

Figure 4: Correlations between W and Z observables. The continuos (red) line is the correlation between σ_W and the W^+/W^- rapidity asymmetry. The long-dashed (green) line is the correlation between σ_Z and $d\sigma/dy_Z$. The short-dashed (blue) line is the correlation between σ_W and $d\sigma/dy_W$.

particular, represents the correlation between σ_W and the W asymmetry. The correlation is weak in the central region (ATLAS/CMS), but becomes more sizable in the forward region (LHCb). This shows that a measurement of σ_W adds a different amount of information if combined with the W asymmetries measured in the central or in the forward region. More explicitly, the impact of these data is highlighted in Figs. 5 and 6, which show the improvements in the determination of the strange quark PDF, when including the information that will arise from 1fb^{-1} of LHC data at 7 TeV [17]. These two figures consider the future knowledge arising from the W asymmetry, as well as from the measurement of $\sigma_{W,Z}$ or of the Z boson rapidity spectrum. Improvements by factors up to 3 are expected for $x \lesssim 10^{-2}$. The figures only consider the impact of future data from ATLAS and CMS, at central rapidity; greater improvements will come, in the region $x \sim 0.1$, from the inclusion of data from LHCb, which are directly sensitive to the large-x range, due to the forward kinematics.

CONCLUSIONS

The main physics driver for the precision of the LHC luminosity determination is the determination of the cross

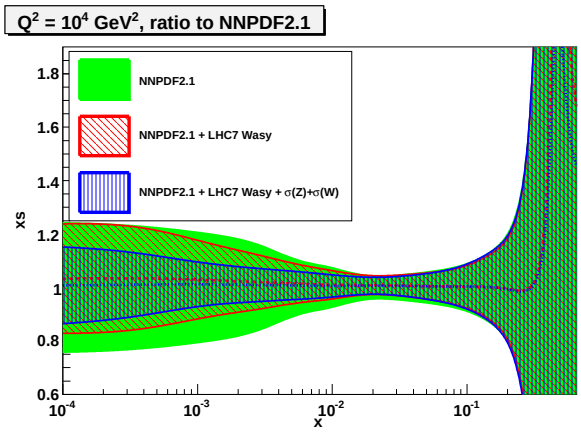

Figure 5: Improvements in the relative uncertainty on the knowledge of the strange quark PDF, when including the information that will arise with 1fb^{-1} of data from the LHC at 7 TeV. The outer (green) band shows the current uncertainty. The lightly-shaded (red) region is the improvement obtained using the W asymmetry measurement from the ATLAS and CMS experiments. The dark-shaded (blue) region is the further improvement obtained with the addition of the σ_W and σ_Z measurements. Figure from Ref. [17].

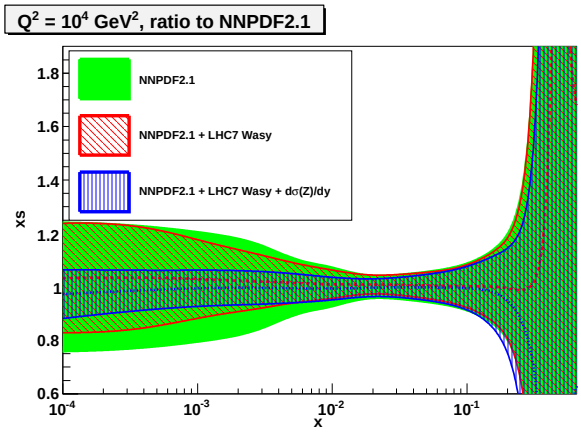

Figure 6: Same as the previous figure, but the last step (dark band) arising from the addition of the Z boson rapidity measurement. From Ref. [17].

section of W and Z bosons. With $\Delta L/L \sim 5\%$, the experimental measure will match the current uncertainty of the theoretical calculation, which is dominated by the PDF uncertanties. Below 5% one will start extracting new information on the proton PDF. Further improvements down to the level of $\Delta L/L \sim 2\%$ are justified by the current level of precision of the partonic cross section. Overall, the improved determination of PDFs will have a direct impact on the systematics of several crucial precision measurements. For example, it is known from the Tevatron experience that the PDF uncertainty must be reduced in order to improve the precision of the W mass measurement. An improved knowledge of the PDFs will also be required to

extract the value of the electroweak coupling $\sin^2\theta_W$ from the Z forward-backward asymmetry [18].

Of course there are many other studies that will benefit from the reduction of $\Delta L/L$ to the few percent level. For example, $\Delta L/L \sim 3\%$ is a necessary ingredient for the indirect measurement of m_t at the level of 1.5-2 GeV.

An interesting observation was made during the discussion following this presentation (W. Krasny): it may be desirabile to monitor the relative $\Delta L/L$ at different beam energies (2.76, 7 and 14 TeV) to higher precision, possibly at the per mille level, in order to achieve high-precision determinations of cross-section ratios at various energies. The theoretical and experimental uncertainty on ratios of cross-sections for the same process at different energies is much better than for individual energies. More work is required to quantify these statements in some concrete cases of interest.

ACKNOWLEDGMENTS

I am grateful to Juan Rojo and Stefano Forte for generating and sharing with me the results on the W and Z distributions presented here.

REFERENCES

[1] V. Khoze, presented at this Workshop.

[2] K. Hiller (ATLAS coll.), in these proceedings.

[3] J. Anderson, (LHCb coll), in these proceedings.

[4] S. Schnetzer (CMS coll.), in these proceedings.

[5] M. Deile (TOTEM coll.), in these proceedings.

[6] LEP/SLC EW working group, Phys. Rept. **427** (2006) 257 [arXiv:hep-ex/0509008].

[7] M. Cacciari *et al.*, JHEP **0809** (2008) 127.

[8] R. Hamberg, W. L. van Neerven and T. Matsuura, Nucl. Phys. B **359** (1991) 343 [Erratum-ibid. B **644** (2002) 403].

[9] C. Anastasiou, L. J. Dixon, K. Melnikov and F. Petriello, Phys. Rev. D **69** (2004) 094008 [arXiv:hep-ph/0312266].

[10] S. Alekhin *et al.*, arXiv:1101.0536 [hep-ph].

[11] G. Aad *et al.* [Atlas Collaboration], JHEP **1012** (2010) 060 [arXiv:1010.2130 [hep-ex]].

[12] V. Khachatryan *et al.* [CMS Collaboration], JHEP **1101** (2011) 080 [arXiv:1012.2466 [hep-ex]].

[13] M. Schott (ATLAS coll.), in these proceedings

[14] J. Werner (CMS coll.), in these proceedings

[15] G. Aad *et al.* [ATLAS Collaboration], arXiv:1103.2929 [hep-ex].

[16] V. Khachatryan *et al.* [CMS Collaboration], http://cdsweb.cern.ch/record/1336774.

[17] R. D. Ball *et al.*, arXiv:1101.1300 [hep-ph]. The figures shown here were provided as private communication from the authors.

[18] S. Haywood *et al.*, arXiv:hep-ph/0003275.

Indirect Luminosity Measurements: Theoretical Assessment

V.A. Khoze
Durham University, England.

A paper was not submitted to the proceedings. However, the slides presented are available in electronic form at http://indico.cern.ch/conferenceOtherViews.py?view=standard&confId=109784. The cover slide from this talk is given as reference.

LHC Lumi Days

13-14 January 2011 CERN

Selected topics on the precision of luminometry at the LHC (as seen through the theorist's eyes)

V.A. Khoze (IPPP, Durham)

Special thanks to Misha Ryskin for discussions.

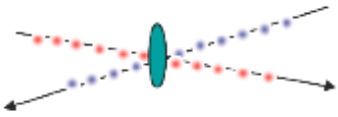

1

TOTEM: PROSPECTS FOR TOTAL CROSS-SECTION AND LUMINOSITY MEASUREMENTS

M. Deile, CERN, Geneva, Switzerland
on behalf of the TOTEM Collaboration

Abstract

With the installation of the T1 telescope and the Roman Pot stations at 147 m from IP5, the detector apparatus of the TOTEM experiment has been completed during the technical stop in winter 2010/2011. After the commissioning of the dedicated beam optics with $\beta^* = 90$ m, a first measurement of the total pp cross-section σ_{tot} and – simultaneously – the luminosity L will be possible in the upcoming running season 2011. The precision envisaged is 3% and 4% for σ_{tot} and L, respectively. An ultimate beam optics configuration with $\beta^* \sim 1$km will later reduce the uncertainty to the 1% level.

INTRODUCTION

The motivation and concept of measuring σ_{tot} and L at LHC with the method based on the Optical Theorem have been discussed at length elsewhere [1, 2]. The central equations expressing σ_{tot} and L in terms of the measured inelastic and elastic rates, N_{inel} and N_{el}, and the extrapolation of the differential elastic rate to the optical point, $t = 0$, are

$$\sigma_{tot} = \frac{16\pi}{1+\rho^2} \cdot \frac{dN_{el}/dt|_{t=0}}{N_{el}+N_{inel}} \quad \text{, and} \qquad (1)$$

$$\mathcal{L} = \frac{1+\rho^2}{16\pi} \cdot \frac{(N_{el}+N_{inel})^2}{dN_{el}/dt|_{t=0}} \,, \qquad (2)$$

where $\rho = 0.1361 \pm 0.0015^{+0.0058}_{-0.0025}$ [3] will as a first step be taken from theory. At a later stage, a measurement at $\beta^* \sim 1$km can be attempted (see last section of this article).

This article aims at giving an update on the expected performance, taking into account recent studies for the reduced centre-of-mass energy of 7 TeV and the running experience in 2010.

The Roman Pot (RP) stations at ± 220 m from IP5 and the forward GEM telescope T2 had already been fully operational in 2010, whereas the second half of the RP spectrometer – i.e. the ± 147 m stations – as well as the CSC telescope T1 were installed during the technical stop in winter 2010/2011, thus completing TOTEM's detector apparatus (Figure 1) in time for the running season 2011.

MEASUREMENT OF THE INELASTIC RATE

The inelastic trigger acceptance predicted by simulation for the TOTEM detector configuration is given in Table 1.

The trigger losses are dominated by low-mass diffractive events where the diffractive system escapes to rapidities beyond the reach of T2, i.e. $\eta > 6.5$ or masses $M \lesssim 10$ GeV. The missing part of the diffractive mass spectrum can be partially recovered by extrapolating it according to the empirical relation $\frac{dN}{dM^2} \propto \frac{1}{M^n}$ with $n \approx 2$.

Table 1: *Trigger losses at $\sqrt{s} = 7$ TeV, requiring 3 tracks pointing to the IP. The cross-sections given are the central values of rather wide ranges of predictions [4].*

Event class	σ	T1/T1 trigger and selection loss
Minimum Bias	50 mb	0.05 mb
Single Diffractive	12.5 mb	4.83 mb
Double Diffractive	7.5 mb	1.21 mb
Total	70 mb	6.1 mb

The systematic uncertainty of this procedure depends on the purity of the diffractive event sample used for the extrapolation. For example, minimum bias events misidentified as diffractive events will introduce a bias. To improve the identification of event topologies, e.g. rapidity gaps, CMS detectors at rapidities below 3.1 (central detectors) or above 6.5 (FSC [5] and ZDC) could be used.

A principal problem of the extrapolation is that the $1/M^2$ dependence of the spectrum is not theoretically justified [6]. There may be sizeable deviations at low masses; even the presence of resonances cannot be excluded. However, an independent handle on Single Diffractive (SD) events can be exploited: At $\beta^* = 90$ m [8], the leading protons of all diffractive events with $|t| > 10^{-2}$ GeV^2 are detected in the RPs, irrespective of the diffractive mass. Thus, SD events whose diffractive system escapes detection by T2 will have the signature of *unpaired* protons in the kinematic region of elastic protons (i.e. $\xi \approx 0$).

After all corrections a total uncertainty of 1 mb (or 1.4%) in N_{inel} is expected.

MEASUREMENT OF THE ELASTIC RATE AND EXTRAPOLATION TO T = 0

Predictions [7] for the differential cross-section of elastic pp scattering at $\sqrt{s} = 7$ TeV in the low-$|t|$ region are displayed in Figure 2(left). Deviations from the apparent exponential behaviour become visible when the exponential slope, $B(t) = \frac{\mathrm{d}}{\mathrm{d}t} \ln \frac{\mathrm{d}\sigma}{\mathrm{d}t}$ is plotted (Figure 2, right). This non-constant $B(t)$ has to be taken into account in the extrapolation fit for obtaining $\frac{\mathrm{d}\sigma}{\mathrm{d}t}(t = 0)$. The procedure is identical to the one described in [2] for $\sqrt{s} = 14$ TeV.

The comparison of the RP acceptances in t for the two

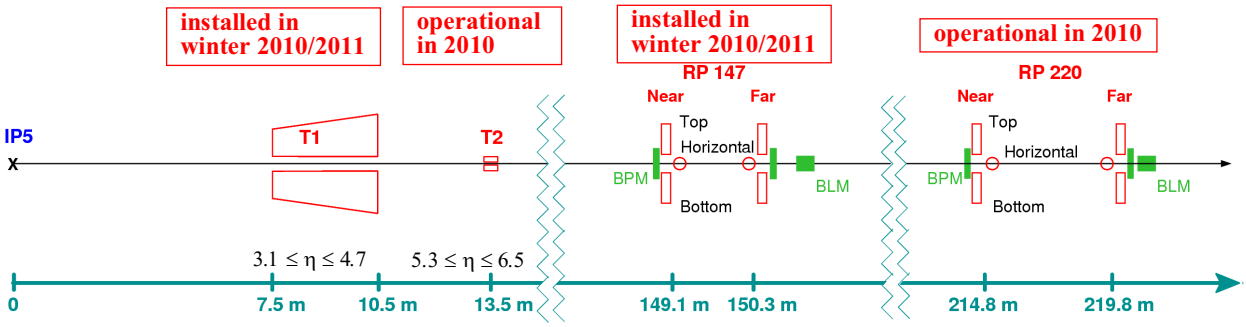

Figure 1: *Schematic overview of the TOTEM detector configuration. The apparatus is symmetric w.r.t. IP5, but only the arm in Sector 5-6 is drawn.*

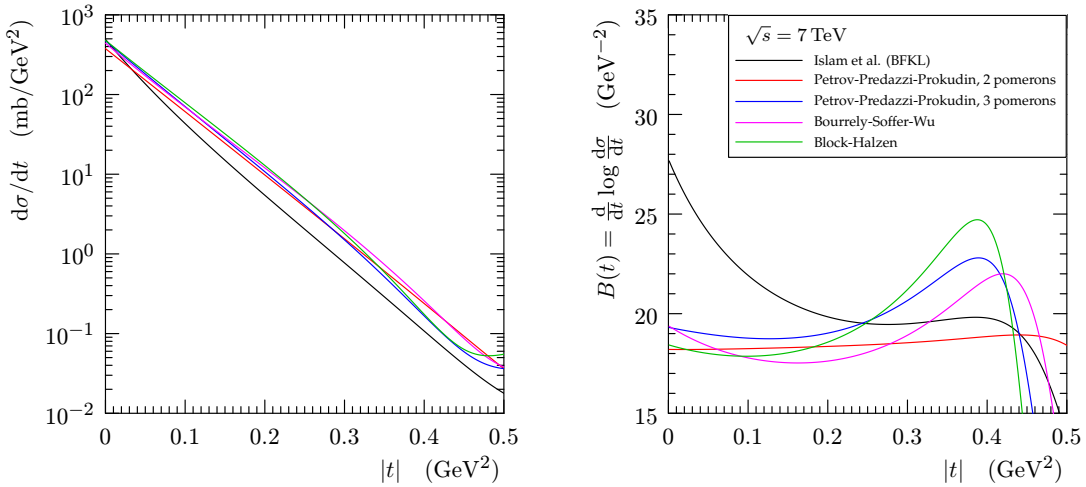

Figure 2: *Left: elastic differential cross-section at low $|t|$ as predicted by different models [7]. Right: exponential slope of (left).*

high-β^* optics foreseen (Figure 3) shows the significantly better reach of the $\beta^* = 1540\,\text{m}$ to low $|t|$ as compared to 90 m. In both cases, the lower centre-of-mass energy is advantageous: reducing $\sqrt{s}$ from 14 TeV to 7 TeV results in a factor 0.5 in the lowest reachable $|t|$-value (see Figure 4 and [4]).

Extrapolation at $\beta^* = 90\,m$

The contributions to the extrapolation uncertainty at $\sqrt{s} = 7\,\text{TeV}$ are expected to be very similar to those at $\sqrt{s} = 14\,\text{TeV}$ discussed in [2]. The key advantage of the lower energy, however, is the about 50% shorter extrapolation interval, which will reduce the fit-induced statistical error and the systematic uncertainty contribution from the model dependence of the extrapolation function. The beam divergence at 7 TeV is higher than at 14 TeV by a factor $\sqrt{14/7} = \sqrt{2}$ (i.e. $3.3\,\mu\text{rad}$ instead of $2.4\,\mu\text{rad}$), but as explained in [2] (Section 6.3.2), this effect leads to a shift in the extrapolation result which can be corrected for. The optical functions are expected to be known to within ∼1%, which would translate into an extrapolation uncertainty contribution of 1.5%. The statistical uncertainty after an 8 hour long run – with conditions explained in the next section and Table 2 – would be on the 1% level.

In summary, a total error estimate of ∼ 2% for the extrapolation at $\beta^* = 90\,\text{m}$ and 7 TeV can be considered as conservative.

Running Scenario for the $\beta^* = 90\,m$ Optics in 2011

After the commissioning of the unsqueeze from the injection optics to $\beta^* = 90\,\text{m}$ [9], TOTEM is aiming at four well separated runs of typically 8 hours length, enabling systematic comparisons between the individual results and successive improvement of the beam conditions. As outlined above, the key element in reducing the extrapolation uncertainty is the minimisation of the $|t|$-interval to be bridged, by extending the acceptance to the lowest possible $|t|$ and hence by moving the RPs as close as possible to the beam. As shown in Table 2, this is accomplished by a twofold strategy:

- Reduce d_{RP}/σ_{beam}. In special runs in 2010, success-

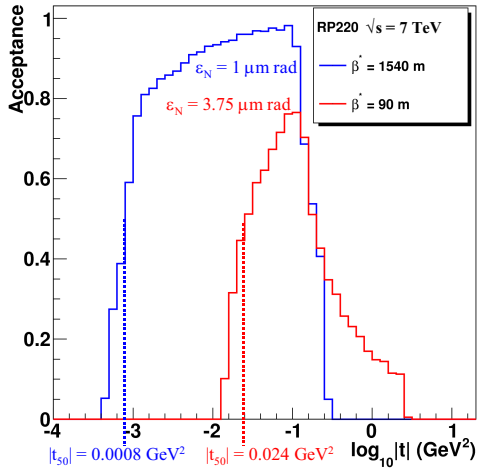

Figure 3: *Acceptance of the RP220 station for elastically scattered protons in terms of t for the two high-β^* optics and for a detector-beam distance of $10\,\sigma$. The point where the acceptance reaches 50% on the lower-$|t|$ side is called t_{50}; it characterises the typical minimum $|t|$ useable for extrapolation purposes.*

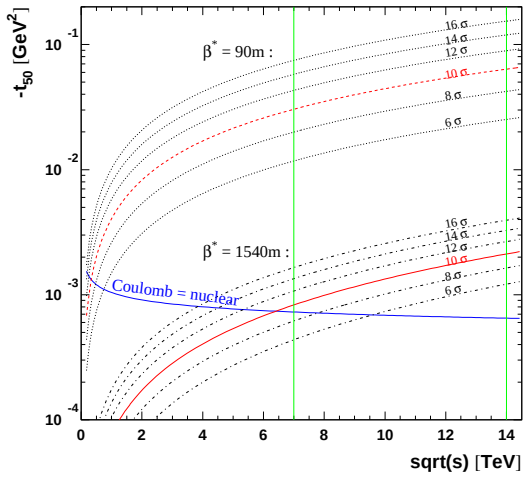

Figure 4: *$|t|$-value at which the RP220 acceptance reaches 50%, as a function of the centre-of-mass energy, for different distances between the RP window and the beam. The sensitive detector volume begins $\delta = 0.5$ mm further away (due to window thickness and window-detector gap). The $|t_{50}|$-values take δ into account. The upper and lower blocks of curves represent the $\beta^* = 90$ m (with $\varepsilon_n = 3.75\,\mu$m rad) and $\beta^* = 1540$ m (with $\varepsilon_n = 1\,\mu$m rad), respectively. At the blue line, the Coulomb and the nuclear scattering amplitudes have equal moduli.*

ful data taking took place as close as $7\,\sigma$ from the beam, i.e. in the shadow of only the primary collimators. For machine protection reasons, this approach imposes a limit on the total beam current[1].

- Reduce the transverse beam emittance and hence the width σ_{beam}. Thus for a given d_{RP}/σ_{beam}, the pots are moved to a smaller absolute distance d_{RP}.

The bunch population N is not only limited by the low-current requirement but most importantly in view of keeping the inelastic pile-up fraction $\mu_{inelastic}$ below 10% which is essential for an accurate measurement of the inelastic rate. With one bunch of $(6 \div 7) \times 10^{10}$ p/b, each of the four runs requested can provide an elastic extrapolation with the required precision $\sim 1\%$.

Table 2: *Tentative scenario for the beam conditions in four physics runs with the $\beta^* = 90$ m optics at 3.5 TeV beam energy[2]. d_{RP} denotes the distance between the outer window surface of the pots and the centre of the beam. The additional distance of 0.5 mm to the sensitive detector volume has been taken into account in the calculation of $|t_{50}|$, i.e. the $|t|$-value where the acceptance reaches 50%. $\mu_{inelastic}$ is the inelastic pile-up fraction. $\delta\sigma_{el}(t=0)$ is the precision of the elastic cross-section extrapolation to $t = 0$.*

Run	1	2	3	4
ε_n [μm rad]	3	3	1	1
d_{RP}/σ_{beam}	8	6	8	6
$N/10^{10}$	7	7	6	6
L [10^{27}cm^{-2}s^{-1}]	6.1	6.1	13	13
$\mu_{inelastic}$	0.04	0.04	0.08	0.08
$\lvert t_{50}\rvert$ [GeV^2]	0.016	0.0096	0.0060	0.0037
$\int_0^{8h} L\,dt$ [nb^{-1}]	0.2	0.2	0.3	0.3
$\delta\sigma_{el}/\sigma_{el}(t=0)$	$\sim 1.5\%$	$\sim 1\%$	$< 1\%$	$< 1\%$

COMBINED UNCERTAINTY AT $\beta^* = 90$ m

The error contributions from all measured quantities and from the theoretical knowledge of ρ are listed in Table 3. The combined uncertainties in σ_{tot} and L result from an error propagation calculation taking into account the correlations. Note that the precision in L is slightly worse due to its squared dependence on $(N_{el} + N_{inel})$, as compared to the linear dependence of σ_{tot} (see Eqns. (1) and (2)).

Table 3: *Error contributions from all ingredients to Eqns. (1) and (2) for $\beta^* = 90$ m.*

Extrapolation of $\frac{d\sigma_{elastic}}{dt}$ to $t = 0$	$\pm 2\%$
Total elastic rate (strongly correlated with extrapolation)	$\pm 1\%$
Total inelastic rate	$\pm 1.4\%$
Error contribution from $(1+\rho^2)$ using full COMPETE error band $\delta\rho/\rho = 33\%$	$\pm 1.2\%$
Total uncertainty in σ_{tot} incl. correlations	$\pm 3\%$
Total uncertainty in L incl. correlations	$\pm 4\%$

[1] The quantitative current limit for $\beta^* = 90$ m runs remains to be decided by the Machine Protection Panel and the collimation group.

[2] This table has been modified w.r.t. the 4.0 TeV version presented in the workshop slides.

OUTLOOK: PERFORMANCE AT $\beta^* = 1540\,\mathrm{m}$

The $\beta^* = 1540\,\mathrm{m}$ optics, studied in detail for $\sqrt{s} = 14\,\mathrm{TeV}$ [2], extends the measurable $|t|$-range to values of the order $10^{-3}\,\mathrm{GeV}^2$ and thus enables an elastic extrapolation with an uncertainty at the 0.2% level. Consequently, the precision in σ_{tot} improves to $\sim 1\%$.

Scaling the optics properties to $\sqrt{s} = 7\,\mathrm{TeV}$ shows an even further enhancement of the acceptance reach to low $|t|$ (Figure 4, bottom block of curves). Inserting the RPs to 8 or 6 σ_{beam} would give access to the elastic scattering zone dominated by the Coulomb interaction and thus permit a measurement of ρ, avoiding any need for theoretical input to the σ_{tot} determination via the Optical Theorem. At $\sqrt{s} = 14\,\mathrm{TeV}$ this opportunity will not be offered.

However, the current version of the $\beta^* = 1540\,\mathrm{m}$ optics for TOTEM is only compatible with operation at $\sqrt{s} = 10\,\mathrm{TeV}$ to $14\,\mathrm{TeV}$ [9]. At lower energy the two main limiting parameters are the minimum strength allowed in the insertion quadrupoles and the aperture. One way to avoid these limitations would be to loosen the constraints on the phase advance by abandoning the condition to have "parallel-to-point focussing" in both transverse projections. Alternative optics at very high β^*, compatible with operations at $\sqrt{s} = 7\,\mathrm{TeV}$ are under study.

REFERENCES

[1] TOTEM Collaboration: Technical Design Report, CERN-LHCC-2004-002; addendum CERN-LHCC-2004-020.

[2] G. Anelli et al. (TOTEM Collaboration): The TOTEM Experiment at the CERN Large Hadron Collider, 2008 JINST 3 S08007.

[3] J.R. Cudell et al.; Benchmarks for the Forward Observables at RHIC, the Tevatron-Run II, and the LHC; PRL **89**, (2002) 201801.

[4] The TOTEM Collaboration: TOTEM Results and Perspectives for 2010/2011, CERN-LHCC-2010-014 / LHCC-G-154; and references therein.

[5] A. J. Bell et al.: Physics and Beam Monitoring with Forward Shower Counters (FSC) in CMS, CMS-NOTE-2010-015.

[6] see e.g. V. Khoze: Indirect luminosity measurements: theoretical assessment, these proceedings.

[7] C. Bourrely, J. Soffer and T. T. Wu: Impact picture phenomenology for pi+-p, K+-p and pp, anti-p p elastic scattering at high-energies, Eur.Phys.J. C28 (2003) 97-105.
V. A. Petrov, E. Predazzi and A. Prokudin: Coulomb interference in high-energy p p and anti-p p scattering, Eur. Phys. J. C28 (2003) pp. 525–533.
M. M. Block, E. M. Gregores, F. Halzen and G. Pancheri: Photon proton and photon photon scattering from nucleon nucleon forward amplitudes, Phys. Rev. D 60 (1999) 054024.
M. M. Islam, R. J. Luddy and A. V. Prokudin: Near forward pp elastic scattering at LHC and nucleon structure, Int. J. Mod. Phys. A 21 (2006) pp. 1–42.

[8] TOTEM Collaboration: Early TOTEM Running with the 90 m Optics, CERN-LHCC-2007-013 / G-130, 9 March 2007.

[9] H. Burkhardt: High-Beta Optics, these proceedings.
H. Burkhardt and S. White: High-Beta Optics for the LHC, LHC Project Note 431, May 2010.

Prospects for indirect luminosity measurements at LHCb

Jonathan Anderson, Physik-Institut der Universität Zürich, Switzerland.
For the LHCb collaboration

Abstract

We summarise the prospects for indirect luminosity measurements at LHCb. Two candidate processes have been identified for such measurements: electroweak boson production and elastic dimuon production via two photon fusion. The cross-section for W and Z production at LHCb has been calculated at NNLO with an uncertainty of $\sim 4\%$, where the dominant theoretical error is due to the uncertainty on the parton distribution functions (PDFs). Using the first 16.5 pb^{-1} of data, a very clean sample of 833 Z bosons and a larger, but less clean, sample of W bosons have been recorded at LHCb. Using the currently available sample of W^+ (Z) events an integrated luminosity measurement with an uncertainty of $\sim$5% ($\sim$6%) could be made. Once 150 pb^{-1} of data has been collected a measurement using a high purity Z sample could be performed that would have an uncertainty of 4%. Cross-section predictions for elastic dimuon production via two photon fusion have been performed with an uncertainty of $< 1\%$. With the first 17.5 pb^{-1} of data, 250 candidate events of this type have been observed. While work is still ongoing to understand the purity and efficiency of this sample, the prospects for using this process to make a precision luminosity measurement at LHCb are promising.

INTRODUCTION

LHCb [1], one of the four large experiments at the Large Hadron Collider (LHC), has been designed for CP violation and rare decay studies in the heavy quark sector. Due to the $b\bar{b}$ production topology at the LHC, whereby both B hadrons are mostly produced in the same forward or backward cone, LHCb has been constructed as a forward single-arm spectrometer with an approximate coverage in terms of pseudorapidity of $1.9 < \eta < 4.9$. Since March 2010 the experiment has been successfully taking proton-proton collision data at a centre of mass energy of 7 TeV.

Knowledge of the integrated luminosity is necessary to make cross-section measurements and monitor running performance at colliding beam experiments. At LHCb the integrated luminosity will be determined both directly, by measuring the beam profiles and currents, and indirectly by measuring the production rates of processes that have cross-sections that are theoretically well known.

Two methods have been employed to measure the beam profiles at LHCb: the commonly used Van der Meer scan method [2], where the colliding beams are moved transversely across each other, and a recently proposed method [3] that utilises reconstructed beam-gas interaction vertices near the beams' crossing point to determine the beam shapes. Combining these techniques with measurements of the beam currents has allowed two luminosity measurements to be made. Both measurements give compatible results and have associated uncertainties of $\sim 10\%$. A more complete description of these measurements can be found elsewhere in these proceedings [4, 5].

The integrated luminosity can also be measured indirectly by recording the event rate of a process with a cross-section that can be accurately calculated from theory. The accuracy of a luminosity measurement using this method is usually limited by the theoretical uncertainty on the calculated cross-section. Two candidate processes have been identified for such measurements at LHCb: W and Z production which has been calculated at NNLO with an uncertainty of $\sim 4\%$, where the dominant theoretical error is due to the uncertainty on the PDFs, and elastic dimuon production via photon fusion which has a cross-section that has been calculated with a theoretical uncertainty of $< 1\%$ [6] but has a lower event rate.

This contribution summarises the progress that has been made towards indirect luminosity measurements at LHCb using electroweak boson production and elastic dimuon production via photon fusion.

PREDICTIONS FOR W AND Z PRODUCTION

Figure 1 shows the kinematic region probed by events at LHCb as a function of the longitudinal momentum fraction x carried by the interacting parton and Q^2, the square of the four momentum exchanged in the scattering process. For particle production processes at LHCb, the momenta of the two interacting partons will be highly asymmetric, meaning that events at LHCb will simultaneously probe a region at high-x and a currently unexplored region at very low-x. The main theoretical uncertainties on cross-section predictions for electroweak boson production at the LHC stem from the level of knowledge of the input proton PDFs. At high x they have been determined from fixed target and HERA data and confirmed at higher Q^2 by W and Z production at the Tevatron. For the smaller x values, the PDFs have been measured by HERA alone but at much lower Q^2 from where they must be evolved to higher energies using the DGLAP equations.

Figure 2(a) shows the percentage uncertainty on cross-section predictions for W and Z production at the LHC due to the uncertainty on the PDFs for the MSTW2007 PDF set. For boson rapidities between 2 and 4.5 the PDF uncertainty for Z and W^+ production is in the range 2 to 4%. The PDF uncertainty on W^- production, being dominated by

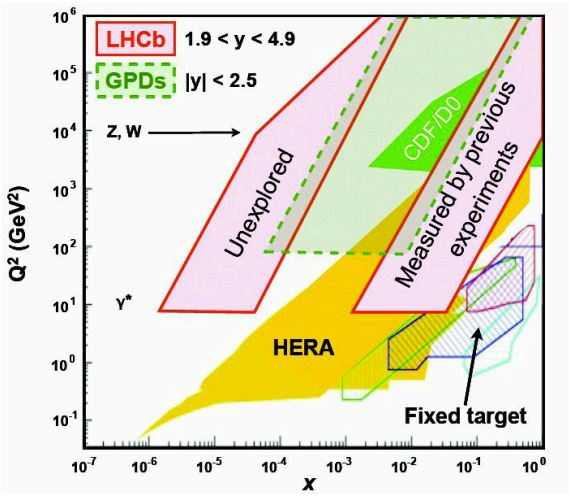

Figure 1: The kinematic region x-Q^2 probed by the LHCb experiment with electroweak boson production together with the region probed by a variety of previous experiments.

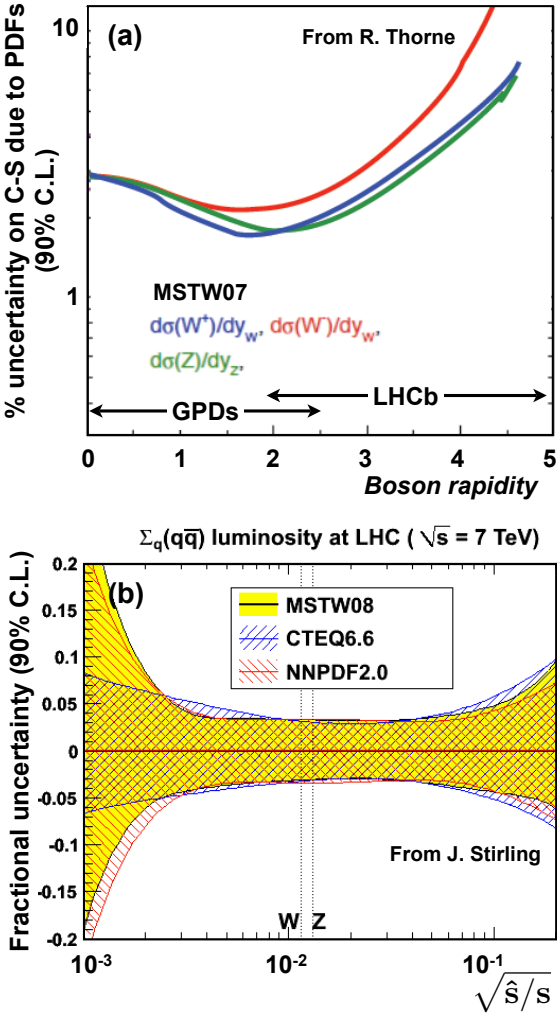

Figure 2: (a) Percentage uncertainty on cross-section predictions for W, Z and low mass Drell-Yan pairs at the LHC due to the PDFs as a function of rapidity. The regions fully instrumented by LHCb and the GPDs are shown (from [7]). (b) The fractional uncertainty on the $q\bar{q}$ luminosity as a function of $\sqrt{\hat{s}/s}$ for the MSTW2008, CTEQ6.6 and NNPDF2.0 PDF sets (From J. Stirling).

the valence down quark distribution at large rapidities, is larger and ranges between 3 and 10%. The compatibility of the results obtained using different PDF sets is illustrated in figure 2(b) which shows the fractional uncertainty on the $q\bar{q}$ luminosity as a function of $\sqrt{\hat{s}/s}$ for the MSTW2008, CTEQ6.6 and NNPDF2.0 PDF sets. It can be seen that in the region corresponding to W and Z production ($\sqrt{\hat{s}/s} \sim 10^{-2}$) all three sets give comparable results and suggest a PDF uncertainty of $\sim 4\%$.

W AND Z MEASUREMENTS

Events containing Z or W bosons are initially selected at LHCb via a single muon trigger that requires the presence of at least one muon that has a transverse momentum (p_T) greater than 10 GeV/c.

Z candidate events are then selected offline by requiring two muons with $p_T > 20$ GeV/c and $2.0 < \eta < 4.5$, which combine to a mass between 81 and 101 GeV/c^2. To ensure a good track quality, cuts on the fractional momentum uncertainty and the χ^2 probability of the track are applied. No impact parameter or isolation cut is imposed. In total 833 Z candidates are selected using 16.5 pb^{-1} of data, their mass distribution is shown in figure 3. The background contribution in the selected mass region is very low and is estimated to be 1.2 ± 1.2 events, where the dominant contribution comes from events containing two semi-leptonic heavy quark decays. This background was estimated from data by selecting events with two muons with an impact parameter significance (IPS) greater than 5.

W candidate events are selected offline by requiring one muon with $p_T > 20$ GeV/c, $2.0 < \eta < 4.5$ and IPS < 2. In order to reduce a variety of QCD backgrounds, coming either from semi-leptonic heavy quark decays or hadron misidentification, further cuts are applied to three variables that are related to the other activity in the event: the invariant mass of the rest of the event ($M^{rest} < 20$ GeV/c^2), the transverse momentum of the vector sum of all other tracks in the event ($p_T^{rest} < 10$ GeV/c) and the transverse momentum of the vector sum of all other particles inside a cone $\Delta R = 0.5$ around the muon ($p_T^{cone} < 2$ GeV/c). In total 7624 (5732) W^+ (W^-) candidates are selected using 16.5 pb^{-1} of data. The selection efficiency has been determined from data using Z events with one of the muons removed from the event. Since the cuts on the impact parameter and the activity in the rest of the event are independent of the muon they have the same characteristic shape for W and Z bosons, a fact that has been confirmed using Monte-Carlo simulations. A selection efficiency of $55 \pm 1\%$ was measured. Since only one high p_T muon is required, the back-

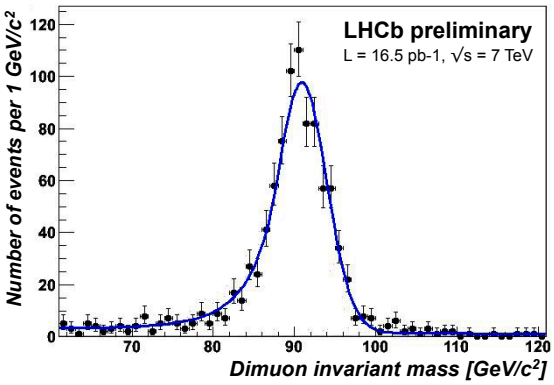

Figure 3: Invariant mass of the dimuon system.

ground contamination for the selected sample is considerably higher than for the offline selected Z sample. The contamination due to both electroweak processes (tauonic W and Z decays and muonic Z decays where only one of the muons is produced inside the LHCb acceptance) and QCD processes (semi-leptonic heavy quark decays and hadron mis-identification) have been determined by a fit to the muon transverse momentum distribution as shown in figure 4. The shapes for the p_T distributions for muons from electroweak processes are taken from simulation while the shape for the QCD background is taken from data by selecting a sample with a very small signal contribution.

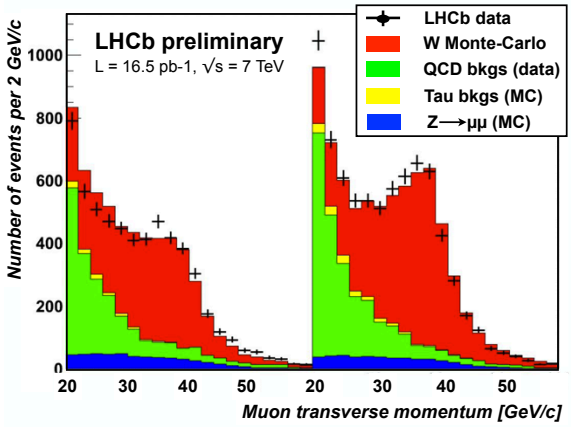

Figure 4: Distribution of the muon pT for negative(left) and positive (right) charged leptons. The data points are shown in black, the W contribution in red, the Z background in blue, the tau background in yellow and the QCD background in green.

The efficiencies for triggering, muon identification and track finding have all been estimated from data. The trigger efficiency has been determined using an offline selected Z sample. By requiring that one of the muons in the event caused the single muon line to fire the other muon can be used to determine the trigger efficiency. The single muon trigger efficiency is measured to be $80 \pm 1\%$, exhibits no evidence for a charge bias and is found to be flat in muon ϕ, η and p_T. For Z events, where either muon can cause the trigger to fire, the efficiency is determined to be $96 \pm 1\%$. The track finding and muon identification efficiencies are measured using a tag and probe method and an offline selected Z sample where the tag muon is required to have fired the single muon trigger line. The track finding and muon identification efficiencies for muons from W and Z events are found to be $92 \pm 2\%$ and $98 \pm 1\%$ respectively.

For muons with $2 < \eta_\mu < 4.5$, $p_T > 20$ GeV/c and Z boson masses between 81 and 101 GeV/c^2, the following preliminary results are obtained for the W and Z production cross-sections:

$$\sigma_Z = 74 \pm 2 \pm 3 \pm 7 \text{ pb}$$

$$\sigma_{W^+} = 1007 \pm 48 \pm 33 \pm 101 \text{ pb}$$

$$\sigma_{W^-} = 680 \pm 40 \pm 22 \pm 68 \text{ pb}$$

where the first error is statistical, the second systematic and the third comes from the luminosity determination. For the W measurements the statistical uncertainty also includes the uncertainty from the efficiency and purity estimation, however, the uncertainty due to the fit procedure is not included in the systematic uncertainty. The integrated luminosity was determined using the Van der Meer scan method and has a 10% uncertainty. These measured values are consistent with the NLO predictions from MCFM [8].

Currently, using the high purity sample of 833 Z events, the efficiencies that have been determined from data and the NNLO Z cross-section prediction, an indirect luminosity measurement could be made that would have an uncertainty of $\sim$6%. The precision is currently limited by the available statistics in two ways: firstly by the relatively large statistical uncertainty (3.5 %) and secondly, since the trigger, tracking and muon identification efficiencies are determined from data using an offline selected Z sample, a large systematic uncertainty on the determined reconstruction efficiency (3.5%). Once $\sim$150 pb^{-1} of data are collected the statistical and systematic uncertainties will be reduced to the 1% level and the uncertainty on a luminosity determination using the Z sample will be dominated by the PDF uncertainty of 4%. Using the currently available W^+ sample the luminosity could be determined with an uncertainty of $\sim$5%, though here the sample purity is lower and the systematics associated with the fit procedure that determines the purity has yet to be evaluated.

CROSS-SECTION PREDICTIONS FOR ELASTIC DIMUON PRODUCTION VIA PHOTON FUSION

Being primarily a QED process, the cross-section for elastic dimuon production via two photon fusion at the LHC has been calculated very precisely. The main features of the process can be illustrated within the Effective Photon Approximation. Here the cross-section can be calculated as a convolution of the direct cross-section of the two colliding photons that produce a muon pair and the fluxes of

virtual photons surrounding the two colliding protons. For elastic events the virtual photon fluxes will be equal to

$$dn_{el} = \frac{\alpha}{\pi}\frac{d\omega}{\omega}\frac{\vec{q}_T d^2\vec{q}_T}{(\omega^2/\gamma^2+\vec{q}_T^2)^2}\frac{G_E^2 - q^2/(2m_pG_M)^2}{1-(q/2m_p)^2} \quad (1)$$

where $q(\omega, \vec{q})$ is the four-momentum of the photon and m_p, G_E and G_M are the mass and electric and magnetic form factors of the proton respectively. The characteristic value of the the total transverse momentum of the dimuon pair produced in such elastic events is small ($\sim$ 10 MeV/c) and the cross-section can be calculated very accurately with an uncertainty of much less than 1%. However, there are two possible QCD contributions that can increase this uncertainty: strong interactions within the colliding protons that can cause one or both of the protons to dissociate during the photon emission, resulting in inelastic dimuon production via photon fusion, and rescattering contributions that are due to strong interactions between the colliding protons.

Due to uncertainties in the momentum distributions of the quarks within the proton and the collective excitations of these quarks, the matrix element describing inelastic vertices is not as well known as the matrix element for elastic vertices. This results in much higher uncertainties in the predicted cross-section for inelastic dimuon production via photon fusion ($\sim$ 20%). Fortunately, the characteristic dimuon pair p_T for inelastic production is higher ($\sim$ 250 MeV/c) enabling this contribution to be reduced by offline selection.

The rescattering corrections, which can be viewed as pomeron exchange between the colliding protons, can be either elastic or inelastic. It has been shown by Khoze et. al. [6] that the elastic rescattering contribution has the effect of modifying the phase of the matrix element but does not change the predicted cross-section, while the inelastic rescattering contribution effectively reduces the elastic cross-section and increases the inelastic cross-section. However, the calculations of Khoze et. al. have also shown that for events with small dimuon pair p_T ($\lesssim$ 100 MeV/c) these inelastic rescattering contributions are small ($\sim$ 0.2%).

MEASUREMENTS OF ELASTIC DIMUON PRODUCTION VIA PHOTON FUSION

The elastic production of dimuons via photon fusion is an exclusive process that leaves the interacting protons intact and deflected by a negligible amount. In the context of a hadron collider, therefore, these events are highly distinctive containing two muons and having no other activity.

At LHCb they are initially selected by a dedicated exclusive dimuon trigger line that requires the presence of two muons with a dimuon invariant mass greater than 1 GeV/c^2, a dimuon transverse momentum smaller than 900 MeV/c and a distance of closest approach between the muons smaller than 150 μm.

Candidate events are further isolated offline by exploiting the exclusivity of the events by requiring: no other tracks reconstructed in the vertex detector and less than five hits in the Scintillator Pad Detector (SPD) which is located before the calorimeters and covers the full acceptance of the experiment. In addition, since the trigger also accepts exclusive J/ψ and Υ events, produced via photon-pomeron fusion, and exclusive χ_c events, produced via pomeron-pomeron fusion, events that have an invariant mass near the J/ψ or Υ masses are rejected. In total 250 candidate events have been recorded in the first 17.5 pb^{-1} of data collected at LHCb. The dimuon invariant mass distribution of these events is shown in figure 5. The shape of the measured invariant mass distribution is in good agreement with the shape predicted by the LPAIR [9] Monte-Carlo generator. The expected background contamination in the selected sample is expected to be dominated by inelastic dimuon production via photon fusion and dimuons produced via pomeron fusion. These backgrounds have been investigated using Monte-Carlo samples produced using the LPAIR and Pomwig [10] generators respectively. While still under investigation, the overall purity of the sample is currently estimated to be above 95%. Data driven techniques to determine the trigger, tracking and muon identification efficiencies are currently being developed. In the future it is hoped that these efficiencies can be determined with uncertainties of O(1%), enabling a luminosity measurement with an uncertainty of $\sim$ 1% with 700 pb^{-1} of data.

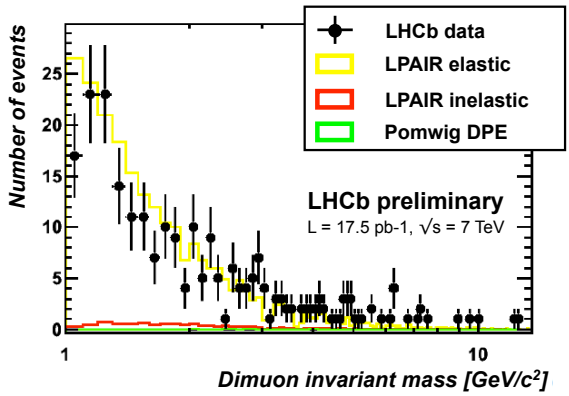

Figure 5: Invariant mass distribution for offline selected exclusive dimuon events at LHCb. The J/ψ and Υ mass regions have been excluded. The predicted distributions for signal and background are also shown.

CONCLUSIONS

Two candidate processes have been identified for indirect luminosity measurements at LHCb: electroweak boson production and elastic dimuon production via two photon fusion.

The cross-section for W and Z production at LHCb has been calculated at NNLO with an uncertainty of $\sim$ 4%, where the dominant theoretical error is due to the uncertainty on the parton distribution functions (PDFs). Using

the first 16.5 pb^{-1} of data, a very clean sample of 833 Z bosons and a larger, but less clean, sample of W bosons have been recorded at LHCb. Using the currently available W^+ sample an integrated luminosity measurement could be made that would have an uncertainty of $\sim$5%. However, the systematic uncertainty associated with the fit procedure that is used to determine the sample purity has yet to be evaluated. Using the currently available Z sample would enable a luminosity determination with a $\sim$6% uncertainty. Here the measurement is currently limited by the available statistics. Ultimately, with 150 pb^{-1} of data, a measurement using a high purity Z sample would be limited by the current PDF uncertainties of 4%.

Cross-section predictions for elastic dimuon production via two photon fusion have been performed with an uncertainty of $< 1\%$. With the first 17.5 pb^{-1} of data, 250 candidate events of this type have been observed. The shape of the dimuon invariant mass distribution of these events is compatible with the shape predicted by the LPAIR generator. Work is still ongoing to understand the purity and efficiency of this sample. It is hoped that with 700 pb^{-1} of data, a luminosity measurement with an uncertainty of $\sim$ 1% will be possible using this process.

REFERENCES

[1] The LHCb collaboration, *The LHCb Detector at the LHC*, JINST **3** S08005 (2008).

[2] S. Van der Meer, *Calibration of the effective beam height at the ISR*, ISR-PO/68-31 (1968).

[3] M. Ferro-Luzzi, *Proposal for an absolute luminosity determination in colliding beam experiments using vertex detection of beam-gas interations*, CERN-PH-EP/2005-023 (2005).

[4] V. Balagura, *LHCb 2010 luminosity determination*, LHC Lumi Days workshop, CERN (2011).

[5] P. Hopchev, *LHCb beam-gas imaging results*, LHC Lumi Days workshop, CERN (2011).

[6] V. A. Khoze et. al., *Luminosity monitors at the LHC*, IPPP/00/01 (2000).

[7] R. Thorne, *Parton Distributions and QCD at LHCb*, DIS2008 London, arXiv:0808.1847v1 [hep-ph] (2008).

[8] J. M. Campbell and R. K. Ellis, *A Monte Carlo for FeMtobarn processes at Hadron Colliders*,http://mcfm.fnal.gov/mcfm.pdf

[9] J. Vermaseren, Nucl. Phys. **B229**, 347 (1983).

[10] B. E. Cox and J. R. Forshaw, Comput. Phys. Commun.144:104-110, (2002).

STATUS AND PROSPECTS OF THE ALFA ROMAN POT STATIONS

K.Hiller, DESY, Zeuthen, Germany

Abstract

ALFA is a sub-detector of the ATLAS experiment to measure the luminosity based on the rate of elastic proton scattering. It consists of fibre trackers in Roman Pots in a distance of 240m form the central ATLAS detector. The installation of all components in the LHC tunnel was finished in February 2011 and preparations for the physics data taking are going on.

LUMINOSITY MEASUREMENT

The main goal of the ALFA detector is a precise luminosity measurement [1]. It is based on the process of elastic proton-proton scattering and independent from the knowledge of beam currents. Due to the simplicity of the physical process which does not affect any other ATLAS detector the model-dependency of this method is very small. Based on these facts the luminosity measurement with ALFA is a valuable proof of the systematic errors of other luminosity measurements.

The elastic scattering is a traditional tool for luminosity measurement. This is related to the optical theorem which relates the total cross section σ_{tot} to the elastic scattering amplitude f_{el} in forward direction: $\sigma_{tot} = 4\pi \mathrm{Im}[f_{el}(t=0)]$. The 4-momentum transfer squared t can be obtained from the scattering angle Θ and proton momentum p: $t = -(p\Theta)^2$. Using the luminosity definition as the proportional factor between total cross section and event rate $R_{tot} = L\,\sigma_{tot}$ the luminosity L can be obtained from the elastic rate R_{el} and the total rate R_{tot}:

$$\frac{1}{L} = \frac{1}{16\pi}\frac{\sigma_{tot}\left(1+\rho^2\right)}{dR_{el}/dt(t=0)}$$

with ρ = Re[f_{el}(t=0)] / Im[f_{el}(t=0)]. This method requires a good knowledge of the total event rate. Since ATLAS has a poor coverage at large values of the pseudo-rapidity η[1)] uncertainties enter from the extrapolation. A way to avoid this uncertainty is to express the total rate by the total cross section from an independent measurement e.g. the TOTEM experiment [2].

The main concept of the ALFA luminosity measurement is independent from any external input. It consist of the use of the well-known Coulomb cross section at smallest t as additional constraint. At smallest distances the scattering is dominated by the Coulomb force between the colliding protons. At larger distances the strong interaction mediated by the exchange of colour-neutral objects is the leading process. Ignoring smaller corrections like the proton form factor the elastic rate can be parametrized by only 4 parameters:

$$\frac{dN}{dt} \approx \pi \cdot L \left| \frac{-2\alpha}{|t|} + \frac{\sigma_{tot}}{4\pi}(i+\rho)\exp\left(-b|t|/2\right) \right|^2$$

The fit of the measured t-dependency gives the luminosity L as well as the other parameters σ_{tot}, ρ and the slope parameter b. Fig.1 shows the rate on dependence of t with the steep Coulomb behaviour and the flatter exponential part from the strong interaction.

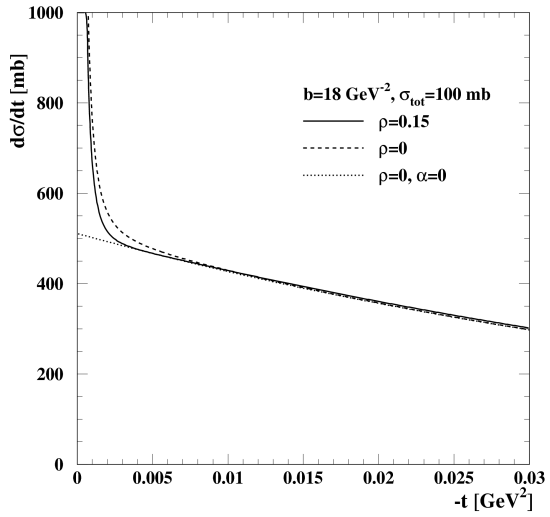

Fig.1: The t-dependency of the elastic proton scattering.

[1)] $\eta = -\ln[\tan(\Theta/2)]$

The difficulty in this kind of luminosity measurement is to access the Coulomb region at very small t on the order of a few 10^{-4} GeV^2. This requires special beam conditions to reduce the beam divergence at the interaction point well below the anticipated minimum t-value. The beam divergence is determined by the β function and the emittance ε at the interaction point: $\sqrt{\varepsilon/\beta}$. The special optics scenario for ALFA combines high β = 2625m with low ε = 1μm. To detect elastic protons at smallest scattering angles requires to move the ALFA detectors very close to the circulating beam. The acceptance of ALFA detectors in a distance of 1.5 mm to the beam is about 50%. A phase advance of 90° in the vertical plane delivers a so-called parallel-to-point optics where protons emerging the interaction point under the same angle are focused to the same position in the ALFA detectors. Another condition for ALFA running is the zero crossing angle of colliding protons. This requires a rather limited number of colliding bunches. Together with the dilution of the beam due to the high β the specific luminosity will be on the order of 10^{-27} cm^{-2}s^{-1}. Due to the special beam conditions the ALFA luminosity measurements will be performed only in short periods of a few days. At this low specific luminosity the consistency with other methods of luminosity measurements can be checked. The simulations carried out with the proposed optics and the detector performance described in [1] predict a luminosity error of 3% with similar contributions from the statistical and systematic sources.

DETECTORS PERFORMANCE

The tracking in the ALFA stations is based on multi-layer scintillating fibre detectors. Altogether 20 layers of staggered fibres with a squared cross section of 0.5x0.5 mm^2 measure the two coordinates perpendicular to the beam. In the upper and lower hemisphere the scattered protons can be traced by two identical detectors. The detectors, sketched in Fig.2, are housed in movable plunger vessels, so-called Roman Pots, which allow to bring them closer to the beam.

The fibres precisely glued on both sides of Titanium plates are inclined by +- 45° in respect to the vertical axis. By a staggering of 50 μm the theoretical resolution is pushed to 14 μm. The tracking detectors are covered by 2 scintillator tiles for triggering. For the physics analysis a distance measurement of the detectors in respect to the beam is needed. So-called overlap detectors measure the distance of the upper and lower fibre detectors and give an additional constraint to the positioning. Both overlap detectors are traversed by halo particles and the positions of tracks can be transformed into a distance. Similar to the main detectors the overlap detectors consist of 3 staggered fibre layers. The anticipated precision of the distance measurement given by a large amount of halo particles is 10 μm.

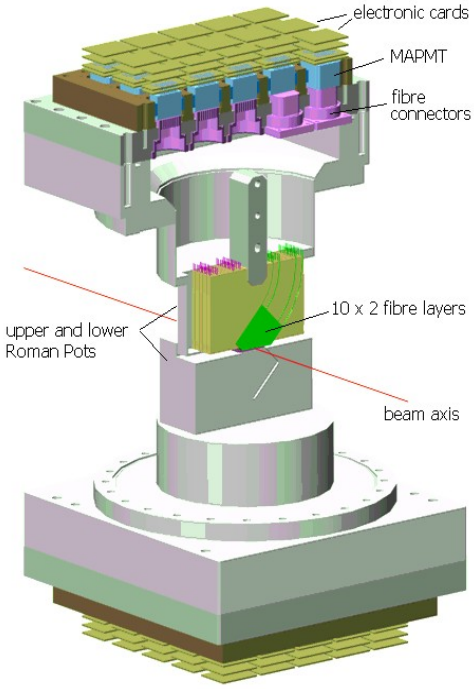

Fig.2 Upper and lower Roman Pot with the main fibre detectors and the routing to the MAPMTs. The overlap detectors are not shown.

The light signals generated by charged particles passing the scintillator material are guided to Multi-Anode Photo-Multipliers (MAPMT). The typical fibre signal gives about 4 photo-electrons on a Bialkali photo-cathode. Altogether 23 MAPMTs[2)] with a grid of 8 x 8 readout pixels amplify the fibre signals. The readout of the trigger tiles is performed by clear fibre bundles glued to two tile edges. Both bundles result in a signal of about 40 photo-electrons from the trigger PMT[3)] photo-cathode.

The front-end electronics is compressed in a compact package of boards directly sitting at the MAPMT back side. The active board contains a 64 channel MAROC chip which amplifies and discriminates all signal which are sent by flat Kapton cables to the motherboard.

In the year 2010 the final sets of all detectors, motherboards and Roman Pots were investigates in a CERN hadron test beam. An important parameter for efficient tracking is the efficiency of the fibre layers. Here a typical value of 94 % was measured. The resulting tracking efficiency is close to 100%.

[2)]Hamamatsu R7600, [3)]Hamamatsu R7400, R9880

Another performance parameter is the spatial resolution. For these studies the EUDET Silicon Pixel telescope [3] was used as an external reference. The ultimate resolution in the centre of the telescope is about 2 μm. Due to space constraints the ALFA stations had to be placed in a distance of 1.2 m to the telescope. At this distance the EUDET resolution is about 8 μm. The residuals of the ALFA coordinate measurement in respect to the extrapolated EUDET tracks are shown in fig.3. Typically values around 30 μm were achieved, best values are at 25μm. The difference to the theoretical resolution of 14μm is caused by deviations from the regular staggering, noise contributions and cross talks from physics processes and in the MAPMTs.

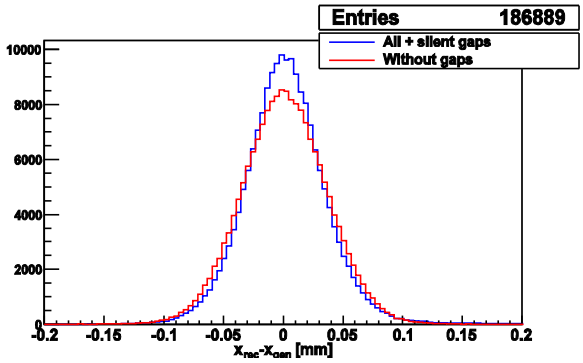

Fig.3 Typical resolution of an ALFA fibre detector.

Another important parameter to access lowest *t*-values in the Coulomb region is the sensitivity of the fibre detectors at the edge close to the beam. For the same reason the gap at the detector edge to the Roman Pot window has to be minimized. A tomography image of the fibre detectors and the Roman Pot windows reconstructed from the EUDET reference tracks is shown in fig.4 The large flat plat tops corresponds to tracks triggered by the main trigger tiles while the small peaks are related to particles interacting in window and trigger the readout by shower particles. The first preliminary results confirm a good edge smearing of about 25μm. Furthermore the gap between the bottom window and the detector edge can be measured directly and compared with the values from the 3D survey. The nominal value of the gap is 150μm. Sometimes deviation on the order of 50μm were observed in the tomography plots. The calibration of the overlap detectors is another purpose of the test beam analysis. Before the assembling of the detectors all fibre positions were measured by microscope and the position of tracks is well-known in the coordinate system of individual plates. However the assembling can introduce small additional offsets which in turn change the position of the reconstructed track. Especially for the overlap detector with only 3 fibre layers the correction of additional offsets is of importance. Monte Carlo simulations have shown that after calibration the distance measurement can achieve a precision of 5μm.

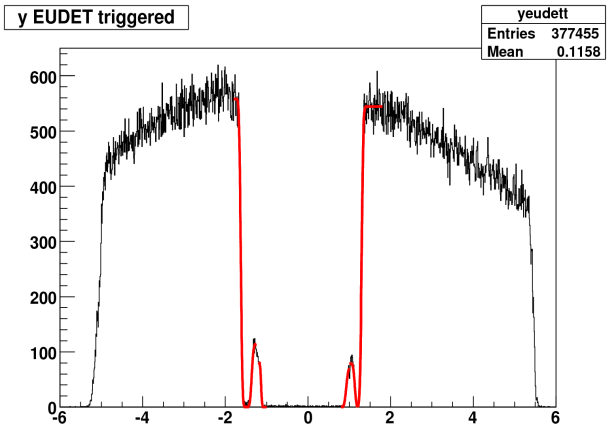

Fig.4: Vertical tomography of upper and lower detector edges with small peaks indicating the windows.

STATUS OF INSTALLATION

The installation in the tunnel started with the integration of the the Roman Pot stations in the ring of LHC beam pipes. While the LHC vacuum was protected by closed valves a short intermediate piece of the outgoing pipe was removed and replaced by a Roman Pot station.

The insertion of the Roman Pots itself into the stations is a time-consuming operation. First there is a very small clearance between the thin bellows and the sharp outer edges of the Roman Pots. And second also the thin 200μm windows of the Roman Pots have to be protected against mechanical impact. The pots were closed by blind flanges and pumped until a pressure of few mbar in the Roman Pots. This secondary vacuum is needed to prevent the windows against bending inside the beam pipe by the atmospheric pressure.

Due to the tight mechanical environment at the positions of the ALFA stations the installation of the stations including insertion of Roman Pots took about 2 weeks. The subsequent bake out of the stations and surrounding elements lasted about 5 days and was finished in December 2010.

The first activity in 2011 was the insertion of the fibre detectors. Since the fibres and the trigger tiles are glued on Titanium plates mechanical impact on these structures must be avoided. Also here the clearance is in some cases only a few hundred μm. The insertion of the detectors took about one day per station. The insertion of a lower fibre detector is shown in fig.5.

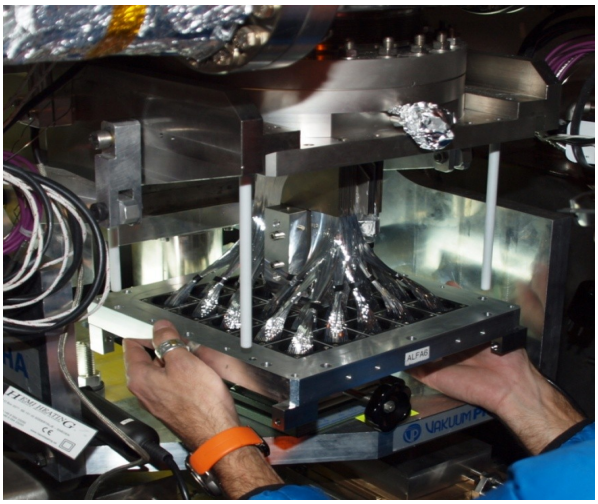

Fig.5: Insertion of a lower fibre detector in the RomanPot.

The next activities were related to the readout electronics. The so-called base plates with all MAPMTs were put onto the detector frame with all the fibre feedthroughs. The front-end electronics of all MAPMTs is connected by flat Kapton cables to the motherboard where data are packed and prepared for the readout.

The main trigger signal for each detector is formed by a coincidence of signals in both trigger tiles. These signals are sent in air-core cables to a VME crate in USA15 and further to the ATLAS Central Trigger Processor (CTP). The CTP produces the L1A trigger signal which is sent by optical fibres back to the ALFA stations to start the data readout from the motherboards. The data packets are transferred via fibre optics to the Read OUT Drivers (ROD) and further to the central ATLAS TDAQ.

An important condition for the measurements with the ALFA detectors is the knowledge of the detector positions in the LHC coordinate system. Apart from the detector positioning this information is also a safety issue for LHC. This positioning was done in two steps. First all stations were aligned to the nominal LHC beams. This can be arranged by a level gauge and the known positions of beam line elements on both sides of the ALFA stations. The second step is the calibration of the detector positions to the nominal LHC beams. For this procedure a laser tracker has been used. The laser tracker measures positions and angles of the detectors via 3 laser targets fixed to the Roman Pots. The positions of these targets have been precisely measured in the Roman Pot coordinate system by a 3D device. For the position measurement of the movable Roman Pots so-called Linear Variable Differential Transformers (LVDT) are used. A sliding core results in changes of the induced voltages in the secondary coils. This voltage ratio will be calibrated to the distance of the outer Roman Pot window to the nominal beam position obtained from the laser measurements.

After the cabling of the electronics and low level connectivity tests the commissioning of the detector readout was performed. The main tool for this purpose are the online histograms implemented in the ATLAS TDAQ. For these tests the TDAQ is running in a standalone partition without affecting the central ATLAS TDAQ. Without particles from the LHC beams the detector commissioning is based on LED data. Each detector is equipped with 2 LEDs which are located inside the Roman Pot with the fibre detectors. The LEDs flash the whole volume of the Roman Pot and light enters the MAPMTs via the transparent glue in the fibre feedthroughs. Such LED pulses generate a typical pattern with more intensive light in two cones on both sides of the detector arm as shown in fig.6.

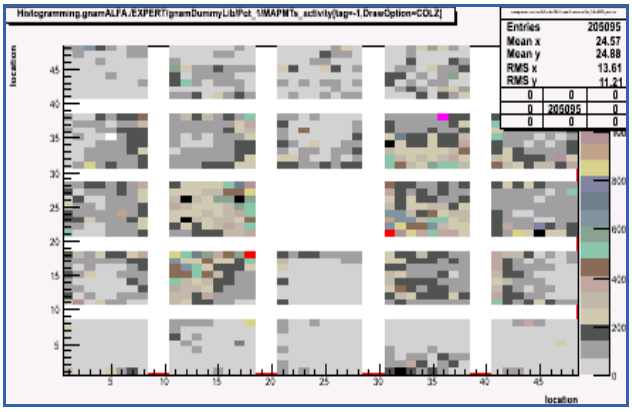

Fig.6: MAPMT images produced by pulsed LED signals illumination the fibres inside the Roman Pot.

The LED pulses are also used to adjust the latencies and to synchronize the data readout of all 8 ALFA detectors. Latencies are roughly adjusted in 25 nsec bunch crossing units given by the 40 MHz LHC clock. The fine timing is organized by firmware and shifts the phase of the LHC clock inside a certain bunch crossing. The LED signals are also used to verify the threshold behaviour of the faint light signals passing the MAROC front-end chip. For this purpose the LEDs are tuned to low light level below the 1 photo-electron signal. In so-called S-curves measurement the MAROC threshold is step by step enlarged and the rate shows a typical behaviour. With the increase of the threshold first the pedestal signal disappears, than a flat part with equal efficiency follows before the signal drops to zero at high threshold. At the end point the threshold increase is extremely steep and even large signals are rejected. The S-curves are different in the flat part due to the varying amount of light in

dependency on the fibre position in the Roman Pot. A band of S-curves of one MAPMT is shown in fig.7.

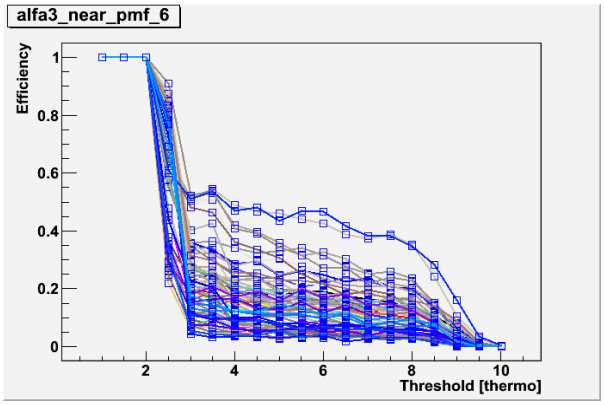

Fig.7: S-curves indicating the 1 photo-electron threshold and saturation around 2.5 and 9.5 thermo.

DATA TAKING 2011

The final goal of the luminosity measurement can only be performed in special runs with the very high β and low specific luminosity. The special optics has to prepared by simulations followed by dedicated machine studies. Before the very high β optics it is foreseen to have data taking with an intermediate β of 90m together with the TOTEM experiment. Taking into account all the necessary steps of commissioning with LHC beams the intermediate β run seems to be a realistic goal for 2011. The experience in this process will allow a better prediction of the time scale for the ultimate β = 2625m run.

The 2011 time line of integration steps into the ATLAS CTP and TDAQ and the evolution of detector positions is summarized in table 1.

Tab.1: ALFA commissioning steps in 2011

Step	Position	Trigger	DAQ	Goal
1	Garage	ALFA NIM	Local stream	Rate
2	Garage	any ATLAS	Local stream	Trigger bits, latency
3	~10mm	ALFA NIM	Local stream	Rate
4	~10mm	ALFA in menu	Local stream	Trigger bits, latency
5	~10mm	ALFA in menu	ATLAS stream	Latency
6	~10mm	ALFA in menu	ATLAS stream	ATLAS latency
7	Close to beam	ALFA in menu	ATLAS stream	cross section

There are three relevant parameters which can be changed: the detector position, the trigger processor and the data stream. The detector position will change from the garage position to out of garage in a safe distance to the beam and finally close to beam for a physics run. For the trigger handling there are 2 options. Since the signals are split before entering the CTP and the readout can be triggered by a local NIM logic, or after integration by a L1A signal of CTP menu. The logging of data can be performed fully locally. After the implementation in the ATLAS trigger menu the ALFA data are integrated in the global ATLAS data stream.

All the commissioning steps until the β 90m run will be performed during normal ATLAS data taking with collision optics.

In the garage position only fragments of shower particles can hit the detectors. With a local NIM based trigger logic one can watch the rates and check the performance of individual detectors. The composition of the trigger bits at the input to CTP can be investigated. Later, still in garage position the data readout can be triggered by any ATLAS L1A trigger. In this spy mode the fraction of events with activity in the ALFA detectors will be low since the coincidence rate of the L1A signal with showers at the ALFA positions is accidentally. These runs can be used to exercise the adjustment of latencies.

In the next step the detectors are moved out of the garage but are still fully in the shadow of the collimators. Shower and halo particles can hit two neighbouring detectors in coincidence. The first measurements aims for feedback about the coincidence rate as an input for a more precise estimation of the radiation dose. In runs with standard collision optics and high specific luminosity the radiation is a critical parameter for the positions of the fibre detectors. Preliminary estimates indicate that the detectors in a distance of ~ 10 mm (~ 30 σ of the beam envelope) to the beam are irradiated by an acceptable low rate. After the rate measurement with local trigger logic data taking continues in spy mode by ATLAS L1A triggers. The latencies will be checked and tuned for halo particles. In the next step the ALFA readout will be first time triggered using an ALFA trigger from the central ATLAS CTP menu. In these runs the final ALFA latency adjustment will be performed. Due to the large distance of the ALFA stations from the IP the latency is on the order of 10 bunch crossings behind the present ATLAS latency. In a temporary phase without correcting the latencies of all ATLAS detectors only the ALFA data are meaningful. To make sure that the data from all ATLAS detectors belong to the same event all latencies have to be adapted to the ALFA latency. This is the last commissioning step before ALFA is ready for a physics run with β 90m optics.

In the very first commissioning step with LHC beams the readout of ALFA data will be triggered by an OR of all detectors in all stations. This is necessary for an overall adjustment of the latencies of all detectors to ensure that data from all detectors belong to the same event. For this purpose ALFA will feed 8 trigger signals of all detectors via the PIT bus to the CTP. The trigger for halo particles can be arranged by coincidences of 2 neighbouring detectors and the amount of inputs to CPT can be reduced to 4 PIT bus units. The final ALFA physics trigger is shown in fig.8.

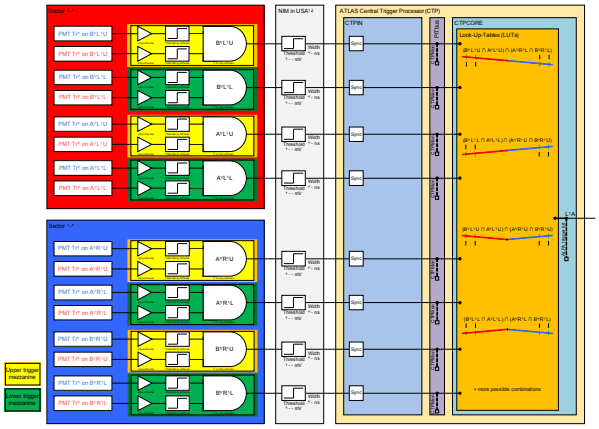

Fig.8: ALFA main trigger logic for elastic scattering.

The elastically scattered protons are characterized by coincidences of signals in all detectors on both arms. The opposite scattering angles of the outgoing protons combines in each case particles in the upper and lower detectors in opposite sides. In this case the 8 trigger inputs are compared in the CTP with pre-defined signal combinations. A L1A signal is related to elastic events and for background studies to some accidental combinations.

ACKNOWLEDGEMENTS

The construction of the ALFA stations, detectors and electronics has been performed by people from many institutions: CERN, DESY, LAL Orsay and universities in Berlin, Giessen, Lisbon, Krakow, Prague and Olomouc. The author acknowledges the good preparation and the smooth procedure of the installation and commissioning in the LHC tunnel. A special thanks for plots and photos to H.Stenzel, M.Heller, K.Korcyl and S.Jakobsen.

REFERENCES

[1] ALFA Technical Design Report, CERN /LHCC/ 2008/004.

[2] TOTEM Technical Design Report, CERN / LHCC/ 2004-002.

[3] J.Behr, EUDET-Report-2010-01, 2010; DESY-THESIS-2010-038, 2010.

Determination of Integrated Luminosity via W and Z Boson Production with the ATLAS Detector

Matthias Schott, on behalf of the ATLAS Collaboration

Abstract

The possibility to determine the recorded integrated luminosity via the measurements of the W and Z boson production cross-sections with the ATLAS detector is discussed. The current results based on 2010 data are briefly summarized. Special attention is drawn to theoretical uncertainties of the measurement. The latter give a large contribution to the systematic uncertainties of the measurements. An outlook on the expected precision of an analysis based on $\int Ldt \approx 1\,\text{fb}^{-1}$ is given and the implications on a possible luminosity determination are discussed.

THEORETICAL PREDICTIONS

The theoretical predicted cross-sections for the W and Z boson production at a p-p collider with $\sqrt{s} = 7$ TeV, discussed in this note, are based on QCD NNLO calculations obtained with the FEWZ program [1, 2]. The central values and their corresponding theoretical uncertainties are summarized in Table 1. The major sources of systematic uncertainties come from PDF and α_s measurements, based on a 90% confidence limit, while electroweak radiative corrections have been assumed to be negligible. A detailed discussion can be found in [3].

	$\sigma_{tot} \cdot BR(W \to l\nu)[nb]$
W^+	6.16 ± 0.31
W^-	4.30 ± 0.21
W	10.46 ± 0.52
	$\sigma_{tot} \cdot BR(Z/\gamma^* \to ll)[nb]$
	$66 < m_{ee} < 116$ GeV
Z/γ^*	0.964 ± 0.048

Table 1: Theoretical predictions of the W and Z boson production cross-sections based on QCD NNLO calculations by FEWZ.

MEASUREMENT OF THE W AND Z BOSON PRODUCTION CROSS-SECTIONS

A detailed description of the preliminary measurements of the inclusive Drell-Yan $W \to l\nu$ and $Z/\gamma^* \to ll$ ($l = e, \mu$) production cross-sections in proton-proton collisions at $\sqrt{s} = 7$ TeV can be found in [4]. This study is based on the complete data collected in 2010, with an integrated luminosity of about 35 pb^{-1}. In the following, only a brief summary of the results is given.

The leptonic (e, μ) decays of W and Z bosons provide clean final states to measure their production cross-sections in proton-proton collisions with the ATLAS detector. The detector and lepton identification strategy are described in [5].

The W and Z boson production cross-sections can be expressed as follows:

$$\sigma_{W/Z} \times BR_{W/Z \to l\nu/ll} = \frac{N_S - N_B}{A_{W/Z} \cdot C_{W/Z} \cdot \int \mathcal{L}dt} \quad (1)$$

where N_S is the number of selected candidate events in data, N_B is the number of estimated background events and $A_{W/Z}$ corresponds to the geometrical and kinematic acceptance for the W/Z boson decays under consideration at purely theoretical level. The factors $C_{W/Z}$ allow to correct the number of observed events for detector effects in the acceptance region. This includes all reconstruction-, trigger- and cut-efficiencies and $\int \mathcal{L}dt$ denotes the integrated luminosity for the channel of interest.

The lepton trigger, reconstruction and identification efficiencies have been estimated in data using the so-called 'tag-and-probe' technique applied on samples of Z bosons decaying into two leptons [6]. In addition, the lepton momentum scale and resolution as well as effects on the $\not\!\!E_T$ scale and resolution have been studied with data-driven approaches [4]. The experimental correction factors C_W and C_Z are determined via Monte Carlo simulations of the ATLAS detector and have been corrected for discrepancies between data and Monte Carlo.

The fiducial regions for the W and Z boson production cross-sections are defined via the following cuts applied at the generator level for the electron and muon decay channels, respectively:

- $W \to e\nu$: $E_T^e > 20$ GeV, $|\eta| < 2.47$, excluding $1.37 < \eta < 1.52$, $E_T^\nu > 25$ GeV, $m_T > 40$ GeV
- $W \to \mu\nu$: $p_T^\mu > 20$ GeV, $|\eta| < 2.4$, $E_T^\nu > 25$ GeV, $m_T > 40$ GeV
- $Z \to e^+e^-$: $E_T^e > 20$ GeV, $|\eta| < 2.47$, excluding $1.37 < \eta < 1.52$, 66 GeV $< m_{ee} <$ 106 GeV
- $Z \to \mu^+\mu^-$: $p_T^\mu > 20$ GeV, $|\eta| < 2.4$, 66 GeV $< m_{\mu\mu} <$ 106 GeV

The purely theoretical factor $A_{W/Z}$ is used to extrapolate from the experimentally accessible fiducial region to the full phase-space and has been determined on Monte Carlo generator level. The systematic uncertainties on $A_{W/Z}$ vary between 3% and 4% and are dominated by PDF uncertainties. The theoretical uncertainties on the detector and efficiency correction factors $C_{W/Z}$ can be assumed to be negligible to a good extend.

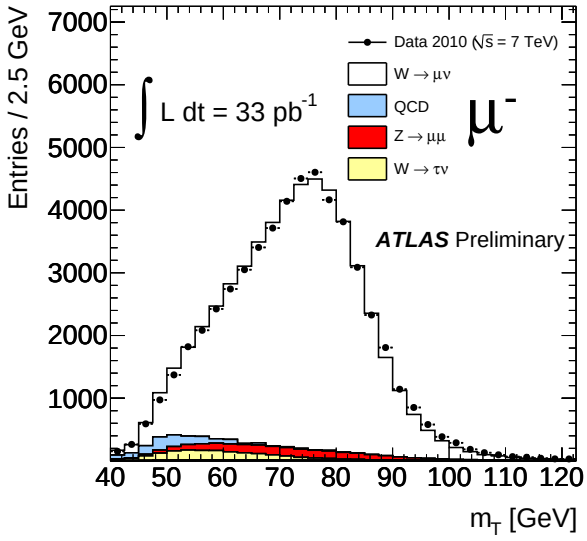

Figure 1: Transeverse mass m_T distribution for $W^- \to \mu^-\nu$ candidates selected in the full 2010 data-set.

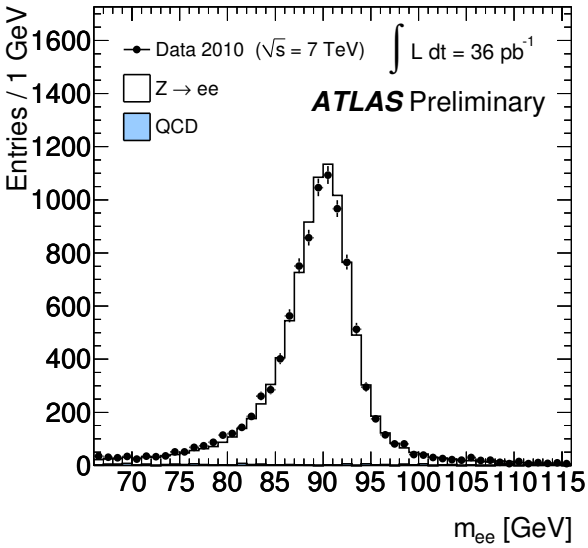

Figure 2: Invariant mass distribution for $Z \to e^+e^-$ candidates selected in the full 2010 data-set.

The recorded electron and muon data samples, used for this analysis, were selected by single lepton triggers, using a combination of hardware and software based triggers. The selection of W boson candidate events requires one identified lepton with a large transverse momentum (p_T) above 20 GeV and within the geometrical acceptance of the detector as already introduced above. Muons are reconstructed in the ATLAS inner detector and muon spectrometer which give rise to two independent p_T measurements. The selected muon candidates are required to be isolated and have a good matching between the muon spectrometer and the corresponding inner detector measurement. The electron candidates have to pass several cuts on their shower shapes in the electromagentic calorimeter, their inner detector track properties and the track-cluster matching between the ATLAS inner detector and the calorimeter system. In addition, it is required that the missing transverse energy ($\not\!\!E_T$) of the event is larger than 25 GeV and that the reconstructed transverse mass (m_T) defined by the lepton-$\not\!\!E_T$ system, is larger than 40 GeV. Figure 1 shows the selected m_T distribution for negative charged W boson candidates in the muon decay channel. The QCD background is estimated by data-driven methods on both the electron and muon channels, while the electroweak contribution is obtained from Monte Carlo simulations.

The selection of $Z \to \ell^+\ell^-$ candidate events requires two oppositely charged leptons with a large transverse momentum $p_T > 20$ GeV. The reconstructed muons must satisfy the same selection criteria and isolation cuts as in the W boson selection. The electron candidates have to pass slightly looser quality criteria. The invariant di-lepton mass m_{ll} is required to be within 66 GeV $< m_{ll} <$ 116 GeV for both decay channels. Figure 2 shows the resulting invariant mass distribution of the selected electron pairs in comparison with the Monte Carlo expectation.

In total, 121,310 $W^\pm \to e^\pm\nu$, 9,721 $Z \to e^+e^-$, 139,266 $W^\pm \to \mu^\pm\nu$ and 11,669 $Z \to \mu^+\mu^-$ candidate events have been selected in the complete 2010 data-set, corresponding to an integrated luminosity of about 35pb^{-1}. The measured cross-sections for the combination of the electron and muon decay channels are summarized in Table 2 together with the statistical and systematic uncertainties. The luminosity uncertainty as well as the uncertainty of the acceptance corrections are shown separately. The experimental uncertainties on the Z boson cross-section is 1.2%, excluding the luminosity uncertainty. This is very close to the ATLAS predictions based on studies at $\sqrt{s} = 14$ TeV with an assumed integrated luminosity of 50 pb^{-1} [7].

	$\sigma_{tot} \cdot BR(W \to l\nu)$				
	Value [nb]	(stat.) [nb]	(syst.) [nb]	(lumi.) [nb]	(acc.) [nb]
W^+	6.257	0.017	0.152	0.213	0.188
W^-	4.149	0.014	0.102	0.141	0.124
$W^\pm$	10.391	0.022	0.238	0.353	0.312
Z/γ^*	0.945	0.006	0.011	0.032	0.038

Table 2: Total averaged cross-sections times leptonic branching ratios for W^+, W^-, W and Z/γ^* production in the combined electron and muon final states. The uncertainties denote the statistical (stat.) , experimental systematic (syst.) errors, the luminosity induced (lumi.) errors as well as the uncertainty of the acceptance factor $A_{W/Z}$ (acc.) in Equation 1.

The results are in very good agreement with the theoretical calculations at NNLO in QCD, as summarized in Table 1. A powerful test of NNLO QCD calculations is provided

by the ratio of W and Z boson production cross-sections, since several theoretical and experimental systematic uncertainties cancel to a good extend in the ratio measurement. The comparison between the measured and predicted ratio is presented in Figure 3 which clearly highlights the large agreement between experiment and theory.

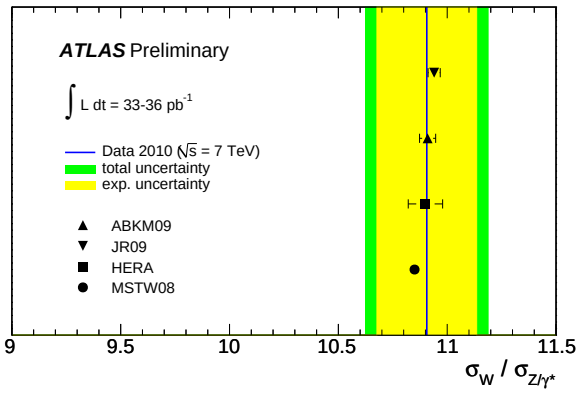

Figure 3: Predicted cross-section ratio $\sigma_W/\sigma_{Z/\gamma^*}$ and the corresponding measurement: 10.906 ± 0.079 (stat.) $\pm$ 0.215 (syst.) $\pm$ 0.164 (acc.) [4]. The experimental uncertainty of the measurement includes statistical and experimental systematic errors. The uncertainties of the predicted cross-section ratios are very small.

LUMINOSITY DETERMINATION BASED ON VECTOR BOSON PRODUCTION

Equation 1 can be rearranged to predict the integrated luminosity of the studied data-sample, by assuming that the theoretically predicted cross-sections agrees with the experimental measurements. In the following it will be discussed which precision on the integrated luminosity can be expected by studying the W and Z boson production at LHC. After the data-taking of roughly 300k Z boson events per lepton decay channel (corresponding to $\int \mathcal{L}dt = 1\,\mathrm{fb}^{-1}$) the statistical component of the measurement is no longer critical in any respect. In addition, data-driven detector performance studies can improve the understanding of the detector performance, leading to a relative uncertainty below 1% on the detector correction factors $C_{W/Z}$ in Equation 1. Hence the dominant systematic in the final luminosity estimate will be the theoretical uncertainty on $A_{W/Z}$, which are currently of the order of 3-4%. This large uncertainty comes mainly from the extrapolation of η beyond the fiducial region, while the extrapolation to lower values of p_T has only a minor effect.

One possibility to lower the uncertainty on $A_{W/Z}$ is to increase the fiducial volume of the measurement by including the ATLAS electron identification up to $|\eta| < 4.5$ in the full cross-section measurement. This would reduce the required extrapolation and thus the systematic uncertainty on $A_{W/Z}$. This has been investigated in [4]. In addition, a differential measurement of the production cross-sections of W and Z bosons as a function of p_T and η can be used to constrain PDF sets and reduce the corresponding systematic uncertainties significantly. One step in this direction was the measurement of the W^+/W^- charge asymmetry, shown in Figure 4 and discussed in detail in [8].

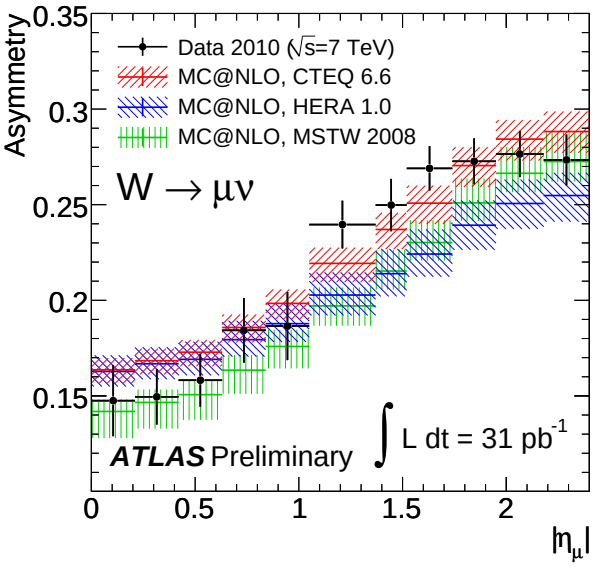

Figure 4: The muon charge asymmetry from W boson decays in bins of absolute pseudorapidity including statistical and systematic contributions. The kinematic requirements applied are $p_T^\mu > 20$ GeV, $p_T^\nu > 25$ GeV and $m_T > 40$ GeV.

Another approach would be to avoid uncertainties on $A_{W/Z}$ at a theoretical level by comparing measured fiducial cross-sections with theoretical predictions in the fiducial region. New versions of NNLO cross-section programs allow the calculation of fiducial cross-sections, i.e. cross-sections within the detector acceptance [2]. These programs have currently no parton show model nor resummation effects included and hence lead to an unrealistic p_T distribution of the decay leptons. Future studies will show how this situation can be improved and uncertainties due to these missing effects can be estimated.

CONCLUSION

The lower bound on the theoretical uncertainty on the W and Z boson production cross-section predictions is given by renormalisation and factorisation scale uncertainties (0.6%-0.8%) which cannot be lowered without significant improvements on the higher order QCD calculations. The current theoretical uncertainties for cross-section predictions in the fiducial region of the detector are estimated at the $\approx$ 3% level, dominated by PDF uncertainties [9]. Those are expected to be significantly lowered in the coming years by future precision measurements at the LHC

while a quantitative statement on the expected uncertainty reduction cannot be made. The expected experimental uncertainties are expected to be significantly below 1%. The expected precision on the integrated luminosity determination via W and Z boson production at the ATLAS detector is therefore expected to be $1 - 3\%$.

However, it should be noted that such an approach essentially relates all cross-section measurements of further physics processes (e.g. the top-quark pair production), to the production cross-section of the electroweak bosons. Hence, production cross-section measurements are essentially replaced by the measurement of cross-section ratios.

REFERENCES

[1] C. Anastasiou, L. J. Dixon, K. Melnikov, and F. Petriello, High precision QCD at hadron colliders: Electroweak gauge boson rapidity distributions at NNLO, Phys. Rev. D69 (2004) 094008, arXiv:hep-ph/0312266

[2] R. Gavin, Y. Li, F. Petriello, and S. Quackenbush, FEWZ 2.0: A code for hadronic Z production at next-to- next-to-leading order, arXiv:1011.3540 [hep-ph]

[3] ATLAS Collaboration, Measurement of the W and Z production cross-sections in proton-proton collisions at $\sqrt{s} = 7\,\mathrm{TeV}$ with the ATLAS detector, JHEP 12 (2010) 060, arXiv:1010.2130 [hep-ex]

[4] ATLAS Collaboration, A measurement of the total W and Z/γ^* cross-sections in the e and μ decay channels and of their ratios in pp collisions at $\sqrt{s} = 7\,TeV$ with the ATLAS detector, ATLAS-CONF-2011-041

[5] ATLAS Collaboration, The ATLAS Experiment at the CERN Large Hadron Collider, JINST 3 (2008) S08003

[6] ATLAS Collaboration, Muon Performance Note, Phys. Rev. Lett. 25 (1997) 56 ATLAS Collaboration, Determination of the muon reconstruction efficiency in ATLAS at the Z resonance in proton-proton collisions at $\sqrt{s} = 7\,\mathrm{TeV}$, ATLAS-CONF-2011-008

[7] The ATLAS Collaboration, Expected Performance of the ATLAS Experiment - Detector, Trigger and Physics, arXiv:0901.0512 [hep-ex]

[8] ATLAS Collaboration, Measurement of the Muon Charge Asymmetry from W Bosons Produced in pp Collisions at $\sqrt{s} = 7\,\mathrm{TeV}$ with the ATLAS detector, arXiv:1103.2929; CERN-PH-EP-2011-036

[9] S. Alekhin, J. Blmlein, P. Jimenez-Delgado, S. Moch, E. Reya, NNLO Benchmarks for Gauge and Higgs Boson Production at TeV Hadron Colliders, arXiv:1011.6259; 2010

MEASUREMENTS OF INCLUSIVE W/Z PRODUCTION CROSS SECTIONS AT CMS AND W/Z AS A LUMINOMETER

The CMS Collaboration, CERN, Geneva, Switzerland

Abstract

Leptonic decays of W/Z bosons provide the first electroweak precision measurements at the Large Hadron Collider (LHC). The results of measurements of inclusive W and Z boson production cross sections in pp collisions at $\sqrt{s} = 7$ TeV are presented [1], based on 2.9 pb^{-1} of data recorded by the Compact Muon Solenoid (CMS) detector at the LHC. The measurements, performed in the electron and muon decay channels, are combined to give $\sigma(\mathrm{pp} \to \mathrm{W}X) \times \mathcal{B}(\mathrm{W} \to \ell\nu) = 9.95 \pm 0.07\,(\mathrm{stat.}) \pm 0.28\,(\mathrm{syst.}) \pm 1.09\,(\mathrm{lumi.})$ nb and $\sigma(\mathrm{pp} \to \mathrm{Z}X) \times \mathcal{B}(\mathrm{Z} \to \ell^+\ell^-) = 0.931 \pm 0.026\,(\mathrm{stat.}) \pm 0.023\,(\mathrm{syst.}) \pm 0.102\,(\mathrm{lumi.})$ nb, where ℓ stands for either e or μ. Theoretical predictions, calculated at the next-to-next-to-leading order (NNLO) in QCD using recent parton distribution functions (PDFs), are in agreement with the measured cross sections. Hence copious production of these well understood and clean signatures suggest the use of W/Z as a "standard candle" for measuring the luminosity at the LHC alongside the current Van der Meer (VdM) separation scan method.

INTRODUCTION

Inclusive leptonic decays of W and Z bosons are benchmark physics processes at hadron colliders. These first electroweak processes studied at the LHC allow validation of high transverse momentum electron and muon reconstruction and identification. In addition, precision measurements of the W/Z are important in testing the Standard Model more rigorously than ever before, constraining the PDF, and potentially uncovering signs of new physics that could appear through radiative corrections.

The results of the W/Z production cross section measurements with pp collisions at a center-of-mass energy of 7 TeV provided by the LHC are reported [1]. The data were collected from April through August, 2010, by the CMS experiment, and correspond to an integrated luminosity of 2.9 ± 0.3 pb^{-1}. The consistency of the results between the different leptonic decay channels and with the NNLO theoretical calculations suggests already considering the use of these electroweak boson decays as "Standard Candles for LHC" to calibrate the absolute luminosity alongside the Van deer Meer separation scan. Comparison of the systematic uncertainties between the two methods is provided.

The precision of the cross section measurements was limited by the systematic uncertainty on the luminosity (11%). In the very near future [1] more detailed understanding of several of the main systematic biases will substantially reduce the uncertainty of these measurements. The statistical uncertainty will also be reduced by about a factor of 3 once the measurement is performed on the entire 2010 data set, corresponding to 36 pb^{-1}. Conservative systematic uncertainty projections for the measurements using the full 2010 data set are provided. [2]

CROSS SECTION RESULTS FOR 2.9 pb^{-1}

Results for electron and muon decay channels are reported separately, and then combined assuming lepton universality in W and Z decays. The electron and muon channels are combined by maximizing a likelihood that accounts for the individual statistical and systematic uncertainties and their correlations. For cross section measurements, correlations are only numerically relevant for theoretical uncertainties, including the PDF uncertainties on the acceptance values. For cross section ratio measurements, the correlations of lepton efficiencies are taken into account in each lepton channel, with other experimental uncertainties assumed uncorrelated; in the combination of lepton channels, fully-correlated uncertainty for the acceptance factor are assumed, with other uncertainties assumed uncorrelated.

Table 1 summarizes the measured electroweak boson production cross sections, and compares them to their theoretical NNLO predictions [3], [4]. The reported Z boson production cross sections pertain to the invariant mass range $M_{\ell\ell} \in (60, 120)$ GeV, and are corrected for the fiducial and kinematic acceptance but not for γ^* exchange. Each cross section result in the table carries an additional uncertainty of 11% from the luminosity that is not listed.

Table 2 lists the measured W/Z and $\mathrm{W}^+/\mathrm{W}^-$ cross section ratios, which are denoted $R_{\mathrm{W/Z}}$ and $R_{+/-}$, respectively. The measured cross section and ratio values are all in agreement with the predictions.

Summaries of the measurements are given in Figures 1, 2, 3, and 4, illustrating the consistency of the measurements in the electron and muon channels, as

[1] As of the publication date of this article the luminosity uncertainty has been reduced to 4%.

[2] Since the LHC Lumi Days workshop, this analysis on 36 pb^{-1} has been completed [2].

Table 1: Summary of the production cross section times branching ratio measurements and their theoretical predictions

Channel		$\sigma \times \mathcal{B}$ (nb)	NNLO (nb)
W	$e\nu$	$10.04 \pm 0.10(\text{stat}) \pm 0.52(\text{syst})$	10.44 ± 0.52
	$\mu\nu$	$9.92 \pm 0.09(\text{stat}) \pm 0.31(\text{syst})$	
	$\ell\nu$	$9.95 \pm 0.07(\text{stat}) \pm 0.28(\text{syst})$	
W^+	$e^+\nu$	$5.93 \pm 0.07(\text{stat}) \pm 0.36(\text{syst})$	6.15 ± 0.29
	$\mu^+\nu$	$5.84 \pm 0.07(\text{stat}) \pm 0.18(\text{syst})$	
	$\ell^+\nu$	$5.86 \pm 0.06(\text{stat}) \pm 0.17(\text{syst})$	
W^-	$e^-\nu$	$4.14 \pm 0.06(\text{stat}) \pm 0.25(\text{syst})$	4.29 ± 0.23
	$\mu^-\nu$	$4.08 \pm 0.06(\text{stat}) \pm 0.15(\text{syst})$	
	$\ell^-\nu$	$4.09 \pm 0.05(\text{stat}) \pm 0.14(\text{syst})$	
Z	ee	$0.960 \pm 0.037(\text{stat}) \pm 0.059(\text{syst})$	0.972 ± 0.042
	$\mu\mu$	$0.924 \pm 0.031(\text{stat}) \pm 0.022(\text{syst})$	
	$\ell\ell$	$0.931 \pm 0.026(\text{stat}) \pm 0.023(\text{syst})$	

Table 2: Summary of the cross section ratio measurements and their theoretical predictions

Channel		$\sigma \times \mathcal{B}$ (nb)	NNLO (nb)
$R_{\text{W/Z}}$	e	$10.47 \pm 0.42(\text{stat}) \pm 0.47(\text{syst})$	10.74 ± 0.04
	μ	$10.74 \pm 0.37(\text{stat}) \pm 0.33(\text{syst})$	
	ℓ	$10.64 \pm 0.28(\text{stat}) \pm 0.29(\text{syst})$	
$R_{+/-}$	e	$1.434 \pm 0.028(\text{stat}) \pm 0.082(\text{syst})$	1.43 ± 0.04
	μ	$1.433 \pm 0.026(\text{stat}) \pm 0.054(\text{syst})$	
	ℓ	$1.433 \pm 0.020(\text{stat}) \pm 0.050(\text{syst})$	

well as the confirmation of theoretical predictions computed at the NNLO in QCD with state-of-the-art PDF sets. For each reported measurement, the statistical error is represented in black and the total experimental uncertainty, obtained by adding in quadrature the statistical and systematic uncertainties, in dark blue. For the cross section measurements, the luminosity uncertainty is added linearly to the experimental uncertainty, and is represented in green. The dark-yellow vertical line represents the theoretical prediction, and the light-yellow vertical band is the theoretical uncertainty, interpreted as a 68% confidence interval.

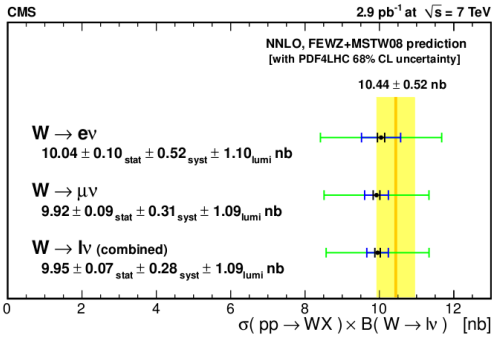

Figure 1: Summary of the W boson production cross section times branching ratio measurements

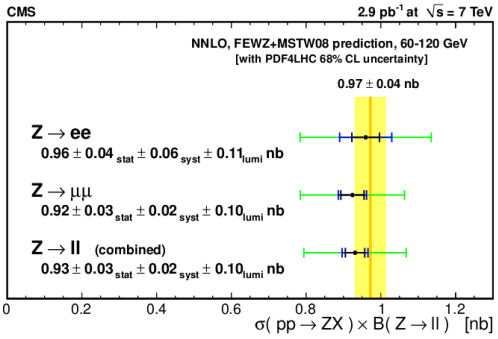

Figure 2: Summary of the Z boson production cross section times branching ratio measurements

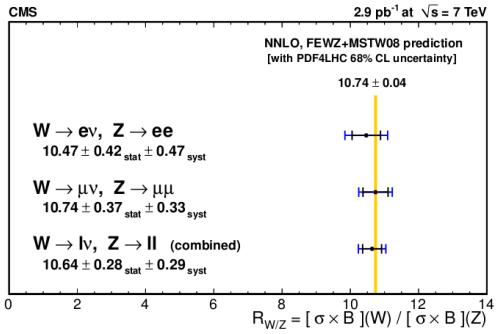

Figure 3: Summary of the $R_{\text{W/Z}}$ cross section ratio measurements

PROJECTED PRECISIONS FOR A 36 PB^{-1} ANALYSIS

The overall uncertainty on the W/Z cross section results will be substantially reduced when measurements are made on the full 36 pb^{-1} dataset, due to larger event yields, more detailed understanding, and improvements in analysis techniques. Table 3 compares the statistical and (non-luminosity) systematic errors reported for the 2.9 pb^{-1} analysis to conservative predictions for the 36 pb^{-1} analysis in the electron and muon channels. The reduction suggests using elec-

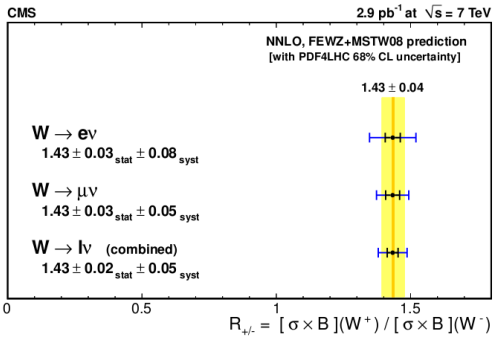

Figure 4: Summary of the $R_{+/-}$ cross section ratio measurements

troweak boson decays as a luminometer will be competitive with VdM scans. This will further be explored in the following section.

Table 3: Production Cross Section Uncertainties and their Projections for the Electron and Muon Channels

$\Delta\sigma/\sigma$ (%)	$W \to e\nu$ 2.9 pb^{-1}	$W \to e\nu$ 36 pb^{-1}	$Z \to ee$ 2.9pb^{-1}	$Z \to ee$ 36 pb^{-1}
Stat	0.6	0.2	3.8	1.1
Syst	5.1	4.0	6.2	4.2
Total	5.1	4.0	7.3	4.3
	$W \to \mu\nu$ 2.9 pb^{-1}	$W \to \mu\nu$ 36 pb^{-1}	$Z \to \mu\mu$ 2.9pb^{-1}	$Z \to \mu\mu$ 36 pb^{-1}
Stat	0.7	0.2	3.1	0.9
Syst	3.1	2.2	2.3	2.1
Total	3.4	2.2	3.9	2.3

COMPARISONS OF W/Z VS. VAN DER MEER SCAN CALIBRATION

Luminosity at CMS is calibrated via Van der Meer scans [5], where horizontal and vertical beam separation scans are performed to measure the beam sizes. The beam sizes along with the other known machine parameters determine the luminosity. The consistency of the results obtained for the cross section measurements in addition to the copious signal yields and precisely known cross sections, suggest the possibility of inverting the cross section measurements to instead use the signal yield to calibrate the luminosity. This can be demonstrated with Z bosons. Table 4 compares the current (with 2.9 pb^{-1}) and projected (36 pb^{-1}) systematic uncertainties of a luminosity calibration using either Z bosons (combined electron and muon channels) or VdM scans.

Table 4: Luminosity Calibration Systematic Uncertainties and their Projections

	VdM Scan 2.9 pb^{-1}	VdM Scan 36 pb^{-1}	$Z \to \ell\ell$ 2.9pb^{-1}	$Z \to \ell\ell$ 36 pb^{-1}
$\Delta\mathcal{L}/\mathcal{L}$ (%)	11	4	6	4-5

The dominant systematic uncertainty on the VdM scans is the beam current measurement. On the other hand, the dominant systematic uncertainty on the Z based calibration comes from the PDF [7]. Table 4 shows that calibrating the luminosity using Z bosons is competitive with the separation scans. It indicates a Z decay based luminosity calibration with a precision of 4-5% should be possible on a daily basis if the LHC provides CMS with approximately 30-40 pb^{-1} of collisions per day. Still, continued improvement of the VdM scans (in particular reducing the uncertainty on the beam current measurement) is advocated since scans can be used to constrain the proton PDF.

Z YIELD STABILITY FOR LUMINOSITY CALIBRATION

Although VdM scans currently provide the primary method to calibrate the luminosity, W/Z bosons could be used as a cross check in the coming periods of data taking. The signal yield must be continuously validated to use these decays for calibration. Irregularities in the signal yield can be uncovered using a Kolmogrov-Smirnov omnibus test [6]. These tests yield the significance or probability value of an observed or claimed deviation in a given frequency distribution from the expected distribution. In Kolmogrov-Smirnov tests, the empirical distribution function (EDF) of the signal yield is plotted vs. an orthogonal variable. The orthogonal variable could be the separation scan based luminosity or the yield of another signal. The EDF is just the fractional yield of the signal. This frequency distribution is then compared to the expected distribution (e.g. the yield increasing linearly with luminosity). The maximal vertical difference between the observed and expected distributions determines a probability. Such a test is shown in Figure 5 where the EDF of the $Z \to ee$ yield observed at CMS is plotted vs. the scan based luminosity for 36 pb^{-1}. The data is shown in black, while the expected distribution is in green. The maximal difference between the 2 distributions is labeled on the plot as D_{stat} and the corresponding probability value is labelled as P_{KS}. The observed distribution agrees well with the expectation and the high probability value indicates a stable signal yield, consistent with the hypothesis that the yield increases linearly with luminosity.

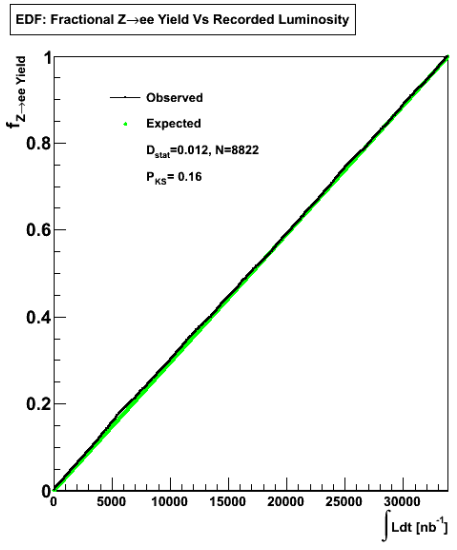

Figure 5: The $Z \to ee$ EDF vs. scan based luminosity

Other useful checks include plotting the signal yield vs. blocks of fixed integrated luminosity. One can then verify that this distribution is flat, having its points

agreeing within errors. Such a plot is shown in Figure 6, where the $Z \to ee$ yield observed at CMS is plotted in 2.4 pb^{-1} luminosity blocks with about 4% relative statistical error per point. The data is shown in black while the corresponding statistical error band is plotted in yellow. The distribution is flat and the yield was stable during data taking.

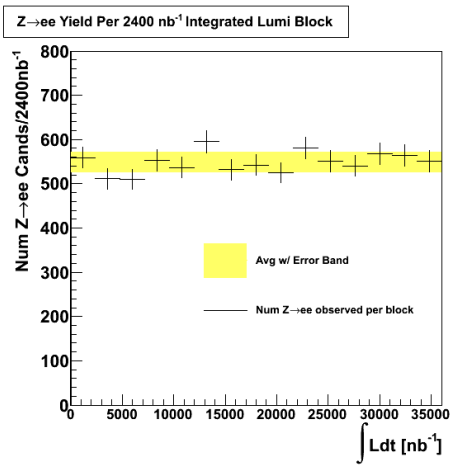

Figure 6: The $Z \to ee$ yield vs. blocks of fixed integrated luminosity

CONCLUSIONS

CMS has performed measurements of inclusive W and Z production cross sections in pp collisions at $\sqrt{s} = 7$ TeV using 2.9 ± 0.3 pb^{-1} of data recorded by the CMS detector at the LHC [1]. The W/Z and W^+/W^- production cross section ratios were also reported. Measurements were performed for both electron and muon decay channels, and were then combined. The measurements are internally consistent and agree well with the theoretical predictions. Conservative systematic uncertainty projections for an upcoming 36 pb^{-1} measurement [2] were provided [3] and the feasibility of using W/Z boson decays alongside the VdM scans to calibrate the luminosity has been examined. Such a calibration is possible for 2011 high luminosity data taking, and usage of W/Z bosons as a standard candle for luminosity could happen as early as this year.

REFERENCES

[1] The CMS Collaboration, "Measurements of Inclusive W/Z Cross Section in pp Collisions at s = 7 TeV", 10.1007/JHEP01(2011)080, http://www.springerlink.com/content/80884781g5708422/

[2] The CMS Collaboration, "Measurement of the W and Z inclusive production cross sections at sqrts=7 TeV with the CMS experiment at the LHC", CMS CMS-PAS-EWK-10-005, 2010, http://cdsweb.cern.ch/record/1337017?ln=en

[3] K. Melnikov and F. Petriello, "Electroweak gauge boson production at hadron colliders through $\mathcal{O}(\alpha_S^2)$", Phys. Rev. D74 (2006) 114017, arXiv:hep-ph/0609070. doi:10.1103/PhysRevD.74.114017.

[4] K. Melnikov and F. Petriello, "The W boson production cross section at the LHC through $\mathcal{O}(\alpha_S^2)$", Phys. Rev. Lett. 96 (2006) 231803, arXiv:hep-ph/0603182. doi:10.1103/PhysRevLett.96.231803.

[5] Van Der Meer, "Calibration of the effective beam height in the ISR", ISR-PO/68-31, KEK68-64

[6] Eadie et al, "Statistical Methods in Experimental Physics", Amsterdam: North-Holland, pp. 269271, ISBN 0444101

[7] Adam et al, "Theoretical Uncertainties in Electroweak Boson Production Cross Sections at 7, 10, and 14 TeV at the LHC" , JHEP 11 (2010) 074, arXiv:1006.3766

[3] Errors reported in [2] are even less: 2.1% for Z production.

CMS Forward Detectors for Luminosity Measurements

S. Schnetzer, Rutgers University, Piscataway, NJ 08854, USA
on behalf of the PLT and FSC CMS groups

Abstract

We describe two CMS forward detector systems that will be used for luminosity measurements. One is the Pixel Luminosity Telescopes (PLT) a dedicated luminosity monitor based on diamond pixel sensors. This device will provide a measure of the relative luminosity in CMS to a statistical and systematic precision of the order of 1%. The other is the Forward Shower Counter (FSC) system of very far forward scintillators. This system could play an essential role in allowing the two-photon process $pp \to pp\mu\mu$ to be used as an absolute luminosity measure by allowing the fraction of events with proton dissociation to be determined.

INTRODUCTION

Two forward detector systems that will contribute to the measurement of luminosity in CMS are the Pixel Luminosity Telescopes (PLT) [1] and the Forward Shower Counters (FSC) [2]. The PLT is a dedicated luminosity monitor based on diamond pixel sensors. It is designed to measure the relative luminosity on a bunch-by-bunch basis to a precision of the order of 1% and to be stable to this precision over the full lifetime of CMS. The FSC is a set of very forward scintillators sensitive to showers produced by high rapidity particles that interact in the beam pipe. It is designed to study forward physics and can be used to tag small angle scattering events in which one or both of the protons undergo dissociation. Discriminating these events will be important for determining the fraction of dissociative events in the two-photon events $pp \to pp\gamma^*\gamma^* \to pp\mu\mu$ that have been proposed [3] for determining the absolute luminosity to high precision.

PLT

The PLT consists of arrays of eight small-angle telescopes, shown in Fig. 1, located on each end of CMS at a distance of approximately 1.75 m from the interaction point and about 5 cm from the beam line corresponding to $|\eta| \approx 4.2$. Each telescope is 7.5 cm long and consists of three equally-spaced planes of mono-crystalline diamond pixel sensors. The pixel sensors have an active area of 4 mm $\times$ 4 mm and are bump-bonded to the CMS PSI46 pixel readout chip [4]. The luminosity measurement consists of counting the number of telescopes with 3-fold coincidences in each bunch crossing using a fast, 40 MHz, output of the PSI46V readout chip. In addition, the addresses and pulse heights of those pixels over threshold will also be readout but at a lower rate of 1 to 10 kHz. As described below, this full pixel information is important in keeping systematics errors at or below the 1% level.

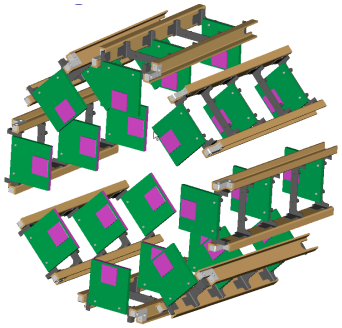

Figure 1: Array of PLT telescopes.

Statistical Precision

Pythia 6.2 was used to simulate particle hits in the PLT. At a luminosity of 10^{34} cm^{-2}s^{-1}, there will be approximately 2 coincidences per bunch crossing in the entire PLT corresponding to a total rate of approximately 80 MHz and a bunch-by-bunch rate of $\approx$ 30 kHz for each of the 2808 filled bunch crossing in an LHC orbit. This is sufficient to yield a statistical precision of 1% on the bunch-by–bunch luminosity in less than a second.

A full pixel readout rate of 1 kHz, gives $\approx$ 2 kHz of tracks recorded in the PLT yielding a 1% statistical precision on the bunch integrated luminosity in 5 s and on the bunch-by-bunch luminosity in four hours.

Systematic Errors

In order to take full advantage of this statistical precision, the systematic errors must be controlled to this precision as well. The main contributions to systematic errors arise from accidentals, track overlaps and the dependence of the acceptance on the position of the interaction point. Particles originating from interactions in material can cause accidental hits in the telescope planes giving a fake 3-fold coincidence rate leading to an overestimate of the luminosity. Fig. 2 shows the fraction of 3-fold coincidences due to accidentals as a function of the number of interactions per bunch crossing. At twenty interactions per bunch crossing, the accidental fraction is about 4%. Two particles passing through a telescope in a single bunch crossing will give only one 3-fold coincidence leading to an underestimate of the luminosity. Fig. 3 shows the fraction of 3-fold coincidences in which two particles overlap in a single telescope. At twenty interactions per bunch crossing, the overlap fraction is about 8%. Both of these effects can be corrected to

a few per cent of themselves by using the track information from the full pixel readout.

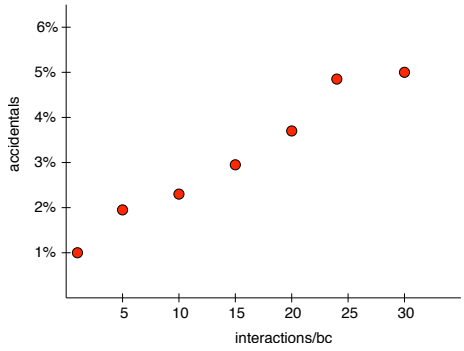

Figure 2: Percentage of accidental 3-fold coincidences as a function of the number of interactions per bunch crossing.

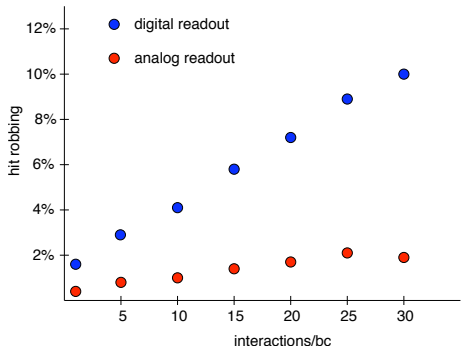

Figure 3: Percentage of 3-fold coincidences with track overlap as a function of the number of interactions per bunch crossing. Blue points are with the whole 4 mm $\times$ 4 mm sensor as a single active area. Red points are with the active area segmented into 300 μm-wide columns.

The solid angle acceptance of each PLT telescope is determined by the most downstream plane that is slightly smaller in active area than the other two. This makes the acceptance insensitive to radial drifts of the interaction point. As shown in Figs. 4 and 5, the acceptance is flat to 1% for a radial displacement of up to 1 cm if the radial displacement is directly toward a telescope and up to 4 mm if the radial displacement is directly between two telescopes. In the longitudinal direction, the acceptance is flat to 1% for displacements up to $\pm$ 30 cm. These displacements are well within the expected excursions of the interaction point.

Long Term Stability

In order for the luminosity measurement to be consistent to 1% throughout separated running periods, the PLT must have long term stability. There are three aspects to the PLT stablity. First, the PLT must be insensitive to changes in CMS acceptance and trigger. It has, therefore, been designed to be an independent system with its own data acquisition and trigger. Second, since the PLT must be removed for access to the CMS pixel detectors, its repositioning accuracy must be such to keep resulting changes in acceptance less than 1%. This is achieved with a cassette and carriage system that allows for precise surveying of the telescope positions and assures repositioning accuracy. Third, the efficiency of the PLT sensors must be known to better than 1% throughout the entire lifetime of CMS. This is achieved in two ways. Use of mono crystalline diamond sensors assures that the signal distribution, Fig. 6, will be well above the 3,000 electrons pixel threshold setting. The pulse height of the diamond sensor will decrease with irradiation, however, the separation of signal from threshold will be maintained up to a fluence of greater than 1.5 $\times 10^{15}$ 24 GeV protons per cm^2, as shown in Fig. 7, corresponding to the full LHC lifetime of 500 fb^{-1} of integrated luminosity. In addition, the information from the full pixel readout will allow continual monitoring of the efficiency of each sensor plane.

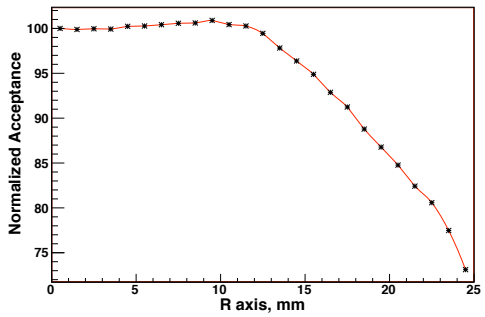

Figure 4: Percent acceptance as function of interaction point radial displacement directly toward a telescope.

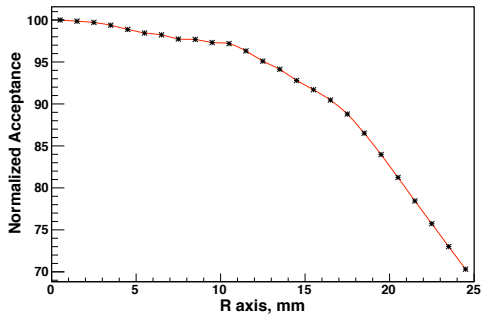

Figure 5: Percent acceptance as function of interaction point radial displacement directly between two telescopes.

FSC

The FSC consists of pairs of 25 cm $\times$ 25 cm scintillators surrounding the beam pipe at distances of 59 m and 85 m and four scintillators at 114 m on either side of the interaction point covering the rapidity range, $6 < |\eta| < 8$. It will detect showers produced by very forward particle interacting in the beam pipe.

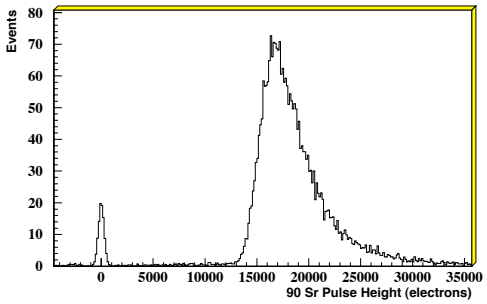

Figure 6: Pulse height distribution in electrons of a monocrystalline diamond sensor for traversing ^{90}Sr β particles.

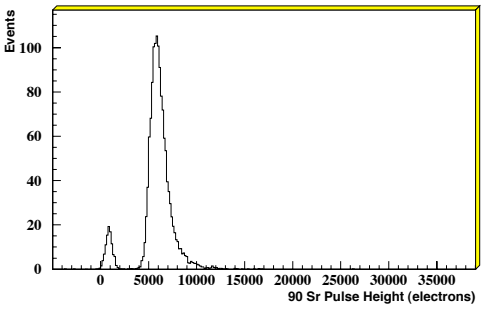

Figure 7: Pulse height distribution in electrons of a monocrystalline diamond sensor for traversing ^{90}Sr β particles irradiated to 1.5 $\times 10^{15}$ 24 GeV protons per cm^2.

Two Photon Process

The two photon process shown in Fig. 8 where X is a lepton pair is a purely electromagnetic process and can, therefor, be calculated to high precision. It has been proposed as a way of obtaining a high precision measure of the absolute luminosity. This method requires: triggering on the low mass lepton pair, identifying events in the presence of pile up and, since the scattered protons are not detected, distinguishing events without proton Coulomb dissociation from those where one or both protons dissociate.

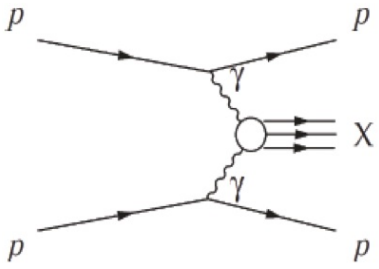

Figure 8: Two photon process.

Event Selection

The two photon events are distinguished by a low mass lepton pair. The trigger will be limited to low mass muon pairs due to the difficulty of triggering on low mass electron pairs. Events without pile up will be rare and it will, therefore, be necessary to identify the two photon events in the presence of pile up. In order to reduce background, events will be selected for which there are no other tracks associated with the di-muon vertex. The only remaining handle on background rejection is the kinematics of the muon pair. These will be back-to-back in the transverse plane and will have a small total transverse momentum. Fig. 9 shows the difference between π and the azimuthal angle between the muons, $\left|\pi - |\Delta\phi_{\mu\mu}|\right|$ while Fig. 10 shows the transverse momentum of the muon pair, $p_T^{\mu\mu}$ where the distributions are from a generator level LPAIR simulation [5] with no detector smearing. In addition to the non-dissociative events of interest, the distributions for events with single and double proton dissociation are also shown. Since these type of events are not as precisely calculated as the non-dissociative events and since they contribute approximately 30% and 10%, respectively, to the event sample, they will need to be corrected for.

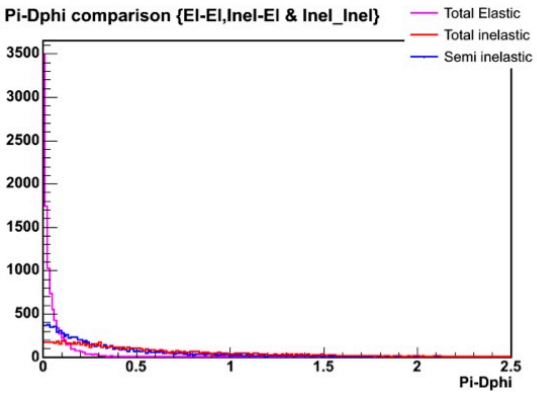

Figure 9: Difference between π and the azimuthal angle between the two muons, $\left|\pi - |\Delta\phi_{\mu\mu}|\right|$, in $pp \to pp\mu\mu$ events. Curves shown are for events without proton Coulomb dissociation (magenta), single proton dissociation (blue) and double dissociation (red) and were generated with LPAIR.

Rejection of Events with Proton Coulomb Dissociation

Although tight cuts on the kinematical distributions in Figs. 9 and 10 could be used to reduce the non-dissociative backgrounds, the efficiency and rejection factor of the cuts must be known very precisely and the simulation is not reliable to the level needed. Instead, single, double and non-dissociative events can be tagged based on whether there is activity in the FSC on one or both detector sides. The relative amounts and the kinematical distributions of the three types of events can then be experimentally determined and used as templates to determine the fraction of single and double dissociation events that remain after the cuts.

Using the activity in the FSC to tag the three types of events requires that the events be free of pile up. Events without pile up can be selected by requiring that there be no

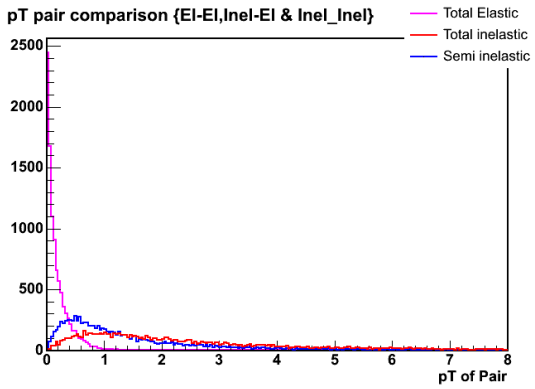

Figure 10: Transverse momentum of the the muon pair, $p_T^{\mu\mu}$, in $pp \rightarrow pp\mu\mu$ events. Curves shown are for events without proton Coulomb dissociation (magenta), single proton dissociation (blue) and double dissociation (red) and were generated with LPAIR.

particle activity except for the the two muons in the CMS detector excluding the FSC. Since events without pile up will be rare if the average number of interactions per bunch crossing is large, this measurement will need to be made during early running while the luminosity is not too large.

The effective luminosity, $L_{\rm eff}$, of single interaction (no pile up) bunch crossings as a function of the instantaneous luminosity is shown in Fig. 11. For instantaneous luminosities between 10^{32} and 10^{33} cm^{-2}s^{-1}, the integrated effective luminosity is 1 to 4 pb^{-1} per 10 hour store. Assuming, 200 hours of running at instantaneous luminosities between 10^{32} and 10^{33} cm^{-2}s^{-1} and using the LPAIR estimated $pp \rightarrow pp\mu\mu$ cross section of 12 pb, there will be about 2,000 two photon events.

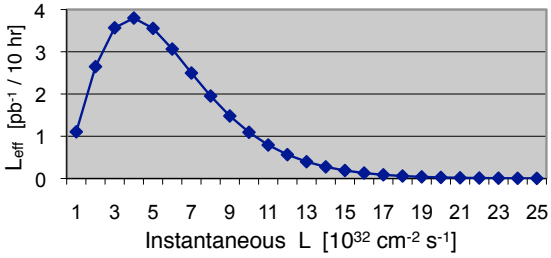

Figure 11: Effective luminosity, $L_{\rm eff}$ of single interaction bunch crossings in units of pb^{-1} per 10 hours as a function of the instantaneous luminosity. [6]

SUMMARY

The PLT will achieve a 1% resolution on the relative bunch-by-bunch luminosity in approximately 1 s. Its hybrid readout that includes a full readout of pixel hit information will allow the systematic errors to be controlled to the 1% level. It is designed to have long term stability through precision repositioning and through control of efficiencies by the use of mono-crystalline diamond sensors. The FSC by allowing for corrections due to proton dissociative events will be key for obtaining an absolute luminosity calibration from the two-photon process, $pp \rightarrow pp\mu\mu$. In order, to determine the $\mu\mu$ kinematical distributions for single and double dissociative events, events without pile up will need to be selected. Estimates indicate that there may be approximately 2,000 $pp \rightarrow pp\mu\mu$ no pile up events in the 2011-2012 LHC run.

ACKNOWLEDGMENTS

I am grateful to members of the PLT and FSC CMS groups and in particular to Mike Albrow for teaching me about the FSC and generously sharing his ideas and results.

REFERENCES

[1] R. Hall-Wilton et al, "Results from a Beam Test of a Prototype PLT Diamond Pixel Telescope", Nucl. Instrum. Meth. A636: S130-S136 (2011).

[2] A. Bell et. al (The FSC Collaboration), "Physics and Beam Monitoring with Forward Shower Counters (FSC) in CMS", CERN-CMS-NOTE-2010-015.

[3] V. Khoze, these proceedings.

[4] H.Chr. Kastli et al., Design and performance of the CMS pixel detector readout chip, Nucl. Instrum. Meth. A 565, 188 (2006).

[5] J. Vermaseren, Nucl. Phys. B229, 347 (1983).

[6] Mike Albrow, private communication.

Bunch Current Normalisation Analysis Results

T. Pauly*, CERN, Geneva, Switzerland

Abstract

This paper presents the results of the LHC Bunch Current Normalisation Group, on the absolute normalisation of the bunch populations during LHC fills in April/May 2010 dedicated to Van der Meer scans, as well as an estimation of the systematic uncertainties for Van der Meer scans in October 2010. The analysis methods are discussed, which are based on data from the LHC beam instrumentation and LHC detectors, as well as the estimation of the systematic uncertainties.

INTRODUCTION

During 2010, the LHC performed a series of Van der Meer scans in April, May, and October, for its four experiments ALICE, ATLAS, CMS, and LHCb, in order to obtain an absolute measurement of the luminosity via beam parameters. An important ingredient for this measurement are the bunch population products $N_i^{(1)} \cdot N_i^{(2)}$, where the bunch populations $N_i^{(j)}$ denote the number of protons of bunch i of beam j, where $j = 1, 2$. This note discusses the procedures and results of the measurement of the absolute bunch populations for the series of fills in 2010 dedicated to Van der Meer scans.

The first series of Van der Meer scans took place in April and May 2010, during LHC fills 1058, 1059, 1089, and 1090, with typically 2 or 3 bunches per beam with total beam populations of around 1 to 4×10^{10} protons, colliding head-on without crossing angle. More information is shown in tables 1 and 2. A preliminary analysis provided first beam population results that were used for ICHEP 2010. A more detailed and rigorous analysis followed, which is subject of this paper and described in more detail in [1].

A second series of Van der Meer scans followed in October 2010, in fills 1386 for ATLAS and partially for CMS, and in fill 1422 for LHCb, CMS, and ALICE. A 19-bunch scheme was used with total beam populations of about 1.5×10^{12} protons. The analysis of this data is still in progress; in this paper, we only make an estimate of the expected systematic uncertainties.

* on behalf of the LHC Bunch Current Normalisation Working Group: G. Anders, N. Bacchetta, V. Balagura, C. Barschel, D. Belohrad, D. Berge, H. Burkhardt, S.I. Cooper, M. Ferro-Luzzi, G. Franzoni, C. Gabaldon, M. Gagliardi, J.J. Gras, V. Halyo, B. Heinemann, P. Hopchev, A. Hunt, W. Kozanecki, S. Kwan, M. Ludwig, D. Marlow, P. Odier, S. Pagan Griso, J. Panman, T. Pauly, S. Thoulet, S. White, J.C. Yun , M. Zanetti

ANALYSIS

The analysis of the bunch population normalisation is based on several independent systems: the DC current transformers (DCCT), the fast beam current transformers (FBCT), the ATLAS timing pick-ups (BPTX), and the LHC detectors. The DCCT measure the total current of the circulating beam (bunched and unbunched). A calibration winding allows an absolute calibration via the injection of a known generated current. The FBCT are used for per-bunch measurements of the beam populations; they are only sensitive to bunched beam and measure the current over a threshold of about 5×10^8 protons. The BPTX are electro-static button pick-ups that provide as by-product a per-bunch relative intensity, which is used to cross-check the results from the FBCT. The LHC detectors are used for detailed studies on ghost charge and satellite bunch contributions. In the context of this paper, we define *ghost charge* as the summed charge for all those 25 ns slots which are not visible by the FBCT, i.e. unbunched or below the FBCT threshold. As *satellite bunches*, we denote captured charge in RF buckets with a few tens of nanoseconds around the nominal buckets.

The total beam population N_{tot}^{DCCT} is derived from the DCCT readings S_{DCCT} by applying the DCCT calibration scale factor α and correcting for a non-zero baseline offset N_0^{DCCT}, which is estimated from DCCT data:

$$N_{tot}^{DCCT} = \alpha \cdot S_{DCCT} - N_0^{DCCT} \quad (1)$$

The per-bunch populations for bunch i are then obtained from the FBCT readings S_i^{FBCT} in the following way: the ghost charge contribution N_{ghost}, which is included in N_{tot}^{DCCT} but not in the per-bunch population, is removed from the total bunch population, which is subsequently split in proportion to the per-bunch fractions from the FBCT:

$$N_i^{FBCT} = \left(N_{tot}^{DCCT} - N_{ghost}\right) \cdot \frac{S_i^{FBCT}}{\sum\limits_i S_i^{FBCT}} \quad (2)$$

In the following, we discuss the procedures for determining the DCCT baseline corrections and its uncertainties, the uncertainty of the DCCT scaling factor α, the uncertainty on the per-bunch fractions, and the ghost-charge population. Note, that if not stated otherwise, all systematic uncertainties are taken as uncertainty bands; a quantity with a systematic uncertainty of Δ is conservatively assumed to follow a flat distribution in the interval $[-\Delta, +\Delta]$ around the central value.

Table 1: Summary of the April-May 2010 LHC luminosity calibration experiments with the Van der Meer method.

Van der Meer scans, April-May 2010							
LHC fill	Approx. start date	time	Approx. stop date	time	IP scanned	Bunch pattern	Approx. bunch population
1058	April 24	11:00	April 24	12:30	IP5	3-bunch	$1.0 \cdot 10^{10} p$
1059	April 26	02:30	April 26	06:00	IP8, IP1	2-bunch	$1.0 \cdot 10^{10} p$
1089	May 8	23:00	May 9	03:30	IP5, IP1	2-bunch	$2.0 \cdot 10^{10} p$
1090	May 10	05:00	May 10	07:00	IP2	2-bunch	$2.0 \cdot 10^{10} p$

Table 2: List of bunch crossings in the four insertion regions for the 3-bunch and 2-bunch patterns. In each line the RF bucket of the encountered Beam2 bunch is given for each IP and for the corresponding bucket of the Beam1 bunch. The numbers in brackets indicate a longitudinally displaced crossing, at 11.23 m (anticlockwise) from the actual IP.

Fill 1058 3-bunch pattern					Fills 1059, 1089 and 1090 2-bunch pattern				
Beam1 RF bucket	Colliding Beam2 RF bucket IP1	IP2	IP5	IP8	Beam1 RF bucket	Colliding Beam2 RF bucket IP1	IP2	IP5	IP8
1	1	8911	1	-	1	1	8911	1	-
8941	(8911)	17851	(8911)	1	17851	-	-	-	8911
17851	17851	-	17851	8911					

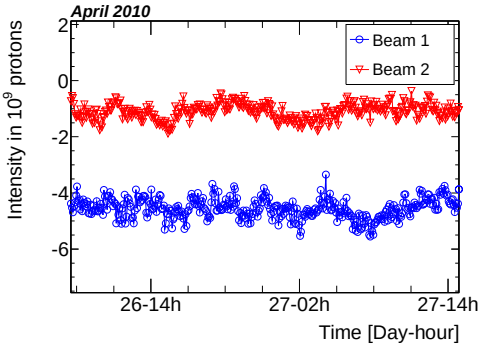

Figure 1: A period without beam (April 26/27, 2010). The DCCT signal is shown versus time for Beam1 (blue circles) and Beam2 (red triangles), with 300 s averaging time.

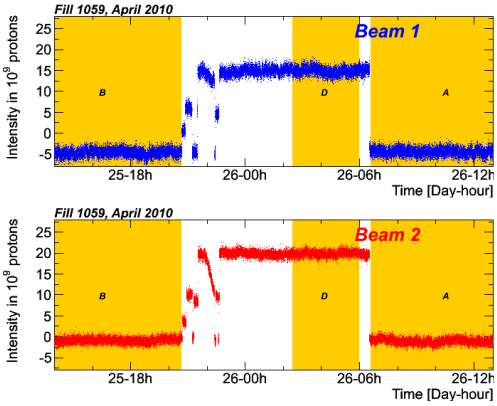

Figure 2: DCCT data for the Van der Meer scan during fill 1059. The periods *before*, *during*, and *after* the scan used to determine the beam populations are indicated by the shaded bands B, D, and A, respectively.

DCCT Baseline Drifts

DCCT baseline drifts have been studied in periods without beam. The white noise of the raw data is about 10^9 protons RMS. It is efficiently suppressed by averaging over time bins of 300 seconds, an appropriate choice large enough to suppress white noise and small compared to the length of a Van der Meer scan. The time-averaged data are shown in Figure 1. Significant baseline drifts are visible. Although their origin is yet unknown, possible causes could be temperature drifts, electromagnetic pick-up in cables and electronics, or mechanical vibrations in the transformer assembly. For a given Van der Meer scan, the DCCT baseline offset N_0^{DCCT} is reconstructed by interpolating between the average baseline offsets determined in a period before and a period after the fill. Figure 2 shows, for fill 1059, the periods before (B), during (D), and after (A) the fill. The DCCT value during these periods is simply the average of the measurements. The systematic uncertainty from the baseline drifts is taken as the maximum of the peak-to-peak variation of the period B and A; numerically $\pm 0.8 \times 10^9$ protons. In the preliminary analysis, a conservative estimate of $\pm 2 \times 10^9$ protons was used.

Table 3: DCCT total population measurements for all April-May and October 2010 fills with Van der Meer scans. Values marked with $*$ are still under study and not yet finalised.

Fill nr.	LHC ring j	Detailed analysis LHC intensity $N_{\mathrm{tot},j} \cdot 10^{-9}$ baseline-corrected	Preliminary analysis LHC intensity $N_{\mathrm{tot},j} \cdot 10^{-9}$ baseline-corrected
1058	1	32.3 ± 0.8	31.8 ± 2.0
	2	30.3 ± 0.8	28.4 ± 2.0
1059	1	19.2 ± 0.8	18.9 ± 2.0
	2	20.7 ± 0.8	20.6 ± 2.0
1089	1	38.4 ± 0.8	38.1 ± 2.0
	2	43.5 ± 0.8	43.7 ± 2.0
1090	1	37.4 ± 0.8	37.4 ± 2.0
	2	40.6 ± 0.8	40.0 ± 2.0
1386	1	$1737.1 \pm 0.8^*$	N/A
	2	$1710.8 \pm 0.8^*$	N/A
1422	1	$1195.6 \pm 0.8^*$	N/A
	2	$1191.3 \pm 0.8^*$	N/A

Correlations between the DCCT baseline drifts of the two beams have been studied using long empty periods in addition to the Van der Meer scan fills, but no correlations have been found. For this reason, the baseline uncertainties of the two beams can be added quadratically.

Scaling Factor Uncertainty

The uncertainty of the absolute scale factor α is dominated by the long-term time stability, which is estimated as $\pm 2\,\%$ from the evolution between calibration periods and Van der Meer scan periods, based on 5 precise calibration points during technical stops. Other possible uncertainties, such as misbehaviour of the DCCT linked to the LHC filling pattern, inaccuracy of the commercial current generator used for calibration, and non-linearities between the working point and the calibration point, have been estimated to be less than $0.1\,\%$ each. It is conservatively assumed that the scale uncertainty is correlated between the two beams in a fill, as well as correlated between two fills.

Per-bunch Uncertainty

In order to study systematic effects of the per-bunch fractions $S_i^{FBCT} / \sum_i S_i^{FBCT}$, cross-checks with measurements from the independent ATLAS BPTX systems have been performed. Figure 3 shows for fill 1295, a fill with a larger spread of bunch intensities, and for each bunch, the proton population measured by the FBCT and the BPTX (uncalibrated). There is a linear correlation between the two systems of better than 1 %, although a non-zero offset is present which is not yet understood. In the presence of this offset, deviations between the two systems of up to

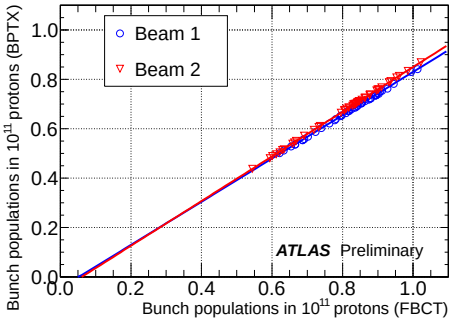

Figure 3: ATLAS BPTX signal versus FBCT signal for LHC fill 1295 (August 2010). Each data point corresponds to a different bunch. The lines are the results of a straight line fit

3 % have been observed for the April/May scans, whereas for the October scans the deviations are fill-dependent and are 1.1 % for fill 1386 and 1.7 % for fill 1422. These uncertainties are taken as not correlated between the two beams, thus the quadratic sum is taken for the bunch population product.

Ghost Charge and Satellite Bunches

The ghost charge has been estimated using beam gas events recorded by LHCb. Small levels of ghost charge have been identified and corrected for, less than 1 % for the April/May scans and less than 0.5 % for the October scans.

Satellite bunches have been studied by ATLAS and CMS using displayed vertices, as well as timing information from the CMS endcap electromagnetic calorimeters. All methods show consistent results: negligible satellite contributions of less than 2 permil have been identified.

RESULTS

Table 4 lists the uncertainties and their treatment for the preliminary analysis (left) and the detailed analysis (right) for the bunch population product $P_{ij} = N_i^{(1)} \cdot N_j^{(2)}$, where i and j denote the bunch number. In the preliminary analysis, uncertainty bands were converted standard deviation by a factor of $1/\sqrt{3}$. As this corresponds to a confidence level of only 57.7 %, the conversion was changed for the detailed analysis, where the factor of 0.682 gives the preferred 68.2 % confidence level. For the DCCT baseline uncertainty, a conservative single beam uncertainty of $\pm 2 \times 10^9$ was chosen in the preliminary analysis; it was assumed to be fully correlated between the two beams, but uncorrelated between fills. In the more detailed analysis, the uncertainty was reduced to $\pm 0.8 \times 10^9$ and is assumed to be uncorrelated between the two beams and between fills. Note, that the baseline uncertainty is the largest uncertainty for the low-intensity beams used in April and May 2010, while it is negligible for the higher intensity beams used in October 2010.

Table 4: Summary of the treatment of uncertainties for the preliminary and detailed analyses.

Preliminary analysis		Detailed analysis	
$\frac{\sigma_{P_{ij}}^{\text{baseline}}}{P_{ij}}$	$= \frac{1}{\sqrt{3}}\left(\frac{\Delta N_{\text{tot},1}}{N_{\text{tot},1}} + \frac{\Delta N_{\text{tot},2}}{N_{\text{tot},2}}\right)$	$\frac{\sigma_{P_{ij}}^{\text{baseline}}}{P_{ij}}$	$= 0.682 \cdot \sqrt{\left(\frac{\Delta N_{\text{tot},1}}{N_{\text{tot},1}}\right)^2 + \left(\frac{\Delta N_{\text{tot},2}}{N_{\text{tot},2}}\right)^2}$
$\frac{\sigma_{P_{ij}}^{\text{scale}}}{P_{ij}}$	$= \frac{2}{\sqrt{3}}\frac{\Delta\alpha}{\alpha} = 2.3\%$	$\frac{\sigma_{P_{ij}}^{\text{scale}}}{P_{ij}}$	$= 0.682 \cdot 2 \cdot \frac{\Delta\alpha}{\alpha} = 2.7\%$
$\frac{\sigma_{P_{ij}}^{\text{FBCT}}}{P_{ij}}$	$= 0$	$\frac{\sigma_{P_{ij}}^{\text{FBCT}}}{P_{ij}}$	$= 0.682 \cdot \sqrt{\left(\frac{\Delta N_{i,1}}{N_{i,1}}\right)^2 + \left(\frac{\Delta N_{j,2}}{N_{j,2}}\right)^2} = 2.9\%$
$\sigma_{P_{ij}}$	$= \sigma_{P_{ij}}^{\text{baseline}} + \sigma_{P_{ij}}^{\text{scale}}$	$\sigma_{P_{ij}}$	$= \sqrt{(\sigma_{P_{ij}}^{\text{baseline}})^2 + (\sigma_{P_{ij}}^{\text{scale}})^2 + (\sigma_{P_{ij}}^{\text{FBCT}})^2}$

Table 5: Summary of the systematic uncertainties for the detailed analysis. The values for the preliminary analysis are shown in parenthesis. The uncertainties marked with * are not yet finalised and under study.

LHC Fill	1058	1059	1089	1090	1386	1422
Baseline drift	2.5 % (7.7 %)	3.9 % (11.7 %)	1.9 % (5.7 %)	2.0 % (6.0 %)	< 0.1 %	< 0.1 %
Scale factor	2.7 % (2.3 %)	2.7 % (2.3 %)	2.7 % (2.3 %)	2.7 % (2.3 %)	2.7 % (2.3 %)	2.7 % (2.3 %)
Per-bunch	2.9 % (0)	2.9 % (0)	2.9 % (0)	2.9 % (0)	1.1 %*	1.7 %*
Combined	4.4 % (10.0 %)	5.5 % (14.0 %)	4.4 % (8.0 %)	4.4 % (8.3 %)	2.9 %*	3.2 %*

The uncertainty on the absolute scale factor is 2 % and assumed to be fully correlated between fills and between the two beams, for both the preliminary analysis and the detailed one.

Per-bunch uncertainties were not considered in the preliminary analysis, while for the detailed analysis, they are taken to be 3 % for the April/May fills and 1.1-1.7 % for the October fills, without correlation between the two beams and between fills.

All uncertainty contributions were conservatively considered correlated in the preliminary analysis, while in the detailed analysis they are assumed to be uncorrelated.

In table 5 the numeric values of the systematic uncertainties are listed. The values are for the detailed analysis, the values of the preliminary analysis are shown in brackets.

The bunch population results for the April and May 2010 scans are shown in Table 6 for the detailed analysis, as well as the results on the bunch population products; the results of the preliminary analysis are shown in parenthesis.

SUMMARY

In this paper we outlined the detailed bunch current normalisation analysis performed on the Van der Meer scan fills in April, May, and October 2010. For the April and May scans, the central values were updated with respect to the preliminary analysis, and the systematic uncertainties were reduced considerably. The normalisation for the October 2010 Van der Meer scans is still work in progress; its systematic uncertainty is dominated by the absolute scale factor and the relative per-bunch population, while the baseline offset uncertainty is negligible.

REFERENCES

[1] G. Anders *et al.*, *"LHC Bunch Current Normalisation for the April-May 2010 Luminosity Calibration Measurements,"* CERN-ATS-Note-2011-004 PERF

Table 6: Summary of results from the detailed analysis for the bunch populations and bunch population products for the April and May 2010 Van der Meer scan fills. Here, the bunches are identified by their nominal RF bucket number b in bracket $N(b)$. The uncertainties are given for 68.2% confidence level. The results given in brackets are those of the preliminary analysis and are standard deviations (57.7% confidence level).

		Fill number			
		1058	1059	1089	1090
Populations $N \cdot 10^{-9}$					
Beam1	$N(1)$	9.56 ± 0.29 (9.42 ± 0.36)	8.98 ± 0.34 (8.85 ± 0.55)	18.99 ± 0.54 (19.01 ± 0.62)	19.91 ± 0.57 (20.00 ± 0.66)
	$N(8941)$	11.70 ± 0.35 (11.53 ± 0.44)	- -	- -	- -
	$N(17851)$	11.02 ± 0.33 (10.85 ± 0.41)	10.20 ± 0.38 (10.05 ± 0.62)	19.08 ± 0.54 (19.09 ± 0.62)	17.33 ± 0.50 (17.40 ± 0.57)
Beam2	$N(1)$	10.19 ± 0.31 (9.56 ± 0.40)	10.35 ± 0.37 (10.30 ± 0.59)	22.18 ± 0.61 (22.34 ± 0.64)	19.54 ± 0.55 (19.34 ± 0.60)
	$N(8911)$	10.66 ± 0.33 (10.00 ± 0.42)	10.35 ± 0.37 (10.30 ± 0.59)	21.20 ± 0.59 (21.36 ± 0.62)	20.88 ± 0.59 (20.66 ± 0.64)
	$N(17851)$	9.43 ± 0.29 (8.85 ± 0.37)	- -	- -	- -
Population products $P_{ij} \cdot 10^{-18} = N_{i,1} \cdot N_{j,2} \cdot 10^{-18}$					
IP1&5	$N(1) \cdot N(1)$	97.5 ± 4.6 (90.0 ± 9.0)	92.9 ± 5.2 (91.1 ± 12.8)	421.1 ± 18.5 (424.6 ± 33.8)	389.0 ± 17.3 (386.6 ± 32.0)
	$N(17851) \cdot N(17851)$	103.9 ± 4.9 (96.0 ± 9.6)	- -	- -	- -
IP2	$N(1) \cdot N(8911)$	101.9 ± 4.8 (94.2 ± 9.4)	92.9 ± 5.1 (91.1 ± 12.8)	402.7 ± 17.7 (406.0 ± 32.4)	415.8 ± 18.4 (413.2 ± 34.2)
	$N(8941) \cdot N(17851)$	110.4 ± 5.2 (101.9 ± 10.2)	- -	- -	- -
IP8	$N(8941) \cdot N(1)$	119.2 ± 5.6 (110.1 ± 11.0)	- -	- -	- -
	$N(17851) \cdot N(8911)$	117.5 ± 5.5 (108.5 ± 10.8)	105.6 ± 5.9 (103.5 ± 14.5)	404.5 ± 17.8 (407.9 ± 32.5)	361.9 ± 16.0 (359.6 ± 29.7)
Relative errors on population products $\sigma_{P_{ij}}/P_{ij}$					
		4.7% (10%)	5.6% (14%)	4.4% (8%)	4.4% (8.3%)

Analysis of the May 2010 van der Meer scan in ALICE

K. Oyama* for the ALICE Collaboration
University of Heidelberg, Philosophenweg 12, 69120 Heidelberg, Germany

Abstract

A reference trigger cross section has been measured by the ALICE experiment in p+p collisions at $\sqrt{s} = 7$ TeV at the LHC, using the van der Meer scan method to evaluate the convolution of the beam profiles. The description of the measurements and analysis is presented in this document.

INTRODUCTION

The measurement of the absolute value of the cross-section σ_{trig} of a reference trigger process allows the determination of an absolute scale normalization for other cross-section measurements in the experiment and enables the on-line calculation of the luminosity based on the measurement of the trigger process' rate R_{trig}, via the relation $R_{trig}(t) = L(t) \cdot \sigma_{trig}$.

In the ALICE experiment[1], such a reference cross-section has been measured using the van der Meer (vdM) scan method [2]. In this method, the rate of the reference process is measured as function of the beams separation, providing information on the spatial convolution of the two colliding beams. This information, combined with the knowledge of the beam intensities, allows to determine the absolute luminosity, and hence to obtain a measurement of the absolute value of the cross-section of the reference process.

Target Precision

In ultra-relativistic heavy-ion collision experiments particle production in nucleus-nucleus collisions is often compared with the extrapolation from elementary pp collisions via binary scaling. The nuclear modification factor $R_{AA}^{(X)}$ for a given process X is defined as the ratio between the process yield in AA collisions $N_{AA}^{(X)}/N_{evt}$ and the yield expected by scaling the pp cross-section $\sigma_{pp}^{(X)}$ by the average nuclear overlap function $\langle T_{AA} \rangle$, that quantifies the average nucleon-nucleon "luminosity" per nucleus-nucleus collision for the sample under consideration:

$$R_{AA}^{(X)} = \frac{N_{AA}^{(X)}/N_{evt}}{\langle T_{AA} \rangle \cdot \sigma_{pp}^{(X)}} \qquad (1)$$

For processes expected to scale like the number of binary nucleon-nucleon collisions (such as hard processes), deviation from unity in the nuclear modification factor allows to quantify the importance of nuclear effects such as parton energy loss in the medium formed in heavy ion collisions.

* oyama@physi.uni-heidelberg.de

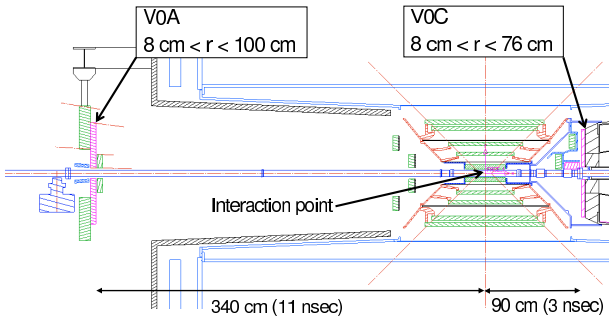

Figure 1: Locations of V0 detectors, V0-A and V0-C.

The desired precision for $R_{AA}^{(X)}$ studies is typically 10% or better. In order for the uncertainty on $\sigma_{pp}^{(X)}$ not to be dominant in the overall uncertainty, a precision of the order of 5% on absolute cross-sections in pp collisions, and hence on the vdM scan reference trigger process, is desired.

V0 TRIGGER SETUP

For the present study, the coincidence between the trigger signals from the two V0 scintillator arrays [1] has been chosen as the reference trigger process. The V0 layout is shown in Fig. 1. The detector consists of two arrays of scintillators placed at z =340 cm and 90 cm respectively for the A-side (V0-A, covering $2.8 < \eta < 5.1$) and C-side (V0-C, covering $-1.7 > \eta > -3.7$), with the scintillator tiles arranged in 2 (radial) $\times$ 16 (azimuthal) segments with individual photomultiplier-tube readout.

The V0 front-end electronics measures the pulse height and arrival time of the signals, with 32 channels of readout electronics each for the V0-A and V0-C arrays.

For each of the two arrays, pulse height thresholds are applied and discriminator outputs are fed into trigger logic circuits that combine the 32 channels into a logical OR. The individual thresholds are well separated from both the pedestal and the minimum ionization peak.

The two resulting trigger signals from V0-A and V0-C can then be combined in two ways: with an "OR" logic (VBOR) and with an "AND" logic (VBAND). To reduce the sensitivity to beam-gas and other machine-backgrounds, the VBAND logic was chosen for the present study. The VBAND logic requires at least one charged particle to be detected both on V0-A and V0-C. During the vdM scan the noise level of the VBAND trigger was negligibly small (below 0.1 Hz).

The photomultiplier tubes of the V0 detector are affected by after-pulsing: secondary pulses may follow the primary one up to 1 μs later. The effect of after-pulses is also

suppressed to a negligible level using the VBAND coincidence.

VAN DER MEER SCAN

During the scan, the luminosity is varied by changing the distance between the two beams in the horizontal (x) and vertical (y) directions ($x-y$ being the plane transverse to the beam axis). The trigger rate follows the luminosity, and the dependence on the beam displacement in $x-y$ reflects the shape of the convolution of the two beams, as discussed below.

Principle of Cross Section Determination

In this analysis, the trigger cross section ($\sigma_{\rm V0}$) of VBAND is measured. The luminosity depends on the transverse profiles ρ_1 and ρ_2 of the two colliding beams Beam-1 and Beam-2, and on the transverse displacement of the two beams (D_x, D_y):

$$L(D_x, D_y) = k_b f \iint \rho_1(x - D_x, y - Dy)\rho_2(x, y)dxdy \tag{2}$$

where k_b is the number of colliding bunches in the orbit, and f is the orbital frequency. The beam profiles are often approximated by gaussian shapes with standard deviations σ_{1x} and σ_{1y} for Beam-1 and σ_{2x} and σ_{2y} for Beam-2. With the above notation one obtains:

$$L(0,0) = \frac{k_b f N_1 N_2}{2\pi\sqrt{(\sigma_{1x}^2 + \sigma_{2x}^2)(\sigma_{1y}^2 + \sigma_{2y}^2)}} \tag{3}$$

where N_1 and N_2 are the average bunch intensities of the two colliding two beams.

During the vdM scan, one of either D_x or D_y was scanned, while beams were kept colliding head-on (zero separation) in the other direction, and the trigger rate

$$R_{\rm V0} = \sigma_{\rm V0} L \tag{4}$$

was recorded. Taking, for instance, the case of the horizontal scan (x-scan), in the gaussian approximation, the VBAND trigger rate will be reduced from the top luminosity value $R_{\rm V0}(0,0)$ to

$$R_{\rm V0}(D_x, 0) = R_{\rm V0}(0,0) \cdot \exp\left(-\frac{D_x^2}{2\sigma_{scan-x}^2}\right) \tag{5}$$

with the "scan standard deviation" defined as:

$$\sigma_{scan-x,y} = \sqrt{\sigma_{1x,y}^2 + \sigma_{2x,y}^2} = \sqrt{2}\sigma_{x,y}. \tag{6}$$

The width of the shape obtained by the vdM scan corresponds to the quadratic sum of the widths of the two beams.

Non-Gaussian Beam Profile

The above considerations are extended here to a more general case of non-gaussian beam profile.

Assuming the two beams to have the same shape in the transverse direction, and assuming factorization of the shapes in x and y, the beam profile can be written as

$$\rho_{1,2}(x, y) = N_{1,2} p_x(x) p_y(y) \tag{7}$$

where $p_x(x)$ and $p_y(y)$ are the normalized density profiles of the beams in the x and y directions.

For convenience, we define the "*shape factors*" as:

$$\int p_x^2(x)dx = Q_x, \quad \text{and} \quad \int p_y^2(y)dy = Q_y. \tag{8}$$

Using the above assumptions and definitions, the trigger rate for the x-scan becomes:

$$R_{\rm V0}(D_x, 0) = \sigma_{\rm V0} k_b f N_1 N_2 Q_y \int p_x(x - D_x) p_x(x) dx. \tag{9}$$

The integral of the convolution of the beams in the x direction is:

$$S_x = \int R_{\rm V0}(D_x, 0) dD_x, \tag{10}$$

and similarly for y. The two convolution integrals can then be expressed as:

$$S_x = \sigma_{V0} k_b f N_1 N_2 Q_y \ \text{ and } \ S_y = \sigma_{V0} k_b f N_1 N_2 Q_x. \tag{11}$$

The maximum value of the rate, corresponding to zero displacement, can be written as:

$$R(0,0) = \frac{k_b f N_1 N_2 Q_x \cdot Q_y}{\sigma_{V0}}. \tag{12}$$

From (11) and (12):

$$\frac{R(0,0)}{S_x} = Q_x \quad \text{and} \quad \frac{R(0,0)}{S_y} = Q_y. \tag{13}$$

The vdM scan can therefore be used to extract the shape factors $Q_{x,y}$ and, knowing the bunch intensities $N_{1,2}$, to evaluate the luminosity and hence the cross-section for the reference process.

VDM DATA ACQUISITION

Table 1 shows the summary of the conditions for the vdM scan performed in May 2010, that shall be referred to in the following as Scan-I.

During the scan, the data was recorded in coordination between ALICE (via the Detector Control System, DCS) and the LHC. The LHC operator scanned the beam separation in ALICE, while ALICE monitored the trigger rate ($R_{\rm V0}$) every 10 seconds, and recorded it on a dedicated data-base along with time stamps. In order to avoid measuring the rate while the beams are in movement, an "*acquisition flag*" (AF) is sent by the LHC. The AF can take on a value of 0 or 1, with 1 indicating that the flag is active and the data is valid.

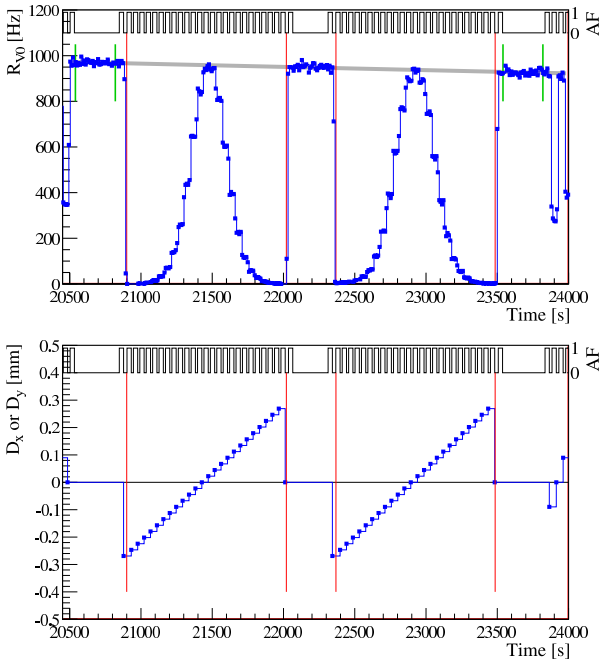

Figure 2: R_{V0} vs time (top) and separation value vs time (bottom) recorded in the ALICE DCS. For each plot, the status of the Acquisition Flag is shown on the upper part.

Fig. 2 shows the full view of the vdM scan period retrieved from the data-base before any correction is applied. The two peaks in the rate plot (top) correspond to the two scans. The scan was done first in the x direction, keeping the y position centered, and then in the y direction, keeping the position centered in x. Only data points recorded during the AF=1 periods are used in the analysis. An AF=1 period was declared at each separation step, for $\sim$ 30 seconds, allowing the recording of three R_{V0} data points with 10 seconds averaging time. In the present analysis, the data points belonging to the same separation value were combined and averaged.

BEAM INTENSITY

The absolute bunch intensities N_1 and N_2 are monitored by LHC beam instruments based on inductive current pickup devices. The corrections and calibrations of intensity data for the vdM scan fill were performed by the Beam Current Normalization Working Group (BCNWG), that provided intensity results together with systematic uncertainties[3]. According to the BCNWG result, the product of the two beam intensities ($N_1 \cdot N_2$) during the scan was 415.8×10^{18} with a systematic uncertainty of 4.4%.

The decrease of the bunch intensity during the scan time was as much as 0.25% and 0.06% for Beam-1 and Beam-2, respectively. This effect was corrected for in the analysis as part of the luminosity decay correction (see below).

Since the beam instrumentation used for the bunch intensity determination is not sensitive to the distribution of the charge within one LHC bunch (corresponding to 10 RF buckets), the effects of the decrease in the intensity of the main bucket due to debunching must be corrected for. The effect of such satellite bunches can be studied by reconstructing the interaction vertices from collisions displaced from the main luminous region. The intensity of satellite bunches and the ghost charge (charge distributed at longer distances over the orbit) were evaluated within the BCNWG. The collision rate involving satellite bunches is estimated to be less then 0.2% of the total rate. The amount of ghost charge in all slots is approximately (0.42$\pm$0.06)% and (0.41$\pm$0.06)% for Beam-1 and Beam-2, respectively. with an amount contained in slots near the colliding bunches of (0.24$\pm$0.05)% and (0.36$\pm$0.06)% for Beam-1 and Beam-2, respectively. The corrections based on these numbers (less than 1%) are already applied to the bunch intensity values provided by the BCNWG.

Table 1: Summary of the first ALICE vdM scan conditions

item	value, conditions
date	May 10, 2010
LHC fill number	1090
LHC fill scheme	Single_2b_1_1_1
intensity (Beam-1, Beam-2)	3.4×10^{10}, 3.8×10^{10}
nominal bunch size	1.8×10^{10}
β^*	2 m
nominal μ at head-on	0.09
crossing angle	internal only
beam spot size (σ_x, σ_y)	(44 μm, 47 μm)
ALICE run numbers	119156 (vdM)
	119159 (LSC)
scanned triggers	VBAND (DCS)
scan points	25 for each plane
scan step	22.42 μm
scan range	$\sim \pm 6\sigma$
scan points for LSC	3

DATA ANALYSIS

The vdM scan data were first corrected for pile-up and for the effect of the decrease in the luminosity during the fill due to emittance blow-up and bunch intensity decay. Then, the shape factors were calculated using different methods and compared. The separation values were checked using the results of the Length Scale Calibration (LSC) measurement. The individual analysis steps are described in the following subsections.

Pile-up Corrections

During Scan-I the trigger rate reached a maximum of about 1 kHz, with only one bunch crossing per orbit and an average number of collisions per bunch crossing (μ) of $\sim$0.1. Bunch crossings in which more than one interaction

occurs are still counted as one interaction in the VBAND rate. This pile-up effect must therefore be corrected for.

Indicating with μ the average number of triggers per bunch crossing and using Poisson statistics, the probability of one ore more triggers in a bunch crossing is given by:

$$P_{V0}(0;\mu) = 1 - e^{-\mu} \tag{14}$$

The value of μ can therefore be obtained from the raw trigger rate:

$$R_{\rm V0}^{raw} = k_b f(1 - e^{-\mu}), \tag{15}$$

and the corrected interaction rate can then be evaluated as:

$$R_{\rm V0} = k_b f \mu. \tag{16}$$

This correction has been applied to the V0 rates point by point. At about 1 kHz of interaction rate, the correction is as much as 5%.

Correction for the Luminosity Decay

As can be seen in Fig. 2, there is a systematic decrease of the top rate with time. This is dominated by the increase of the beam emittance. The bold gray line in the Fig. 2 is the result of a straight line fit using data points recorded outside of the scanning time. The fitting region is indicated by thin green vertical lines. The individual data points were then normalized so that the head-on luminosity corresponds to the value measured at an arbitrarily chosen neutral point at 22160 s in the plot. The maximal correction factors are -1.7% at the beginning of the x-scan and $+2.0\%$ at the end of the y-scan.

Length Scale Calibration

The scan separation values D_x and D_y were provided by the LHC. The calibration of the length scale has been verified by analyzing the data taken during a dedicated ("Length Scale Calibration", LSC) run during which both beams were moved in the same direction in either x or y. The data were then analyzed offline by reconstructing the primary vertex positions in order to determine the transversal displacement of the luminous region.

Fig. 3 shows the LSC data, with straight line fits to the data points for the x and y scans. According to the result of the fits, the actual separation is $\sim$1.3% and $\sim$0.9% smaller than the recorded values of D_x and D_y, respectively. In addition, there is some deviation from linearity, especially in the y direction ($\sim$2 μm). These values have been used in the evaluation of the systematic uncertainty (see later).

Shape Analysis with the Fitting Method

The data, corrected for pile-up and luminosity decrease, were analyzed using various fitting methods. The first is based on the use of a simple gaussian distribution (3 free parameters):

$$R_{\rm V0}(D_{x,y}) = A_{x,y} \exp\left\{-\frac{(D_{x,y} - m_{x,y})^2}{2\sigma^2_{scan-x,y}}\right\}. \tag{17}$$

Table 2: Summary of fit results with calculated luminosity and $\sigma_{\rm V0}$.

parameters	**single gaussian**	**double gaussian**
A_x [Hz]	970.4$\pm$2.9	1000.1$\pm$3.5
m_x [μm]	8.8$\pm$0.1	8.8$\pm$0.1
α_x	-	0.463$\pm$0.046
σ_{scan-x} [μm]	62.0$\pm$0.1	50.0$\pm$1.2
σ_x [μm]	43.8	35.4
$\sigma_{scan-xb}$ [μm]	-	68.8$\pm$0.7
σ_{xb} [μm]	-	48.6
fit $\chi^2/n.d.f.$	406.0 / 22	72.2 / 20
A_y [Hz]	984.4$\pm$2.8	998.8$\pm$2.8
m_y [μm]	-1.6$\pm$0.2	-1.7$\pm$0.0
α_y	-	0.978$\pm$0.000
σ_{scan-y} [μm]	66.4$\pm$0.1	64.3$\pm$0.0
σ_y [μm]	47.0	45.5
$\sigma_{scan-yb}$ [μm]	-	123.8$\pm$1.3
σ_{yb} [μm]	-	87.5
fit $\chi^2/n.d.f.$	637.2 / 22	168.5 / 20
$L(0,0)$ $\left[10^{28}\frac{1}{\rm cm^2 s}\right]$	1.81$\pm$0.01	1.89$\pm$0.04
$\sigma_{\rm V0}$ [mb]	54.06$\pm$0.17	52.95$\pm$1.00
with centering corr.	54.34$\pm$0.18	53.23$\pm$1.01

The results are shown in Fig. 4 as bold gray curves. While the single gaussian fit is acceptable for the x-scan, non-gaussian – and possibly asymmetric – tails are observed for the y-scan.

To improve on this, fits based on a double gaussian distribution were also performed, using the functional form:

$$\begin{aligned} & R_{\rm V0}(D_{x,y}) \qquad (18) \\ = \;& A_{x,y}\left[\alpha_{x,y}\exp\left\{-\frac{(D_{x,y} - m_{x,y})^2}{2\sigma^2_{scan-x,y}}\right\}\right. \\ + \;& \left.(1-\alpha_{x,y})\exp\left\{-\frac{(D_{x,y} - m_{x,y})^2}{2\sigma^2_{scan-x,yb}}\right\}\right] \qquad (19) \end{aligned}$$

where the two gaussians have a common center $m_{x,y}$, but different magnitudes and widths. The relative amplitudes of the primary and secondary gaussians are determined by $0 < \alpha_{x,y} < 1$.

The results of the double gaussian fits are shown in Fig. 4 as solid lines, while the dashed lines show the secondary gaussian part of the fit function.

Table 2 shows the values of the parameters extracted from the fits, together with the values of the luminosity and cross-section. The values for σ_x and σ_y, and σ_{xb} and σ_{yb} are simple estimates of the beam spot sizes obtained by dividing $\sigma_{scan-x,y,xb,yb}$ by $\sqrt{2}$. It should be noted that the two widths of the double gaussian fits are anti-correlated, resulting in an over-estimation of the fit uncertainty. In addition, the value of α in the double gaussian fit is not strongly constrained if the shape is close to gaussian. Since

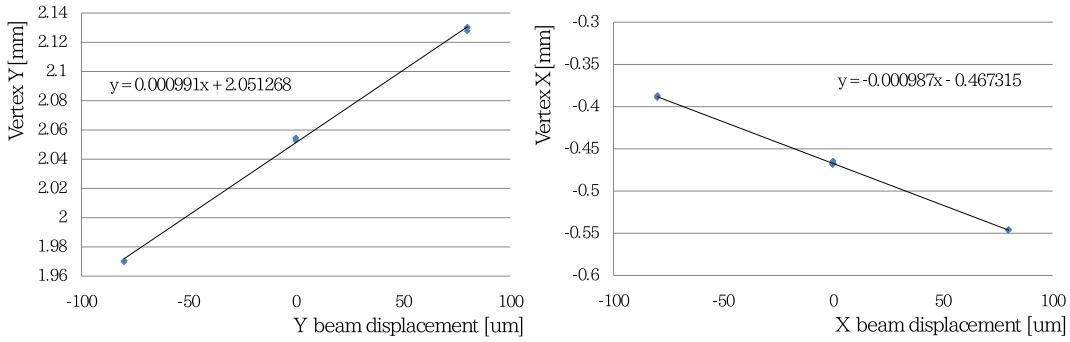

Figure 3: Results of straight line fits to the bump calibration data for the x-scan (left) and the y-scan (right).

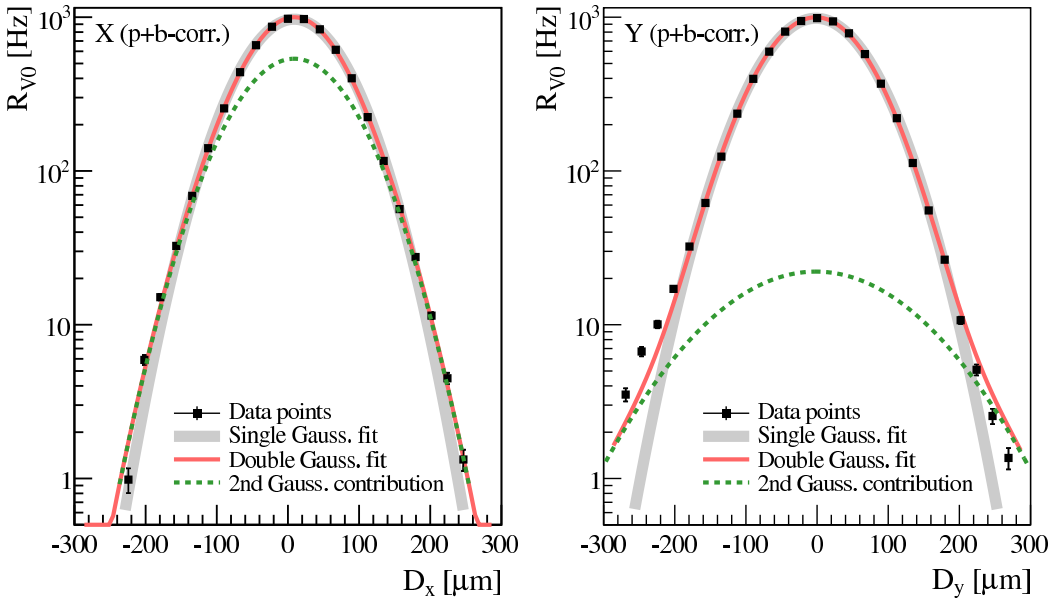

Figure 4: Data corrected for pile-up and luminosity decay, with fits by single gaussian (bold line) and double gaussian (solid line). The dashed lines show the secondary component of the double gaussian fit function.

the central value for the reference VBAND cross-section in this note will not be based on gaussian fits, but on numerical integration, the correlation of the fit errors is not discussed further here.

Beam Centering Correction

As can be seen from the fit results shown in Table 2, the values of D_x and D_y at which the luminosity is maximized are not exactly zero: $(m_x, m_y) = (8.8\ \mu\text{m}, -1.6\ \mu\text{m})$. During the scan, the separation $D_{x,y}$ for one direction is kept neutral (zero) while the beam is scanned in the other direction, which is therefore kept at the residual displacement determined by the values of (m_x, m_y).

The resulting luminosity decrease factors to be corrected for are estimated using (17). They are: 99.97% and 99.00% for the x- and y-scans, respectively.

The effect on the final value on cross section is +0.52%, taking into account the correlations among the parameters. In addition, conservatively, a 1% uncertainty is included in the final systematic error to account for possible residual centering effects.

Shape Analysis by Numerical Integration

The convolution integral can be calculated independently of the gaussian fits by numerical integration:

$$S_x = \sum_{i=1}^{n_x} R_{xi}\Delta_{xi} \quad \text{and} \quad S_y = \sum_{i=1}^{n_y} R_{yi}\Delta_{yi} \qquad (20)$$

where $n_{x,y}$ are the numbers of measured data points for each horizontal and vertical scan, R_{xi} and R_{yi} are the measured trigger rates, and Δ_{xi} and Δ_{yi} are the sizes of the bins. The results are shown in Table 3.

Table 3: Results of the numerical integration method for pile-up- and luminosity loss-corrected data together with intermediate results. σ_x and σ_y are the equivalent gaussian standard deviations corresponding to $S_{x,y}$.

parameters	**values**
$R(0,0)_x$ [Hz]	976.4±5.8
S_x [μm/s]	150696±339
Q_x [/cm]	64.79±0.41
σ_x [μm]	43.5
$R(0,0)_y$ [Hz]	986.4±5.9
S_y [μm/s]	164219±358
Q_y [/cm]	60.07±0.38
σ_y [μm]	47.0
$\langle R(0,0)\rangle$ [Hz]	981.4±4.1
with centering corr.	986.5±4.2
$L(0,0)$ $\left[10^{28}\frac{1}{\mathrm{cm^2 s}}\right]$	1.82±0.02
σ_{V0} [mb]	53.93±0.28
with centering corr.	54.21±0.28

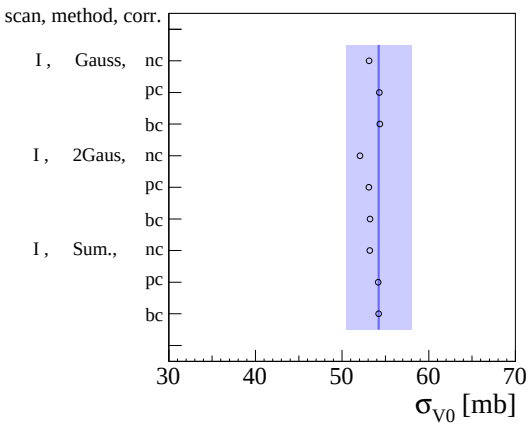

Figure 5: Comparison of the values obtained σ_{V0} for different methods and corrections (nc: no correction, pc: only pile-up correction, bc: full correction). The final value extracted from Scan-I and its systematic uncertainty are indicated by the vertical line and the gray band.

The numerical integration method does not rely on any assumption on the beam shape. In particular, the inclusion of any tails is straightforward. The result obtained based on numerical integration is used as final central value in the present note.

Fig. 5 summarizes how the cross section value varies according to the calculation methods and corrections. For the overall systematic uncertainty on the calculation of the convolution integral we have estimated a somewhat conservative value of 2%. The gray band in Fig. 5 indicates the range of the total systematic uncertainty.

Table 4: List of the systematic uncertainties on σ_{V0} taken into consideration.

item	**rel. uncertainty**
uncert. for $\delta(N_1 \cdot N_2)$	
bunch intensity	4.4%
uncert. for $\delta(S_x \cdot S_y)$	
length scale	2% $\oplus$ 2%
different methods	2%
rate determination	negligible
V0 time window	negligible
beam centering	1%
background and noise	negligible
pile-up	negligible
uncert. (additional)	
luminosity decrease	1%
scan-to-scan variation	2.5%
total $\delta\sigma_{\mathrm{V0}}$	7%

SYSTEMATIC UNCERTAINTIES

Table 4 summarizes the systematic uncertainties associated with the σ_{V0} determination that have been taken into consideration in the present analysis:

Bunch intensity $\cdots$ for the uncertainty on the product of the bunch intensities $N_1 \cdot N_2$, the BCNWG estimate of 4.4% has been used.

Length scale $\cdots$ from the Length Scale Calibration described above, we estimate an uncertainty of 2% for each scan direction. No correlation between x and y is assumed, thus 2%$\oplus$2% is applied.

Integration methods $\cdots$ the variation of the results for the different shape analysis methods was of the order of 1%. Somewhat conservatively, we take a value of 2% for the product $S_x \cdot S_y$.

Rate determination $\cdots$ the rate is measured by the V0 electronics integrating the counts every 10 seconds. The timing is very well controlled, since the integration is performed on an FPGA driven by the 40 MHz LHC clock. We estimate the precision of the integration to be better than 1 ms / 10 s. The systematics associated to the rate measurement is therefore taken to be negligible.

V0 time window $\cdots$ the V0 coincidences are counted within a tunable time window, which was set to its maximum width during the vdM scan in order to avoid possible counting inefficiencies. The resulting systematics is considered to be negligible.

Beam centering $\cdots$ we estimate a residual systematics after the centering correction of the order of 1%.

Table 5: Summary of the Scan-II conditions.

item	value, conditions
date	Oct. 15, 2010 (vdM)
	Oct. 29 and 30, 2010 (LSC)
LHC fill number	1422 (vdM)
	1453 and 1455 (LSC)
LHC fill scheme	Single_16b_3_1_12_allVdmB
intensity in each Beam	1.2×10^{12}
nominal bunch size	7.5×10^{10}
β^*	3.5 m
μ at head-on	$\sim$0.75
crossing angle	internal + external
beam spot size (σ_x, σ_y)	(57 μm, 65 μm)
ALICE run numbers	134779 (candle run)
	134780 (vdM)
scan points in x and y	25 or 21
scan range	$\sim \pm 6\sigma$
scan points for LSC	3 to 5

Background and noise $\cdots$ the total level of background is below 1 Hz, resulting in a negligibly small ($<$0.1%) effect on the luminosity calculation.

Pile-up $\cdots$ the residual systematics due to pile-up once the pile-up correction is applied is estimated to be negligible.

Luminosity decay $\cdots$ the rates have been corrected for the decrease of the luminosity during the fill due to emittance blow-up and intensity decay, as described above. A 1% discrepancy remains after the correction is applied. A 1% uncertainty has therefore been included in the systematics.

Scan-to-scan variation $\cdots$ a second scan was performed later during the year (Scan-II). The preliminary results (see below) give values of the VBAND cross-section up to 2.5% lower. This could be due to a systematics in the preliminary determination of the beam current, which would then in principle be included in the bunch intensity uncertainty. However, for safety, for the moment we include an additional systematic uncertainty of 2.5%.

Adding up quadratically the above uncertainties and rounding off, we obtain a total uncertainty on $\sigma_{\rm V0}$ of 7%. This estimate is somewhat conservative. We intend to review it once the results of the second scan will be final.

PRELIMINARY RESULTS OF THE SECOND VDM SCAN

The second vdM scan at 7 TeV (Scan-II) was performed in October 2010. In Scan-II, besides VBAND, other triggers were also measured. In the present document, we concentrate mainly on the results of the VBAND scan. Since

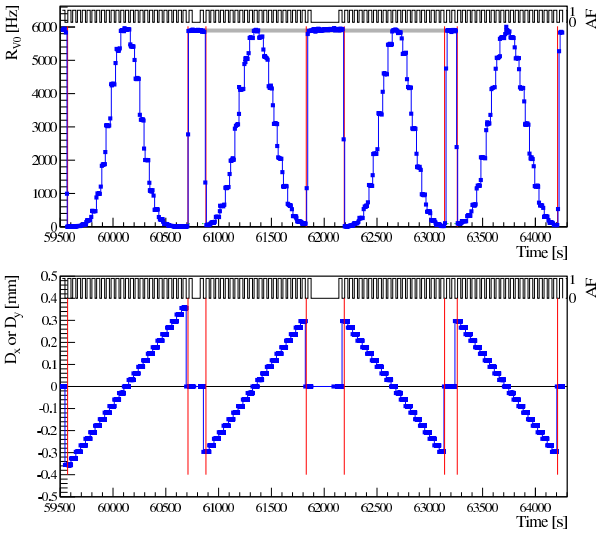

Figure 6: History of raw VBAND trigger rates (upper) and separation values (lower) during Scan-II.

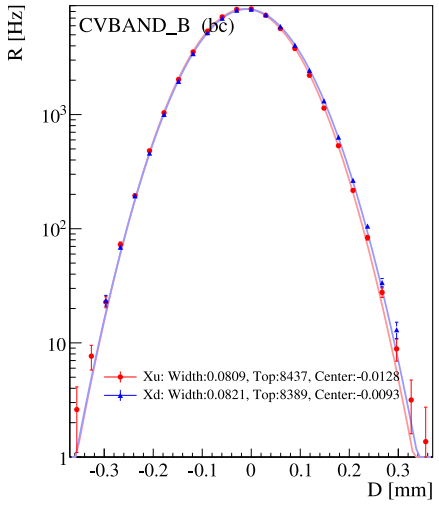

Figure 7: Comparison of scan shapes between u- and d-scans.

the beam current analysis is still being finalized by the BCNWG at the time of writing this document, the results presented here are still preliminary. They are compared with those of Scan-I with the aim of obtaining an estimate of the possible systematics due to differences in the beam or instrumental conditions from scan to scan.

Table 5 summarizes the conditions for Scan-II. In addition to the vdM scan, two Length Scale Calibration scans were also performed.

The vdM scan scheme during Scan-II, was different from that of Scan-I. As can be seen from Fig. 6, four successive scans were performed. The first two are an x-scan and a y-scan for which D_x or D_y were increasing with time (u-

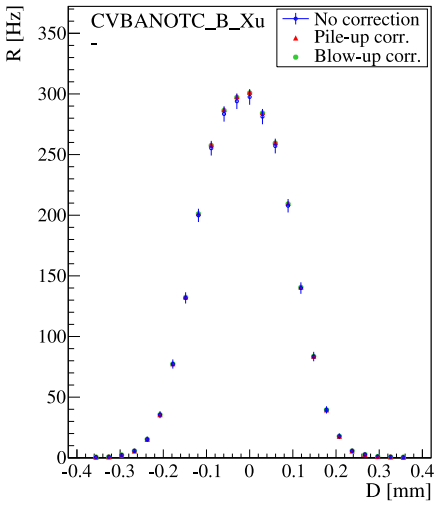

Figure 8: Obtained rate v.s. beam separation for $\mathrm{VBA\overline{C}}$.

scan), the last two are again an x-scan and a y-scan, but this time D_x or D_y were decreasing with time (d-scan).

Scan-to-Scan Shape Stability

Fig. 7 shows the comparison between the data of the u-scan and d-scan in the x direction. The fits were performed using a gaussian function, on emittance-corrected data.

The shapes of the u-scan and of the d-scan deviate from one another for separations D$>$ 0.1 mm. While at D=0 the two scans agree within 0.15%, the discrepancy reaches 15% at high values of D. For the vertical scan, the differences are much smaller. The effect of these discrepancies on the fitted widths is about 1.5%, in x and 0.5% in y. The reason for these discrepancies is currently under investigation.

Beam Intensity

The beam intensity data are not yet fully corrected. The decrease of the bunch intensity during the vdM scan time is less than 0.13%, and can therefore be neglected. The preliminary values for the average intensities during the scan used here are: 83.6×10^{10} and 78.7×10^{10} for Beam-1 and Beam-2, respectively.

Pile-up of Excluded Events

In view of the high trigger rate values expected in Scan-II, two exclusive triggers were set up in order to estimate the effect on the VBAND rate of the pile-up of two events for which only V0-A had fired in one event and only V0-C in the other.

The two exclusive triggers are: $\mathrm{VBA\overline{C}}$, firing when V0-A has fired but V0-C has not, and $\mathrm{VB\overline{A}C}$, doing the opposite.

Fig. 8 shows the result of the scan of $\mathrm{VBA\overline{C}}$. The top rate for $\mathrm{VBA\overline{C}}$ and $\mathrm{VB\overline{A}C}$ are approximately 300 Hz and 250 Hz, to be compared with a top VBAND rate after pile-up correction of 8 kHz.

The scan shape for $\mathrm{VBA\overline{C}}$ and $\mathrm{VB\overline{A}C}$ is close to gaussian, but slightly flattened at the top, precisely due to exclusive pile-up events of the type discussed above. With rates of the exclusive triggers of the order of 5% or less of the top interaction rate, the effect of exclusive pile-up on the top VBAND rate will be of the order of 0.3 %, and is neglected in the present analysis.

Table 6: Trigger cross sections measured in Scan-II.

trigger (scan dir.)	**cross sections [mb]**	
	Gauss fit	**numerical sum**
VBAND (u-scan)	53.09 ± 0.20	52.90 ± 0.20
VBAND (d-scan)	53.93 ± 0.20	53.51 ± 0.20
MUS5 (u-scan)	0.77 ± 0.01	0.77 ± 0.03
MUS5 (d-scan)	0.76 ± 0.02	0.75 ± 0.03

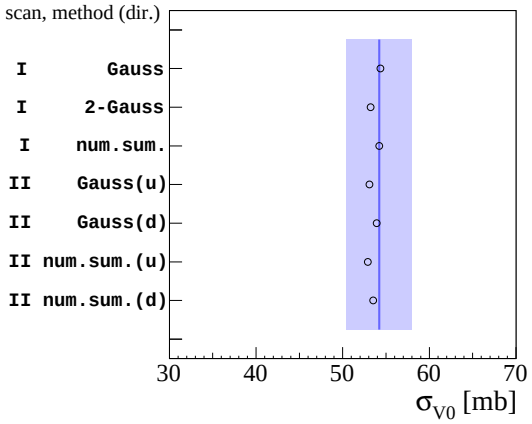

Figure 9: . Comparison between Scan-I and Scan-II results. Only pile-up and luminosity loss corrected data are compared. "(u)" and "(d)" indicate the scan direction. The final value extracted from Scan-I and its systematic uncertainty are indicated by the vertical line and the gray band.

Cross Sections and Comparison Between Fills

Table 6 shows the preliminary values of the cross section extracted from Scan-II data for VBAND and for one of the additional triggers scanned: MUS5 (single muon trigger at forward rapidity [1]). The values for the VBAND cross section vary from 52.9 to 53.9 mb depending on the integration method and on the scan direction. The variation between the u-scan and the d-scan is as much as 1.8%.

The scan-to-scan consistency is visualized in Fig. 9 for the VBAND trigger. The Scan-II values are somewhat lower than the Scan-I value of 54.2 mb which is indicated by the vertical bar, and within the systematic error of the Scan-1 measurement, indicated by the gray band.

The lowest value is the one obtained from numerical in-

tegration of the u-scan, which is 2.4% smaller than the Scan-I value. As discussed above, a 2.5% systematic uncertainty has been added in quadrature to the Scan-I results, to account for the possible systematics due to instrumental or beam-related effects.

As an additional consistency check, the ratio between the MUS5 and VBAND trigger cross-sections is compared to the ratio measured offline extracting the fraction of MUS5 events from the VBAND triggered sample recorded in low pile-up conditions. The two ratios agree to better than 1% accuracy, providing an important cross-check of the pile-up correction, which for Scan-II amounts to about 40% for VBAND, while it is negligible for MUS5.

CONCLUSION

Data from the May 2010 ALICE vdM scan (Scan-I) and, partially, from the October 2010 scan (Scan-II) have been analyzed.

The results obtained with different analysis methods (single gaussian fit, double gaussian fit and numerical integration) have been compared in order to estimate the systematics due to the uncertainty on the beam profile. The beam intensity calibration and the Length Scale Calibration for Scan-I are considered to be final.

The preliminary results of Scan-II have been compared to those of Scan-I in order to estimate the systematic uncertainty from scan-to-scan variations due to instrumental or beam effects.

The cross section for the process triggered by the ALICE V0 detector with the VBAND logic for 7 TeV p+p collision has been measured as:

$$\sigma_{\mathrm{V0}} = 54.2 \text{ mb} \pm 0.6\%(\text{stat.}) \pm 7.0\%(\text{syst.}), \qquad (21)$$

and can now be used as a reference cross-section by the ALICE experiment.

REFERENCES

[1] The ALICE Collaboration and K Aamodt et al 2008 *JINST* **3** S08002 (`http://iopscience.iop.org/1748-0221/3/08/S08002`).

[2] S. van der Meer, ISR-PO/68-31, KEK68-64 (`http://cdsweb.cern.ch/record/296752/`).

[3] G. Anders et al., CERN-ATS-Note-2011-004 PERF, 31 Jan 2011

LHCb 2010 luminosity determination with van der Meer scans

V. Balagura, CERN, Geneva, Switzerland & ITEP, Moscow, Russia

Abstract

The absolute calibration of LHCb 2010 luminosity performed with van der Meer scans is discussed.

INTRODUCTION

The luminosity in LHCb is constantly monitored with randomly triggered at 1 kHz events. They are usually called "nano-events" because they contain only an information relevant for the luminosity measurement and everything else is stripped off. The load on LHCb data acquisition system is therefore almost negligible. This approach of luminosity monitoring was proposed in [1]. "Nano-events" contain so called "luminosity counters", i.e. quantities proportional to the luminosity and easily measurable online. In 2010 we used as counters a number of vertexes, tracks and hits in a vertex detector (VELO), a number of hits in a scintillator pad detector (SPD) in front of calorimeters, and a transverse energy deposition in the calorimeters.

The relative luminosity can be determined from the average value of any counter. Alternatively one may determine it from the fraction of empty events with the counter close to zero, which we denote by $P(0)$. The luminosity should be proportional to $-\log P(0)$. This is obvious for the Poisson distribution, but in fact is also valid generally. Indeed, let's suppose that the counter x *can not take negative* values. Suppose, there are two independent sources contributing to x and they individually give spectra P_1 and P_2. The resulting spectrum is a convolution $P = P_1 \otimes P_2$. Since both sources can not produce negative x, a zero sum means zero contributions from P_1 and P_2, so that $P(0) = P_1(0) \cdot P_2(0)$ and $\log P(0) = \log P_1(0) + \log P_2(0)$. Therefore $\log P(0)$ is an additive quantity which should be proportional to the luminosity. This also implies that in the presence of backgrounds its contribution $-\log P_{\rm bgr}(0)$ may be subtracted. Note, that the background distribution should not necessarily follow Poisson law. $-\log P_{\rm bgr}(0)$ is estimated in LHCb from the crossings where one bunch is filled and the other is empty. In the crossings with pp-collisions it is renormalized assuming that the dominating beam-gas background is proportional to the beam currents.

We define an "empty" event as having $x \le x_0$ with some threshold x_0. The above arguments hold only for $x_0 = 0$ since we assumed that $x = x_1 + x_2 = 0$ implies $x_1 = x_2 = 0$. If $x_0 > 0$, some systematic error appears. To avoid it, one may use the average value of the counter $< x >$ instead of $-\log P(0)$. In this case another systematics may appear however, if the counter is not exactly proportional to the luminosity. The discussion of both methods and their comparison with the luminosity estimation from the fit of the x spectrum, which is the most precise procedure, is discussed in [2]. In particular, it explains how the x spectrum can be conveniently described using Fourier transforms.

During commissioning in 2010 several modifications have been made in LHCb subdetectors influencing luminosity counters. We chose the number of tracks reconstructed in VELO in R-Z projection as the best and the most stable counter. We used $-\log P(0)$ method for it and defined an "empty" event as having zero or one track. The systematics associated with this choice of threshold is negligible since the average interaction produces ~ 30 tracks. Modifications and alignment variations of VELO also produced almost negligible impact on the method, since the efficiency of reconstruction of at least two tracks in an inelastic event was always close to 100%. The stability of the counter is demonstrated in Fig. 1 which shows the ratio of the relative luminosities determined with $-\log P(0)$ method from the multiplicity of hits in the upmost layer of VELO and from the number of R-Z tracks. The former was also stable throughout LHCb 2010 running, and we used it as a cross check. Fig. 1 covers the whole period of LHCb operation, with both low and high number of interactions per crossing. Two counters have different systematics, and by comparing them we assign a systematic error of 0.5% to the relative luminosity measurement.

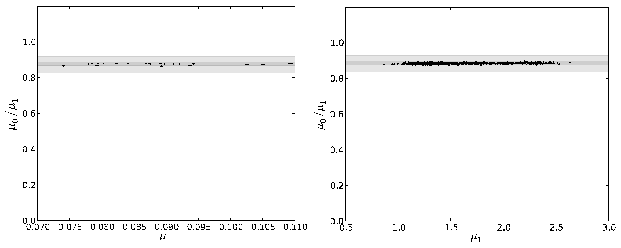

Figure 1: Ratio of average numbers of interactions per crossing μ_{PU}/μ_{RZ} determined with $-\log P(0)$ method from the number of hits in the upmost (so called pile-up or PU) layer of VELO and the number of R-Z tracks, versus μ_{RZ}. The deviation from unity is due to the difference in acceptance. Left (right) plot is for the beginning (the end) of LHCb 2010 running with lower (higher) values of μ.

The absolute calibration of LHCb luminosity was performed in 2010 using a beam-gas imaging method and van der Meer scans. In the former the images of two beams were developed from their interactions with a small amount of gas remaining in the beam pipe, assuming the uniform

gas distribution across the beams. The luminosity was calculated from the beam overlap integral obtained from the beam images. The method was proposed in [3] and first applied in LHCb in [4, 5]. At this workshop it was discussed in [6]. Here we concentrate on the alternative absolute luminosity calibration proposed by van der Meer [7].

The calibrations obtained with two methods were consistent and were averaged for the final result. The methods had similar sensitivity limited in 2010 by uncertainties in beam intensities. Other systematic errors were different, therefore usage of both in LHCb provided an important cross check of the results.

VAN DER MEER SCAN EXPERIMENTAL CONDITIONS

Van der Meer scans in LHCb have been performed in the dedicated LHC fills in the beginning and in the end of 2010 running, in April and in October. The characteristics of the beams are summarized in Table 1. In both fills there were two scans where either both beams moved symmetrically or only one at a time. Beam movements recorded with LHC Beam Position Monitors (BPMs) up- and downstream of LHCb are shown in Fig. 2. Note, that for the following analysis we did not use this information since BPM measurements were temperature dependent and were drifting with time. Precise beam positions were calculated from LHC magnet currents and cross checked with LHCb VELO detector, see later.

Table 1: Parameters of LHCb van der Meer scans. $I_{1,2}$ is a typical number of protons per bunch in units 10^{10}, $n_{\rm all}$ ($n_{\rm coll}$) is the total number of bunches per beam (number of colliding bunches), $\mu_{\rm max}$ is the maximal average number of interactions per crossing, $\tau_{I1\times I2}$ and τ_L are the decay times of the bunch intensity product and of the luminosity, respectively, in hours.

	25 Apr	**15 Oct**
LHC fill	1059	1422
$I_{1,2}$	1	7-8
$\beta^\star$	2	3.5
$n_{\rm coll}/n_{\rm all}$	1/2	12/16
$\mu_{\rm max}$	0.03	1
trigger	min.bias	22.5 kHz random <1 kHz min.bias beam-gas
$\tau_{I1\times I2}$	950	700
τ_L	30	46

In April the maximal beam separation was achieved only in the first scan, as in the second only the first beam was allowed to move. In October, in the second scan both beams moved one after the other. This allowed to cover the whole separation range. However, the beam steering procedure was such that in the middle of the scan the first beam jumped to an opposite end point and then returned back, so

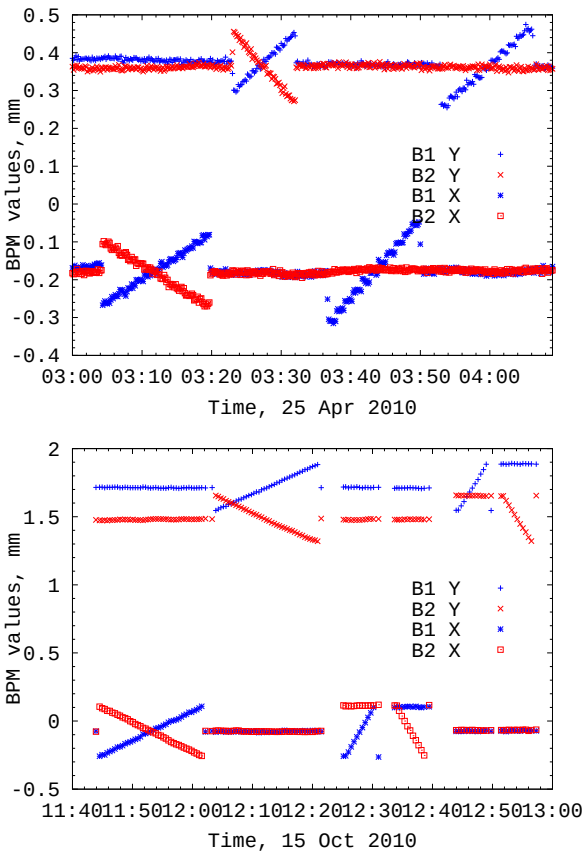

Figure 2: Beam movements recorded with LHC Beam Position Monitors (BPMs) around LHCb point in April (top) and in October (bottom). The zero points on the vertical axes are arbitrary. Top (bottom) curves show time dependent coordinates of two beams, $y_{1,2}$ ($x_{1,2}$). In both LHC fills there were two scans, first in $\Delta x = x_1 - x_2$ and then in $\Delta y = y_1 - y_2$. In the first scan both beams moved symmetrically, in the second scan either only the first beam was moved (April) or the first in the beginning and the second in the end (October).

that the beam movement was not continuous. This could potentially increase hysteresis effects in the LHC magnets. In addition, second scan in October had twice less data points, so we used it only as a cross check to estimate systematic errors.

In April the event rate was low and it was possible to record all events with pp interactions. We used loose minimum bias trigger with the minimal requirements on number of SPD hits (≥ 3) and transverse energy deposition in the calorimeters (≥ 240 MeV). In October the bunch intensities were higher by ~ 7.5, therefore in spite of slightly broader beams ($\beta^\star$=3.5 instead of 2), the rate was significantly larger, by a factor of ~ 30. In addition, there were 12 colliding bunches instead of one in April. Therefore we used selective trigger with three lines running in parallel. The first line accepted random "nano-events" at 22.5 kHz (20 kHz were devoted to 12 crossings with colli-

sions, $1+1$ kHz - to $4+4$ crossings where only one of two beams was present, and 0.5 kHz to all other empty crossings). The second line was the same loose minimum bias trigger but rate limited at 1 kHz. The third line collected events for the beam-gas analysis.

Both in April and in October the systematic error was dominated by uncertainties in the beam intensities. In April it was higher (5.6%) because of larger contribution from the offset uncertainty at lower beam intensities [8]. In October the calibration factor in the intensity measurement (2.7%) became dominant [9]. Both scans gave consistent results, and in the following we concentrate on the later scan with about twice better precision.

Time stability

Beam intensities in LHC are measured with Direct Current (DC) and Fast Beam-to-Current Transformers (BCTs) [10]. The former provides ultimate precision for the total current in the ring, while the latter gives information on relative bunch populations. Fig. 3 shows the DC BCT beam intensities before, during and after van der Meer scan fill in October. Fig. 4 presents the relative evolution of the individual bunch charges during LHCb scans. The LHC filling scheme was chosen in such a way that all bunches were collided only in one (or two for ATLAS/CMS) experiment, namely 12 in LHCb, 3 in ATLAS/CMS and 1 in ALICE. It is interesting that LHCb bunches demonstrated the best time stability. They changed during two LHCb scans by less than 0.1%. Therefore we did not normalize the rates by the intensity product $I_1 \times I_2$ at every scan point, but instead used only one average product per scan. This was done to avoid the noise associated with $I_{1,2}$ measurement. The averaged bunch intensities are given in Table 2. The same procedure was applied for the April scan, when the decay time of $I_{1,2}$ was even longer, 950 instead of 700 hours in October.

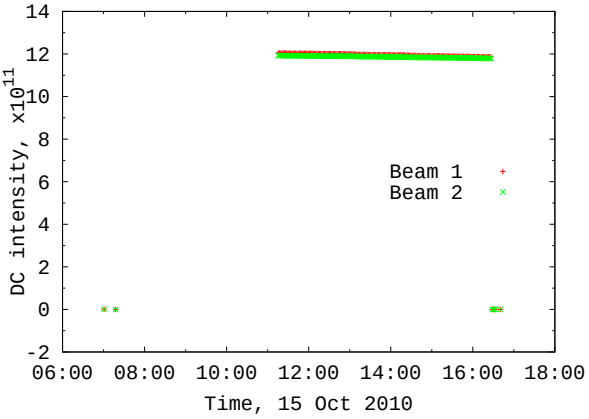

Figure 3: Intensities of two beams measured with DC BCT (system A) before, during and after van der Meer scan fill in October.

In addition to the beam intensity changes the luminosity stability may be limited by the changes in the bunch profiles, e.g. by an emittance growth. The luminosity stability was checked several times during the scans when the beams were brought to their nominal positions. The measured luminosities are shown in Fig. 5 for the October scan. The luminosity decay time was measured to be 46 hours (30 hours in April). This corresponds to 0.7% luminosity drop during the first (longer) scan along either Δx or Δy (0.9% in April). As it will be discussed later, in van der Meer method one needs the integrals of the luminosity over the separations Δx and Δy. The scan points have been taken from lower to higher Δx, Δy values, therefore the luminosity drop effectively enhances slightly the left part of the integral and reduces its right part, so that the net effect to the fist order cancels, since the curve is symmetric. The luminosity at the nominal beam positions also entering van der Meer formula, was measured in the beginning, the middle and the end of every scan, so that the luminosity drop also cancels to the first order. Therefore the systematic error due to the luminosity drop was much less than 0.7% and was neglected.

Table 2: Beam intensities averaged over two scan periods. The bottom line is DC BCT measurement, everything else is Fast BCT. The first 12 rows are the measurements in bunch crossings (BX) with collisions at LHCb, and the last two lines are the sums over all 16 bunches.

	Scan 1		Scan 2	
BX	I_1	I_2	I_1	I_2
2027	8.425	7.954	8.421	7.951
2077	7.949	7.959	7.944	7.957
2127	7.457	7.563	7.452	7.561
2177	6.589	7.024	6.584	7.021
2237	7.315	8.257	7.311	8.255
2287	7.451	7.280	7.446	7.278
2337	7.016	7.219	7.012	7.217
2387	7.803	6.808	7.798	6.805
2447	7.585	7.744	7.580	7.742
2497	7.878	7.747	7.874	7.745
2547	6.960	6.244	6.955	6.243
2597	7.476	7.411	7.472	7.409
All, Fast	120.32	119.07	120.18	118.99
DC	120.26	119.08	120.10	118.98

Fig. 6 shows the luminous region profiles when the beams were brought to their nominal positions during the first and the second scans in Δx and Δy. One can see that the widths did not change within the statistical errors which also presents an evidence of the negligible emittance growth. In addition, in the following it will be demonstrated that the widths of van der Meer plots with the luminosity dependence on Δx, Δy are also stable.

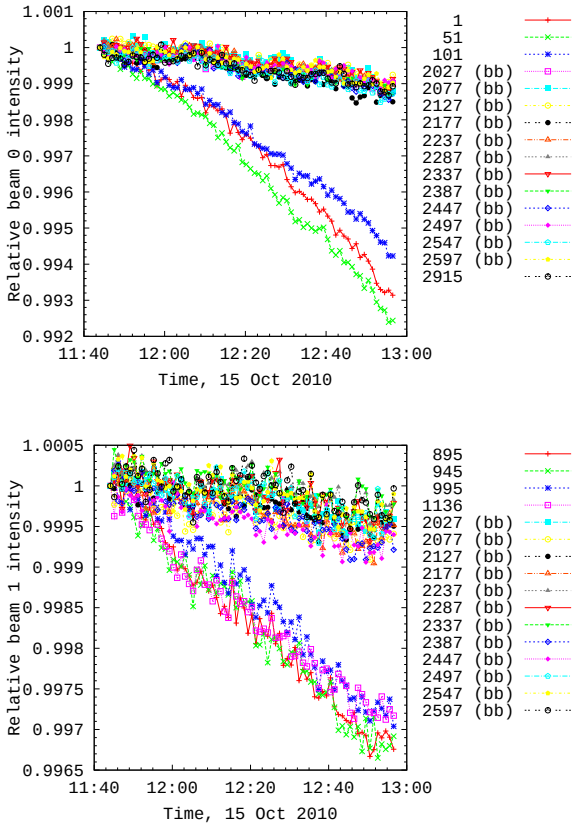

Figure 4: Relative evolution of the individual bunch charges measured with Fast BCT (system A) during two LHCb scans in October. Top (bottom) plot corresponds to the first (second) beam. Three (four) bunches in the bottom with faster decay time collided in ATLAS/CMS (or in ALICE).

CROSS SECTION DETERMINATION

In case of x-y factorization the cross section can be determined from Δx, Δy scans with van der Meer formula

$$\sigma = \frac{\int \mu(\Delta x, \Delta y_0)\, d\Delta x \;\times\; \int \mu(\Delta x_0, \Delta y)\, d\Delta y}{N_1 N_2 \mu(\Delta x_0, \Delta y_0) \cos\alpha}, \qquad (1)$$

where $N_{1,2}$ are the bunch intensities, μ is the average number of interactions per crossing and α is a half of the beams crossing angle (270 and 170 μrad in April and in October, respectively). It is assumed that protons in the beams move with the speed of light. $(\Delta x_0, \Delta y_0)$ is the crossing point where the beams return to their nominal positions, which is not necessarily the point of the maximal luminosity. The derivation of this formula is given in [11]. The interaction definitions for μ and for σ should be the same, but otherwise are arbitrary. We defined it as a pp interaction with ≥ 2 VELO tracks in R-Z projection, in accordance with the definition of our best luminosity counter.

12 bunches collided in October were analysed individually. The separation Δx, Δy dependence of μ averaged over all bunches is shown in Fig. 7. Two scans are over-

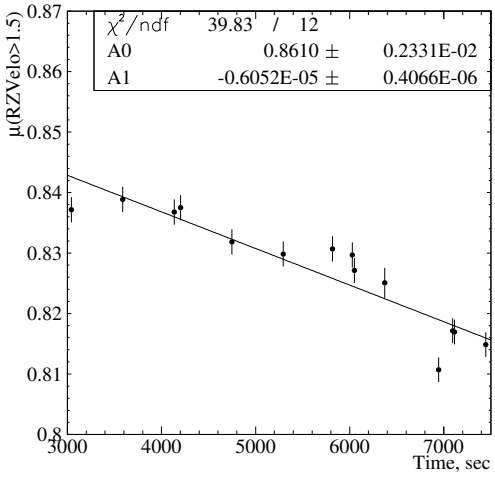

Figure 5: The evolution of the average number of interactions per crossing at the nominal beam positions during October scans. In the first (second) scan both in Δx and Δy the nominal point parameters were measured three (four) times. The line is a fit to the first order polynomial, the fit parameters are given in the top right corner. The luminosity decay time is $1/0.605 \cdot 10^{-5}$ sec $= 46$ hours.

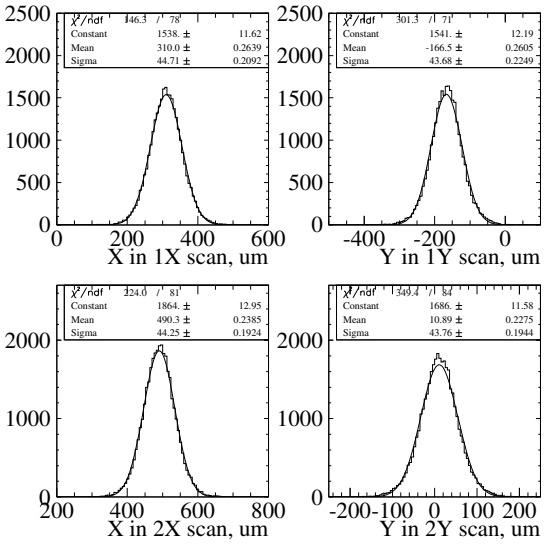

Figure 6: The luminous region profiles measured with the beams at their nominal positions during the first and the second scan in October in Δx and Δy. 12 colliding bunches are combined. The curve is a Gaussian fit with the parameters listed in the top right corner.

laid, the second was taken at the same points but with twice larger step. One can see that its Δy curve is shifted from the first scan by 7 μm on the left and by 4 μm on the right side. The reason of non-reproducibility is not understood. It may be attributed to the hysteresis effects enhanced in the second scan.

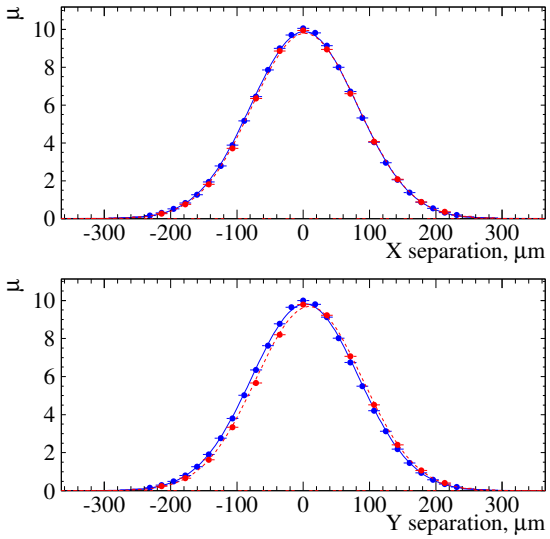

Figure 7: Averaged over 12 bunches number of interactions per crossing versus the separations Δx, Δy in October. The first (second) scan is represented by blue (red) points and solid (dashed) lines.

Similar curves for the April scans are shown in Fig. 8 where some shift in Δx is present.

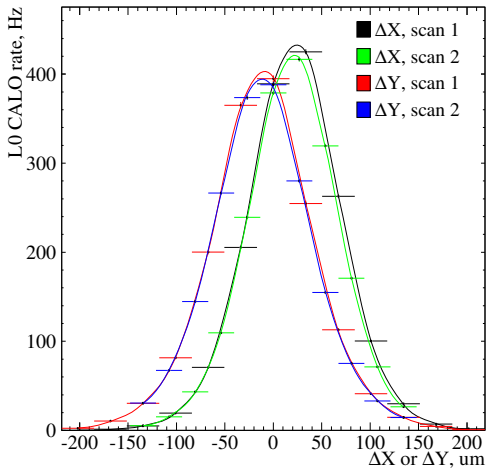

Figure 8: Trigger rate in April scan corrected for a small probability of multiple interactions and thus proportional to the luminosity versus the beam separations Δx, Δy. First and second scans are overlaid.

The curves were fit to single and double Gaussian. The results of the former for the October scans together with the mean and RMS values are listed in Table 3. There is no evidence for the emittance growth as the widths in two scans were the same within the errors.

Table 3: Mean, RMS and single Gaussian fit results for the October scans averaged over 12 bunches.

	Δx scan	Δy scan
mean	1.29	3.10
	2.79	9.16
RMS	80.56	80.82
	80.49	80.71
χ^2/ndf	1881 / 38	827 / 38
	1362 / 18	819 / 18
constant	9.880 ± 0.008	9.820 ± 0.008
	9.789 ± 0.010	9.681 ± 0.009
center	1.30 ± 0.05	3.10 ± 0.05
	2.77 ± 0.07	9.11 ± 0.07
sigma	80.25 ± 0.04	80.73 ± 0.04
	79.95 ± 0.05	80.35 ± 0.05

Double Gaussian fit gives a much better description. We fit all bunches individually, Fig. 9 gives one example for the first two bunches in October. The Δy curve is shifted from zero to the right for illustration purposes to be distinguished from Δx. It was found that the fit errors can be reduced approximately by half if the fit of Δx and Δy curves was performed simultaneously and the value at the nominal point $\mu(\Delta x_0, \Delta y_0)$ was constrained to be the same in both scans. The first fit parameter was chosen to be $\int \mu\, d\Delta x \cdot \int \mu\, d\Delta y / \mu(\Delta x_0, \Delta y_0)$, the term appearing in Eq. (1), so that a cross correlation of both integrals and the value at the nominal point is correctly taken into account in the resulting fit error. Other fit parameters listed in Fig. 9 are: two integrals along Δx and Δy, σ_1, $\Delta\sigma$ and a common Gaussian center for Δx and then for Δy curves. Here σ_1 is the width of the first Gaussian, while $\sigma_2 = \sqrt{\sigma_1^2 + \Delta\sigma^2}$, ensuring $\sigma_2 > \sigma_1$. Relative normalization of two Gaussians and the value at the nominal point were derived from nine fit parameters listed above. χ^2/ndf for all bunches was always between 0.7 and 1.8.

The product of bunch intensities $I_1 \cdot I_2$ in 12 colliding bunches is shown in Fig. 10. In spite of RMS spread of 12%, the bunches give cross sections consistent within statistical errors, having an average of 0.29% in the first scan. The sensitivity of the method is so high that we decided to use it to cross calibrate the *relative* bunch populations $I^i_{1,2} / \sum_{j=1}^{16} I^j_{1,2}$ measured with Fast BCT system. Here i runs over 12 LHCb bunches. By comparing Fast BCT with ATLAS BPTX measurements it was observed, that both may have a non-zero offset, see [8], [9]. Therefore we fit our 12 cross section measurements with three parameters: common cross section σ and Fast BCT offsets for two beams $I^0_{1,2}$. The offset uncorrected cross sections

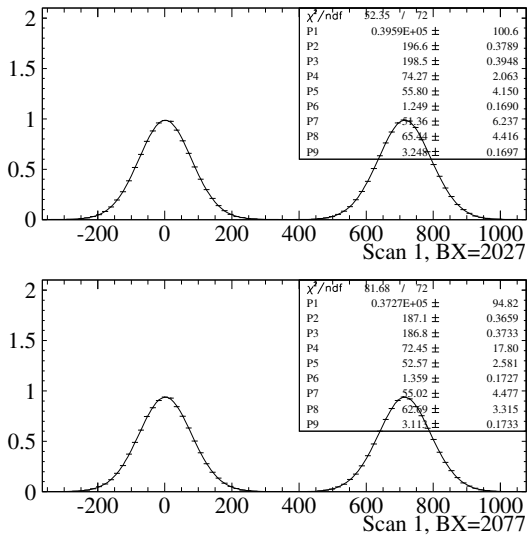

Figure 9: Number of interactions per crossing μ versus the separations Δx, Δy for the first two colliding bunches in the first October scan. Δx and Δy curves are stacked one after the other for illustration purposes. Fitting curves and parameters are discussed in the text.

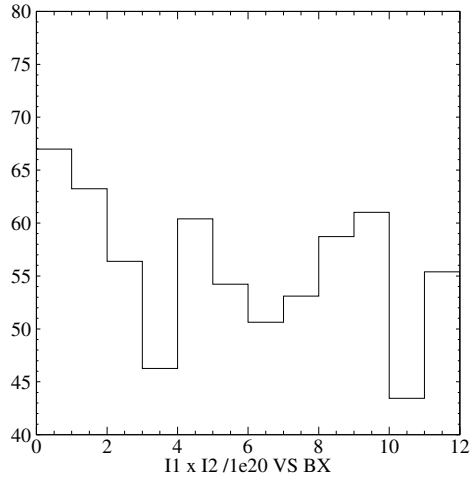

Figure 10: Bunch intensity products $I_1 \cdot I_2$ for 12 colliding bunches in October.

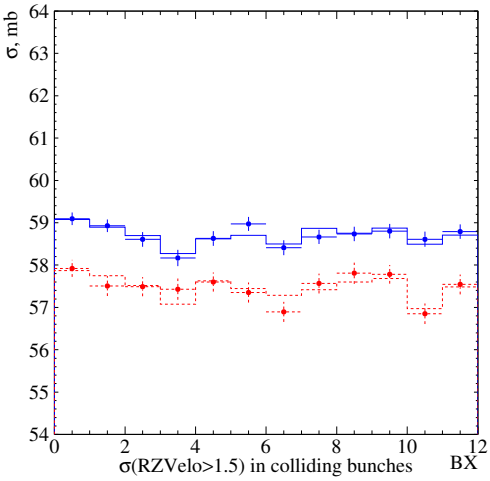

Figure 11: Cross sections not corrected for Fast BCT offset for 12 LHCb bunches in October. The upper (lower) curve is obtained in the first (second) scan. The fit takes into account Fast BCT offset and is discussed in the text. The fit results are summarized in Table 4.

are shown in Fig. 11. They are fit to the function

$$\sigma \cdot \prod_{b=1,2} (I_b^i - I_b^0)/I_b^i \cdot \sum_{k=1}^{16} I_b^k / \sum_{j=1}^{16} (I_b^j - 16 \cdot I_b^0)$$

which uses Fast BCT offset corrected relative populations and implies DC BCT $I_{1,2}^{\rm DC}$ total beam intensities. Two offsets improve the description of the points compared to the uncorrected simple fit by a constant. The latter has a goodness of fit probability of 1.5% and 2.5% in two scans, or $2.3 \cdot 10^{-3}$ if they are combined. The χ^2/ndf and all other fit results are summarized in Table 4, which also contains a section when ATLAS BPTX was used instead of Fast BCT system.

One can see that the offset errors in the first scan are $(0.10 - 0.12) \cdot 10^{10}$, or 1.5% relative to the average bunch intensity $< I_{1,2} >= 7.5 \cdot 10^{10}$. The sensitivity of the method, therefore, is very high, in spite of the fact that the RMS spread of intensities $I_1 \cdot I_2$ was only 12%. It may be very advantageous to make bunches in the future scans as different as possible, to become even more sensitive to the offsets and also to probe other effects like beam-beam interactions which may be visible at high but not at low intensities.

The offset and cross section errors are only statistical. Since the fits return good χ^2/ndf values, the bunch crossing dependent systematics should be at a lower or at a comparable level. The relative cross section error is only 0.09%, although the cross section difference between Fast BCT and BPTX fits is twice larger. One can also see that the BPTX offset I_2^0 for the second beam differs in two scans by 1.6 σ.

This gives the level of systematic errors. All main sources of systematics which will be discussed later (DC BCT uncertainty, hysteresis, ghost charges etc.) cancel when comparing bunches.

In spite of a good agreement between the bunches within the same scan, there is an overall 2.1% discrepancy between the scans. The reason is not understood, and may be attributed to the potential hysteresis or similar effects resulting to uncontrollable shifts of the beam as a whole. We took the results of the first scan with Fast BCT offsets for the final LHCb luminosity determination. 2.1% is the second largest systematic error in the cross section measure-

Table 4: Results of the cross section fit over 12 LHCb bunches in October. $I^0_{1,2}$ are Fast BCT or BPTX offsets in units 10^{10}. They should be subtracted from the values measured for individual bunches. Last two columns are for the first and the second scan, respectively. The cross section from the first scan obtained with Fast BCT intensities with offsets is used for LHCb luminosity calibration.

	Fast BCT	
σ, mb	$\mathbf{58.73 \pm 0.05}$	57.50 ± 0.07
I^0_1	0.40 ± 0.10	0.29 ± 0.15
I^0_2	-0.02 ± 0.10	0.23 ± 0.13
χ^2/ndf	5.8 / 9	7.6 / 9
	with zero offsets	
σ, mb	58.73 ± 0.05	57.50 ± 0.07
χ^2/ndf	23.5 / 11	21.9 / 11
	ATLAS BPTX	
σ, mb	58.62 ± 0.05	57.45 ± 0.07
I^0_1	-0.10 ± 0.12	-0.23 ± 0.17
I^0_2	-0.63 ± 0.12	-0.34 ± 0.15
χ^2/ndf	6.9 / 9	7.3 / 9
	with zero offsets	
σ, mb	58.63 ± 0.05	57.46 ± 0.07
χ^2/ndf	66.5 / 11	23.5 / 11

ment after uncertainties in the beam intensities. If DC BCT accuracy will improve in future 2011 scans, this may become a dominating error. In April the situation was similar, the discrepancy was $(4.4 \pm 1.2)\%$, the results may be found in Table 5. Since the April measurement was performed with the trigger rates proportional to the luminosity, instead of R-Z VELO tracks, we corrected the results for the difference in acceptances $\sigma(RZ)/\sigma(\text{April trigger}) = 1.066$. At that time Δx and Δy curves were fit separately. To obtain the average number of interactions from the trigger rates we used LHC revolution frequency 11.245 kHz.

Table 5: Cross section results in April. R is the trigger rate corrected for the small probability of multiple interactions and thus proportional to the luminosity. $\sigma(RZ)$ is the cross section of the interaction with ≥ 2 R-Z VELO tracks.

	Scan 1	Scan 2
$\int R\, d\Delta x$, cm·Hz	5.107 ± 0.017	4.875 ± 0.016
$\int R\, d\Delta y$, cm·Hz	5.094 ± 0.025	4.994 ± 0.016
$R(\Delta x_0, \Delta y_0)$, Hz	392	383
$I_1 \cdot I_2$, $\times 10^{10}$	1.056	1.056
$\sigma(RZ)$	**59.6**	**57.0**

SYSTEMATIC ERRORS

Δx and Δy length scale

Δx and Δy beam separation values at every scan step are calculated from the LHC magnet currents. There was a small non-reproducibility in the results of two scans, as it may be seen from Figs. 7 and 8, which may be attributed to the mismatch of the beam positions. Therefore it is important to check Δx and Δy values, and in particular their scales which linearly enter the cross section formula (1).

We made two cross checks with VELO detector, first, by comparing the luminous region positions measured in two scans, and second, we made a dedicated mini-scan in October when we moved the beams with constant separation.

In case of identical beams the luminous region is centered at the middle between them, otherwise it is shifted towards the narrower beam. The deviation from the middle is a function of the beam separation which we denote by $\Delta\vec{r}_{\rm Lum}(\Delta x,\, \Delta y)$. When the beams are moved symmetrically in the first scan, the middle is always at zero, so the deviation coincides with the luminous region center, $\Delta\vec{r}_{\rm Lum}(\Delta x,\, \Delta y) = \vec{R}^I_{\rm Lum}$. Here I stands for the first scan and "Lum" is for the luminous center. When only the first or the second beam is moved by $\vec{R}^{II}_{b1,2}$ in the second scan, the middle between the beams is at $\vec{R}^{II}_{b1,2}/2$ and $\Delta\vec{r}_{\rm Lum}(\Delta x,\, \Delta y) = \vec{R}^{II}_{\rm Lum} - \vec{R}^{II}_{b1,2}/2$. Since $\Delta\vec{r}_{\rm Lum}(\Delta x,\, \Delta y)$ should be the same function in both scans, we have a constraint $\vec{R}^{II}_{b1,2}/2 = \vec{R}^{II}_{\rm Lum} - \vec{R}^{I}_{\rm Lum}$ independently of the beam shapes. The luminous region centers $\vec{R}^{I}_{\rm Lum}$ and $\vec{R}^{II}_{\rm Lum}$ can be precisely measured in VELO. Its dependence on the beam separation in April is shown in Fig. 12. Blue solid lines (red dashed) is for the first (second) scan. One can see that the former is not linear as it should be for single Gaussian beams. At the scan ends the center is closer to the first beam meaning that the second is broader.

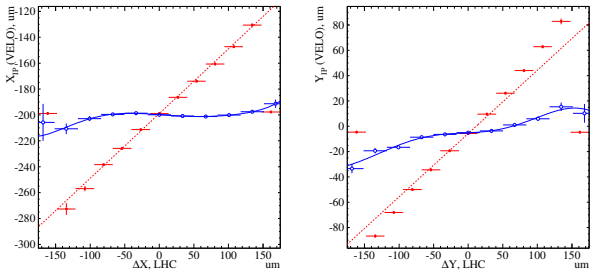

Figure 12: The luminous region center measured in VELO versus the beam separation Δx (left) or Δy (right), in April. The first (second) scan is shown by blue open (red filled) points. The curves are the fit by 7th order polynomial. Horizontal bars represent not the errors but the bin width.

The difference between the curves for the second and for the first scan, multiplied by two, is shown in Fig. 13. Inde-

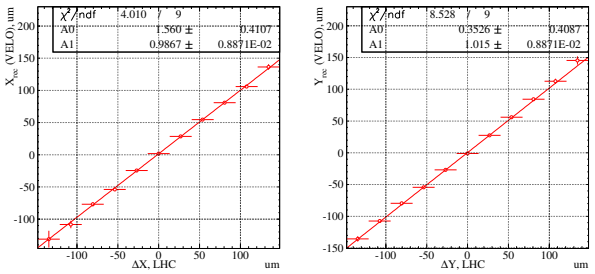

Figure 13: Difference between two curves in Fig. 12 multiplied by two. Results of the fit by a straight line are shown in the top right corner.

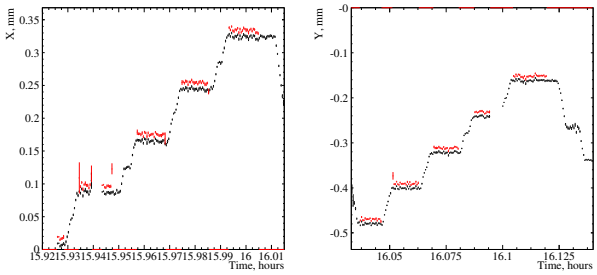

Figure 14: Evolution of the luminous center in x (left) and in y (right) during length scale calibration scans in October. Red points above flat intervals distinguish periods used in the following analysis. They are shifted upwards only for illustration purposes. During the first (second) scan the beams were moved in 5 equidistant steps of 80 μm along x (y) with the constant separation $\Delta x = 80\mu$m, $\Delta y = 0$ $(0,\ 80\ \mu\mathrm{m})$.

pendently of the bunch shapes it should be linear. The fit returns the slopes compatible with unity within $-1.3 \pm 0.9\%$ and $1.5 \pm 0.9\%$ for Δx and Δy, respectively. In spite of opposite signs of Δx and Δy corrections, we conservatively assigned 2% systematic error for the length scale calibration in April. Note, also that in Δx there is a shift by 1.5 μm at zero between the two scans.

Dedicated length scale calibration scan in October

In October we used another calibration method. Beams have been moved in 5 equidistant steps in Δx and Δy but the separation between them was kept constant. The luminous center movement is shown in Fig. 14. Red points above flat intervals distinguish periods with fixed beam positions which we used in the following analysis. They are shifted upwards only for illustration purposes. During the scan along x the beam separation was $(\Delta x,\ \Delta y) = (-80\ \mu\mathrm{m},\ 0)$. Here 80 μm is approximately one sigma of van der Meer luminosity dependence on $\Delta x = x_1 - x_2$. This separation was chosen to maximize the derivative $dL/d\Delta x$, i.e. the luminosity sensitivity to possible difference in the two beam scales. If e.g. the first beam moves slightly faster than the second, the separation Δx gets smaller and the effect can be visible in the increase of the luminosity. The same separation $\Delta y = 80$ μm was chosen in the y scan.

Difference between beam scales. The luminosity behaviour during the scans is shown in Fig. 15. As one can see it is not constant. This may be attributed to the different scales of two beams. Mote specifically, we assumed that the real positions of the beams $x_{1,2}$ can be obtained from the predicted numbers $x^0_{1,2}$ by applying a correction

$$x_{1,2} = (1 \pm \epsilon_x/2) \cdot x^0_{1,2}, \qquad (2)$$

and the same for $y_{1,2}$. Assuming a Gaussian shape of van der Meer luminosity dependence on Δx, with sigma σ, we get in this case

$$\frac{1}{L} \cdot \frac{dL}{d(x_1 + x_2)/2)} = -\epsilon_x \frac{\Delta}{\sigma^2}. \qquad (3)$$

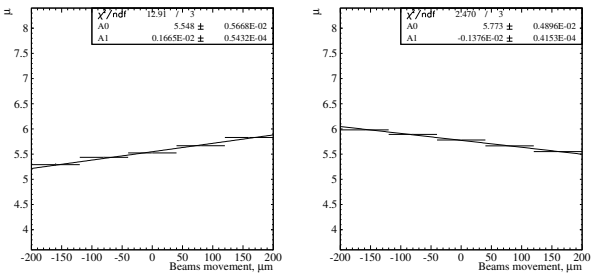

Figure 15: Average number of interactions summed over 12 colliding bunches versus the luminous center during length scale scans in x (left) and in y (right) in October. The fit by a straight line is overlaid, the fit results are given in the top right corner.

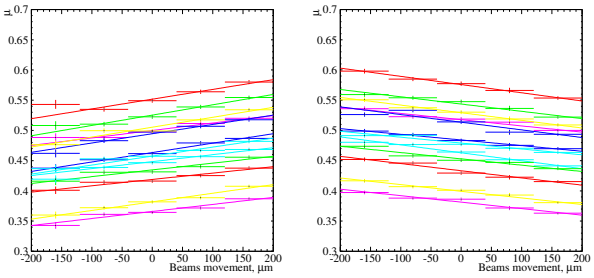

Figure 16: The same as in Fig. 15 but separately for different bunches.

Since $\Delta x = (x^0_1 - x^0_2) + \epsilon \cdot (x^0_1 + x^0_2)/2$, it depends on the

middle point between the beams $(x_1^0 + x_2^0)/2$. In the first scan it is always at zero, therefore no correction is needed. During the second scan this point moved $0 \to 355.9\,\mu\text{m} \to 0$. Therefore a correction of Δx values in Fig. 7 is required. The central point should be shifted to the right (left) for the x (y) scan. The left (right) side is thus stretched and the opposite side is shrunk. The corrected curves are shown in Fig. 17. One can see, that the shift between the scans is reduced in y, but appears in x, so that the discrepancy can not be fully explained just by a linear correction.

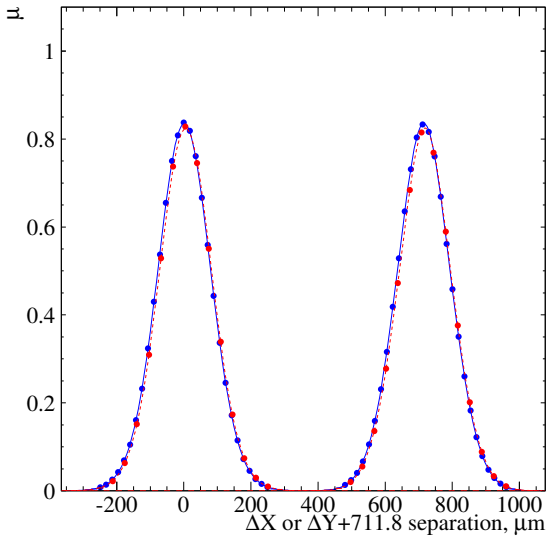

Figure 17: The same plots as in Fig. 7 but with $\epsilon_{x,y}$ correction discussed in the text. Δx and Δy curves are stacked one after the other for illustration purposes.

Stretching and shrinking the second scan curves influences the integrals and the resulting cross sections very little. The latter changes in average only by 0.1%, which we include into a systematic error. In fact, in Table 4 and in Fig. 9 the numbers are given after the correction.

Cross check of a common beam scale. In case of parallel translation of both beams, the luminous center should follow the beam positions regardless of the bunch shapes. Since it is approximately at $(x_1 + x_2)/2 = (x_1^0 + x_2^0)/2$ and similar for y, the corrections due to $\epsilon_{x,y}$ are negligible. The luminous center can be measured with VELO. This provides a precise cross check of the common beam scales $(x_1^0 + x_2^0)/2$ and $(y_1^0 + y_2^0)/2$.

The result is shown in Fig. 18. The LHC and VELO scales agree within $-0.97 \pm 0.17\%$ and $-0.33 \pm 0.15\%$ in x and y, respectively. For the cross section determination we took a more precise VELO scale and multiplied the values from Table 4 by $(1 - 0.0097) \cdot (1 - 0.0033)$. In addition, we conservatively assigned 1% systematic error due to the common scale uncertainty.

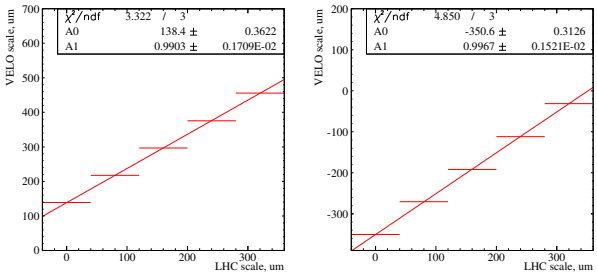

Figure 18: Luminous center reconstructed in VELO versus the position predicted from LHC magnets. The horizontal bars represent the bin widths, not the errors. The points are fit to a linear function. The slope, shown in the top right corner, calibrates the common beam scale.

x-y coupling

LHC ring tilt. Van der Meer formula (1) is valid only if the particle distributions in x and in y are independent. To check this statement we measured the movement of the luminous center along y during length scale scan in x and vice versa, see Fig. 19. The slope is compatible within errors with the expected at LHCb 13 mrad tilt of the LHC ring [12] with respect to vertical and horizontal axes of VELO. Note, that due to this tilt the LHC and VELO scales differ by $1 - \cos(13\text{ mrad}) = 0.84 \cdot 10^{-4}$ both in x and y. The corresponding correction to the cross section is negligible.

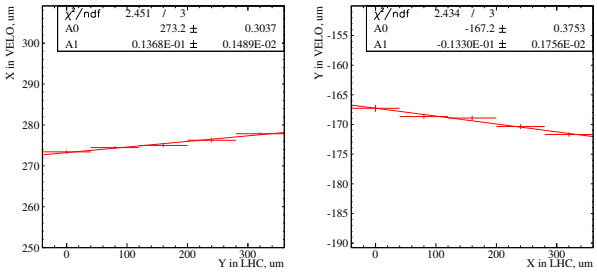

Figure 19: Luminous center position in x during length scale scan in y (left) and vice versa (right). The points are fit to a linear function. The slope, shown in the top right corner, is compatible with the expected 13 mrad tilt of LHC ring at LHCb.

x-y independence of the luminous region. In addition we checked x-y independence of the vertex distribution. To increase statistics we used data collected in the same LHC fill 1422 after van der Meer scan at LHCb when the beams collided head-on. Fig. 20 shows RMS spread of vertexes in y in different slices in x and vice versa. From the first glance there is a big x-y correlation. However, the same plot for the sample of vertexes with > 40 tracks and thus better resolution, is much more flat, see Fig. 21.

Clearly, the x tails of the luminous region contain more poorly measured vertexes, which produce larger RMS in y. This explains Fig. 20, x-y correlation appears via a cross correlation with the vertex resolution.

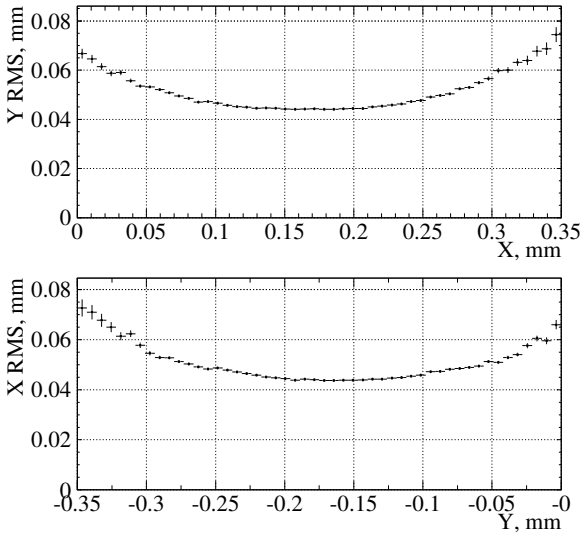

Figure 20: Luminous center RMS in y in different x slices (top) and vice versa (bottom). The data was collected after LHCb van der Meer scan, with head-on beams.

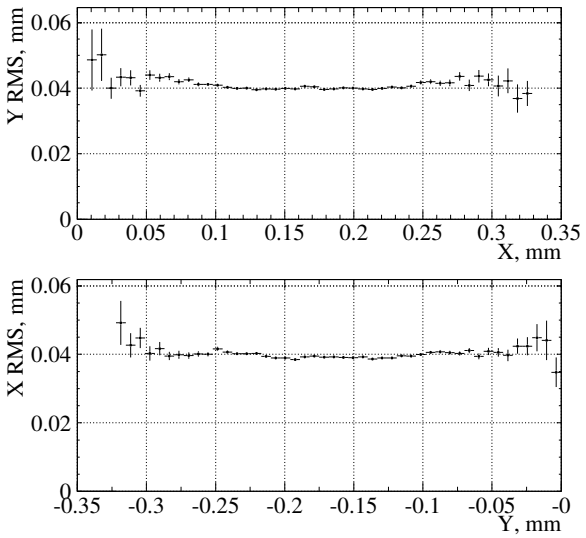

Figure 21: The same as in Fig. 20 but only for vertexes with > 40 tracks.

Fig. 22 shows the x-y profile of the luminous region. There is a slope of 79 mrad. Its origin is not understood. The corresponding x-z and y-z profiles are given in Fig. 23. The slopes of -92 and 44 μrad are due to the known fact that the middle line between LHC beams is inclined from the z axis. This was observed with beam gas events, the inclination varies slightly from fill to fill. Taking into account these x and y cross correlations with z and also the known 13 mrad tilt of LHC ring, one can calculate the residual x-y correlation slope, which was found to be 77 mrad.

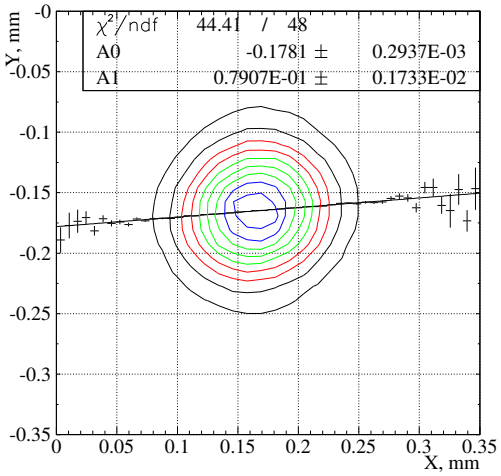

Figure 22: Contours of x-y luminous region profile. The points represent y-coordinates of the luminous center in different x slices. They are fit with the linear function. The slope (A1) is given in the top right corner.

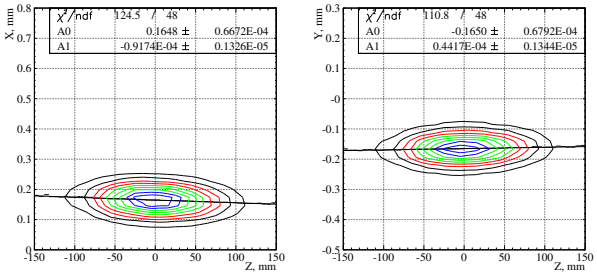

Figure 23: Similar to Fig. 22 but in x-z and y-z projections.

If the beam profiles are two-dimensional Gaussians of the general type with a non-zero correlation between x and y, the cross section formula should be corrected. The details are given in Appendix. We assumed that the correlation coefficients of two beams were similar and therefore close to the measured correlation in the luminous distribution $\xi = 0.077$. In this case the cross section correction is $\xi^2/2 = 0.3\%$. We did not apply this correction, but included 0.3% as a systematic error.

Ghost charge in LHC ring

There is a small fraction of "ghost" protons contained in not nominal LHC RF buckets. This is discussed in [8], [9]. Their contribution to the total LHC beam current should be subtracted.

Ghost charge in not nominal bunches. With the dedicated trigger in LHCb we were able to measure the rates of beam-gas events produced by ghost and nominal protons, and to determine the ghost fraction from their ratio. The results for the October and April fills are summarized in Table 6. LHCb trigger efficiency is timing dependent, it is optimized for the interactions in the nominal RF buckets. For the satellite buckets the efficiency drops as it is shown in Fig. 24. This was measured in van der Meer October fill by shifting LHCb clock by 5, 10 and 12.5 nsec and by comparing the total beam-gas rates in the nominal crossings. Since the RF bucket number within 25 nsec bunch is not measured in LHCb, this uncertainty through the efficiency dependence introduces some systematics in ghost charge measurement. We considered two extreme cases, when all ghost charge was contained at the nominal RF positions and thus the timing efficiency was 100%, and when the efficiency was at the average level for 5, 10 and 12.5 nsec points. The latter should be below the efficiency averaged over *all* RF buckets. We took the average between these two extremes as an approximation of the efficiency and half of the difference between them as an error. We also fit four available points at 0, 5, 10 and 12.5 nsec to the periodic function $R_{\rm max} \cdot (\epsilon + (1-\epsilon) \cdot \cos(2\pi\Delta t/25 \text{ nsec})$. Here $R_{\rm max}$ is the maximal rate at zero and ϵ estimates the average efficiency due to timing for the random distribution of the ghost charges in RF buckets. The obtained ϵ values are close to our efficiency central values, as it can be seen from Table 6. Finally, the cross section correction due to the ghost charge is $\frac{0.12\pm0.06}{0.86\pm0.14} + \frac{0.00\pm0.03}{0.84\pm0.16} = 0.14 \pm 0.08\%$ in April and $\frac{0.20\pm0.02}{0.86\pm0.14} + \frac{0.36\pm0.03}{0.84\pm0.16} = 0.66 \pm 0.10\%$ in October.

Table 6: From top to bottom: total ghost charge fraction outside nominal bunches in October. Fractions localized in ± 3 bunches around the nominal positions. The same two lines for April. Ratio of the average rate measured with 5, 10, 12.5 nsec time shifts and the rate at zero. Estimation of the efficiency due to timing. Average efficiency from the fit to the sum of a cosine and a constant.

	Beam 1	Beam 2
Fraction in Oct., %	0.20 ± 0.02	$0.36 \pm 0.03)$
(in ± 3 BX)	(0.12 ± 0.01)	(0.25 ± 0.02)
Fraction in Apr., %	0.12 ± 0.06	$0.00 \pm 0.03)$
(in ± 3 BX)	(0.12 ± 0.06)	(0.00 ± 0.03)
5, 10, 12.5 ns avr.	0.73	0.67
Efficiency	0.86 ± 0.14	0.84 ± 0.16
ϵ	0.83 ± 0.04	0.78 ± 0.04

Ghost charge in the satellite RF buckets in the nominal bunches. It is known that there may be a ghost charge in the satellite RF buckets in the nominal bunches. Usually it may be present in $\pm 2, 4, \ldots$ buckets around the nominal position which is attributed to the SPS frequency of 200 MHz [8], [9]. Due to LHCb crossing angle of 170 μrad in October, ± 2 and the nominal buckets are separated in x and can not collide if the beams are head-on. However, as it is schematically illustrated in Fig. 25, when the beams are separated in x by about 225 μm the collisions are possible at $z = \pm 75$ cm. The z distribution of vertexes accumulated with the minimum bias trigger in October is shown in logarithmic scale in Fig. 26. To estimate the fraction of the ghost charge, we counted a number of vertexes at $z = 0, \pm 75$ cm versus the separation x, see Fig. 27. Since the rate of the minimum bias events was biased by the trigger rate limiter, we took vertex distributions with the weights determined from the sample of nano-events taken with random trigger. Assuming similar efficiencies and distribution of particles in the nominal and the satellite ± 2 RF buckets, the fraction of the charge in the latter is determined to be 0.1%. We did not correct for this effect but assigned a systematic error of 0.1%.

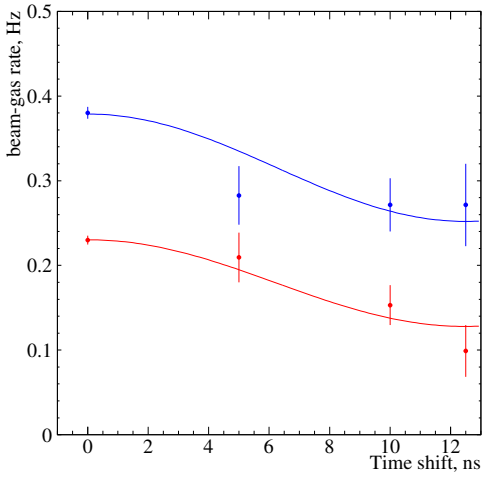

Figure 24: Beam-gas rate proportional to the trigger efficiency versus the time shift of the interaction from LHCb clock. The curve is the fit to the function $R_{\rm max} \cdot (\epsilon + (1-\epsilon) \cdot \cos(2\pi\Delta t/25 \text{ nsec})$, which returns the timing trigger efficiency for the random distribution of ghost charge $\epsilon = 0.83 \pm 0.04$ and 0.78 ± 0.04 for the first and the second beam, respectively.

Reproducibility of the luminosity at the nominal beam positions

As it can be seen from Fig. 5, when the beams were brought to their nominal positions, the luminosity not always returned to the expected value. $\chi^2/\text{ndf} = 40/12$, so the non reproducibility can not be fully attributed to statistical fluctuations and some systematic error should be present. It is origin is not understood but the effect may be similar to the non reproducibility of the beam positions visible from the shift of two scan curves in Figs. 7, 8 and 17.

We denote sigma of the statistical fluctuations by $\sigma_{\rm stat}$

and assume that the extra systematic fluctuations may also be described by a Gaussian with sigma $\sigma_{\rm syst}$. A luminosity measurement time, an accumulated statistics and thus $\sigma_{\rm stat}$ at different points were the same. Since the statistical error alone gives $\chi^2/{\rm ndf} = \sum_i(\Delta_i)^2/\sigma^2_{\rm stat}/{\rm ndf} = 40/12$, to bring it to unity one should add the systematics $\sigma_{\rm syst}$ determined from $(\sigma^2_{\rm syst} + \sigma^2_{\rm stat})/\sigma^2_{\rm stat} = 40/12$. The relative statistical error is $\sigma_{\rm stat} = 0.00209/0.8356 = 0.25\%$, so that $\sigma_{\rm syst} = \sigma_{\rm stat}\sqrt{39.84/12 - 1} = 0.38\%$. The absolute scale of μ measurement enters the cross section formula (1) twice in the enumerator and once in the denominator, so the overall dependence is linear. Therefore we assigned an extra systematic error of 0.4% to the cross section measurement.

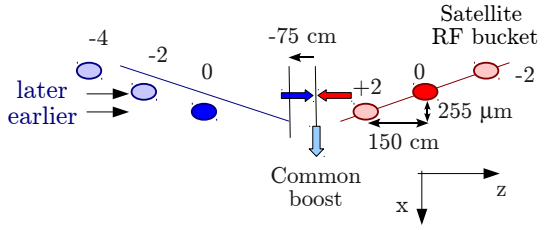

Figure 25: Collision of protons from the nominal and ± 2 satellite RF buckets in van der Meer scan.

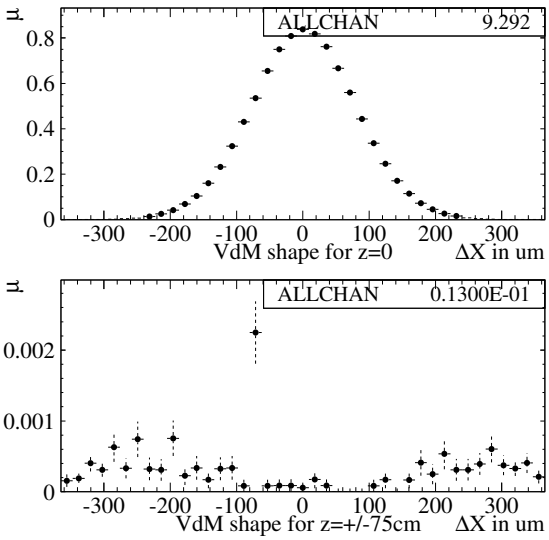

Figure 27: Average number of interactions μ at $z = 0$ (top) and $z = \pm 75$ cm (bottom) versus the beam separation Δx corrected for the trigger bias of the minimum bias sample. It is assumed that the efficiencies and the distribution of particles in the nominal and the satellite $\pm$ RF buckets are the same.

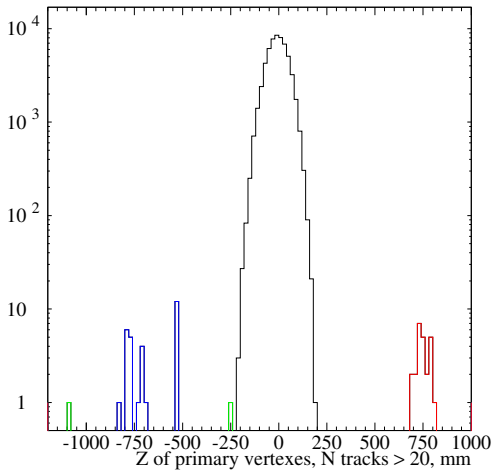

Figure 26: z distribution of vertexes in the minimum bias sample in the first Δx scan. Vertexes at ± 75 cm are due to interactions of protons in the nominal and ± 2 satellite RF buckets.

BEAM IMAGING DURING VAN DER MEER SCAN

During van der Meer scan the transverse beam images can be reconstructed [11]. One should accumulate transverse vertex distributions visible from the beam center and unfold them with the transverse vertex resolution. This should give the beam image in its transverse plane for arbitrary beam shapes. The approach is complementary to the beam-gas method.

The beam imaging was used to cross check the widths of van der Meer luminosity versus separation curves in October data. The x and y VELO vertex resolution was determined from data in the following way. N vertex tracks were randomly split into two equal halves to form two independent vertexes. Their separation divided by $\sqrt{2}$ gave a resolution estimate for a vertex with $N/2$ tracks. The resolution was then parameterized with the function $\sigma/N^\alpha + \delta$ with σ, α and δ parameters and their errors given in Table 7. For the beam imaging we used only tracks with $N > 10$. The average resolution function was reconstructed for the N-distribution observed in data. This was done for the central values of σ, α and δ parameters, and for the values shifted by one sigma to the left or to the right to simultaneously minimize or maximize the resolution. To simplify deconvolution, the obtained resolution functions, shown in Fig. 28, were approximated as Gaussians. The beam images were also approximated as Gaussians, the corresponding widths after unfolding are shown in fig. 29. The beam transverse planes were defined using the known crossing angle of 170 μrad and the measured inclination of the luminous ellipsoid from the z axis. As it is discussed in [11], the luminosity depends on the beam profiles along x, while the beam imaging gives the widths $\sigma_{x1,2}$ of the profiles perpendicular to the beams. Due to the crossing angle $\alpha = 170$ μrad, the former is broader due to

a contribution from the z-length of the bunch. To correct for this effect we assumed that the bunches of two beams were of the same length and determined it from the width of the luminous region as $\sqrt{2}\sigma^z_{\rm Lum}$. The widths of van der Meer luminosity versus separation curves finally can be obtained as $\sqrt{\sigma^2_{x1}+\sigma^2_{x2}+4(\sigma^z_{\rm Lum})^2\alpha^2}$, their ratio with the measured values is show in Fig. 30. The points (band) corresponds to the central values (one sigma change) of the vertex resolution parameters. As one can see the method is very sensitive, the band width is about 1.2% and the RMS spread of the points is 0.5-0.8%. Assuming equal weights of the points, they were fit to a constant. The obtained average ratio is compatible with unity within 0.4-0.6%. This proves both the widths of van der Meer luminosity versus separation curves which effectively enter the cross section formula (1), and the vertex resolution at LHCb which is important in the beam-gas luminosity determination.

Table 7: VELO vertex resolution parameters and their errors.

	x	y
σ, μm	0.2148 ± 0.01962	0.2023 ± 0.01806
α	1.023 ± 0.05375	1.008 ± 0.05257
δ, $\times 10^{-3}$ μm	5.463 ± 0.675	4.875 ± 0.6451

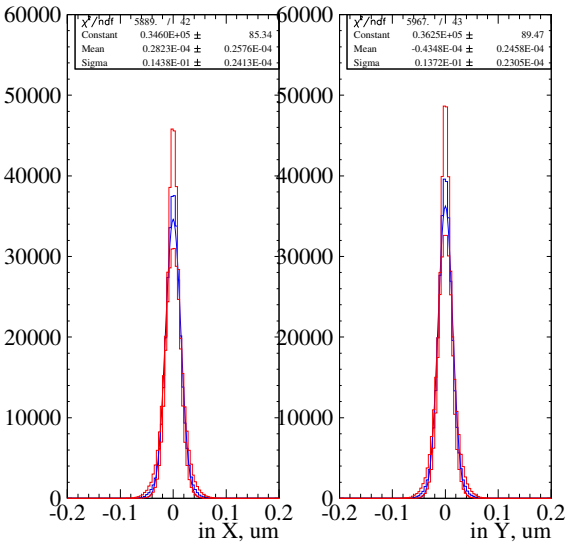

Figure 28: VELO resolution functions obtained for the observed distribution of the number of vertex tracks N. Middle curve corresponds to the central values of σ, α and δ resolution parameters discussed in the text. Narrower and wider curves are obtained for the parameters simultaneously shifted by one sigma in the direction minimizing or maximizing the resolution.

The width of van der Meer Δx curve was also checked by measuring the z-movement of the luminous center dur-

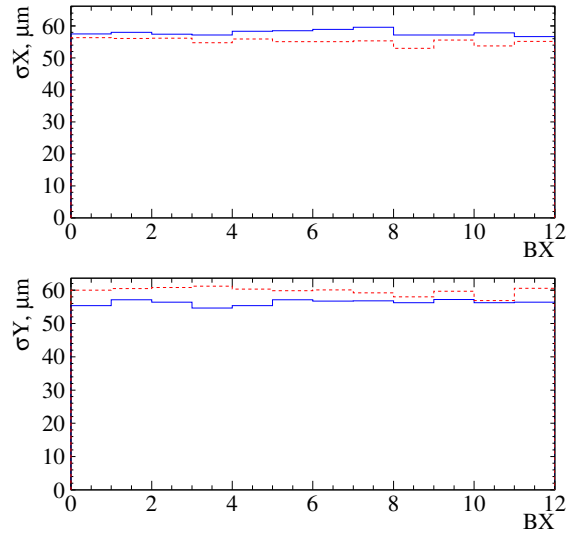

Figure 29: Gaussian widths of the reconstructed beam profiles after unfolding with VELO resolution in the plane transverse to the beam in different bunch crossings. Solid blue (dashed red) curves are for the first (second) beam.

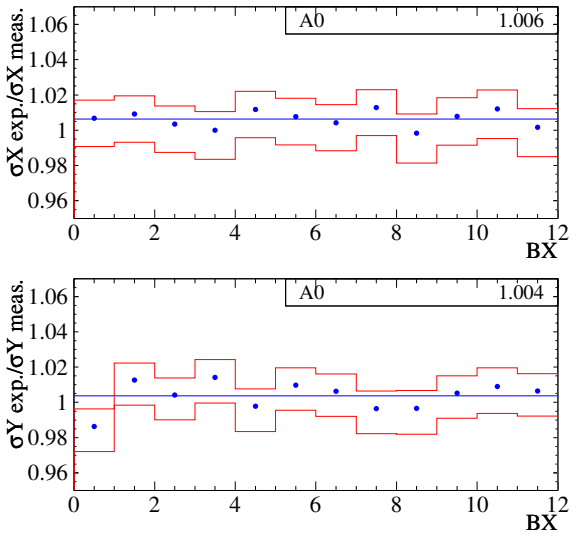

Figure 30: Ratio of expected from the reconstructed beam images and measured widths of van der Meer luminosity versus Δx (top) or Δy (bottom) curves in different bunch crossings. The band corresponds to one sigma variation of the resolution parameters. The points are fit to a constant, the result is shown in the top right corner.

ing the first scan in x. It is shown in Fig. 31. According to [13], in case of identical beams the slope should be equal to

$$\frac{\delta z}{\Delta x} = \frac{\sin 2\alpha}{4} \frac{\sigma_z^2 + \sigma_x^2}{\sigma_x^2 \cos^2\alpha + \sigma_z^2 \sin^2\alpha},$$

where $\sigma_{x,z}$ are the transverse and longitudinal beam widths, δz is the induced z-shift of the luminous center. We approximate again σ_z as $\sqrt{2}\sigma^z_{\rm Lum}$. Since VELO resolution in z is much better than $\sigma^z_{\rm Lum} = 52.0 \pm 0.3$ mm, it is neglected. Using the slope from Fig. 31 one gets the expected width of van der Meer Δx curve $\sigma_x^{\rm VDM} = \sqrt{2}\sigma_x = 78$ μm in agreement with the measured value of 80 μm.

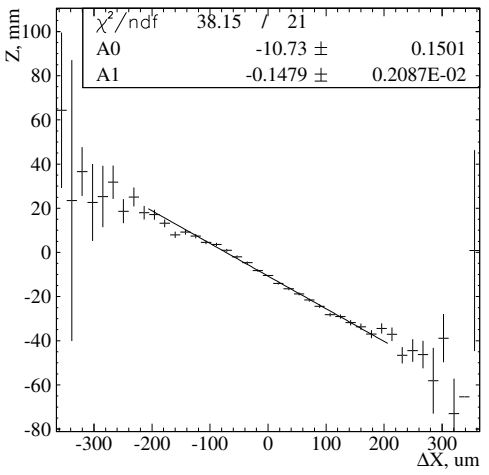

Figure 31: Movement of the luminous center in z during the first scan in Δx. The slope (A1) is given in the top right corner.

CONCLUSIONS

The absolute calibration of luminosity was performed in LHCb in 2010 using two van der Meer scans and the beam-gas method. They gave similar accuracy dominated by the bunch intensity uncertainties. Here we concentrate on the results of van der Meer scans in April and in October. The visible cross section is measured for events having at least two VELO tracks in R-Z projection. The fraction of such events in randomly triggered sample is continuously monitored during LHCb data taking. This allows to extrapolate our measurements to the whole LHCb statistics.

The cross section results are given in Table 8[1]. They are all consistent with each other. For the final LHCb luminosity calibration we averaged the cross sections measured in the first scan in October and in the beam-gas method. During the second scan in October the beam movements were not continuous, so the results might suffer from the hysteresis effects. Both in April and in October measurements the difference between the scans was included as a systematic error. The complete list of errors is given in Tables 9 and 10.

Table 8: Cross section of the interaction producing at least two VELO tracks in R-Z projection, measured in two van der Meer scans in April and in October and obtained with the beam-gas method. Cross sections from the first October scan and from the beam-gas analysis were averaged for the final LHCb luminosity calibration in 2010.

	$\sigma(RZ)$, mb	rel. error, %
April	59.6, 57.0	7.5
October	**58.4**, 57.1	3.6
Beam-gas method	**60.8**	4.5

Table 9: Summary of cross section relative errors for van der Meer scan in April. Last column contains correction to the cross sections listed in Table 5.

Source	error, %	corr., %
$I_1 \times I_2$	5.6	
Diff. btw. scans	4.4	
Length scale	2	
Stat. error	0.9	
RZVelo stability	0.5	
Ghosts in other BX	0.08	+0.14
Ghosts in ± 2 RF	neglig.	
$I_1 \times I_2$ drop	neglig.	
Emittance growth	neglig.	
Total	7.5	

In the future van der Meer scans in 2011 the DC BCT accuracy should be improved. Note, that Fast BCT did not contribute to October systematics since we determined the Fast BCT offsets directly from the fit, and therefore the statistical error 0.09% already includes this contribution. With significantly improved BCT scale uncertainty, the error will be dominated by non reproducibility of the scans. This is not fully understood but may be attributed to the uncertainties in the beam positions during the scan. Note, that there is always a very good agreement between different bunches, so the problem should be in the beam as a whole.

To push the error further down one may think of either the precise measurement of the beam positions or of precisely controllable beam movements, which should not necessarily be linear but may be more complicated, e.g. sinusoidal.

To study systematic effects further it will be advantageous to have as different bunches as possible. Difference in bunch intensities may provide better sensitivity to the Fast BCT offset measurement. Comparing the bunches with high and low intensities allows to estimate possible beam-beam effects. Broad and narrow bunches could help reveal systematics which depends on the bunch shapes.

[1] The beam-gas results is an update of [6]

Table 10: Summary of cross section relative errors for van der Meer scan in October. Last column contains corrections to the cross section central values from Table 4 with Fast BCT intensities.

Source	error, %	corr., %
BCT scale	2.7	
Diff. btw. scans	2.1	
Length scale	1	-1.3
RZVelo stability	0.5	
Working point stability	0.4	
Non-diag. xy cov.matrix	0.3	
Ghosts in other BX	0.15	+0.66
Ghosts in ± 2 RF	0.1	
Beam scale difference	0.1	
Stat. error	0.09	
$I_1 \times I_2$ drop	neglig.	
Emittance growth	neglig.	
Total	3.6	

In LHCb it is also very advantageous to perform beam-gas measurements during van der Meer LHC fill.

APPENDIX

Here were calculate the cross section correction in case when the beam profiles are two-dimensional Gaussians of the general type with non zero x-y correlation term,

$$\rho_{1,2}(r) = \frac{1}{\sqrt{|2\pi\Sigma_{1,2}|}} \exp(-\frac{1}{2}(r - r_{1,2})^T \Sigma_{1,2}^{-1}(r - r_{1,2})).$$

Here

$$\Sigma_{1,2} = \begin{bmatrix} \Sigma_{x1}^2 & \xi_{1,2}\Sigma_{x1,2}\Sigma_{y1,2} \\ \xi_{1,2}\Sigma_{x1,2}\Sigma_{y1,2} & \Sigma_{y1,2}^2 \end{bmatrix}, \; r_{1,2} = \begin{bmatrix} x_{1,2} \\ y_{1,2} \end{bmatrix}$$

are the covariance matrices and Gaussian centers. $|2\pi\Sigma_{1,2}|$ denote the determinants of the matrices $2\pi\Sigma_{1,2}$. It may be shown that the overlap integral $\rho = \int \rho_1(r)\rho_2(r)\, d^2r$ is

$$\rho(\Delta r) = \frac{1}{\sqrt{|2\pi\Sigma_0|}} \exp(-\frac{1}{2}\Delta r^T \Sigma_0^{-1} \Delta r),$$

where

$$\Delta r = r_1 - r_2 = \begin{bmatrix} \Delta x \\ \Delta y \end{bmatrix},$$

$$\Sigma_0 = \Sigma_1 \frac{1}{\Sigma_1 + \Sigma_2} \Sigma_2 = \begin{bmatrix} \Sigma_{x0}^2 & \xi_0\Sigma_{x0}\Sigma_{y0} \\ \xi_0\Sigma_{x0}\Sigma_{y0} & \Sigma_{y0}^2 \end{bmatrix}$$

are the beam separations and the two-dimensional analog of the width of van der Meer luminosity versus separation function. The analog of the luminous width is $\Sigma = \Sigma_1 + \Sigma_2$. If the Δx-Δy correlation coefficient is not zero, $\xi_0 \neq 0$, the cross section formula (1) should be modified. Instead of Δr it is convenient to use the normalized coordinates

$$\chi = \begin{bmatrix} \chi_x \\ \chi_y \end{bmatrix} = \begin{bmatrix} \Delta x/\Sigma_{x0} \\ \Delta y/\Sigma_{y0} \end{bmatrix}.$$

Since

$$\Sigma_0^{-1} = \frac{1}{1-\xi_0^2} \begin{bmatrix} 1/\Sigma_{x0}^2 & -\xi_0/\Sigma_{x0}/\Sigma_{y0} \\ -\xi_0/\Sigma_{x0}/\Sigma_{y0} & 1/\Sigma_{y0}^2, \end{bmatrix}$$

we have then

$$\Delta r^T \Sigma_0^{-1} \Delta r = \chi^T \widetilde{\Sigma}_0^{-1} \chi$$

where

$$\widetilde{\Sigma}_0 = \begin{bmatrix} 1 & \xi_0 \\ \xi_0 & 1 \end{bmatrix}$$

and

$$\rho(\chi) = \frac{1}{2\pi\Sigma_{x0}\Sigma_{y0}\sqrt{1-\xi_0^2}} \exp\left(-\frac{\chi_x^2 - 2\xi_0\chi_x\chi_y + \chi_y^2}{2(1-\xi_0^2)}\right).$$

We'll denote the cross section calculated from Eq. (1) by $\sigma_{\rm fact}$ since it is valid only in the case of x-y factorization. The general formula is

$$\sigma_{\rm true} = \frac{\int \mu(\Delta x,\, \Delta y)\, d\Delta x\, d\Delta y}{N_1 N_2 \cos\alpha},$$

and the required correction

$$\frac{\sigma_{\rm true}}{\sigma_{\rm fact}} = \frac{\mu(\Delta x_0,\, \Delta y_0) \cdot \int \mu(\Delta x,\, \Delta y)\, d\Delta x\, d\Delta y}{\int \mu(\Delta x,\, \Delta y_0)\, d\Delta x \cdot \int \mu(\Delta x_0,\, \Delta y)\, d\Delta y}.$$

With the non-diagonal covariance matrix, if

$$\mu(\Delta x_0,\, \Delta y_0) \propto \exp\left(-\frac{\chi_{x0}^2 - 2\xi_0\chi_{x0}\chi_{y0} + \chi_{y0}^2}{2(1-\xi_0^2)}\right),$$

then with the same proportionality factor

$$\int \mu(\Delta x,\, \Delta y)\, d\Delta x\, d\Delta y \propto 2\pi\Sigma_x\Sigma_y\sqrt{1-\xi_0^2},$$

$$\int \mu\, d\Delta_i \propto \int \exp\left(-\frac{(\chi_i - \xi_0\chi_{y0})^2 + (1-\xi_0^2)\chi_{y0}^2}{2(1-\xi_0^2)}\right) \times$$

$$\times\, d(\Sigma_i\chi_i) = \sqrt{2\pi(1-\xi_0^2)}\Sigma_i \exp\left(-\frac{\chi_{y0}^2}{2}\right),$$

where $i = x, y$ and $(\chi_{x0},\, \chi_{y0})$ denote the normalized coordinates of the crossing point $(\Delta x_0/\Sigma_{x0},\, \Delta y_0/\Sigma_{y0})$. Therefore, *the measured widths* of van der Meer μ versus Δ_i functions are

$$\Sigma_{x,y}^{\rm meas} = \Sigma_{x,y}\sqrt{1-\xi_0^2}.$$

Finally,

$$\frac{\sigma_{\rm fact}}{\sigma_{\rm true}} = \sqrt{1-\xi_0^2} \exp\left(-\frac{\xi_0\chi_{x0}\chi_{y0}}{1-\xi_0^2} + \frac{\xi_0^2(\chi_{x0}^2 + \chi_{y0}^2)}{2(1-\xi_0^2)}\right)$$

$$\approx 1 - \frac{\xi_0^2}{2} - \xi_0\chi_{x0}\chi_{y0}$$

The exponent term coming from $\mu(\Delta x_0,\, \Delta y_0)$, gives a correction only if the crossing point $(\chi_{x0},\, \chi_{y0})$ is not centered at zero. For the October LHCb scan it is negligible. The coefficient ξ_0 is determined by the covariance matrices of both beams $\Sigma_{1,2}$. It is impossible to obtain it only from the measurable matrix $\Sigma = \Sigma_1 + \Sigma_2$ of the luminous region. However, for the systematic error estimation we assumed that ξ_0 is at the same level as the correlation coefficient in Σ (0.077), which is the case e.g. for the similar beam covariance matrices.

REFERENCES

[1] H. Dijkstra and O. Schneider, "Online and offline monitoring of the relative luminosity at LHCb", LHCb note 2008-034.

[2] V. Balagura, "Analysis methods for luminosity data", LHCb note LHCb-INT-2009-001.

[3] M. Ferro-Luzzi, Nucl. Instrum. and Methods A 553 (2005) 388.

[4] R. Aaij *et al.*, LHCb collaboration, Phys. Lett. B 693 (2010) 69.

[5] R. Aaij *et al.*, LHCb collaboration, Phys. Lett. B 694 (2010) 209.

[6] P.Hopchev, "LHCb beam-gas imaging results", contribution to this LHC Lumi Days workshop, CERN (2011).

[7] Van der Meer, "Calibration of the Effective Beam Height in the ISR", internal CERN report, ISR-PO/68-31 (1968).

[8] G. Anders *et al.*, "LHC Bunch Current Normalisation for the April-May 2010 Luminosity Calibration Measurements", CERN-ATS-Note-2011-004 PERF.

[9] G. Anders *et al.*, "LHC Bunch Current Normalisation for the October 2010 Luminosity Calibration Measurements", CERN-ATS-Note-2011-016 PERF.

[10] J.J. Gras, M Ludwig and P. Odier, "The 2010 LHC DC BCT measurement system and its main sources of uncertainties", CERN-LHC-Project-Note-432;
D. Belohrad, J.J. Gras, M. Ludwig, "The 2010 LHC ring Fast BCT measurement system and its main sources of uncertainties", CERN-LHC-Project-Note-433;
D. Belohrad *et al.*, "Commissioning and First Performance of the LHC Beam Current Measurement Systems", 1st IPAC, Kyoto, Japan, 23 - 28 May 2010.

[11] V. Balagura, "Notes on van der Meer Scan for Absolute Luminosity Measurement", arXiv:1103.1129 [physics.ins-det], submitted to Nucl. Instrum. and Methods A.

[12] C. Lasseur *et al.*, "Gomtrie Du LHC : Points Caractristiques, Formules De Transformation", CERN-LHC-Project-Note-95 (1997).

[13] M. Ferro-Luzzi, private communication.

LHCb BEAM-GAS IMAGING RESULTS

P. Hopchev, LAPP, IN2P3-CNRS,
Chemin de Bellevue, BP110, F-74941, Annecy-le-Vieux
For the LHCb Collaboration

Abstract

The high resolution of the LHCb vertex detector makes it possible to perform precise measurements of vertices of beam-gas and beam-beam interactions and allows beam parameters such as positions, angles and widths to be determined. Using the directly measured beam properties the novel beam-gas imaging method is applied in LHCb for absolute luminosity determination. In this contribution we briefly describe the method and the preliminary results obtained with May 2010 data.

INTRODUCTION

The methods for measuring the absolute luminosity are generally divided into indirect and direct ones. Some of the indirect methods to be used at the LHC are:

- Optical Theorem - can be used to determine the absolute luminosity without knowing the beam intensities. ALTAS-ALFA [1] and TOTEM [2] are going to measure the elastic scattering of protons with detectors located about 200 m away from IP 1 and 5 respectively.
- Use precisely calculable process. For example in e+/e- colliders the Bhabha scattering process is used. At LHC the most promising candidates are the QED processes of Z and elastic muon pair production, both of which are going to be used in LHCb. A more complete description of the prospects for these measurements can be found elsewhere in these proceedings [3].
- Reference cross-section - once any absolute cross-section has been measured it can be used as a reference to calculate the cross-section for other processes.

The direct methods determine the luminosity by measuring the beam parameters:

- Wire method [4] - scan thin wires across the beams and measure rates.
- Van der Meer method [5] - scan beams across each other and measure rates.
- Beam-gas imaging method [6] - reconstruct beam-gas interaction vertices to measure the beam angles, positions and shapes. Results from the application of this method are discussed in this contribution.
- Beam imaging during van der Meer scan - a recently proposed method [7] to measure the beam profiles and overlap by vertex reconstruction of beam-beam interactions.

For absolute luminosity normalization in 2010 the LHC and each of its large experiments performed van der Meer scans. Detailed descriptions of the procedure and the results can be found elsewhere in these proceedings [8, 9, 10, 11].

The beam-gas method for absolute luminosity determination was proposed by M. Ferro-Luzzi in 2005 and was applied for a first time in LHCb (see [12, 13, 14]) using the first LHC data collected in the end of 2009. This measurement represents the only absolute cross-section normalization performed by the LHC experiments at 900 GeV.

In this contribution we report on the further application and results of the method, using 7 TeV center-of-mass energy data collected by LHCb in 2010. Apart from the common beam current measurement, the beam-gas imaging provides an absolute luminosity normalization, which is independent from the one obtained with the van der Meer method.

BEAM-GAS IMAGING METHOD

The luminosity for a single pair of counter-rotating bunches can be expressed with the following general formula [15]:

$$L \;=\; f N_1 N_2 K \int \rho_1(\vec{r},t)\rho_2(\vec{r},t)\; d^3\vec{r}\, dt, \qquad (1)$$

where f is the bunch revolution frequency, N_i are the number of particles in the colliding bunches, $K = \sqrt{(\vec{v_1}-\vec{v_2})^2 - \frac{(\vec{v_1}\times\vec{v_2})^2}{c^2}}$ is the Møller kinematic relativistic factor, c is the speed of light, $\vec{v_i}$ are the bunch velocities and $\rho_i(\vec{r},t)$ are the bunch densities, normalized such that their integral over full space is equal to 1 at any moment t: $\int \rho_i(\vec{r},t)\; d^3\vec{r}\, dt = 1$.

As described in [7], for the case of no crossing angle, the luminosity formula can be written as a function only of the transverse profiles of the colliding bunches $\rho_i^{\perp}(x,y)$:

$$L \;=\; f N_1 N_2 \int \rho_1^{\perp}(x,y)\rho_2^{\perp}(x,y)\; dx\, dy \qquad (2)$$

The effect on the luminosity for the case of non-collinear beams is described later, in the section *Analysis Overview*. The beam-gas imaging method aims at measuring the overlap integral for a given bunch-pair by measuring the angles, offsets and transverse profiles of the two colliding bunches. This is achieved by reconstructing beam-gas interaction vertices. The gas used as a *visualizing medium* can be the residual gas in the beam vacuum pipe, which

consists mainly of relatively light atoms like hydrogen, carbon and oxygen, or a specially designed gas-injection system can be used to create a controlled pressure bump in the region of the LHCb vertex detector. The later would allow to perform the beam profile measurements in a shorter time, thus reducing the effects from potential beam instability. In addition, the injection of gas with high atomic number, like xenon, will result in high multiplicity interaction vertices and improved primary vertex resolution.

An important prerequisite for the proper reconstruction of the bunch profiles is the transverse homogeneity of the visualizing gas. A dedicated test performed in October 2010 measured the beam-gas interaction rates as function of beam displacement in a plane perpendicular to the beam axis. The beams were moved within ± 150 μm (approximately 3 times the beam width) from their nominal position in both x and y. This allowed us to set a limit on the distortion of the measured beam profiles due to transverse inhomogeneity of the residual gas. The needed beam overlap correction from a non-uniform transverse distribution of the residual gas was found to be smaller than 0.05% and was neglected.

The principal precision limitations of the beam-gas method are:

- Vertex resolution - its knowledge plays increasingly important role as the beam sizes become smaller than the resolution.
- Beam-gas rate - determines the time needed to *snapshot* the beam profiles and the associated statistical uncertainty.
- Beam stability - in case of fluctuations of the beam orbits and sizes non-trivial systematic effects need to be taken into account.

It is important to note that in contrast to the van der Meer method the beam-gas imaging method does not involve movement of the beams. This means that possible beam-beam effects are constant and potential effects which depend on the beam displacement, like hysteresis, can be avoided. Furthermore, the beam-gas imaging method is applicable during physics fills.

PRELIMINARY RESULTS FROM MAY 2010 DATA

LHCb [16] is a forward spectrometer covering the pseudo-rapidity range of $\eta \in [2; 5]$. It is equipped with a vertex detector (Vertex Locator, VELO), positioned around the interaction point. The VELO consists of two retractable halves, each having 21 modules of radial and azimuthal silicon-strip sensors with half-circle shape, see Fig. 1. Its excellent acceptance for beam-gas and beam-beam interactions is determined by its length of almost a meter and the small inner radius of the sensors, which approach the beam to merely 8 mm when the VELO is at its nominal, closed position. The two most upstream stations (left side of figure 1), the so called *Pile-Up System*, are used in the Level-0 trigger. The VELO is the sub-detector essential for the application of the beam-gas imaging method at LHCb.

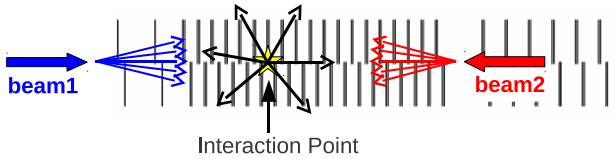

Figure 1: A sketch of the VELO, including the 2 Pile-Up stations on the left. The thick arrows indicate the direction of the LHC beams (beam1 going from left to right), while the thin ones show example directions of flight of the products of the beam-gas and beam-beam interactions.

Running Conditions and Beam-gas Trigger

The data used for the results described in this contribution was taken in May 2010 when there were between 2 and 13 bunches per beam and the number of colliding pairs at LHCb varied between 1 and 8. The trigger included a dedicated selection for events containing beam-gas interactions. The relevant hardware (Level-0) triggers are:

- Beam1-gas: select events with a Calorimeter transverse energy sum larger than 3 GeV and a Pile-Up System multiplicity lower than 40.
- Beam2-gas: select events with a Calorimeter transverse energy sum smaller than 6 GeV and a Pile-Up System multiplicity larger than 9.

These triggers were enabled in all b-e and e-b crossings (throughout this contribution 'e' is used for denoting an empty bunch slot and 'b' - a bunch slot filled with protons). For the colliding bunches no beam-gas Level-0 trigger was used and the beam-gas events were selected only if they passed any of the 'physics' trigger channels or if they happen to coincide with a proton collision, which fired any of the Level-0 trigger channels. In May 2010 the LHCb hardware trigger was non-selective and the beam-gas interactions in b-b crossings were triggered efficiently. At the High Level Trigger a simple proto-vertexing algorithm selected events by looking for accumulation of tracks around a point on the z axis. The same algorithm was used for the b-e, e-b and b-b crossings, but different z-selection cuts were applied. For example during b-b crossings only interactions with $z < -350$ mm or $z > 250$ mm were selected.

VELO Vertex Resolution

The VELO primary vertex resolution was determined from data in the following way. We randomly split the reconstructed VELO tracks in two equal samples, run a vertexing algorithm on each of them and require that the two reconstructed vertices have equal number of tracks. The width of the distribution of the distance between the two vertices divided by $\sqrt{2}$ gives the resolution estimate for the

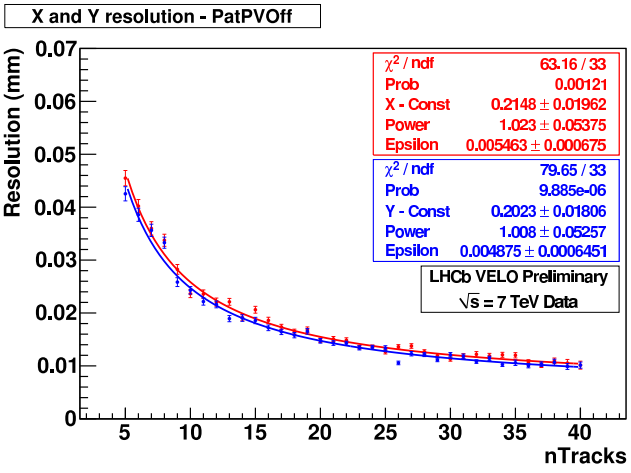

(a) Beam-beam resolution in x and y.

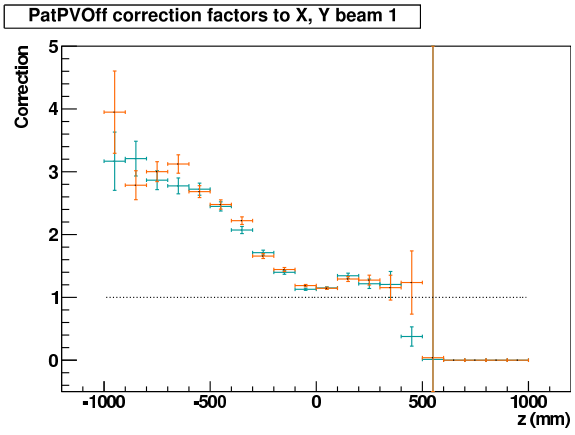

(b) Beam1-gas resolution correction factor in x and y.

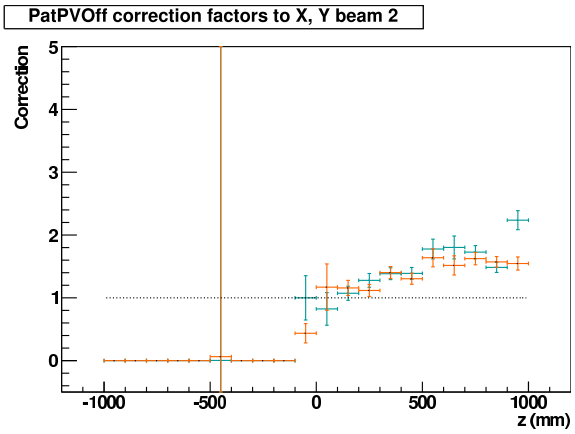

(c) Beam2-gas resolution correction factor in x and y.

Figure 2: (a) VELO primary vertex resolution in the transverse directions x and y for beam-beam interactions. (b) and (c) resolution corrections in x and y for beam1-gas and beam2-gas interactions, accounting for the z-dependence of the resolution.

half-track vertices. The resolution is parametrized with a Gaussian in two steps. First we estimate the resolution for beam-beam interactions as function of the number of tracks in the vertex, see Fig. 2(a). The used parametrization function has the following form:

$$R(N) = \frac{\sigma_0}{N^{0.5+\frac{\delta}{N^2}}} + \epsilon, \qquad (3)$$

where σ_0 is a parameter determining the resolution for small number of tracks, N is the number of tracks per vertex, the power δ accounts for the deviation from the $1/\sqrt{N}$ behavior and ϵ is the asymptotic resolution for large number of tracks per vertex. Later, by comparing the resolution for beam-gas and beam-beam vertices with the same number of tracks, we calculate a correction factor which takes into account the z-dependence of the resolution. Fig. 2(b) and Fig. 2(c) show the beam-gas correction factor as function of z. Finally, the parametrized vertex resolution is used to unfold the true size of the beams.

Analysis Overview

To measure the beam positions and transverse profiles we plot the position of the beam-gas vertices in the x-z and y-z planes. In Fig. 3 we show an example for the case of b-e and e-b crossings. The straight line fits provide the beam angles in the corresponding planes. In general we observe an agreement between the expected and measured beam angles. It is important to note that the colliding bunches are the only relevant ones for the luminosity measurement, because we need to measure the overlap integral for the colliding bunch-pairs.

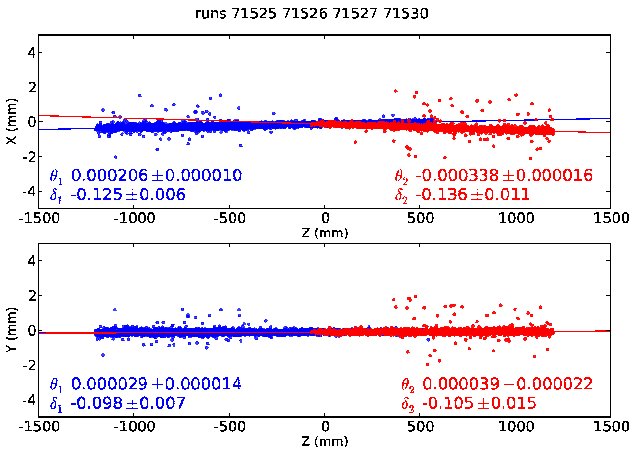

Figure 3: Position of reconstructed beam-gas interaction vertices during b-e and e-b crossings for a May 2010 fill. The measured crossing angles in the horizontal and vertical planes (544 ± 26 and -10 ± 36 μrad respectively) agree reasonably well with the expectations (540 and 0 μrad respectively).

The bunch x and y profiles are obtained from the projection of the x-z and y-z beam-gas vertex distributions onto a plane perpendicular to the beam direction. As an example

in Fig. 4 we show the x and y profiles of three colliding bunch-pairs.

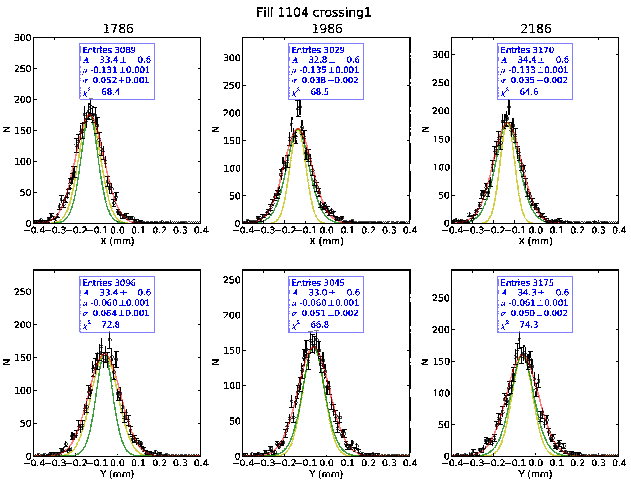

(a) Bunches of beam1. Top: x profile, Bottom: y profile.

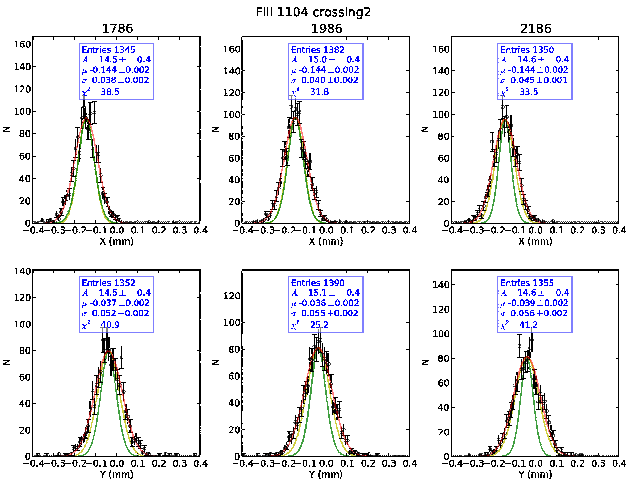

(b) Bunches of beam2. Top: x profile, Bottom: y profile.

Figure 4: x and y profiles of three colliding bunch-pairs. The different lines represent the raw measured size, the vertex resolution and the unfolded size.

The true bunch size is obtained after deconvolving the vertex resolution. Equally importantly, we use the following relations between the position and size of the luminous region (μ_{BB} and σ_{BB}) and the positions and sizes of the individual beams (μ_1, μ_2, σ_1 and σ_2) as a constraint in the fits.

$$\sigma_{BB}^2 = \frac{\sigma_1^2\sigma_2^2}{\sigma_1^2+\sigma_2^2} \qquad \mu_{BB} = \frac{\mu_1\sigma_2^2+\mu_2\sigma_1^2}{\sigma_1^2+\sigma_2^2} \qquad (4)$$

This improves significantly the precision of the beam size measurements.

The calculation of the overlap integral is done initially by integration of the product of two Gaussians representing the widths and positions found with the procedure mentioned above. As the beam profiles are measured in a plane perpendicular to the beam direction we have not yet taken into account the fact that the bunches are tilted and do not collide head-on. The crossing angle correction to be applied on the overlap integral can be approximated with the following formula:

$$C_{\text{crossing angle}} = \sqrt{1+\left(\frac{\theta_c\,\sigma_z}{\sigma_x}\right)^2}, \qquad (5)$$

where θ_c is the half crossing angle and σ_x and σ_z are the bunch sizes in the crossing angle plane. The longitudinal beam size is measured from the beam spot assuming that the two beams have equal size. For the beam conditions in May 2010 the crossing angle overlap correction factor was about 0.95. Formula 5 is a good approximation for the case of no transverse offsets and equal bunch sizes. We now use a numerical calculation which makes a small difference (0.5%).

Preliminary Results with May 2010 Data

With the use of the beam-gas imaging method and following the outlined procedure we performed seven independent measurements of an LHCb-specific reference cross-section. The beam currents, essentially needed for this method, were obtained following the same procedure as described in [17]. The main uncertainties contributing to the overall precision of the cross-section measurement come from the bunch widths (3%), their relative positions (3%) and crossing angle (1%). The measurement of the beam intensities was done with precision of 5% and has dominant contribution to the overall uncertainty. The preliminary results of the analysis are summarized in Fig. 5. For multi-bunch fills the results obtained for each colliding pair were averaged.

The absolute scale knowledge is propagated through the full LHCb dataset with the use of several independent luminosity monitors.

CONCLUSIONS

The beam-gas imaging method was applied on data collected by LHCb in May 2010 and provided an absolute luminosity normalization with uncertainty of 10%, dominated by the knowledge of the beam intensities. The measured LHCb-specific cross-section is in agreement with the measurement performed with the van der Meer method.

In the beginning of 2011 a more refined analysis was performed, providing an improved precision of the beam parameters measured by LHCb. Most notably this later analysis profited from an improved knowledge of the beam currents which allowed a significant reduction of the absolute luminosity normalization uncertainty.

Further precision improvements are possible in dedicated fills with broader beams or fills where both beam-gas and van der Meer methods can be applied simultaneously. In a addition, a controlled pressure bump in the LHCb interaction region would allow us to apply the beam-gas imag-

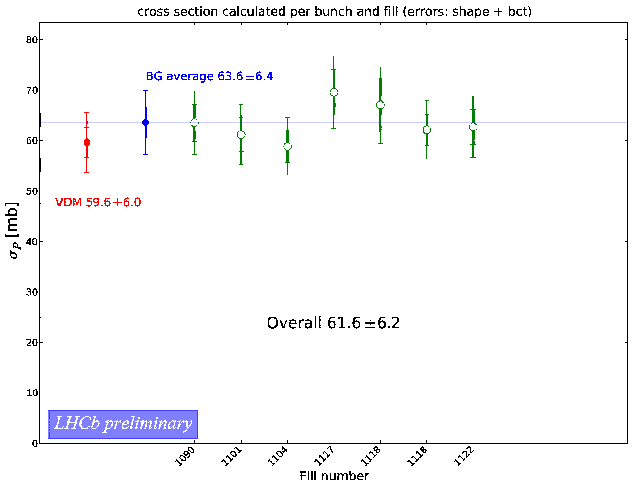

Figure 5: Preliminary results for an LHCb-specific cross-section measured with the beam-gas imaging method. The results for seven different physics fills taken in May 2010 are compared with the ones obtained from a van der Meer scan performed in April 2010.

ing method in a shorter time, decreasing the effects from beam instabilities.

REFERENCES

[1] The ATLAS Collaboration, Review of the ATLAS Technical design report on the forward detectors for the measurement of elastic scattering and luminosity, CERN-LHCC-2008-004, ATLAS TDR 18 (2008).

[2] The TOTEM Collaboration, TOTEM Technical Design Report, CERN-LHCC-2004-002, TOTEM-TDR-001.

[3] J. Anderson, Prospects for indirect luminosity measurements at LHCb, LHC Lumi Days workshop, CERN (2011).

[4] J. Bosser et al., Nucl. Instrum. Methods A235 (1985) 475

[5] S. van der Meer, Calibration of the effective beam height in the ISR, ISR-PO/68-31 (1968).

[6] M. Ferro-Luzzi, Nucl. Instrum. Methods A553 (2005) 388.

[7] V. Balagura, Notes on van der Meer Scan for Absolute Luminosity Measurement, arXiv:1103.1129v1, submitted to Nucl. Instrum. Methods A

[8] K. Oyama, ALICE 2010 Luminosity Determination, LHC Lumi Days workshop, CERN (2011).

[9] M. Huhtinen, ATLAS 2010 Luminosity Determination, LHC Lumi Days workshop, CERN (2011).

[10] M. Zanetti, CMS 2010 Luminosity Determination, LHC Lumi Days workshop, CERN (2011).

[11] V. Balagura, LHCb 2010 Luminosity Determination, LHC Lumi Days workshop, CERN (2011).

[12] The LHCb Collaboration, Prompt K-short production in pp collisions at sqrt(s)=0.9 TeV, arXiv:1008.3105v2.

[13] V. Balagura, Luminosity measurement in the first LHCb data, proceedings of Rencontres de Moriond QCD and High Energy Interactions, 2010.

[14] P. Hopchev, The beam-gas method for luminosity measurement at LHCb, proceedings of Rencontres de Moriond Electroweak Interactions and Unified Theories, 2010.

[15] O. Napoly, Particle Acc., 40 (1993) 181.

[16] The LHCb collaboration, The LHCb Detector at the LHC, JINST 3 S08005 (2008).

[17] G. Anders et al., LHC Bunch Current Normalisation for the April-May 2010 Luminosity Calibration Measurements, CERN-ATS-Note-2011-004 PERF.

Beams scan based Absolute Normalization of the CMS Luminosity Measurement

M. Zanetti, MIT, Cambridge, MA 02142, USA

Abstract

A campaign of dedicated measurements based on the scan of the LHC beams in the transverse plane at the interaction points have been performed in October 2010. Based on a technique first proposed by Van der Meer, these experiments are used to determine the effective crossing area of the beams that together with the measurement of the beam currents provide an absolute estimation of the LHC luminosity. This document describes the analysis of the CMS data collected during such beam scans and summarizes the results concerning the normalization factor exploited to evaluate the integrated luminosity delivered at the CMS interaction point.

INTRODUCTION

The precise measurement of the production cross sections is a key component of the LHC physics program. The accurate determination of the accelerator luminosity and its related uncertainties is therefore mandatory to achieve this result. The CMS detector [1] exploits the measurements of the forward hadronic calorimeters (HF) to estimate the instantaneous luminosity in real time [2] (in the following referred to 'HF online' method), by means of a dedicated data acquisition system. The event data logged by the central DAQ are also used offline ('HF offline' and 'vertex counting' methods) as cross checks of the online estimates.

A commonly used way to calibrate the instantaneous luminosity measurement consists in determining at the same time in a dedicated experimental setup, both the event rate (R_0) and the absolute luminosity (L_0) on the basis of the beam and optics parameters

$$R_0/L_0 = \sigma_{vis} \tag{1}$$

The quantity σ_{vis} (visible cross section) is then used as constant factor to obtain the instantaneous luminosity during the standard physics operations:

$$L(t) = R(t)/\sigma_{vis} \tag{2}$$

A method originally proposed by Simon Van der Meer and first exploited at the CERN ISR [3] has been adopted at the LHC during the 2010 run [4]. The procedure consists in scanning the beams against each other in the transverse plane to determine their overlap region, hereafter named effective area (A_{Eff}). At the same time the individual bunch currents are measured by dedicated devices (DC BCT and fast BCT [5]). The mathematical bases of the method are described in details for instance in [6], here we only summarize the relevant conclusions. We assume that beams' directions are parallel and that the tridimensional particle density functions can be factorized into the product of three independent one-dimensional functions ($\rho(\vec{r},t) = \rho_x(x)\rho_y(y)\rho_z(z,t)$). Both these assumptions will be discussed later. The luminosity (and thus the interaction rate) dependence on the beams displacements $\Delta x, \Delta y$ in the transverse plane results in this case to be:

$$\frac{L(\Delta x,\Delta y)}{\nu N_1 N_2} = \frac{R(\Delta x,\Delta y)}{\nu N_1 N_2 \sigma_{vis}} = \int \rho_{1,x}(x)\rho_{2,x}(x-\Delta x)dx \int \rho_{1,y}(y)\rho_{2,y}(y-\Delta y)dy \tag{3}$$

Where we considered only two circulating bunches with frequency ν and total charge population N_1 and N_2 for beam 1 and beam 2. The visible cross section can then be measured by separating the beams in the transverse plane and by integrating in $\Delta x \Delta y$ over the whole plane, obtaining:

$$\sigma_{vis} = \frac{\int R(\Delta x,\Delta y_0)d\Delta x \cdot \int R(\Delta x_0,\Delta y)d\Delta y}{\nu N_1 N_2 R(\Delta x_0,\Delta y_0)} \tag{4}$$

It is worth noticing that this formulation does not set any requirements on the original beam separation $\Delta x_0, \Delta y_0$ (those who are not integrated out), in particular they do not need to be exactly null, i.e. a perfect overall is not necessary at the beginning of the transverse plane scan [6].

In the traditional Van der Meer method, the information related to the luminous region, i.e. the distribution of the collision vertices at the interaction point, is integrated away (cfr. Formula 3). A modern collider experiment as CMS features extremely powerful tracking and vertexing devices, capable of reconstructing collision vertices with a precision of $\mathcal{O}(10)$ micrometers [7]. Recently a new approach has been proposed which makes use of the luminous region as measured by the detector and exploits that to estimate the effective area by means of the reconstruction of the individual beam shapes [6]. The basic idea is rather simple and consists in inverting the integrations in Equations 3 and 4, i.e. first perform the integration over the beam separation and then on the coordinate variable. Hereafter we refer to the scan coordinate as ξ with the latter corresponding with enough precision to either of the CMS transverse axes. Still assuming the possibility of factorizing the density functions, we get for the rate $R(\xi)$ the following relation:

$$R(\xi) \propto \int \rho_1(\xi)\rho_2(\xi-\Delta\xi)d\Delta\xi = \rho_1(\xi)\int \rho_2(\xi-\Delta\xi)d\Delta\xi = \rho_1(\xi) \tag{5}$$

where the last equality arises from the normalization of the beam density functions. The Van der Meer scans (VdM scans) are performed with the beams progressively displaced by finite steps, the integral of Eq. 5 is therefore replaced by a sum:

$$R(\xi) \propto \rho_1(\xi) \sum_s \rho_2(\xi - \xi_s)(\Delta\xi_{s+1} - \Delta\xi_s) = \rho_1(\xi) \sum_s \rho_2(\xi - \xi_s)\delta\xi \quad (6)$$

where the sum extends over the number of steps performed during the scan. Here we assume the step sizes to be the same along the scan ($\forall s, \Delta\xi_{s+1} - \Delta\xi_s = \delta\xi$). This spots out the main feature of this alternative approach: as long as they are the same, the actual beams' displacements during the scan do not need to be known.

The finite vertex position resolution (V) smears the distribution of the collision vertices affecting therefore the measurement of the beam density functions:

$$R(\xi) \propto \sum_s [(\rho_1(\xi)\rho_2(\xi - \xi_s)) \otimes V]\delta\xi = \rho_1(\xi) \otimes V \quad (7)$$

where the last equality holds for density functions represented by linear superpositions of Gaussian functions. The vertex resolution V has then to be known and unfolded from $R(\xi)$ to obtain the bare beam density function.

Once $\rho_1(x, y)$ and $\rho_2(x, y)$ are determined (as $\rho_i(x, y) = \rho_i(x)\rho_i(y)$), the effective area is simply computed from the integration in the transverse plane of their product:

$$A_{\mathrm{Eff}} = \frac{1}{\int \rho_1(x, y)\rho_2(x, y)dxdy} \quad (8)$$

EXPERIMENTAL SETUP

Two sets of VdM scans have been performed at the CMS interaction point (IP5) in October 2010, during LHC fills 1386 (October 1^{st}) and 1422 (October 15^{th}). The beam optics parameters relevant for the luminosity analysis for the two fills were the same as for the standard physics operations. The expected beam width (σ_b) at the interaction point was $\sim 60\ \mu\mathrm{m}$, whereas the half crossing angle was $\sim 100\mu\mathrm{rad}$. The other beam parameters not affecting the optics were set such to improve the conditions for the luminosity measurement. The number of colliding bunch pairs at IP5 were limited to 6 and 3 for fill 1386 and 1422 respectively in order to be capable of recording enough statistics to allow an independent analysis of each of them. The chosen value for the bunch intensity resulted from the tradeoff between the optimal working point for the beam current measuring devices (the higher current the less relevant the effect of the constant noise [8]) and the need to limit the beam-beam effect (the lower the intensity the more negligible the collective interaction among the bunches in collision[9]). For both fills the bunch intensity resulted to be $\sim 7{\cdot}10^{10}$ protons per bunch corresponding to an average number of 1.2 inelastic events per crossing.

The scans performed during the two fills differed in the way the beams were moved against each other: during fill 1386 ('double beam scan'), the beams were both taken away from their nominal position symmetrically along a given transverse coordinate up to a total separation of 6 nominal σ_b The beams were then moved at the same time towards each other at steps of $\frac{\sigma_b}{2}$ till they reached the positions opposite to their initial ones. Both the horizontal and the vertical planes were scanned in this way. The scan of fill 1422 ('single beam scan') was performed instead with one beam at the time kept at its nominal position and the other steered from $-280\mu\mathrm{m}$ to $+280\mu\mathrm{m}$ corresponding to a maximum separation of $4.5\sigma_b$ Both beams were scanned in both vertical and horizontal planes with a step size of $\frac{\sigma_b}{2}$. The resulting four individual beam scans are named X1, X2, Y1 and Y2 hereafter in the document (where for instance X1 stands for the scan with beam 1 at rest and beam moved along the horizontal plane). In all cases the time spent on each scan step was 25 seconds.

As mentioned in the introduction, CMS uses a dedicated and independent data acquisition system to record continuously the HF signals allowing the online measurement of the luminosity. For both fills 1386 and 1422, the CMS central trigger and DAQ adopted a special configuration conceived specifically for the VdM scans. It was chosen not to record data from more than 3 bunch crossings, therefore for fill 1386, three out six bunch crossings were masked out at trigger level. Only two kind of triggers were exploited:

- **Zero Bias.** The coincidence of beam-pickup transformer (BPTX) signals from both beams was the only trigger requirement. The first trigger level (L1) output rate (corresponding exactly to the beams revolution frequency times the number of colliding bunch pairs in CMS) was reduced by the High Level Trigger (HLT) to ~ 500 Hz by applying a constant pre-scale factor.

- **Minimum Bias.** At L1, in addition to the coincidence of the BPTX signals, at least one hit from one of the beam scintillator counters (BSC) was required. The corresponding event rate was therefore luminosity dependent with a maximum of ~ 25 kHz when the beams were perfectly overlapping. The rate fell exponentially with the beam separation as $\exp\left(-\frac{\delta^2}{4\sigma_b^2}\right)$. In order to maximize the logging rate a variable pre-scale factor was applied at HLT level such to keep the minimum bias event rate to disk below 1.5 kHz throughout the scan.

The overall recorded event rate never exceeded 2 kHz corresponding to a data bandwidth to disk of $\sim 500\ \mathrm{MB/sec}$ well affordable by the CMS storage system. The average dead time resulted to be negligible.

As explain in the next session, in addition to the standard VdM scans, a calibration scan has been performed

to calibrate the length scale of the effective area measurement. This has been done parasitically during a standard LHC physics fill, 1439, with nominal bunch intensity ($\sim 1.1 \cdot 10^{11}$ protons per bunch) and large number of bunches. During both vertical and horizontal scans, the beams were kept at a distance $d_{LS} = \sqrt{2}\sigma_b \sim 70\mu$m and steered along the scan plane such that each beam spanned $5d_{LS}$ (5 steps per plane, 30 seconds each). The distance d_{LS} was chosen in order to maximize the sensitivity of the instantaneous luminosity on the beam separation, i.e $\max\{\frac{\partial L}{\partial d}\} = \frac{\partial L}{\partial d}\big|_{d_{LS}}$.

LENGTH SCALE CALIBRATION

In the standard VdM procedure the relative positions of the two beams is computed on the bases of magnetic field model of the corrector dipoles magnets used to steer the beams at the interaction points. In order to calibrate this length scale, the measurements of the experiments tracking systems are used as reference. This is achieved by comparing the predicted displacement of the beams with the movement of the center of the luminous region (known as beam-spot) obtained from the distribution of the reconstructed interaction vertices. Each beam would in principle require a different calibration factor for each plane. The definitions that follow are used to correlated such factors for a given plane, namely α_1 and α_2 for beam 1 and beam 2 respectively, to the position of the beam-spot and the instantaneous luminosity variation. For x_i and x'_i respectively the nominal and actual displacements for the i^{th} beam we thus have:

$$x'_i \equiv \alpha_i x_i \tag{9}$$

At the start of the scan, the two beams are positioned as shown in Fig.1 and their displacements are

$$x'_{10} = x_{10} \equiv 0 \qquad \text{and} \qquad x'_{20} = \alpha_2 x_{20} = \alpha_2 d_{LS} \tag{10}$$

where d_{LS} is the nominal separation ($= \sqrt{2}\sigma_b$).

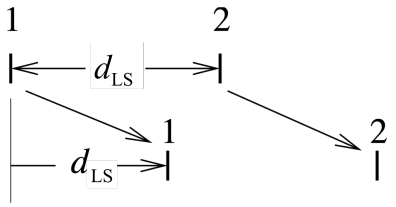

Figure 1: Distance parameters for length-scale scan.

It is convenient to define the average scale factor ($\bar{\alpha}$) and the difference between the scale factors of the two beams (ϵ):

$$\bar{\alpha} = \frac{\alpha_1 + \alpha_2}{2} \qquad \text{and} \qquad \epsilon = \alpha_2 - \alpha_1 \tag{11}$$

where $\bar{\alpha} \sim 1$ and $\epsilon \sim 0$. The difference of the beam-spot position between two consecutive scan steps is thus given by:

$$d_{BS} = \bar{\alpha} d_{LS} \tag{12}$$

In the case the two beams shared the same correction factor ($\epsilon = 0$) then the distance between the beams would remain the same through the scan with no variation in the instantaneous luminosity. A variation of the latter between two consecutive scan steps, expressed as variation of the average number of interaction per crossing, can be used to estimate ϵ:

$$\frac{\delta\mu}{\mu} \simeq -\frac{\epsilon\bar{\alpha}d_{LS}^2}{2\sigma_b^2} \Rightarrow \epsilon \simeq -\frac{\delta\mu}{\mu} \tag{13}$$

where the last equality arises from the fact that $d_{LS} \simeq \sigma_b$ has been chosen for the length scale calibration scan.

It is worth noticing that in the case the VdM scan is performed by moving the two beams at the same time ("double beam scans") by a nominally identical amount, $d_j/2$, in opposite directions, the true separation of the beams is given by:

$$\Delta x_j = x'_{2j} - x'_{1j} = \alpha_2 \frac{d_j}{2} + \alpha_1 \frac{d_j}{2} = \bar{\alpha} d_j \tag{14}$$

In other words, the actual beam separation is just the nominal beam separation scaled by $\bar{\alpha}$.

Table reports the values obtained from the fits to the length scale calibration scan data along with the inferred values for α_1 and α_2 in both the x and y scans, assuming that $d_{LS} = 70$ μm and $\sigma_b = 57$ μm[1]. Although the latter two values are uncertain to a few percent, they are used to determine a correction which is itself at the 1% level, so that this slight uncertainty can be neglected.

Table 1: Length scale parameters from the fits and the inferred values of $\bar{\alpha}$, ϵ, α_1 and α_2.

	x		y	
	Value	Error	Value	Error
$\bar{\alpha}$	0.9933	0.0013	0.9902	0.0013
μ_0	1.909	0.004	1.775	0.004
μ slope	-1.47×10^{-4}	0.40×10^{-4}	1.37×10^{-4}	0.37×10^{-4}
ϵ	0.0070	0.0019	-0.0071	0.0019
α_1	0.9898	0.0016	0.9937	0.0016
α_2	0.9968	0.0016	0.9867	0.0016

TRADITIONAL VDM ANALYSIS

In the traditional VdM method, the interaction rate as a function of the beam separation is measured and Equation 4 is used to determine the visible cross section. Double Gaussian function is found out to best fit the data and especially the tail of the distribution. For this analysis we assume the beam density functions to be totally uncorrelated in the vertical and horizontal plane. For each plane we have:

$$f_x(x) = \frac{h_x}{\sqrt{2\pi}\sigma_{1x}} e^{\frac{-x^2}{2\sigma_{1x}^2}} + \frac{(1-h_x)}{\sqrt{2\pi}\sigma_{2x}} e^{\frac{-x^2}{2\sigma_{2x}^2}}, \tag{15}$$

[1]The value of σ_b for fill 1439 was derived from the size of the luminous region under the assumption of identical Gaussian beams.

where the effective beam size[2] $\sigma_{\rm eff}(j)$ for each scan plane j is given by

$$\sigma_{\rm eff}(j) \equiv \left(\frac{\sigma_{1j}\sigma_{2j}}{h_j\sigma_{2j} + (1-h_j)\sigma_{1j}} \right). \qquad (16)$$

In the following the methods used to measure the interaction rate are described. These procedures are based on "zero-counting", i.e. the average number of interactions per crossing is estimated from the fraction p_0 of events with no "counts" through the Poisson relation $\mu = -\ln p_0$. This approach requires in principle very little corrections due to pileup events.

Online methods

The CMS online luminosity measurement employs signals from the HF, which covers the pseudorapidity range $3 < |\eta| < 5$. Two methods for extracting a real-time relative instantaneous luminosity with the HF have been implemented in firmware. The first is based on "zero counting',' in which the average fraction of empty towers is used to infer the mean number of interactions per bunch crossing. The second method exploits the linear relationship between the average transverse energy per tower and the luminosity. In both cases, the detector occupancy and the E_T-sum data are gathered into histograms that have one bin for each of the 3564 possible bunch crossings. The main advantage of the online methods is indeed the very high statistics leading to a statistical precision on the $A_{\rm Eff}$ measurement of $\sim 0.1\%$.

Offline methods

Two offline algorithms were developed for luminosity monitoring. First is based on energy depositions in the HF, while the other uses reconstructed tracks for vertex finding.

- The **HF method** is based on the coincidence of $\sum E_T$ depositions of at least 1 GeV in the forward and backward HF arrays (the sum in each HF runs over all towers). Timing cuts, where $|t_{HF}| < 8$ ns for both HF+ and HF-, are imposed to eliminate non-collision backgrounds.
- The **Vertex method** requires that at least one vertex with at least 2 tracks be found in the event. The z-position of the vertex is required to lie within 150 mm of the center of the interaction region

To remove possible biases associated with trigger efficiency and dead time, events selected by the zero bias trigger are used. For both methods we estimate the mean number of good events per bunch crossing, μ, through "zero counting" by measuring the observed fraction of zero bias triggers with *no* good events. The linearity of the response of the offline methods for different ranges of instantaneous luminosity is verified against the online measurements that benefits from a much higher statistics. The variation in response is tiny and affects the estimations of $A_{\rm Eff}$ from both the HF method and Vertex method by few per mill. The statistical uncertainty on $A_{\rm Eff}$ derived from the fit is $\sim 0.5\%$.

The plots in Figure 2 show a few examples of data distributions and corresponding fitting functions for the double beam scan of fill 1386. Online and offline methods are represented respectively in the upper and lower plots. The individual effective area measurements for both single and double beam scans as obtained by the traditional VdM analysis are summarized in Table 3.

BEAM IMAGING ANALYSIS

Equation 5 states that one beam can be used as a point-like light source to get the image of the other one. To be totally independent on the reference positions given by the accelerator and rely only on the measurement performed by the tracking and vertexing systems, one beam has to be kept at rest with respect to CMS and the other scanned through it (i.e. the reference frame in which Eq. 5 is defined must be the CMS one). This is exactly the way the single beam scan has been performed during fill 1422. The functional form of $R(\xi)$ in Eq. 5 is obtained from the distribution of the reconstructed collision vertices along the scan coordinate. Events selected by the Minimum Bias trigger are considered. In addition offline selections are applied on reconstructed primary vertices (PV) to achieve an average vertex position error of ~ 25 μm. $R(\xi)$ for each beam and each transverse coordinate is constructed by summing up the PV position distribution of each scan step. Every entry of the final distribution is weighted to take into account the pre-scale factor and the dead time associated to the corresponding event.

The bare beam profile functional form ($\rho(\xi)$) is obtained from $R(\xi)$ by performing an unbinned maximum likelihood fit assuming as density function (PDF) a double Gaussian for $\rho(\xi)$ and a simple Gaussian for the vertex position resolution ($V(\xi;\mu=0,\sigma_r)$). In order to properly take into account the event by event dependency on the vertex position error a conditional probability function is used for the vertex resolution. The PDF used for fitting $R(\xi)$ can be expressed as:

$$f(\xi) = [\frac{h_\xi}{\sqrt{2\pi}\sigma_{1\xi}} e^{\frac{(\xi-\mu_\xi)^2}{2\sigma_{1\xi}^2}} + \frac{(1-h_\xi)}{\sqrt{2\pi}\sigma_{2\xi}} e^{\frac{(\xi-\mu_\xi)^2}{2\sigma_{2\xi}^2}}] \otimes V(\xi;\mu=0,\sigma_r|d(\sigma_r)) \qquad (17)$$

here $d(\sigma_r)$ is the density function of vertex resolution's width σ_r obtained from the distribution of the vertex position error as measured from data.

Biases Estimation and Correction

Vertex Position Resolution Scale A bad estimate of the scale of the vertex position error and therefore of the width of the vertex resolution would directly affect the evaluation

[2]The beam size here is the convolution of both beams.

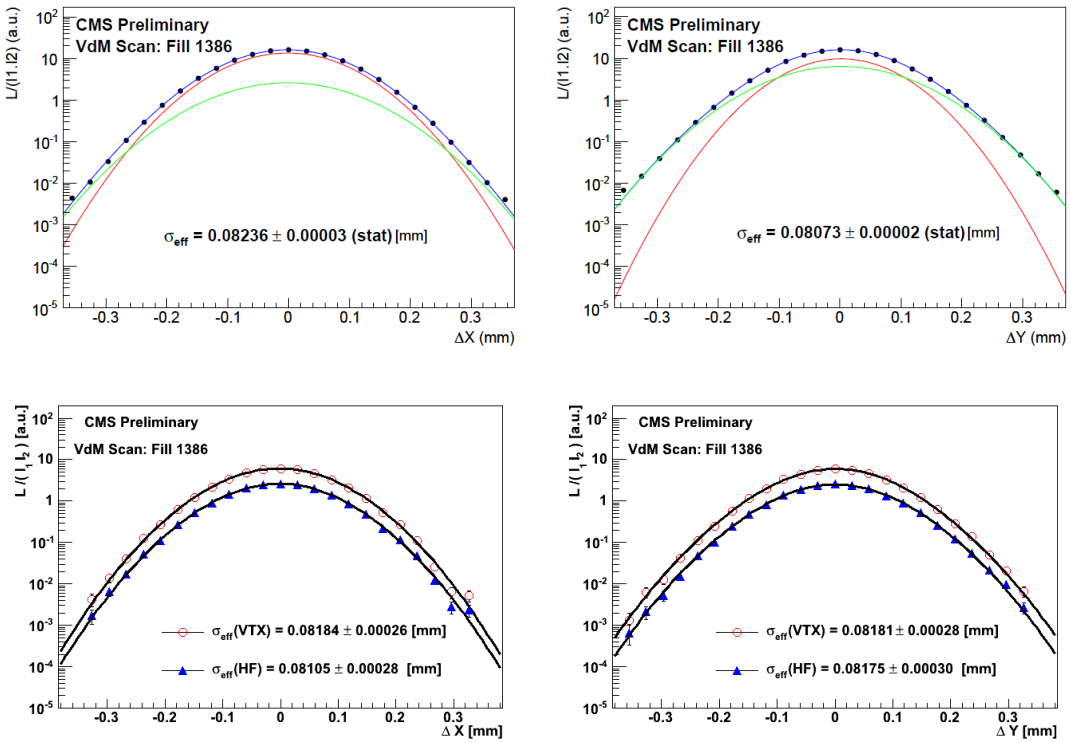

Figure 2: **Upper plots:** Van der Meer scans for the online method summed over all bunch crossings combined in the horizontal (X) and vertical (Y) planes for Fill 1386. For the upper plots, the red, green, and blue curves respectively represent the two Gaussian components of the fit and their sum. **Lower Plots:** Van der Meer scans for the offline methods summed over bunch crossings combined in the horizontal (X) and vertical (Y) planes for Fill 1386. The open circles (red) represent the offline vertex method and the filled triangles (blue) represent the offline HF coincidence method.

of $\rho(\xi)$ (in a rough approximation $\sigma_R^2 = \sigma_\rho^2 + \sigma_r^2$, where σ_R is the width of $R(\xi)$ and σ_ρ is the width of the beam density function). In order to compute accurately the scale of vertex position uncertainty we measure it directly on data adopting a technique described in [7]: the set of tracks used to reconstruct the vertex are randomly spitted into two subsets which are then independently exploited to define two new vertices. The distance between these is thus compared with the position error assigned by the reconstruction algorithm to the original vertex. The width of the relative pull distribution is then used as rescaling factor to be applied to σ_r. Such rescale factor is proved to be independent on the vertex parameters (i.e. mainly the number of input tracks) and results to be $\simeq 0.89$ with a precision of 1%.

Vertex Reconstruction Efficiency The validity of Equations 5-7 relies on the constancy of the primary vertex reconstruction efficiency throughout the scan. Such efficiency possibly depends on the average number of collision per crossing. In order to quantify the relative variation of efficiency during the single beam scan, we studied it on Monte Carlo generated minimum bias events characterized by different pileup scenarios matching what expected for the different beam separations. Given the low value of the maximum pileup occurring in fill 1422, the efficiency variation is very small ($< 0.5\%$), resulting in a negligible overall correction.

Crossing Angle The non zero crossing angle in the horizontal plane implies that the plane orthogonal to the beam being measured is not parallel to the CMS transverse plane, therefore the equalities in Equation 5 do not hold exactly. As demonstrated in [6], it is however possible to reestablish the validity of Eq. 5 by projecting the measurements (i.e. the reconstructed vertex position) into the plane orthogonal to the beam direction accordingly to:

$$x_{1,2} = x - z \sin \alpha_{1,2} \tag{18}$$

This allows measuring the unbiased transverse profile of the beam along its direction. However, as discussed in [6], the actual area contributing to the luminosity result to be wider still due to the presence of the crossing angle. The effective area needs therefore to be rescaled according to the formula:

$$A_{\mathrm{Eff}} \mapsto A_{\mathrm{Eff}} \sqrt{1 + \left(\frac{\sigma_z \sin \alpha}{\sigma_x} \right)^2} \tag{19}$$

where we have assumed the two beams to have the same longitudinal (σ_z) and transverse dimensions (σ_x). The

value of σ_z has been estimated from the data multiplying by a factor $\sqrt{2}$ the longitudinal luminous region size (from the assumption of Gaussian beam profiles), whereas for σ_x we used the average of the values obtained from the fit of the individual beam profiles and reported in table 2. The corrections on the horizontal effective areas deriving from Equations 18 and 19 correspond respectively to $\sim -0.7\%$ and $\sim +1\%$, yielding to a rather small net correction.

Fit Results

The plots in Figure 3 display the data distribution ($R(\xi)$) and the corresponding fitting functions for one of the bunch pair colliding at CMS during fill 1422.

Table 2 lists the widths of the individual beam shapes $\rho_i(\xi)$ defined as $\Sigma^{\xi}_{\mathrm{Eff,i}} = \frac{1}{\sqrt{2}\int \rho_i(\xi)^2 d\xi}$. The uncertainties are statistical from the fit, they have been determined by randomly varying the fit parameters by $\pm 1\sigma$ accordingly to the covariance matrix and considering the 68% range of the corresponding distribution of A_{eff}.

Table 2: Widths of the individual beam images. The reported error are statistical from the fit.

	BX 1	BX 51	BX 101
$\Sigma^{X}_{\mathrm{eff},1}$ (μm)	$54.5^{+0.5}_{-0.1}$	$53.1^{+0.1}_{-0.3}$	$53.1^{+0.1}_{-0.1}$
$\Sigma^{X}_{\mathrm{eff},2}$ (μm)	$54.5^{+0.1}_{-0.2}$	$54.2^{+0.1}_{-0.2}$	$55.0^{+0.1}_{-0.2}$
$\Sigma^{Y}_{\mathrm{eff},1}$ (μm)	$61.1^{+0.1}_{-0.5}$	$59.0^{+0.1}_{-0.1}$	$59.9^{+0.1}_{-0.5}$
$\Sigma^{Y}_{\mathrm{eff},2}$ (μm)	$61.3^{+0.1}_{-0.4}$	$62.2^{+0.5}_{-0.4}$	$61.8^{+0.1}_{-0.5}$

The values for the effective areas averaged over the three colliding bunch pairs of fill 1422 are reported in Table 3. The quoted errors are derived from the RMS of the values for each bunch pair.

Systematic Uncertainties

Three main sources of systematics are identified: those related to the fit procedure, the ones deriving from the finite vertex resolution and finally the uncertainty due to the limited beam scan range. Other possible effects whose contributions are verified to be negligible are listed in the end.

Fit Procedure In order to test the performances of the our fit procedure, a Monte Carlo simulation has been developed reproducing the main features of the single beam scans. Several pseudo experiments have been performed assuming beam parameters similar to what observed from fill 1422 data and the value of the generated A^{ξ}_{Eff} have been compared with the one obtained from the maximum likelihood fit. The fit results to be unbiased and the statistic error ($\sim 0.4\%$) is well in agreement with those obtained from the fit to the data.

Vertex Resolution Scale The precision with which such factor is known translates into an uncertainty on the effective area. We studied this dependency empirically, performing the fit to $R(\xi)$ with the rescale factor varied by $\pm 4\%$ and $\pm 2\%$. The results are shown in the plots of Fig. 4.

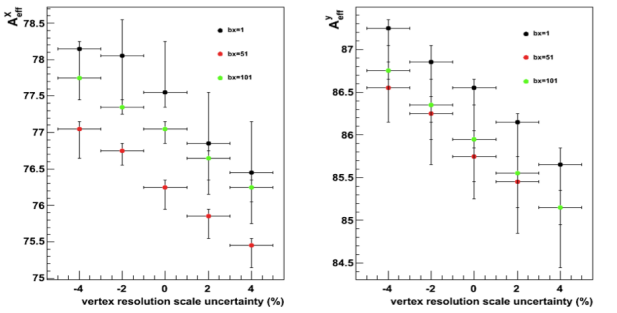

Figure 4: Variation of the computed A_{Eff} (left: horizontal plane, right: vertical plane. The color code represent the three BX colliding a CMS) as a function of the uncertainty on the vertex resolution scale.

For small variations of the scale factor, the relation between the latter and the effective area is linear, $\Delta A_{\mathrm{Eff}}/A_{\mathrm{Eff}} = m\Delta\sigma_r/\sigma_r$. The coefficient m is obtained from the linear fit of the plots in Fig. 4, resulting to be ~ 0.25; given the uncertainty on the vertex resolution scale factor of 1%, the corresponding systematic uncertainty to the estimates on $A^{X,Y}_{\mathrm{Eff}}$ is $\pm 0.25\%$.

Scan Range In order to estimate the effect of the limited scan range in Equation 6 (for the single beam scan, the allowed scan range was ± 4.5 nominal σ_b), we studied the dependency of the measured $A^{X,Y}_{\mathrm{Eff}}$ on the latter: for each plane the value of the effective area resulting from summing the data on restricted ranges (± 3.0, ± 3.5 and ± 4.0 σ_b) are used to extrapolate A_{Eff} beyond the maximum available range.

The Horizontal plane results to be probed completely, whereas for the vertical beam profiles there are indication that a small fraction of the particle distribution may be left not fully probed, i.e. the difference between the extrapolated A_{Eff} values and the actual values obtained on the basis of the available range amounts to 0.5%. Such difference is used to correct the central values for A^{Y}_{Eff}.

Other (negligible) Systematics Uncertainties Other possible sources of systematics effects have been examined and have been confirmed to have a negligible effect on the measured effective area:

- CMS vertex position measurement scale
- Primary Vertex quality cuts
- PV reco performances as a function of BS position
- Tilts between the CMS and LHC reference frames
- Crossing Angle

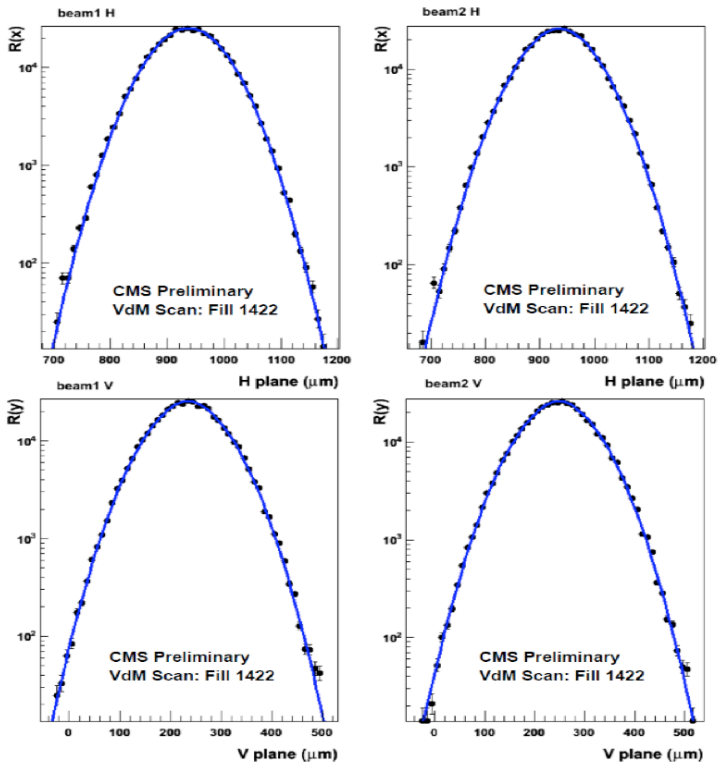

Figure 3: Beam-shape functions for Fill 1422 derived using the beam-imaging method. **Upper Left:** shape of beam 1 in the horizontal direction. **Upper Right:** shape of beam 2 in the horizontal direction. **Lower Left:** shape of beam 1 in the vertical direction. **Lower Right:** shape of beam 2 in the vertical direction.

LUMINOSITY NORMALIZATION RESULTS

Emittance Correction

During the lifetime of a fill, the proton beams in the LHC tend to undergo "emittance blow-up", a process whereby the emittance of the beam increases with time. This effect is important for VdM scans that take place over a period of time such that the instantaneous luminosity of the beams has significantly decreased between the horizontal and vertical scans used to measure σ_x and σ_y. To correct for this effect we exploit the measurements performed by telescopes (BSRT) [10] that provide a bunch by bunch profiling by gathering the synchrotron-light produced by the beam itself. The emittance is then derived from the value of the beta function at the location of these devices.

The visible cross section is best estimated when the dependency of the luminosity on the beams' displacement is minimal, i.e. when the latter is nominally zero. This define the measurement's zero points. The values of the effective areas for the horizontal and vertical plane need to be extrapolated to each zero point accordingly to the specific emittance evolution as obtained from the BRST which in good approximation results to be linear with time:

$$\sigma_{x,y}(t_i) = \sigma_{x,y}(t_0) + m_{\sigma_{x,y}}\Delta t \qquad (20)$$

Here $\Delta t = t_i - t_0$, t_i is the time at a given zero-point and t_0 is the time at the maximum of the scan from which the width was measured; $m_{\sigma_{x,y}}$ are the slopes computed from the fit of the BRST data, corresponding to $\sim 1.3 \cdot 10^{-4}$ μm/s and $\sim 3 \cdot 10^{-4}$ μm/s for the horizontal and vertical plane respectively.

Beam Current Measurement

The intensity of each individual colliding bunch is obtained by the combined measurements performed by the DC BCT and fast BCT as explained in details in [8] where the results and relative uncertainties are also reported. An analysis has been performed to determine the amount of charges present in satellite bunches next to the main colliding bunches (5 ns away) based on timing of the signals in the electromagnetic calorimeter. Due to the crossing angle, possible displaced collisions are very much suppressed limiting the sensitivity of the method. For both fill 1386 and 1422 upper bounds have been however set, constraining the satellite population to a few per mill relative to the main bunch intensity.

Results

The results concerning the visible cross section are summarized in table 3. Each method described before provides

an estimation of the horizontal and vertical $A_{\rm Eff}$ averaged on the values obtained for each colliding bunch pair. The luminosity calibration factor is expressed as a ratio of the visible cross section measured here and the one used during 2010 LHC run in CMS [2]. We combined the results of three methods exploited such to define five estimates of the calibration ratio (the four possible combinations resulting from the standard VdM analysis of the single beam scan are averaged into one single measurement). The standard deviation of the values obtained for this ratio is 2.51%.

SYSTEMATIC UNCERTAINTIES

Several contributions to the systematic error have been evaluated. A summary appears in Table 4. Individual entries of this table are discussed below. The last two listed in the table and discussed in the text ("HF drift" and "Afterglow") do not concern the luminosity normalization but rather the real-time luminosity measurement during standard physics operations.

Table 4: Summary of contributions to the overall systematic error. All values are percentages. The total error is obtained by adding all components in quadrature.

Term	**Error (%)**
Method & Fill Variation	2.5
Beam Background	< 0.1
Beam Shape	0.3
Non-linear correlations	0.9
Length-Scale Calibration	0.3
Emittance Slope	0.2
Beam Intensity	2.9
HF drift	0.5
Afterglow	0.5
Total	4.0

Method and Fill Variation Following a conservative approach we assume the uncertainty on the visible sigma due to the effective are measurement can be estimated from the variation of the results on the latter obtained by the various methods exploited. The RMS of the five estimates of $A_{\rm Eff}$ summarized in table 3 is thus assumed as uncertainty.

Beam Background This refers to possible backgrounds from non-collision sources and was found to be a negligible effect.

Method & Fill Variation This error reflects the observed RMS variation in the five values of $A_{\rm Eff}$ obtained using different methods and fills shown in Table 3.

Beam Shape In carrying out the fits, we assumed that the beam density function is uncorrelated in the vertical and horizontal planes and that in each plane a double Gaussian is best describing the beam profile. The former assumption has been discussed in [11] and is estimated to lead to an uncertainty of 0.9% (quoted as "Non-linear correlation" in Table 4). We tested the latter assumption performing the fit with different density functions: the variation on the resulting $A_{\rm Eff}$ never exceeds 0.3%.

Length-Scale Calibration For the traditional Van der Meer scans the $A_{\rm Eff}$ values depend on knowing the amount by which the beams have been displaced. This information is provided by the LHC. The LHC values are cross-checked and corrected using beam-position measurements from the CMS vertex detector, as described previously. Given the small amount of the correction, the corresponding error is estimated to be 0.3%.

Emittance Slope Since scans in the horizontal and vertical planes inevitably occur at different times, one cannot directly obtain a snapshot in time that includes all of the factors in the luminosity expression (Eq. 20). Rather, one must extrapolate the $A_{\rm Eff}$ values measured during the scans to a common point in time. To take into account evolution of the beam sizes, emittance data provided by the LHC is used. The typical correction is of order 1%. The 0.2% error quoted represents the uncertainty in those corrections.

Beam Intensity The luminosity depends directly on the number of circulating protons. The measurement of this current is the responsibility of the LHC. The systematic uncertainty on this measurement is determined by the Beam Current Normalization Working Group [8]. The quoted error of 2.9% includes scale uncertainties associated with direct current transformers used to measure the beam intensities as well uncertainties in the offset of the fast beam current transformers used to determine how that current is distributed among the circulating bunches.

HF Drift The calibration procedures described in this note were carried out over a relatively short period of time in October 2010, whereas CMS has acquired data over a period extending from March to November of 2010. Drifts in the calibration of the HF, which is the primary luminometer for CMS, could therefore contribute an additional systematic uncertainty to the luminosity value used in a given analysis. To check for such drifts, we compare the ratio of the luminosity measured by the HF online to the luminosity determined using the offline vertex counting method. Based on this study, we conclude that drifts in the calibration of the HF contribute 0.5% to the overall systematic error.

HF Afterglow The response of the HF to pp collisions has a small tail that extends over many (~ 100) bunch crossings. For runs where many bunches are filled, the tails from

Table 3: Summary of relative luminosity calibrations obtained from the various methods. The beam width values have units of microns. Values for the online and offline methods have been corrected for the length-scale calibration. The errors are statistical. The column marked "Ratio" indicates the calibration factor relative to the calibration factor obtained using the scans in spring 2010 [2]. The five numbers in the rightmost column that enter the overall average are highlighted in bold font.

HF Online Method				
Fill	Scan Pair	$A^x_{\rm Eff}$ (μm)	$A^y_{\rm Eff}$ (μm)	Ratio
1386	—	81.81 ± 0.03	79.94 ± 0.02	**1.018**
1422	X1–Y1	76.30 ± 0.04	82.88 ± 0.04	1.007
	X2–Y1	76.83 ± 0.04	82.88 ± 0.04	1.008
	X1–Y2	76.30 ± 0.04	83.80 ± 0.04	0.992
	X2–Y2	76.83 ± 0.04	83.80 ± 0.04	0.993
			1422 Average	**1.000**
Offline Methods				
Fill	Scan Pair	$A^x_{\rm Eff}$ (μm)	$A^y_{\rm Eff}$ (μm)	Ratio
1386	N/A	81.79 ± 0.28	80.33 ± 0.30	**1.013**
1422	X1–Y1	77.53 ± 0.26	84.47 ± 0.30	0.972
	X2–Y1	77.63 ± 0.29	84.47 ± 0.30	0.979
	X1–Y2	77.53 ± 0.26	85.11 ± 0.32	0.961
	X2–Y2	77.63 ± 0.29	85.11 ± 0.32	0.968
			1422 Average	**0.970**
Beam Imaging Method				
Fill	Scan Pair	$A^x_{\rm Eff}$ (μm)	$A^y_{\rm Eff}$ (μm)	Ratio
1422	N/A	77.06 ± 0.21	86.03 ± 0.21	**0.962**
			Overall Average	**0.993**
			RMS	**2.51%**

each bunch crossing add up to contribute an apparent luminosity at the few per-mil level. We conservatively estimate a contribution to the systematic error of 0.5% from this source.

CONCLUSIONS

The Van Der Meer scan performed in October have been used to determine the absolute calibration factor for the CMS luminosity measurement. Different methodologies have been exploited to analyze the scan data to determine the effective area, providing results consistent at 2.5% level. In particular the beam imaging technique has been proved to be a valid complementary approach for the determination of $A_{\rm Eff}$. The new calibration factor is very similar (to 0.7% level) to the one used for the 2010 run. The CMS luminosity measurement uncertainty derived from this analysis amounts to 4%.

REFERENCES

[1] The CMS Collaboration, "The CMS experiment at the LHC", *JINST* 3 (2008) S08004.

[2] The CMS Collaboration, "Measurement of CMS Luminosity", CMS Physics Analysis Summary EWK-10-004.

[3] S. Van der Meer, Calibration of the Eective Beam Height in the ISR, internal CERN report, ISR-PO/68-31 (1968).

[4] S. M. White et al., First Luminosity Scans in the LHC, proceedings of IPAC10, Kyoto, Japan, May 2010.

[5] D. Belohrad et al ., Commissioning and First Performance of the LHC Beam Current Measurement Systems , Proc. IPAC10, Kyoto, Japan, 23 - 28 May 2010.

[6] V. Balagura, "Notes on Van der Meer Scan for Absolute Luminosity Measurement", arXiv:1103.1129v1.

[7] The CMS Collaboration, CMS tracking performance results from early LHC operation, The European Physical Journal C, 4 (2010) 70.

[8] G. Anders et al., "LHC Bunch Current Normalisation for the October 2010 Luminosity Calibration Measurements", CERN-ATS-Note-2011-016 PERF

[9] W. Herr, "Tune shifts and spreads due to short and long range beam-beam interaction in the LHC", CERN/SL/90-06 (AP) and LHC-Note 119.

[10] A.S. Fisher, A. Goldblatt and T. Lefevre, The LHC Synchrotron Light Monitors, Proceeding of the DIPAC Conference, Basel, Switzerland (2009), p164

[11] G. Piacquadio et al., Private Communication. Also mentioned in: M. Huhtinen, "ATLAS 2010 luminosity determination", this proceedings

ATLAS luminosity determination in 2010

M. Huhtinen *CERN, CH-1211 Geneva, Switzerland*
on behalf of the ATLAS Luminosity WG

Abstract

This paper describes the detectors and algorithms which were used for monitoring the ATLAS luminosity in 2010. A main emphasis is on the absolute calibration by van der Meer scans. The systematic uncertainties associated with the calibration are discussed. The resulting uncertainty of the luminosity calibration reached in 2010 is 3.4%.

INTRODUCTION

The absolute luminosity of a particle collider can be written as

$$\mathcal{L} = \frac{R n_b f_r}{\sigma} \tag{1}$$

where n_b is the number of colliding bunches, f_r the revolution frequency, R the average rate of some process and σ the cross-section corresponding to that process.

Eq. 1 implies that any process that can be observed by the detector and for which the cross-section is known can be used to monitor luminosity. In the ideal case the dependence between the true rate (R) and the observed rate (εR) would be linear, but any well understood functional dependence is acceptable.

In ATLAS [1] the online luminosity measurement is based on detectors in the forward hemisphere, which record inelastic pp-collisions with an *a priori* unknown efficiency (ε). For the initial LHC start-up these efficiencies were estimated from Monte-Carlo simulations, and thus were associated with significant uncertainties – estimated to be at the level of 20% [2]. The purpose of an absolute luminosity calibration is to determine these efficiencies as accurately as possible. Provided the efficiencies remain stable in time and their dependence on pile-up can be accurately modelled the calibrated detector will yield an absolute luminosity measurement.

The average number of inelastic collisions per bunch-crossing, μ, follows a Poisson-distribution. We derive a quantity $\mu_{\mathrm{vis}} = \varepsilon\mu$ and correspondingly a visible cross-section

$$\sigma_{\mathrm{vis}} = \varepsilon\sigma_{\mathrm{inel}}, \tag{2}$$

both of which are detector-dependent. These allow to rewrite Eq. 1 as

$$\mathcal{L} = \frac{\mu n_b f_r}{\sigma_{\mathrm{inel}}} = \frac{\mu_{\mathrm{vis}} n_b f_r}{\sigma_{\mathrm{vis}}}, \tag{3}$$

where the luminosity depends only on a "fill constant" $n_b f_r$, the observed μ_{vis} and the calibration constant σ_{vis}.

LUMINOSITY MONITORING IN ATLAS

During the 2010 pp-running several luminosity detectors and algorithms, listed in Table 1, were used in ATLAS. These can be divided into "online" and "offline" methods. While the offline methods allow for more detailed analysis like timing cuts to identify collisions, their drawback in general is that they can only work from recorded events and thus have to deal with significantly lower statistics. Also, they are not available for fast online monitoring, e.g. when optimising the collisions by mini-scans. Online methods use the detector data-stream directly – in the case of MBTS the trigger rates before prescale – and thus have maximum statistics at their disposal. Only the online methods are able to provide luminosity information to the ATLAS control room (ACR) and to the LHC.

Some of the online methods can be applied at a frequency of order 1 Hz. This results in the instantaneous values displayed in the ACR and transmitted to LHC.

In normal stable-beam running of the LHC it can be assumed that the luminosity is essentially stable on the timescale of minutes. Therefore each ATLAS run is subdivided into luminosity blocks (LB) with a typical length of 2 minutes. This is the smallest quantity in which luminosity can be accounted in an offline analysis. The luminosities from all online methods are stored per LB in the COOL database.

One motivation to maintain several luminosity monitors and algorithms is to have fallback alternatives in case of problems with some detector. But an even more important aspect of this redundancy is to have a handle on systematic effects and long term stability. Inter-comparison of the detectors allows to diagnose potential drifts of efficiency in any given detector and enable us to investigate and fix potential problems promptly.

PILEUP DEPENDENCE OF ALGORITHMS

In 2010 only *Event counting* was used in ATLAS. This means counting the bunch-crossings where

- a signal is detected on either side of the detector (Event-OR)
- a signal is detected on both sides of the detector (Event-AND)

Event counting is related to *Zero counting* by

$$P_{\mathrm{Event}} = 1 - P_{\mathrm{Zero}}, \tag{4}$$

where P denotes the probability to observe an event (or zero, i.e. no event) in a given bunch crossing.

Table 1: Luminosity detectors and algorithms commissioned as luminosity detectors during the 2010 pp run. †The track counting algorithm is described in detail in [3].

Detector	Algorithms	per-bunch	Onl/Offl	Comments
LUCID	OR, AND	yes	Online	Provided preferred luminosity
MBTS	AND, (OR)	no	Online	Not usable with 150 ns bunch trains
BCM	OR, AND, XOR	yes	Online	Fully commissioned only end of September
MBTS timing	AND	yes	Offline	Coincidence within 10 ns
LAr timing	AND	yes	Offline	Used only in very early runs
Prim.Vtx	4 tracks	yes	Offline	p_T threshold for tracks 150 MeV/c
Track counting	≥ 1 track†	yes	Offline	Studied for comparisons between experiments

Denoting by $P_0(\mu)$ the probability to have no collision when the average number of Poisson-distributed collisions is μ, we obtain from Eq. 4 the probability $P_{\rm OR}(\mu)$ to have an "OR" event as

$$P_{\rm OR}(\mu) = 1 - P_0(\mu) = 1 - e^{-\mu}. \quad (5)$$

In Event-OR counting also $\mu_{\rm vis} = \varepsilon\mu$ follows a Poisson distribution and Eq. 5 is valid also if $\mu \to \mu_{\rm vis}$.

For Event-AND counting the situation is more complicated. The efficiency to observe a coincidence is given by $P_{\rm AND}(\mu) = P_{\rm A}(\mu) + P_{\rm C}(\mu) - P_{OR}(\mu)$, where A and C denote the two sides of the detector. The probability of a coincidence is then given as [4]

$$P_{\rm AND}(\mu) = 1 - e^{-\mu\varepsilon_{\rm A}} - e^{-\mu\varepsilon_{\rm C}} + e^{-\mu\varepsilon_{\rm OR}}. \quad (6)$$

If $\varepsilon_{\rm A} = \varepsilon_{\rm C}$, this can be simplified to

$$P_{\rm AND}(\mu) = 1 - 2e^{-\mu(\varepsilon_{\rm AND}+\varepsilon_{\rm OR})/2} + e^{-\mu\varepsilon_{\rm OR}}. \quad (7)$$

Using the definitions from Eq. 2 and $\mu_{\rm vis} = \varepsilon_{\rm AND}\mu$ allows to further rewrite this in the form

$$P_{\rm AND}(\mu_{\rm vis}) = 1-2e^{-\mu_{\rm vis}(1+\sigma_{\rm vis}^{\rm OR}/\sigma_{\rm vis}^{\rm AND})/2}+e^{-\mu_{\rm vis}\sigma_{\rm vis}^{\rm OR}/\sigma_{\rm vis}^{\rm AND}} \quad (8)$$

The luminosity determination is based on a measurement of $P(\mu)$ and while Eq. 5 is readily inverted, there is no analytical solution for Eq. 8. Except for approximate solutions for small μ or when $\sigma_{\rm vis}^{\rm OR} \approx \sigma_{\rm vis}^{\rm AND}$, the solution has to be found numerically.

In the special case of a van der Meer scan, when the $\sigma_{\rm vis}$ values are not yet known, the solution has to be found iteratively: first $\sigma_{\rm vis}^{\rm OR}$ is determined from a fit using the correction from Eq. 5 and then $\sigma_{\rm vis}^{\rm AND}$ from Eq. 8 by several iterative fits.

LUMINOSITY DETERMINATION FROM VAN DER MEER SCANS

The luminosity can also be calculated from beam parameters as

$$\mathcal{L} = \frac{n_b f_r n_1 n_2}{2\pi\Sigma_x\Sigma_y} \quad (9)$$

where n_1 and n_2 are the number of particles in the colliding bunches and Σ_x and Σ_y the convolved horizontal and vertical beam sizes.

By setting equal Eqs. 3 and 9 at the peak of the scan we obtain

$$\sigma_{\rm vis} = \frac{2\pi\mu_{\rm vis}^{\rm max}\Sigma_x\Sigma_y}{n_1 n_2} = 2\pi\mu_{\rm vis}^{\rm sp,max}\Sigma_x\Sigma_y, \quad (10)$$

which is the basic equation for the van der Meer (vdM) calibration [5]. The last step in Eq. 10 introduces the specific μ-value, $\mu_{\rm vis}^{\rm sp} = \mu/(n_1 n_2)$. Eq. 10 allows to obtain the calibration parameters $\sigma_{\rm vis}$ from measured scan data ($\mu_{\rm vis}^{\rm max}$, Σ_x and Σ_y) and a simultaneous determination of the bunch intensities. This provides the parameter $\sigma_{\rm vis}$ needed for the absolute calibration of the luminosity.

The values of Σ_x and Σ_y have to be determined in 2 scans along the corresponding axes. Inevitably these two scans are separated in time and due to emittance growth during the scan will result in slightly different $\mu^{\rm max}$-values. In Eq. 10 we use the arithmetic average of these two μ-values, i.e. the final formula for $\sigma_{\rm vis}$ is

$$\sigma_{\rm vis} = \pi(\mu_{\rm vis,x}^{\rm sp,max} + \mu_{\rm vis,y}^{\rm sp,max})\Sigma_x\Sigma_y. \quad (11)$$

The specific luminosity per bunch is obtained from Eq. 9 by dividing with the intensity product $n_1 n_2$ and the number of bunches:

$$\mathcal{L}_{\rm sp} = \frac{f_r}{2\pi\Sigma_x\Sigma_y} \quad (12)$$

It can be seen that, unlike $\sigma_{\rm vis}$, the value of $\mathcal{L}_{\rm sp}$ does not depend on any quantities that would involve properties of the detector or algorithm and therefore is an ideal quantity to study the consistency of different detectors and algorithms.

THE VDM SCANS

In 2010 ATLAS had 5 fills with vdM scans, of which one was dedicated to a length-scale calibration only and one was with heavy-ions. The first 3 fills listed in Table 2 had a total of 5 scan pairs. The very first scan in fill 1059 had a single scan in x and another in y. This was soon followed by a more extensive vdM session with first 2 scans in x, followed by 2 in y. Both of these were done with a single colliding bunch and very moderate μ.

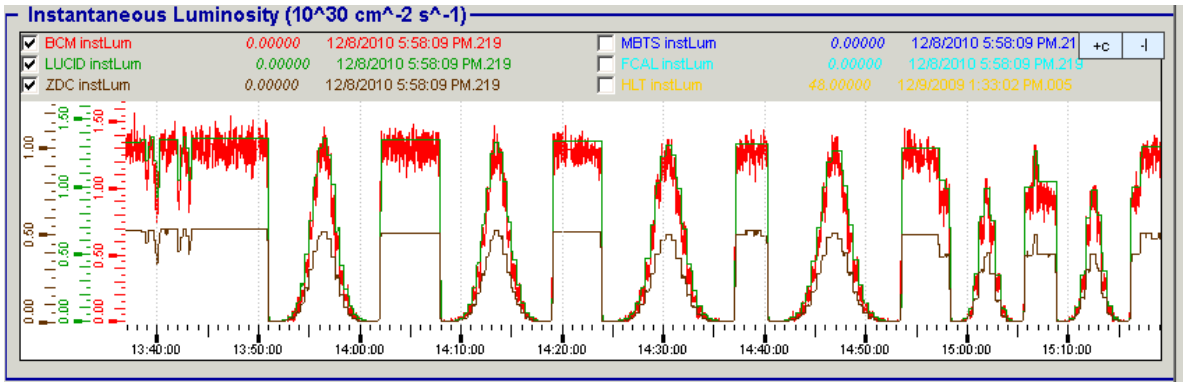

Figure 1: Illustration of the vdM scan procedure in ATLAS during LHC fill 1386. The first four scans are in order x, y, x, y with the other coordinate centred. The last two scans are in order x, y, with the other coordinate displaced by 60 μm. The time axis is in CEST.

Each of the october scans consisted of 25 points where luminosity data was recorded for 15–20 seconds. Between these acquisition points were shorter periods during which the beams were moved. During the scan luminosity recording by ATLAS LB's was disabled, instead a special scan-controller received information from the LHC and issued pseudo-LB boundaries accordingly.

The last vdM scans in October were done by alternating x and y scans. The time between 2 scans was about 20 minutes, i.e. all 4 scans fitted into a bit more than one hour. This procedure is illustrated in Fig. 1 as a function of real time. Scan-data stored in COOL per pseudo-LB was used for the vdM analysis.

The October fill also included 2 scans with a displacement in the other coordinate. This was intended to study xy-coupling, but the analysis of it has not yet finished. The centred scans, however, show no signs of significant coupling.

In all of the scans both beams were scanned simultaneously over $\pm 3\,\sigma_{\rm beam}$ in opposite directions giving a total maximum separation of $\pm 6\,\sigma_{\rm beam}$.

Fig. 2 shows the LUCID-EventOR luminosity as a function of BCID in fill 1386. Five of the colliding bunches are easily recognised, the sixth in BCID 1 is difficult to see in the Figure. Each colliding BCID is followed by a tail of "afterglow", which will be discussed later as a source of systematic uncertainty. On top of this tail sit the 26 non-colliding bunches.

FIT MODEL

Analysing the vdM scan data it was soon discovered that a single Gaussian does not provide a satisfactory fit. Since in most algorithms the background is negligible, adding a constant term did not bring significant improvement. A much better fit was obtained by a double-Gaussian with a constant background term:

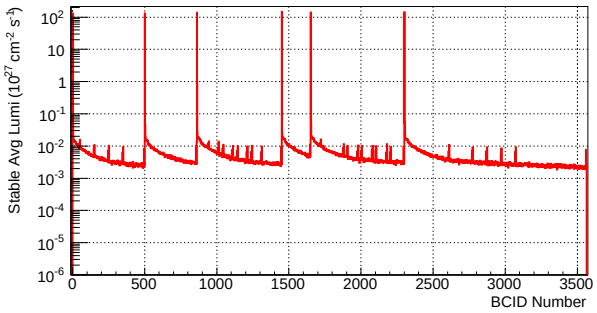

Figure 2: Luminosity as determined from LUCID-EventOR during LHC fill 1386. The large peaks correspond to the 6 colliding bunches while the 26 smaller peaks are due to the 13 unpaired bunches per beam. The slowly decaying tails are the "afterglow" discussed in the text

$$P(x) = \frac{P_0}{\sqrt{2\pi}}\left[\frac{f e^{-(x-x_0)^2/2\sigma_a^2}}{\sigma_a} + \frac{(1-f)e^{-(x-x_0)^2/2\sigma_b^2}}{\sigma_b}\right] + c \tag{13}$$

The convolved beam size can be obtained from these two Gaussians as

$$\frac{1}{\Sigma} = \left[\frac{f}{\sigma_a} + \frac{1-f}{\sigma_b}\right] \tag{14}$$

Setting $x = x_0$ in Eq. 13, we get

$$P(x_0) = \frac{P_0}{\sqrt{2\pi}}\left[\frac{f}{\sigma_a} + \frac{1-f}{\sigma_b}\right] = \frac{P_0}{\sqrt{2\pi}\Sigma} \tag{15}$$

If Eq. 14 is used to substitute, e.g., σ_b in Eq. 13 the resulting equation has Σ conveniently as its fit parameter.

A typical fit with Eq. 13 is shown in Fig. 3 together with the residuals.

Fig. 4 shows the distribution of χ^2/ndf for the fits on LUCID data, illustrating the good quality of the fits, which

Table 2: Summary of the vdM fills used by ATLAS in 2010

Date	Fill	Number of coll. bunches	β^* (m)	Crossing ang. (μrad)	N_b 10^{11}	μ at peak	Comment
Apr 26	1059	1	2	0	0.1	0.03	Scan 1 & length scale
May 9	1089	1	2	0	0.2	0.11	Scans 2 & 3
Oct 1	1386	6	3.5	200	0.9	1.4	Scans 4 & 5
Oct 4	1393	186	3.5	200	1.0	2.4	Length Scale
Nov 30	1533	113	2.5	0	0.1	0.00016	Heavy Ion

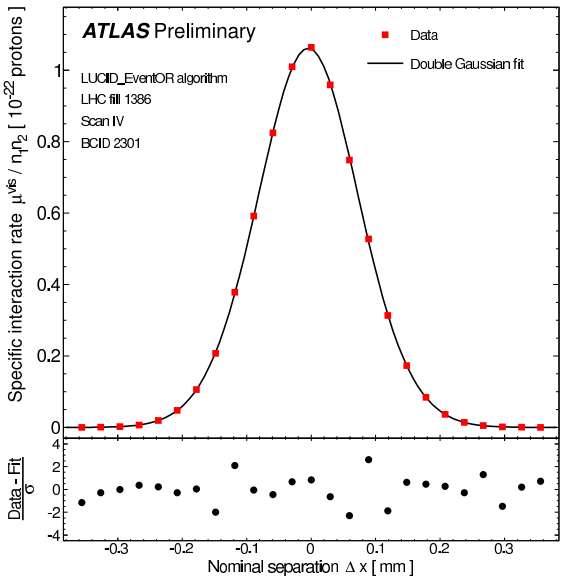

Figure 3: Fit of Eq. 13 to LUCID-EventOR data from scan IV in the x-plane. The residuals on the bottom plot are based on statistical deviations only [6].

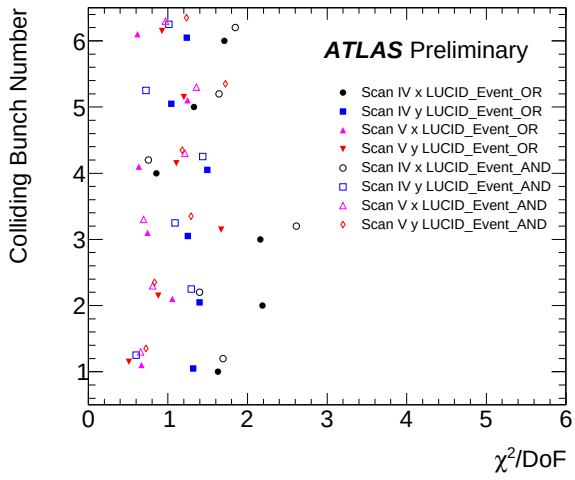

Figure 4: Distribution of $\chi^2/$ per number of degrees of freedom (ndf) values for fits to the LUCID vdM data.

suggests that a possible systematic error due to the fit function is small. Detailed studies using cubic spline fits and comparing the resulting $\sigma_{\rm vis}$ values allow to estimate the associated systematic effect as 0.2% for the october scans.

SYSTEMATIC UNCERTAINTIES

Bunch charge product

The uncertainty on the product n_1n_2 measured during the scan by LHC instrumentation has been significantly reduced by very detailed analysis [7], but with 3.1% remains to be the dominating uncertainty in the October scans.

Background and afterglow

The background due to beam-gas and beam-halo can be measured from the unpaired bunches shown in Fig. 2, but also from the tails of the fits to the scan data. Both methods indicate that this contribution is at the level of 10^{-4} for OR algorithms and negligible for the AND.

Afterglow refers to signals from the luminosity detectors after a colliding bunch pair. After each paired BCID we observe a long tail of signals up to the μs range, which we attribute to slow collision debris. In particular slow neutrons are susceptible to cause delayed signals via nuclear reactions which result in de-excitation by photon emission.

Emittance growth

During a fill the emittance of the beam grows, which results in a simultaneous increase of Σ and decrease of $\mu_{\rm vis}$. In principle these effects cancel each other, but in practice this cancellation is not exact since the values are determined over a longer time, i.e. Σ's result from fits to several data-points spread in time and for $\mu_{\rm vis}$ we use the average of 2 scans, roughly 20 minutes apart.

There are various methods to estimate the emittance growth:

1. From wire-scanner and synchrotron light monitor data recorded by the LHC

2. From the decrease of $\mu_{\rm vis}$ between the scans, when beams were colliding head-on

3. From the fits of Σ and $\mu_{\rm vis}$ to the scan curves

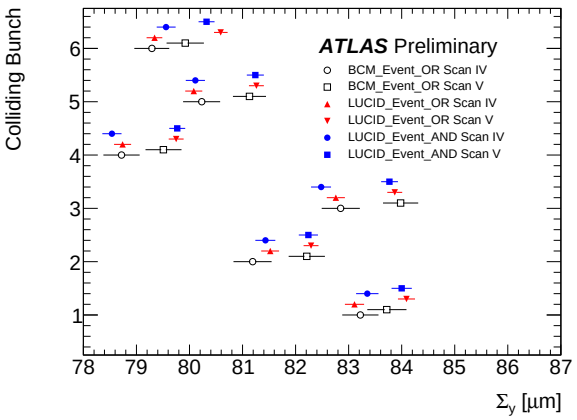

Figure 5: Σ_y for each colliding bunch pair, as determined from LUCID and BCM-EventOR data during the October scans. The error bars are statistical only and thus much larger for BCM which has a smaller count rate.

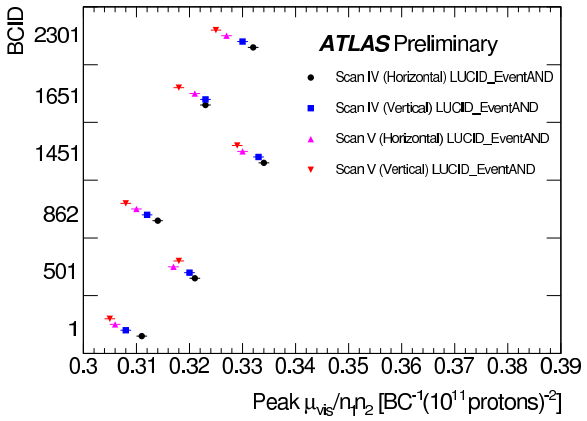

Figure 6: $\mu_{\rm vis}^{\rm sp,max}$ for each colliding bunch pair, as determined from LUCID-EventAND data. The error bars are statistical only.

The last of these can be seen in Figs. 5 and 6 and indicate an emittance increase of about 2% between scans IV and V. This is consistent with observation from the first 2 methods.

However, a comparison of the $\sigma_{\rm vis}$ values, obtained from the two scan-pairs, as shown in Fig. 7, confirms that the effect of emittance growth almost entirely cancels. The residual effect is $< 0.5\%$. It should be noted that this observed discrepancy between the scans accounts not only for the emittance growth but also for any other potential non-reproducibility effect.

Length scale

In Fig. 3 the luminosity data is plotted against the nominal beam separation, which is given by the currents in the separation magnets. In order to check this scale and dedicated length-scale calibration was done. The procedure was to displace one beam at the time and move the other until collisions were optimised at the offset position. At several such points data was taken and the ATLAS Inner Detector was used to reconstruct the primary vertex distribution. The correlation – an example is shown in Fig. 8 – between the shift of the reconstructed luminous centroid and the nominal displacement allowed to establish the length scale correction and uncertainty. The correlation was found to be excellent, so no correction was applied and an uncertainty of 0.3% was derived.

However, also an uncertainty related to the ID geometry enters. If the geometry of the ID would be distorted it could

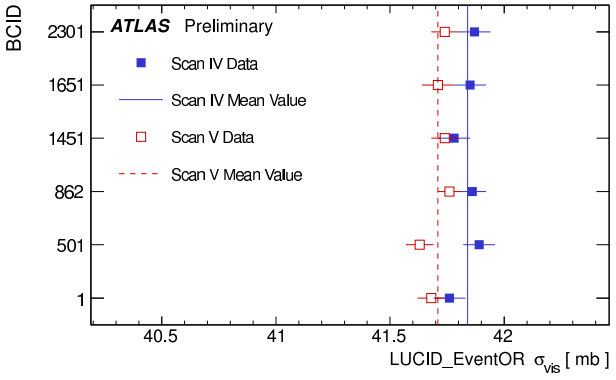

Figure 7: Values of $\sigma_{\rm vis}$ for each colliding bunch pair, as determined from LUCID-EventOR data. The error bars are statistical only.

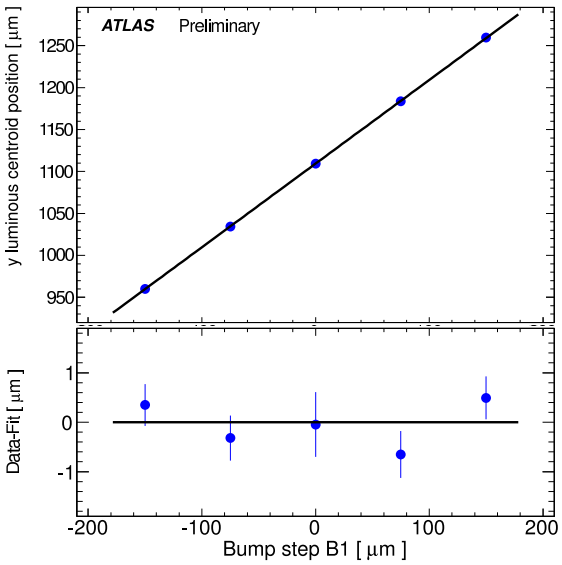

Figure 8: Length-scale calibration scan for the y direction of beam 1. The top plot shows the displacement of the luminous region as a function of the nominal displacement. The lower plot shows the residuals with respect to the linear fit.

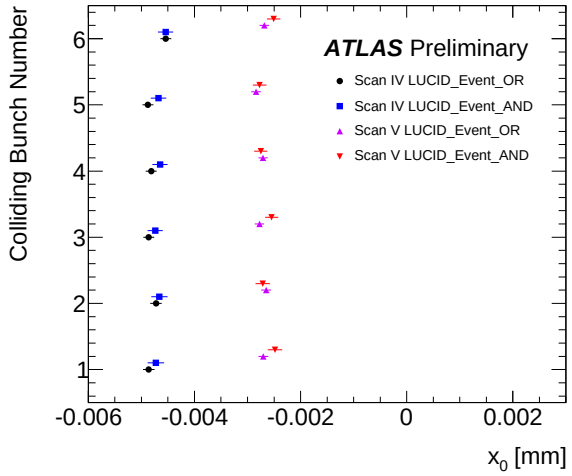

Figure 9: Values of x-displacement obtained from scans IV and V. After scan IV the displacement observed in online monitoring was corrected for. Nevertheless, a slightly smaller shift appeared in scan V.

lead to a wrong reconstructed displacement. These effects were studied by Monte Carlo using the extreme limit of data-driven alignment. These studies allowed to assign a conservative 0.3% uncertainty on the luminosity calibration due to this effect.

Beam centring and jitter

A potential source of error for the vdM scan is if the beams are not properly centred in one coordinate while the other is scanned. Our procedure of interleaved x and y scans allows to estimate the possible displacement and to correct for it if needed. In the October scans we observed perfect stability of the y-coordinate. However, Fig. 9 shows that there was indeed drift in x at the level of few μm. Compared to the beam-sizes during the scan this displacement corresponds to an uncertainty of only 0.04%.

Another source of uncertainty is a possible jitter of the beam position around its nominal value. A jitter of 0.8 μm measured during the length-scale calibration scan translates into an uncertainty of 0.3% on $\sigma_{\rm vis}$ [6]

Transverse correlations

Non-linear transverse correlations were discovered in the final stages of the analysis as a potentially important uncertainty. However, a detailed analysis allowed to estimate their effect to be only 0.9% in the October scans [6].

Summary of systematic effects

The evaluation of all components of the systematic uncertainty are discussed in detail in Ref. [6]. Table 3 summarises these contributions. It can be seen that, despite a significant reduction of the beam current related error, the total uncertainty remains to be dominated by it.

Table 3: Systematic uncertainties, in %, on the value of $\sigma_{\rm vis}$.

Scan Number	I	II-III	IV-V
Bunch charge product	5.6	4.4	3.1
Beam centring	2	2	0.04
Emittance growth & other non-reproducibility	3	3	0.5
Beam-position jitter	—	—	0.3
Length scale calibration	2	2	0.3
Absolute ID length scale	0.3	0.3	0.3
Fit model	1	1	0.2
Transverse correlations	3	2	0.9
Pileup correction	2	2	0.5

The total systematic uncertainty in the October vdM scan is estimated to be 3.4%.

ALGORITHM CONSISTENCY

Fig. 10 gives a comparison of the specific luminosities, as determined during the October vdM scans for all ATLAS luminosity algorithms. The excellent consistency is evident, especially in the plot where all six colliding BCID's are averaged to reduce the statistical scatter.

In the other plots the worse statistics of the offline algorithms is evident. This is no intrinsic deficiency of the algorithms but just a reflection of the smaller number of triggered events available for offline analysis.

LONG-TERM STABILITY

While we have been able to reach a systematic uncertainty well below 5% in the vdM calibration itself, this alone does not assure that we can measure the luminosity with such an accuracy at all times thereafter – or before.

In fact several parameters which can change between ATLAS runs can have an influence on the measured luminosity:

- stability of detector efficiency
- beam-related background
- bunch-spacing (e.g. afterglow level)
- pileup conditions

The first of these points can to a large extent be controlled by frequent calibrations with light pulses – typically once a day for LUCID. The background and afterglow can be estimated from the data and the pileup corrections can be studied by comparing different algorithms.

In all cases, however, it is an asset of ATLAS to have several independent luminosity monitors and algorithms at its disposal. These allow to promptly recognise and diagnose any drifts of individual luminosity algorithms. Such a

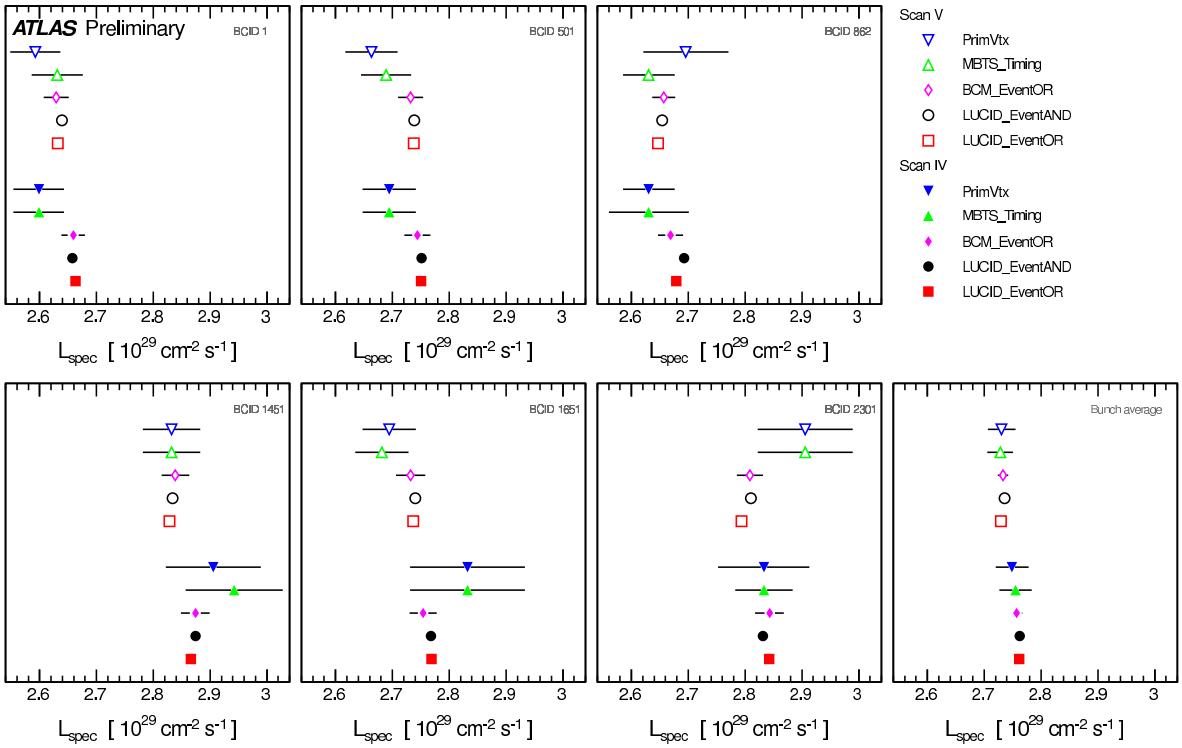

Figure 10: Specific luminosities (Eq. 12 in units of $10^{29}\,\mathrm{cm}^{-2}\mathrm{s}^{-1}$ $(10^{11}$ protons$)^2$ for various ATLAS luminosity detectors and algorithms [6]. The error bars reflect the statistical uncertainties only.

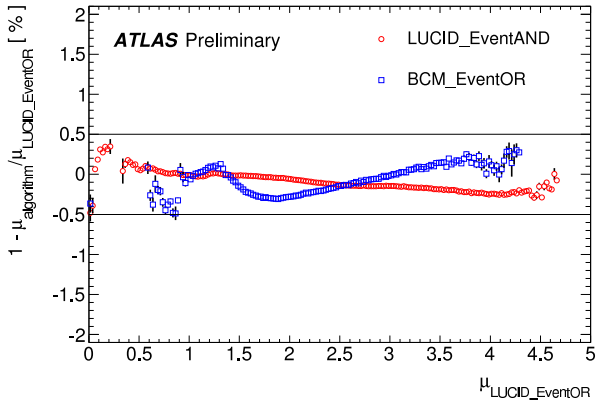

Figure 11: Fractional deviation in average value of μ as obtained using different algorithms with respect to the corresponding value from LUCID-EventOR. The curves are obtained as averages over several runs [6].

constant monitoring ensures that a once established calibration can be maintained stable over long periods of varying beam conditions – although not necessarily over prolonged shutdowns.

In particular, Fig. 11 shows the deviation of the pileup-corrected value of μ for two detectors and algorithms with respect to LUCID-EventOR. All three algorithms are consistent within $\pm 0.5\%$ over the whole range of μ covered by the 2010 LHC run. This indicates that our pileup correction formalism is adequate and also shows that the calibration is stable over time and between runs.

CONCLUSIONS

During the 2010 LHC run the luminosity determination in ATLAS was based on 3 detectors providing online data and additional 4 offline algorithms. This redundancy was very useful for long-term stability monitoring and estimation of detector related systematic effects.

Uncalibrated all of these methods can provide only information about relative luminosity variations. In order to obtain absolute luminosities several van der Meer scans were performed in 2010. These allow to extract the absolute luminosity from beam intensities and detector response as a function of beam separation.

The systematic uncertainties related to the scan procedure have been studied in detail and the final uncertainty in the 2010 luminosity calibration is estimated to be 3.4%. This value does not include stability of the luminosity monitors over time and in varying beam conditions. These effects have to be controlled by intercomparison of the different monitors and algorithms. Such monitoring over the entire 2010 proton-proton operation showed that long-term stability was within $\pm 0.5\%$.

REFERENCES

[1] ATLAS Collaboration, G. Aad et al., *The ATLAS Experiments at the CERN Large Hardon Collider*, JINST **3** (2008) S08003.

[2] ATLAS Collaboration, G. Aad et al., *Luminosity Determination Using the ATLAS Detector*, ATLAS-CONF-2010-060 (2010).

[3] B. Heinemann, these proceedings.

[4] ATLAS Collaboration, G. Aad et al., *Luminosity Determination in pp Collisions at sqrt(s)=7 TeV Using the ATLAS Detector at the LHC*, `arXiv:1101.2185 [hep-ex]` (2011), submitted to EPJC.

[5] S. van der Meer, *Calibration of the effective beam height in the ISR*, CERN-ISR-PO-68-31, (1968).

[6] ATLAS Collaboration, G. Aad et al., *Updated Luminosity Determination in pp Collisions at $\sqrt{s}$=7 TeV using the ATLAS Detector*, ATLAS-CONF-2011-011 (2011).

[7] T. Pauly, these proceedings.

Comparison of the ATLAS and CMS Luminosity Measurements during pp Collisions in 2010 at $\sqrt{s} = 7$ TeV

B. Heinemann, UC Berkeley and Lawrence Berkeley National Laboratory, Berkeley, CA 94720, USA

Abstract

In this article a comparison between the determination of the luminosity from the two large multi-purpose LHC experiments, ATLAS and CMS, is made. The luminosities measured in some individual example LHC fills are compared directly. In addition comparisons between several physics cross sections are made and their agreement is quantified. It is found that the measurement of the luminosity is consistent between the two experiments within the uncorrelated uncertainties.

INTRODUCTION

In this article a comparison of the CMS and ATLAS luminosity and cross section measurements is presented with the aim of understanding if both experiments receive the same luminosity from the LHC. In the following sections we first briefly describe the methods used for calibrating the absolute luminosity with emphasis on the differences between ATLAS and CMS. We then compare directly the luminosity measured by the experiments before we compare the cross section measurements based on that luminosity. Finally we conclude.

METHODS USED FOR THE CALIBRATION OF THE ABSOLUTE LUMINOSITY

Both ATLAS and CMS determine the absolute luminosity calibration using dedicated van-der-Meer scans as reported in these proceedings [1, 2]. This calibrated luminosity is reported online to the LHC and it is used offline by physics analyses in both experiments. The results presented in this report all rely on the preliminary calibrations derived from the van-der-Meer scans from April and May 2010 where the overall precision was 11% on the luminosity measurement. 10% of this uncertainty is, however, due to the beam current measurement and correlated between the two experiments. The strictly uncorrelated part of the luminosity measurement is 4.2% for CMS and 4.7% for ATLAS. The uncertainty on the ratio of the ATLAS to CMS luminosity measurement is thus 6.3% and this will be used to evaluate the consistency between the two experiments.

A major difference between the two experiments is that ATLAS counts *events* while CMS counts *hits*. The ATLAS method is rather sensitive to pileup pp interactions but ATLAS has demonstrated that this can be corrected for with an uncertainty $< 0.5\%$. The CMS method is intrinsically less sensitive to pileup and CMS quotes an uncertainty on this better than 1%.

COMPARISON OF THE LUMINOSITY MEASUREMENTS BY FILL

Both ATLAS and CMS report the luminosity as measured online to the LHC via DIP and these values are stored in the `TIMBER` database. We analysed the 18 fills taken with stable beams between 1364 (Sept. 22nd) and 1418 (Oct. 14th). Fig. 1 shows this comparison for two example LHC fills. In fill 1418 the value of this ratio is stable at 1.02 and this is typical: for 16 of the 18 LHC fills the ratio is consistent with 1.02 ± 0.02. There were two cases where a larger difference was observed, e.g. in fill 1397 also shown in Fig. 1. In this particular fill the ratio is about 1.06 during most of the fill. However, at the end the ratio goes back to 1.02. The reason in this particular case is that CMS did not report any luminosity measurement at the start of the fill so that the LHC was not able to optimize the luminosity. At the end of the fill LHC did a beam optimization scan and after that the ratio returned back to the typical value of 1.02. The other case where a larger difference was observed is 1372 during which the so-called *hump* was present. We observe a much larger emittance growth than usual and an apparent correlation between the horizontal and vertical plane. It is possible that this causes then a real difference in the two experiments due to e.g. the crossing angles being in different planes. This is not yet understood quantitatively.

COMPARISON OF CROSS SECTION MEASUREMENTS

In this section we compare cross section measurements from ATLAS and CMS.

W and Z Boson Production Cross Sections

Both experiments have published measurements of the W and Z boson cross sections based on 0.3 pb^{-1} (ATLAS [3]) and 2.9 pb^{-1} (CMS [4]). The values are given in Table 1.

Considering only the uncorrelated uncertainties the resulting ratios for the ATLAS to CMS cross sections are $1.00 \pm 0.06(\mathrm{stat} + \mathrm{sys}) \pm 0.06(\mathrm{unc.lumi})$ for the W cross section and $0.88 \pm 0.09(\mathrm{stat} + \mathrm{sys}) \pm 0.06(\mathrm{unc.lumi})$ for the Z boson cross section. These ratios are in good agreement within the uncertainties. This comparison is as not yet probing the luminosity to a precision better than 10% but is expected to achieve a precision much better than 5% when the full 2010 dataset is analysed and experimental uncertainties of both statistical and systematic nature will be much improved.

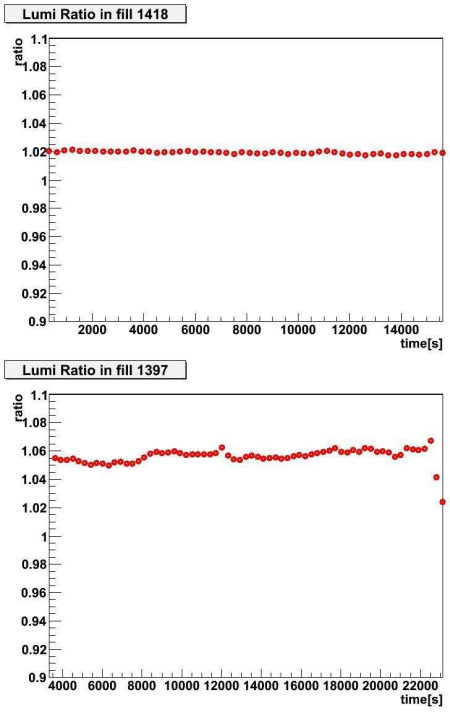

Figure 1: Ratio of the ATLAS to CMS instantaneous luminosity for LHC fills 1418 (top) and 1397 (bottom) as function of time during the fill.

Table 1: Cross sections for W and Z boson production as measured by the ATLAS and CMS collaborations. Also given is the ratio of the ATLAS to the CMS cross section measurement including only the uncorrelated uncertainties on the measurement. The ATLAS measurements are based on an integrated luminosity of 0.3 pb^{-1} and those of CMS are based on 2.9 pb^{-1}.

Experiment	$\sigma(W)$ (nb)
ATLAS	$9.96 \pm 0.55(\text{stat} + \text{sys}) \pm 1.10(\text{lumi})$
CMS	$9.95 \pm 0.29(\text{stat} + \text{sys}) \pm 1.09(\text{lumi})$
	$\sigma(Z)$ (nb)
ATLAS	$0.82 \pm 0.08(\text{stat} + \text{sys}) \pm 0.09(\text{lumi})$
CMS	$0.931 \pm 0.035(\text{stat} + \text{sys}) \pm 0.102(\text{lumi})$

Charged Particle Cross Section

During early LHC running another method was devised to allow for a direct comparion between the LHC experiments fill by fill by using the high statistics cross section of minimum bias interactions. While there exists no high precision theoretical prediction (as is the case for the W and Z boson cross sections [5]) for this process it can serve to compare the experiments fill by fill.

The ATLAS and CMS experiments have measured the cross section for events that have at least one primary charged particle with $p_T > 0.5$ GeV/c and $|\eta| < 0.8$ as this region ensures a high experimental acceptance in ATLAS, CMS and ALICE. Primary charged particles are defined as charged particles with a mean lifetime $\tau > 0.3 \times 10^{10}$ s either directly produced in pp interactions or from subsequent decays of particles with a shorter lifetime. The measurements are performed by selecting minimum bias interactions that have at least one reconstructed track and are corrected for any detector-specific effects such as the tracking and vertex efficiencies, the trigger efficiency, the pileup interactions etc. [6, 7, 8]. LHC fill 1089 taken in May 2010 was chosen for an initial comparison. The instantaneous luminosity in this fill was about 2.1×10^{28} cm^{-2}s^{-1} at the start and 1.3×10^{29} cm^{-2}s^{-1} at the end of the fill, and there was one bunch pair colliding in ATLAS and CMS. The average number of events per crossing is about $\mu = 0.1$. Both CMS and ATLAS did van-der-Meer-scans during this fill, and here only the part of the fill where no scan was performed is compared.

The rates of events are shown in Fig. 2. It is seen that the rate decreases as function of time due to the decrease in luminosity. It is also seen that the correction from the raw to the physical rate is about 10%. For the CMS measurement both the raw and the fully corrected rate is shown. For ATLAS the corrected rate is shown both with and without the pileup correction.

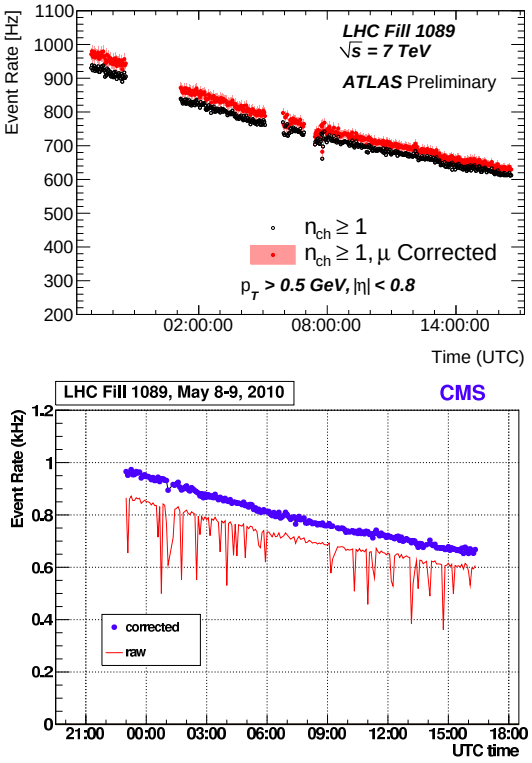

Figure 2: ATLAS (top) and CMS (bottom) measurements of number of events selected by the charged particle analysis. For ATLAS the corrected rate is shown with and without the correction for pileup. For CMS the raw and the fully corrected rate is shown. The dips in the raw CMS rate are due to deadtime and are corrected for in the final result. The overall deadtime correction for CMS integrated over the fill is well below 1%.

The overall correction factor (from raw to fully corrected) is about 10% at the beginning and 8% at the end of the fill: this time dependence is a result of the decreasing value of μ during the run, i.e. the decreasing pileup. In addition there are certain times when a much larger correction is applied due to significant deadtime. The overall correction factor for tracking, vertexing efficiency etc. is 1.040 ± 0.017 in ATLAS.

The cross section is shown for ATLAS and CMS in Fig. 3 after all corrections. ATLAS finds $\sigma_{ATLAS}(\mathrm{ChPart}) = 42.3 \pm 0.7(\mathrm{stat.+sys.})$ mb and CMS finds $\sigma_{CMS}(\mathrm{ChPart}) = 43.99 \pm 0.62(\mathrm{stat.+sys.})$ mb, and thus the ratio of the two cross sections is

$$R = 1.040 \pm 0.022(\mathrm{stat.+sys.}) \pm 0.062(\mathrm{unc.lumi}).$$

This assumes that all the expertimental uncertainties between the ATLAS and CMS measurement are uncorrelated as they are dominated by the understanding of the tracking efficiency. This ratio is again consistent with unity within the uncertainties quoted. Also, note that both measurements are flat vs time during this fill.

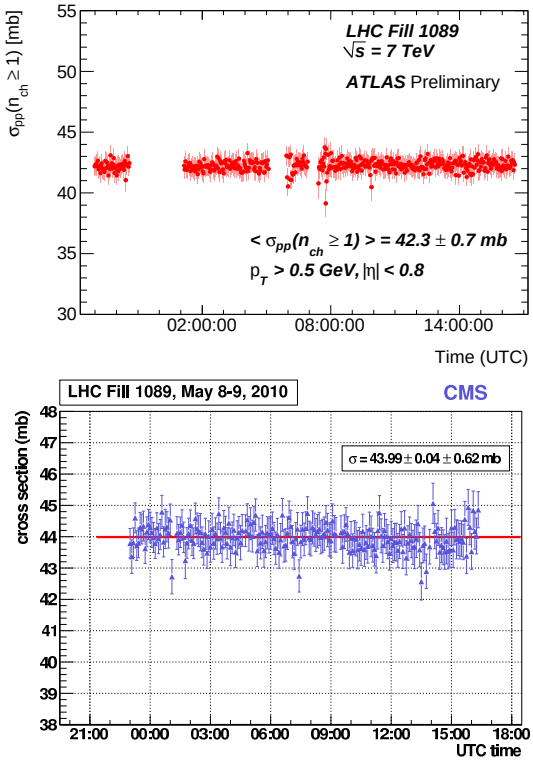

Figure 3: ATLAS (top) and CMS (bottom) measurements of the cross section for charged particles with $p_T > 0.5$ GeV/c and $|\eta| < 0.8$ as function of time during LHC fill 1089.

CONCLUSIONS

A comparison between the CMS and ATLAS measurements for the luminosity has been presented. For most fills the two luminosity measurements agree to within 2%. The cross sections of W and Z boson production and of the production of events with a prompt charged particle with $p_T > 0.5$ GeV/c and $|\eta| < 0.8$ also agree to within the uncorrelated systematic uncertainties. It will be interesting to repeat this comparison when the uncertainty on the W and Z cross section measurements is improved using the full 2010 datasets. Also, since the time of writing these proceedings the luminosity precision has been improved significantly (e.g. to 3.4% by ATLAS [11]) using the van der Meer scan from October 2010, and the much improved understanding of the beam current uncertaunties [9, 10]. These comparisons should be repeated with the updated much more precise luminosity calibration.

ACKNOWLEDGMENTS

I would like to thank N. Bachetta, G. Brandt, L. Malgeri, M. Schmitt, M. Tibbetts and L. Tompkins for providing the information relevant to this article. I am also thankful to the accelerator team of the Large Hadron Collider for the efficient commissioning and operation of the LHC during this initial high-energy data-taking period. I want to express my gratitude to the organizers of this very useful workshop: H. Burkhardt, Massimiliano Ferro-Luzzi and M. Mangano. In addition, I thank the Department of Energy in the United States of America for their financial support.

REFERENCES

[1] G. Aad *et al.* (ATLAS Collaboration), *Luminosity Determination in pp Collisions at sqrt(s)=7 TeV Using the ATLAS Detector at the LHC*, arXiv:1101.2185, submitted to EPJC; M. Huhtinen, these proceedings.

[2] M. Zanetti, these proceedings.

[3] G. Aad *et al.* (ATLAS Collaboration), *Measurement of the $W \to \ell\nu$ and $Z/\gamma^* \to \ell\ell$ production cross sections in proton-proton collisions at $\sqrt{s} = 7$ TeV with the ATLAS detector*, JHEP **1012** (2010) 060.

[4] V, Kachatryan *et al.* (CMS Collaboration), *Measurements of Inclusive W and Z Cross Sections in pp Collisions at $\sqrt{s} = 7$ TeV*, JHEP **01** (2011) 080.

[5] M. Schott, these proceedings.

[6] https://twiki.cern.ch/twiki/bin/view/AtlasPublic/RunStatsPublicResults2010.

[7] The ATLAS Collabortion, *Central charged-particle multiplicities in pp interactions with $|eta| < 0.8$ and $p_T > 0.5$ and 1 GeV measured with the ATLAS detector at the LHC*, ATLAS-CONF-2010-101.

[8] CMS Collaboration, *Luminosity Study: Events with a Central Track*, CMS Note DP-2011/004.

[9] G. Anders *et al.*, *LHC Bunch Current Normalisation for the April-May 2010 Luminosity Calibration Measurements*, CERN-ATS-Note-2011-004 PERF, Feb, 2011.

[10] G. Anders *et al.*, *LHC Bunch Current Normalisation for the October 2010 Luminosity Calibration Measurements*, CERN-ATS-Note-2011-016 PERF, in preparation.

[11] ATLAS Collaboration, *Updated Luminosity Determination in pp Collisions at $\sqrt{s} = 7$ TeV using the ATLAS Detector*, ATLAS-CONF-2011-011.

LUMINOSITY DETERMINATION AT THE TEVATRON*

V. Papadimitriou#, Fermilab, Batavia, IL 60510, U.S.A.

Abstract

In this paper we discuss the luminosity determination at the Tevatron. We discuss luminosity measurements by the machine as well as by using the luminosity detectors of the CDF and D0 experiments. We discuss the uncertainties of the measurements, the effort to maximize the initial and integrated luminosity, the challenges and the lessons learned.

INTRODUCTION

Luminosity measurements are an absolutely necessary component of any experimental beam colliding program since they provide the frequency of the interactions and the needed normalization for the physics processes under study. Luminosity measurements also allow for the monitoring of the performance of the accelerator and for implementation of beam parameter adjustments as needed for optimized performance. We describe here absolute luminosity measurements by the machine based on the measurement of beam parameters, and real time, relative luminosity measurements performed by CDF and D0 which are then normalized to the inclusive, inelastic proton-antiproton cross section.

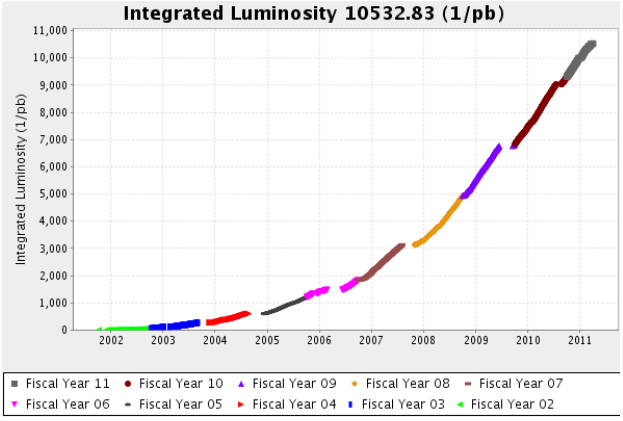

Figure 1: Tevatron integrated luminosity in Run II (averaged over the CDF and D0 experiments) as a function of time.

TEVATRON PERFORMANCE

In 2010 the Tevatron Collider celebrated the 25th anniversary of proton-antiproton collisions that took place for the first time on October 17, 1985. The Tevatron, a proton-antiproton collider, has delivered 110 pb^{-1} per experiment to the CDF and D0 experiments in Run I (1992 – 1996) at a center of mass energy of 1.8 TeV. In Run I, six proton bunches were colliding with six antiproton bunches with a 3.5 μs spacing between collisions. Since the beginning of Run II and by the end of March 2011 the Tevatron has in addition delivered 10.5 fb^{-1} per experiment at a center of mass energy of 1.96 TeV (see Fig. 1). In Run II, thirty six proton bunches are colliding with thirty six antiproton bunches with a 396 ns spacing between collisions. The proton and antiproton beams in the Tevatron share a common vacuum pipe. Their paths are controlled by electrostatic separators which keep the beams apart around most of the Tevatron ring and bring them to collision at the CDF and D0 Interaction Points (IPs).

On April 16, 2010 there was set an initial luminosity record of 4.024 x 10^{32} $cm^{-2}s^{-1}$. Between April 13 and April 20, 2009 the accelerator complex delivered a record of 73.1 pb^{-1} per experiment in a single week and in March 2010 it delivered a record of 272.7 pb^{-1} per experiment within a month. The Tevatron is expected to have delivered 11.1–12.1 fb^{-1} per experiment in Run II by the end of September of 2011.

LUMINOSITY IMPROVEMENTS

Run II started in the summer of 2001 and by the end of the year the instantaneous luminosity was in the range of (5-10) x 10^{30} $cm^{-2}s^{-1}$. A lot of effort was invested in the follow up years in increasing the Tevatron luminosity (see Fig. 1 and 2). There is a long list of upgrades that took place, of which we list a few here. Understanding and tuning the Tevatron optics was a key contributor to the success. In 2002/2003 it was identified that the coupling in the Tevatron was not small, which led to significant emittance growth. During three long accelerator shudowns between 2003 and 2006 the global coupling around the machine was reduced by reshimming the Tevatron dipoles to address the coherent skew quadrupole component that was slowly growing. The completion of the Tevatron Beam Position Monitor (BPM) electronics upgrade in 2005 enabled more accurate beam lattice measurements, helped identify rolled quadrupoles, allowed for orbit stabilization within a store, and better monitoring of orbits store-to-store, resulting therefore in better reproducibility and enhanced reliability. In September 2005 a new Tevatron optics lattice was implemented decreasing the betatron amplitude function at the IPs, β*, from 35 cm to 29 cm. This increased the instantaneous luminosity by ~ 10%. At the same time the number of antiprotons available for Tevatron stores got increased by improvements in beam loading, longitudinal matching and damper optimization at the Main Injector, which resulted in an increase of protons

* Work supported by DE-AC02-07CH11359
# vaia@fnal.gov

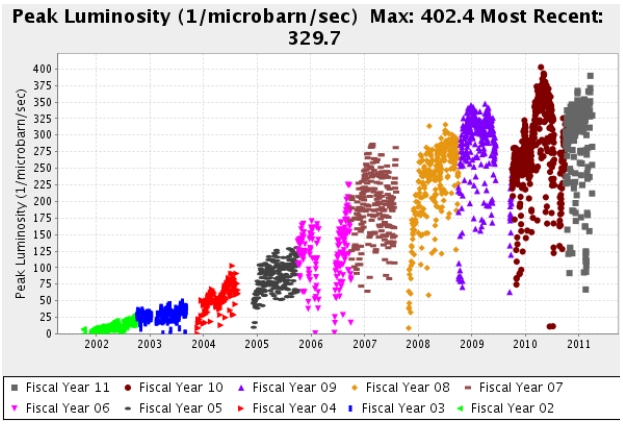

Figure 2: Tevatron peak luminosity in Run II (averaged over the CDF and D0 experiments) as a function of time.

at the antiproton production target by ~ 20%. In 2005 electron cooling at the Recycler became operational (maximum stash size of 6.08 x 10^{12} on March 21, 2011). In the mean time, since 2005 the antiproton stacking rate kept gradually improving with highest average stacking rate for one week of 25.65 x 10^{10}/hr (January 2011). Additional electrostatic separators introduced in 2005/2006 allowed for an about 20% improvement in the luminosity lifetime, and implementation of the 1.7 GHz Schottky monitors and tune feedback improved it even further. The 2nd order chromaticity compensation circuits implemented in 2007 allowed for higher proton intensity and also improved the luminosity lifetime. Tevatron alignment, which was performed almost every year during the long shutdowns, contributed significantly in the good performance of the machine. In 2009-2010 the shot setup duration was also reduced by about 20% allowing for faster turn-around between stores.

Although there has been a lot of effort in increasing the instantaneous luminosity in Run II, the goal in the past few years has been to maximize the integrated luminosity to the experiments instead of trying to achieve higher instantaneous luminosities.

LUMINOSITY MEASUREMENTS

Machine

Absolute luminosity measurements by the machine are based on measurements of beam parameters like intensities, emittances, beam lattice, etc. and have an overall uncertainty of about 15-20%. In Eq. 1 one can see the dependence of the instantaneous luminosity on the number of protons and antiprotons per bunch, the emittances of the two beams and β*. The emittances of the beams are directly related to the standard deviations of the beams spatially at the IPs. In Run II, the revolution frequency (f_0) is ~48 kHz and the number of bunches, *B*, is 36. $F(\sigma_z/\beta^*)$ is an hourglass form factor depending on the bunch length σ_z and on β*.

$$L = \frac{3\gamma f_0 N_p (BN_{\bar{p}})}{\beta^*(\varepsilon_p + \varepsilon_{\bar{p}})} F(\sigma_z / \beta^*) \qquad (1)$$

Intensities of protons and antiprotons are being measured by a Fast Bunch Integrator (FBI) of a Wall Current Monitor and by a Sampled Bunch Display (SBD). Both devices are ultimately scaled to a DC Current Transformer (DCCT) which is the most accurate device we have for measuring the total current in the Tevatron. The DCCT uncertainty is 1-2%. Typically, the measurement of the transverse beam emittances is based on the measurement of the transverse beam profiles. In the presence of dispersion, *D*, the momentum spread of the beam needs to be measured as well (see Eq. 2). Transverse beam profiles at the Tevatron are being measured by Flying Wire monitors, a synchrotron light monitor and ionization profile monitors. This allows for cross checking. The systematics of the Flying Wire (5 μm thick carbon fiber) measurements include the wire position measurement, the scintillator acceptance as a function of the beam position and the influence from previously scattered particles. The systematics of the synchrotron light monitor include the optical magnification, the non-uniformity and degradation of the intensifier as a function of time and the optical acceptance. The systematics of the Ionization Profile Monitors include resolution effects, the baseline subtraction, microchannel plate non-uniformities and degradation, etc.

$$\varepsilon_{tr} = \frac{6\pi(\beta\gamma)_{rel}}{\beta}\left[\sigma^2 - D^2\left(\frac{dp}{p}\right)^2\right] \qquad (2)$$

The momentum spread of the beam is being measured with the SBD. The overall uncertainty of emittance measurements is about 15%. In Fig. 3 we display Flying Wire normalized proton horizontal emittances through the accelerator chain as a function of time.

The beam optics parameters are being measured mainly within proton-only Tevatron stores using the orbit response method [1]. In Table 1 we show the β* and the dispersion at the CDF and D0 IPs as measured in the end of the long shutdown in 2010. The uncertainties vary between 5% (ideal case) and 15% depending on the goal of the measurement and coordination with other machine studies.

We routinely perform electrostatic separator scans to determine if the beam is well centered at the two IPs.

CDF and D0 Experiments

The official Tevatron luminosity measurements are based on the relative luminosity measurements performed by the CDF and D0 experiments which are then normalized to a relatively well known and copious process, in this case the inclusive inelastic proton-

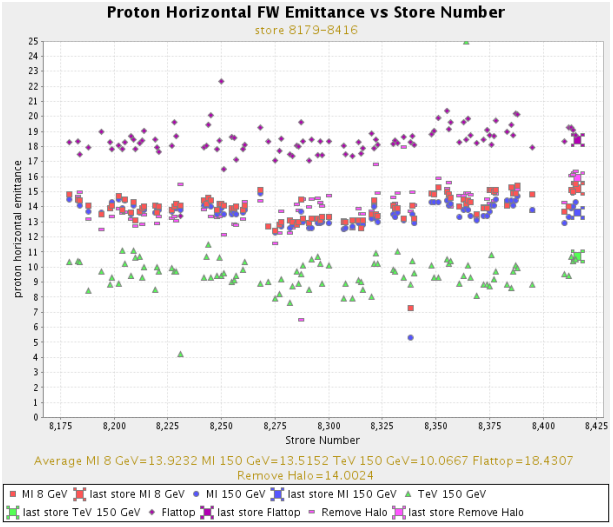

Figure 3:.Normalized, 95% proton horizontal emittances through the accelerator chain as a function of Tevatron store number (time).

Table 1: Measured β* and D* parameters for the CDF and D0 interaction points in the end of August, 2010

	β^*_x proton	**β^*_y proton**	**β^***
CDF	30.7 cm	30.8 cm	30.7 cm
D0	27.7 cm	32.7 cm	30.2 cm
	D**$_x$ proton	***D**$_y$ proton***	***D****
CDF	1.1 cm	1.7 cm	2.0 cm
D0	1.4 cm	-0.7 cm	1.6 cm

antiproton cross section. The instantaneous luminosity $\mathcal{L}$ is being estimated by using Eq. 3, where μ is the average number of interactions per beam crossing, f_{BC} is the frequency of bunch crossings, σ_{in} is the inelastic cross section and ε^{det} the acceptance of the detector. The average number of interactions can be estimated either by measuring the probability of zero interactions ($P_0(\mu)=e^{-\mu}$ for a detector of 100% acceptance) or directly, by counting particles or hits or time clusters in the detector. The CDF and D0 collaborations have agreed to use a common proton-antiproton inelastic cross section for luminosity normalization in Run II. This common cross section has been derived [2] on the basis of averaging the inelastic cross sections measured by the Fermilab CDF and E811 experiments at 1.8 TeV and by extrapolating the cross section at 1.96 TeV.

$$\mu \cdot f_{BC} = \sigma_{in} \cdot \varepsilon^{\det} \cdot \mathcal{L} \qquad (3)$$

In addition, luminosity measurements get cross calibrated with rarer, cleaner and better understood processes like the decay $W \to l \cdot \nu$.

Both experiments have used scintillating counters to measure the luminosity during Run I. For Run II where the instantaneous luminosity is substantially higher, CDF opted for a Cherenkov counter system while D0 for a scintillating system of better granularity than Run I.

The CDF Cherenkov counter system [3] consists of 48 counters per side arranged in 16 layers with 16 counters each covering the pseudorapidity region $3.7 \le |\eta| \le 4.7$. The counters are filled with isobutane and are being read by Hamamatsu R5800QCC Photomultipliers (PMTs) with quartz window. The Cherenkov counter system allows for good separation between primaries and secondaries, good amplitude resolution (~18% from photostatistics, light collection and PMT collection), good timing resolution and in addition it is radiation hard. In Fig. 4 is displayed the amplitude distribution for CDF data vs full simulation with PYTHIA in one Cherenkov counter after an isolation requirement of less than 20 photoelectrons in the surrounding counters. The Single Particle Peak (SPP) is clear. Fig. 5 shows how the average number of particles (total amplitude over the amplitude of the SPP) or hits (counters with amplitude above a certain threshold) varies as a function of the average number of proton-antiproton interactions and compares the data with the Monte Carlo simulation. The data and the simulation compare very well. At the highest luminosities the particle counting algorithm is more linear. As a reference, note that μ approximately equal to 6 corresponds to $\mathcal{L}$ approximately equal to 2 x 10^{32} $cm^{-2}s^{-1}$. The CDF luminosity measurement is based as a default on measuring the probability of zero interactions and uses measuring hits and particles as a cross check. CDF has evaluated that the luminosity measurement using the probability of zero interactions is reliable up to about 3.6 x 10^{32} $cm^{-2}s^{-1}$. The current CDF luminosity measurement uncertainty is 5.8%. The leading contribution is from normalizing to the proton-antiproton inelastic cross section (4%). The next two most important contributions are due to simulating the material in the detector (3%) and the relative contribution from non-diffractive and diffractive processes in the Monte Carlo generator (2%). CDF is cross checking their absolute luminosity measurements by comparing with the inclusive W and Z boson cross section measurements and the comparison is very satisfactory. The yield of J/ψ's and W's through the $J/\psi \to \mu\mu$ and $W \to l\nu$ decays as a function of instantaneous luminosity serves as an additional check of the stability of the luminosity measurements. The aging rate of the PMTs is ~35% per fb^{-1} and is being addressed by High Voltage and PMT gain adjustments or with replacements as needed.

The D0 Run II luminosity system [4] consists of two forward scintillator arrays covering the pseudorapidity region $2.7 \le |\eta| \le 4.4$. There are 24 wedges per array, each read out with a fine mesh PMT. Inelastic collisions are being identified by using the coincidence of in-time hits in the two arrays. Since October 2005 the luminosity

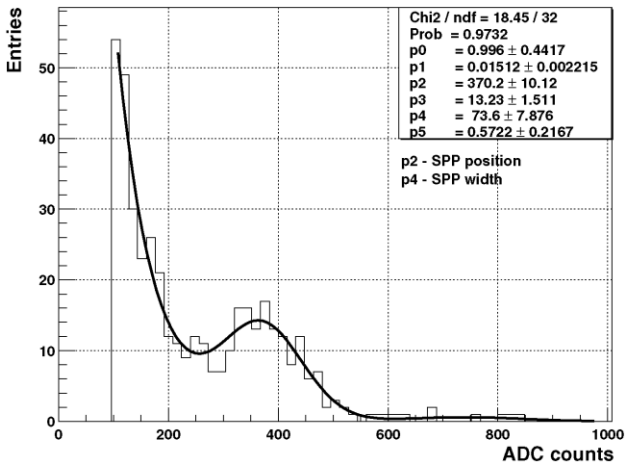

Figure 4:Amplitude distribution for a single Cherenkov counter at CDF. The solid line represents a fit to the data.

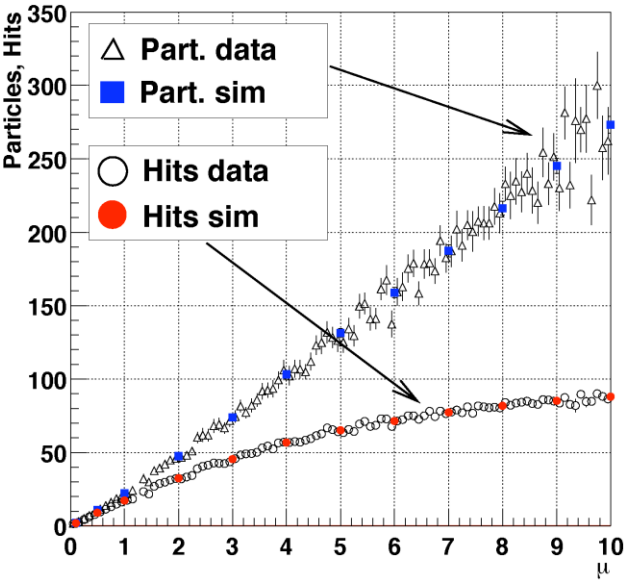

Figure 4: Data vs Monte Carlo simulation comparison of the average number of particles or hits vs the average number of proton-antiproton interactions at CDF.

readout electronics changed from NIM to custom VME [5]. The D0 luminosity measurement is based on measuring the probability of zero interactions. The current D0 luminosity measurement uncertainty is 6.1%. The leading contribution is from normalizing to the proton-antiproton inelastic cross section (4%). The next two most important contributions are due to the determination of the non-diffractive fraction (~4%) and the long term stability (~2.8%). Fig. 5 shows a data-Monte Carlo simulation comparison of counter multiplicity (above a threshold) assuming the final, non-diffractive fraction of 0.687±0.044. D0 is using the yield of forward muons as a function of time and instantaneous luminosity (see Fig. 6) as an additional check of the stability of the luminosity measurements (within ~1% during the past few years). The radiation damage to the scintillator is being addressed by annealing and replacement as needed.

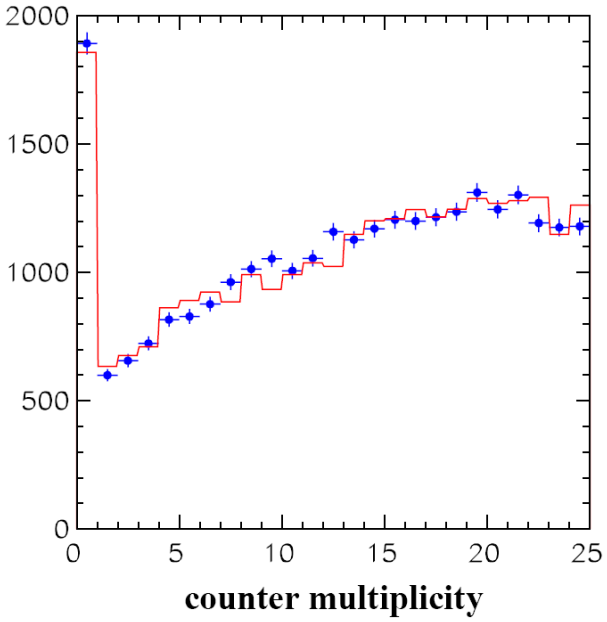

Figure 5: Data vs Monte Carlo simulation comparison of the multiplicity of the luminosity counters at D0 using the non-diffractive fraction. The points represent the data and the solid line the Monte Carlo. The plot corresponds to an instantaneous luminosity of 1.3 x 10^{31} $cm^{-2}s^{-1}$.

Luminosity Task Force

In 2003 there was established the Luminosity Task Force, a joint effort between Accelerator, CDF and D0 colleagues, to address luminosity detector issues, beam position and beam width issues and other Tevatron issues affecting luminosity. We exchange information on a daily basis and meet as a larger group on a monthly basis or as needed. As a result, several machine studies have been performed and we have now a much better understanding of the Tevatron optics, the crossing angles and vacuum at the two IPs, the emittance of the proton and antiproton beams as well as of the luminosity detectors of both experiments. We monitor on a store-by-store basis luminosity related quantities for the experiments and the machine and examine their inter-correlations as well as possible correlations with external factors.

The CDF/D0 ratio of instantaneous luminosities is one of such quantities being checked on a store-by-store basis (see Fig. 7) and being compared with the expected ratio on the basis of beam parameters. The goal is to keep this ratio within a few percent around 1. Significantly larger deviations observed a few times so far have led to thorough investigation on both the machine and experiment sides and resulted to either machine parameter

adjustments or to improvements in the techniques used by the experiments to measure the luminosity.

The CDF and D0 experiments provide as well on a regular basis measurements of beam parameters (beam position, beam emittance and β*) which are then being compared with the corresponding accelerator measurements. The CDF and D0 measurements are results of a fit of beam widths at the IPs as a function of z according to a model, where z is the axis along the direction of the collisions.

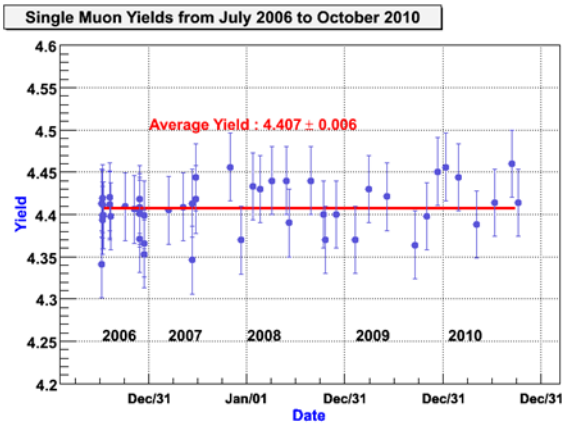

Figure 6: Single muon yields as a function of time, produced regularly by the D0 experiment to cross check the luminosity measurements.

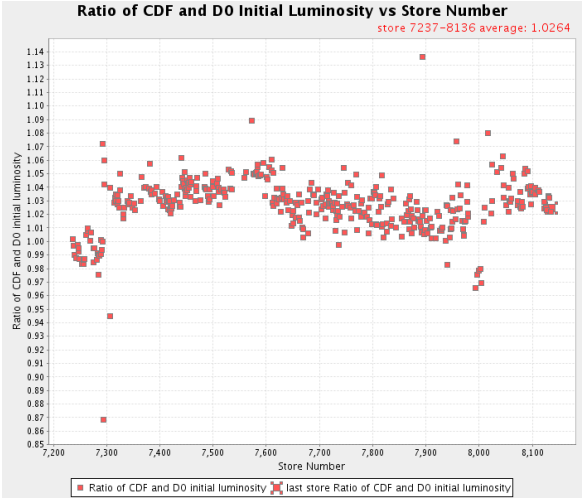

Figure 7: The ratio of the CDF and D0 initial luminosities in Tevatron stores as a function of time (store number) between October 2009 and September 2010.

LESSONS LEARNED

Some of the lessons learned so far from the luminosity measurements at the Tevatron are: a) Continuous cross checking between the luminosities calculated by the machine and the luminosities measured by the experiments, as well as between the experiments themselves, is very valuable. The same is true for other beam parameters measured by the machine and the experiments; b) The method of counting zero interactions works well for the current Tevatron luminosities; c) Fine granularity detectors are needed for high instantaneous luminosities (Run I vs Run II); d) In situ calibration of the detector is very important; e) Detector stability is crucial; f) A good simulation of the processes involved and of the luminosity detector itself is needed as early as possible; g) A good knowledge of the physics cross section the measurement relies upon is necessary; h) Careful monitoring of gas purity when having a gas detector is a must; i) Minimizing - eliminating if possible - the dead time of the luminosity system is critical; j) Watchfulness is needed for aging due to large total luminosity and readinesss to replace consumables.

CONCLUSION

Luminosity measurements at hadron-hadron colliders are very challenging. The luminosity uncertainty achieved at the Tevatron by the CDF and D0 experiments is approximately 6%, dominated by the uncertainty in the proton-antiproton inelastic cross section. The uncertainty achieved by the machine on the absolute luminosity measurement is approximately 15-20%. Cross checking the detector and machine luminosity measurements has been very valuable. We expect that the lessons learned from the Tevatron will be very useful for LHC.

I would like to thank the organizers for a very stimulating Workshop. I would also like to thank several colleagues from the Tevatron for discussions on the information presented here: N. Goldschmidt, B. Lee, R. Moore, A. Sukhanov, R. Tesarek, R. Thurman-Keup, A. Valishev and J. Zagel.

REFERENCES

[1] A. Valishev et al., "Progress with Collision Optics of the Femrilab Tevatron Collider," EPAC'06, Edinburg, UK, June 2006; http://accelconf.web.cern.ch/AccelConf/e06/PAPERS/WEPCH058.PDF .

[2] S. Klimenko, J. Konigsberg, T. M. Liss, Fermilab-FN-0741 (2003) and references therein.

[3] D. Acosta et al. Nucl. Instr. and Meth. A 494 (2002) 57.

[4] V.M. Abazov et al., Nucl. Instr. And Meth. A 565 (2206) 463.

[5] T. Andeen et al., Fermilab-TM-2365 (2007).

EXPERIENCE AT CERN WITH LUMINOSITY MONITORING AND CALIBRATION, ISR, SPS PROTON ANTIPROTON COLLIDER, LEP, AND COMMENTS FOR LHC…

WERNER HERR, RÜDIGER SCHMIDT, CERN, Geneva, Switzerland

Abstract

There is a long history of luminosity calibration at CERN. Already at the ISR, operating during 1968–1983, luminosity calibrations were performed. Beams were crossing at a large angle, to calibrate the luminosity a scan in only one plane (vertical) measuring the beam height overlap was required. Such "Van der Meer" scans were performed by beam displacements with magnets. In the SPS Proton Antiproton collider, operating during 1984-1991, Van der Meer scans were performed by beam displacement with electrostatic separators in both planes. For LEP, operating from 1989-2001, scans were performed in both planes by beam displacement with electrostatic separators, not to precisely measure the luminosity, but to optimise luminosity. From the experience with Van der Meer scans at these very different accelerators some lessons were learned that might be considered when discussing luminosity calibration at the LHC.

PARAMETERS AND LUMINOSITY CALIBRATION AT THE ISR

The ISR was a 2-ring proton-proton collider, but also proton antiproton beams were brought into collision. The beam energy of the ISR was up to 31 GeV. Beams were circulating in two separate vacuum chambers with different orbits for the two beams. The ISR operated with coasting beams (no bunches). The collisions between the beams were at large angle in horizontal plane and the maximum beam current was up to 40 Amperes. Van der Meer scans were performed with reduced beam current of a few Amperes. The transverse beam size at the ISR was very large, in the order of cm. The beams were separated with magnets.

The luminosity calibration was performed for both, proton-proton and proton-antiproton collisions. At the interaction point a wire scanner was installed to measure the beam profile.

The proposal for calibration of the beam height in ISR came from S. van der Meer [1]. The main challenge was the calibration of the beam displacement during the scan. In his paper S. van der Meer wrote: *Of course, this method suffers from all the disadvantages connected with beam displacements outlined in [2]. On the other hand, it might be suitable for somewhat less precise measurements in cases where the experiments requires that the interaction region remains without the obstructions inherent to the wire method.* It seems that S. van der Meer did not expect that his method would turn out to be the most accurate method for calibrating the luminosity of hadron colliders.

The largest challenge was the calibration of the beam displacement at the collision point [3] when the magnet currents were changed. A measurement of the beam displacement was later performed using beam scrapers installed at the collision point. There was a large effort to understand systematic errors.

The results that were finally reported for the total luminosity had an error of 0.7% for proton-proton collisions and 1.1% for proton-antiproton collisions [4], different techniques were used to obtain these results.

PARAMETERS AND LUMINOSITY CALIBRATION AT THE SPS

The SPS was build as a proton synchrotron and later transformed into a proton-antiproton collider with a beam energy of up to 315 GeV. The beams were bunched. The SPS had one beam pipe and both beams had the same orbit when operating with a few bunches colliding head-on. In order to increase the luminosity, electrostatic separators were installed to separate the beams, that allowed to increase the number of bunches. The beam current was less than 0. 1 A. Luminosity calibrations were performed with a special optics (high beta optics, with beta = 2500 m).

The luminosity at the SPS was calibrated with different methods, using the optical theorem, direct coulomb scattering and Van der Meer scans [5][6].

A generalisation of the Van der Meer scan for luminosity calibration in the case of bunched beams was proposed for the SPS in 1977 [7]. Taking into account the difference between ISR (coasting beams, scan in only one plane, and SPS (bunched beams, scans in both planes) the calibrations in the SPS were more challenging.

The technique using Van der Meer scans is not the only method to calibrate the luminosity. Another method for luminosity determination is from beam profile measurements. The horizontal and vertical beam profiles of both beams are measured with a scraper or a wire scanner. With the knowledge of the beta function, the beam size at the collision points can be calculated. The estimated accuracy is about 5–10%.

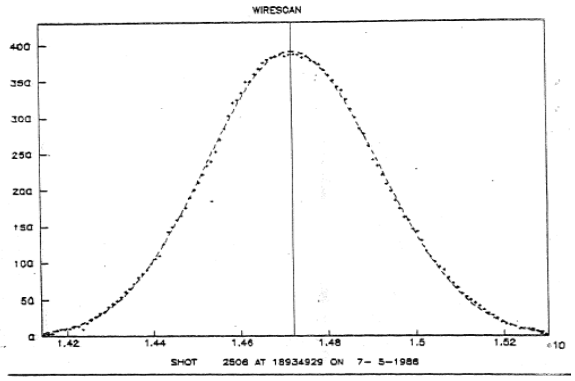

Fig. 1: Profile measured with the linear wire scanner at the SPS proton antiproton collider

In general, Gaussian beams are assumed. This was shown to be very accurate [8] – the r.m.s. beam size is an excellent assumption for any realistic beam distribution. For precise measurement of the beam profile at the SPS with an error better than 0.5% a linear wire scanner was developed. The result of such a scan is shown in Fig.1. The same type of (linear) wire scanner is also used in LHC. It should also be possible to use these instruments for luminosity calibration at LHC.

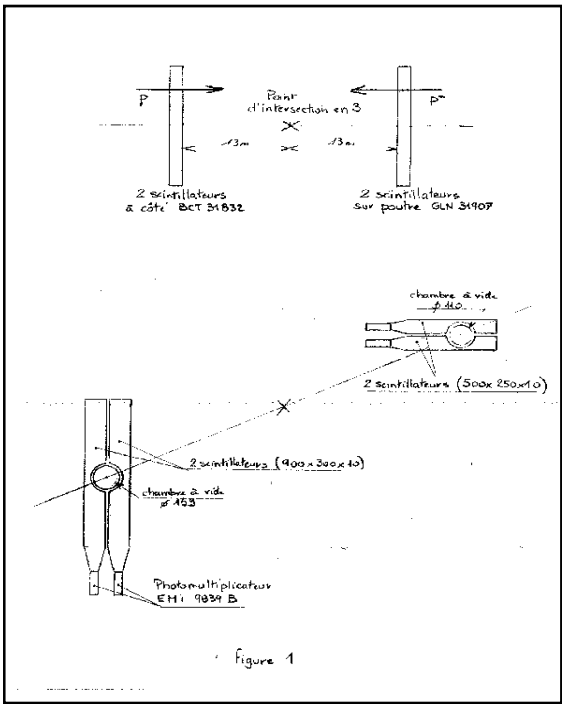

Fig. 2: Schematic drawing of a "poor mans" monitor to measure the overlap integral at the SPS

Fig.2 shows that Van der Meer Scans can be performed with very simple instrumentation. In order to measure the overlap integral of both beam at a collision point without experiments, two sets of scintillation counters were installed and the beams were displaced with electrostatic separators (see fig. 2). The beams were displaced with electrostatic separators, and the counting rate in the monitors was recorded. The results of such a scan in the SPS are shown in fig. 3.

PARAMETERS AND LUMINOSITY CALIBRATION AT LEP

To calibrate the luminosity for an electron positron collider other methods than Van der Meer scans are more accurate, essentially Bhabha scattering. Van der Meer scan for e+e- luminosity calibration do not work correctly due to strong beam-beam effects (much stronger than for hadron colliders). Because of the small cross section the counting rate is very low and the statistical error much larger than for scans at hadron colliders.

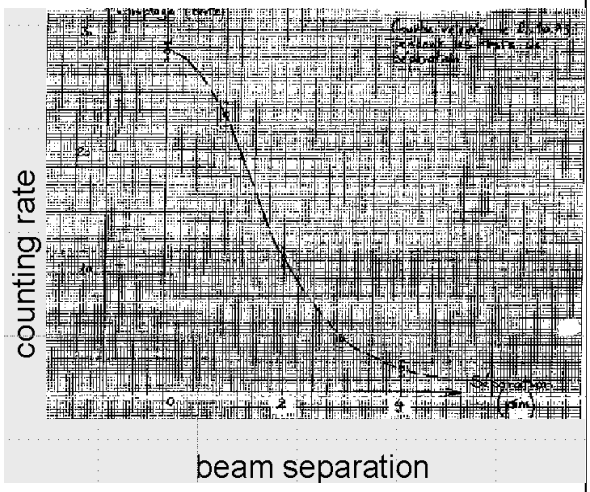

Fig. 3: Result from a Van der Meer scan in the SPS proton antiproton collider, measured with the instruments shown in fig.2.

Both, the beta function and orbit changes during the scan (dynamic beta). The beam sizes are dominated by the balance between damping and quantum excitation due to synchrotron light emission PLUS excitation of resonances driven by the beam-beam effect. The beam size and emittance changes, in general the beam is blown up during a scan. This is very different from beam dynamics at hadron colliders.

Still, at LEP scans were done frequently to optimise the luminosity. This can be done by measuring the counting rate as a function of separation, but for LEP operating at 100 GeV with very low cross-section this method is very lengthy. An alternative is to measure the beam-beam deflection during the scan [9].

At LEP, a large effort went into the precision measurement of the beam energy. The techniques to calibrate the energy are very different from luminosity calibrations, but from the way to approach precision measurement lessons for the LHC can be derived. On of

the lessons is the need for close collaboration between machine and experiments during many years.

IDEAS FOR LUMINOSITY CALIBRATION AT LHC

There are several options for luminosity calibration. The most accurate method is expected to come from the TOTEM and ALFA experiments but need a specific optics with high beta function at the collision points. The calibration based on Van der Meer scans can be performed during normal luminosity operation and it is expected to achieve results with an error of about 5 %. Other methods that use the knowledge of beam parameters rely on measuring the beam sizes at the interaction point. This can be done using direct measurement by LHC experiments using proton-proton collisions (measuring the overlap integral) and collisions with gas molecules (measuring single beam profiles).

Indirect measurement of the beam size at the IP use precise wire scan data and calculating the beam size at the IP with the knowledge of the beta function (the SPS micro wire scanner was invented for very precise measurements of the beam size).

Beta function measurements are performed by exciting beam oscillations with an AC dipole and measuring the beam response. Today, the beta function measurement can be performed with an error of about 5%, in the future it might be possible to reduce the error to about 1% for dedicated studies, but this needs to be demonstrated [10]. This would result in a beam size error of 0.5%.

It is always required to precisely measure the bunch current. Bunch current measurements are not obvious and precise calibration is needed. For utmost precision, an independent measurement of the bunch current is recommended.

When performing Van der Meer scans, the beams are displaced by magnets. The displacement needs to be calibrated, by measuring . The displacement can also be derived from the knowledge from the machine optics and magnetic fields. Both methods should be used and the results should be compared.

Orbit effects when beams are separated need to be considered. This depends on the beam-beam parameter, on the number of bunches and on the number of long range interactions.

Very important are simulations – programs exist and should be used to simulate the entire measurement process with MAD and other programs (to understand possible errors of the measurements and to understand detail of the LHC machine).

Calibration of the luminosity with different methods is recommended since the total cross section is an absolute value to be measured. For the most precise scans it is proposed to operate the LHC in a simple configuration:

- Avoid too many bunches
- Avoid parasitic crossing
- No crossing angle

The luminosity calibration is a precision experiment – the more precise the more difficult. If ultimate accuracy is required this is a long term effort, possibly requiring new ideas, in particular for monitoring of the beam parameters. Precise calibration will take machine time and will have an adverse effect on the integrated luminosity.

It is proposed to use different calibration principles, in order to get confidence in the results and to better understand systematic error (of possibly unknown nature).

The question to the physics community: Is if the physics motivation strong enough to justify such effort and is a (moderate) loss in integrated luminosity acceptable?

REFERENCES

[1] S. van der Meer, Calibration of the effective beam height in the ISR, CERN-ISR-PO-68-31

[2] P.Darriulat, C.Rubbia, CERN internal document, 68/340/5 SIS/si, 1968

[3] P.J.Bryant, K.Potter, Calibration of the beam displacements used in ISR luminosity measurements / CERN-ISR-ES-BOM-82-15, 1982

[4] G.Carboni et al., Precise measurements of proton-antiproton and proton-proton total cross sections at the CERN Intersecting Storage Rings, CERN-EP-84-163, CERN, 1985 and Nucl. Phys. B 254 (1985) 697-736

[5] UA4/2 Collaboration, Measurement of the proton-antiproton total cross section at the SppS collider by a luminosity dependent method , Phys. Lett. B 344 (1995)

[6] UA4/2 Collaboration, A precise measurement of the real part of the elastic scattering amplitude at the SPPS, PHYS. LETT. B 316 (1993)

[7] UA4/2 Collaboration, Measurement of the proton-antiproton total cross section at the SppS collider by a luminosity dependent method, Phys. Lett. B 344 (1995)

[8] H.G.Hereward, E.Keil, Measurements of the luminosity for beams crossing at small angles in a low-section, CERN-ISR-DI-TH-74-41

[9] C.Bovet et al., Luminosity optimisation using beam-beam deflections at LEP, Proc. of the 5th European Particle Accelerator Conference, Sitges, Spain, 1996

[10] R.Tomas, private communication

LHC BEAM CURRENT TRANSFORMERS STATUS AND PROSPECTS

D. Belohrad, J-J. Gras, M. Ludwig, P. Odier CERN, Geneva, Switzerland.

Abstract

This document will present the main issues observed and results obtained with the LHC Beam Current Transformers (BCT) during 2010 a along with the BE-BI strategy and prospects for 2011.

MAIN ISSUES IN 2010

Issues with the DC BCT

The DC BCTs performed well and within specifications at the beginning of the year with low intensity and unbunched beam (once we managed to regularly correct the offsets of the monitors via the LHC sequencer tasks). Unfortunately, things degraded significantly when we started to inject 75 ns batches in the machine. Depending on the filling pattern, the DC BCT started to sometimes over-estimate, sometimes under-estimate the number of protons stored in the machine (see Fig 1.). This effect has been diagnosed, simulated and then reproduced in our laboratory (see Fig 2.).

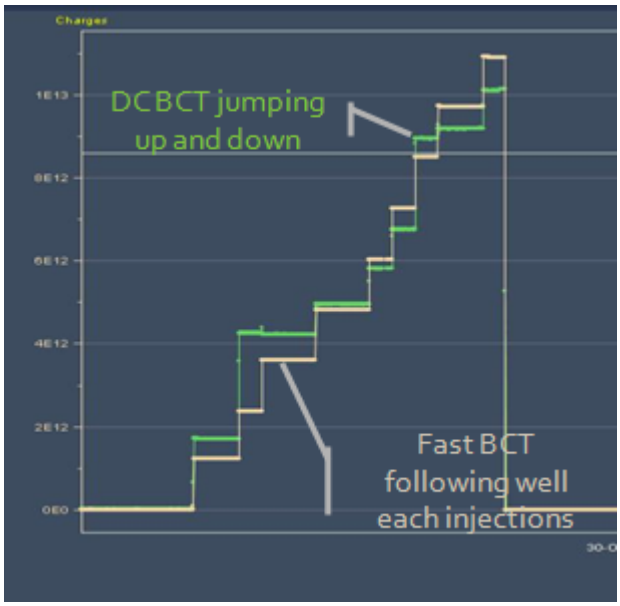

Figure 1: DC BCT dependency on the filling of the machine.

The source of this problem has been identified to be a combination of:

- poor efficiency of our RF by-pass supposed to reduce the HF magnetic field induced by the beam which is seen by the DCCT.
- inappropriate gain partition associated with operational amplifier limitations in the feedback loop (current, voltage swing, slew-rate)

We made several attempts to mitigate this issue during 2010 but without real success.

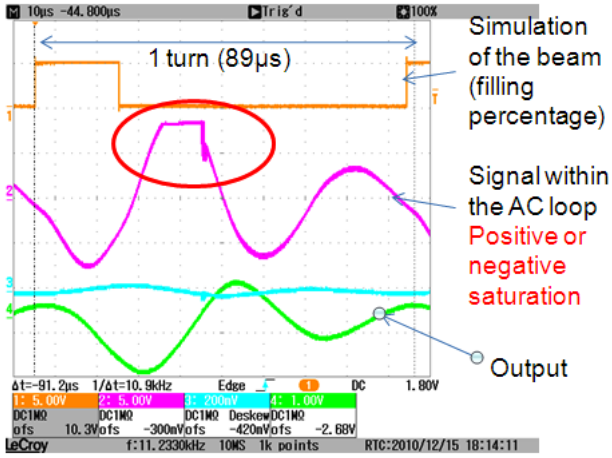

Figure 2: Plot showing a positive saturation of our 2010 AC loop with a given filling pattern. Same set-up with different filling pattern leads to a negative saturation, reproducing the observed over and under estimations seen with beam.

Issues with the Fast BCT

We did not manage to make an independent calibration of our fast BCTs during 2010. Every attempt resulted in a difference of several % of the estimated intensity with respect to the DC BCT measurements.

We discovered that there are several effects which make accurate calibration difficult with these systems:

- A clear position dependence was demonstrated at the end of last year (>1% per mm), which was well outside the specifications given by the manufacturer of these toroids (see Fig. 3). The manufacturer acknowledges this issue, but there is no easy fix for this.

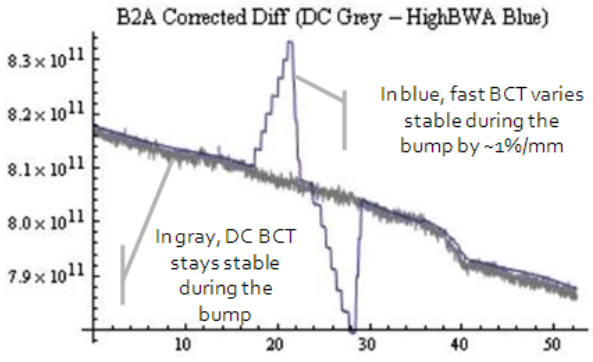

Figure 3: Fast BCT readings vary during controlled orbit bumps around our monitors while DC BCT behaves correctly.

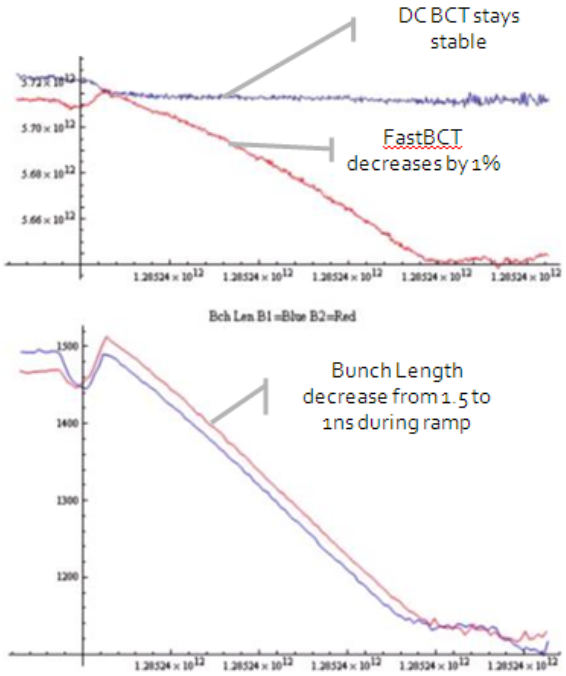

Figure 4: Fast BCT readings decrease with bunch length during the ramp while DC BCT behaves correctly.

- A bunch length dependence has also been seen at the 1% level. This can have many sources, one of which is related to the position dependence mentioned above (see Fig 4).

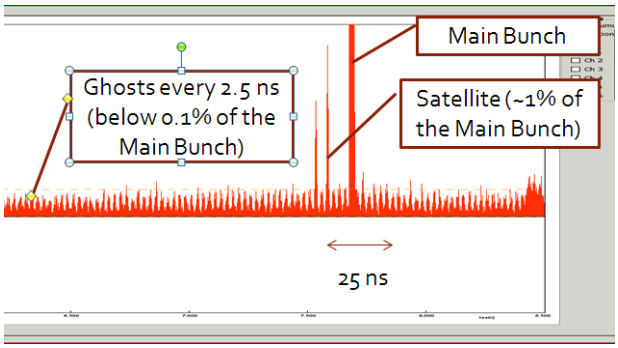

Fig 5: RF bucket population around one main bunch estimated with the Longitudinal Density Monitor during the ion run proves that these satellites and ghost bunch populations cannot always be neglected.

- The bandwidth of the transformer and the acquisition chain do not allow the system to distinguish between charges in the main bunch and in any satellite or ghost bunches. All charges in 21ns out of every 25ns slot is integrated. It is important to remind ourselves that the experiments care about the bunch population in the nominal 2.5ns RF bucket. In addition, fast BCTs are totally insensitive to unbunched beam.

All of these effects meant that we had to rely on cross calibrating the fast BCT with the DC BCTs assuming that the amount of unbunched beam and the ghost/satellite populations were negligible.

OUR STRATEGY AND RESULTS IN 2010

Based on these observations, our strategy to achieve the best possible accuracy during the 2010 luminosity calibration measurements has been the following:

- Define and use filling patterns where the DC BCT was known to be free of issues
- Check and fine tune if necessary the DC BCT offsets before the fill
- Cross-calibrate fast BCT with DC BCT just before stable beam, once orbit and bunch length are stabilized, assuming ghost, satellite and unbunched beam populations were negligible (any unbunched beam is lost during the ramp and satellite populations in the vicinity of the main bunches were measured by the experiments.).

Despite our issues and thanks to our close collaboration with PH and the well defined context of the dedicated Van de Meer scans, we managed to achieve a performance level which is already close to the targets defined in the original LHC functional specifications for beam intensity monitoring [1].

These results are described in details in these proceedings and in 2 notes dedicated to the April-May [2] and October [3] luminosity calibration measurements.

THE SITUATION WITH BEAM CURRENT TRANSFORMERS ELSEWHERE

We took the opportunity of this Lumi workshop to bring together at CERN BCT experts from DESY, GSI and Industry to share our experiences and results. We had many fruitful discussions on how to improve our current systems and some of these actions will be described in the following chapters. But it was also interesting to hear that:

- Similar issues have been observed in all laboratories on many different machines (lepton/hadron, linac/synchrotron)
- These instruments are still poorly understood for phenomena below the % level
- LHC experiments are quite demanding clients

- People tend to be reluctant to mention absolute accuracy as soon as they have more than one intensity monitor in the ring.

OUR STRATEGY AND PROSPECTS FOR 2011

Our Plans for the DC BCTs

In order to eliminate our sensitivity to filling pattern, we made the following modifications during the 2010/11end of year technical stop :

- We improved the RF bypass to limit any components above 11kHz seen by the monitors
- We modified our electronics to prevent saturation in the feedback loop.
- We improved our diagnostic capability in SX4.

We repeated our tests in the laboratory with these modifications and found that they were successful in eliminating fill pattern dependence for all the patterns we can currently simulate. Fig.6 shows a summary of these tests which covers the beams we may expect in 2011/12.

I_mean_batch = #charges_per_bunch*elementary_charge/bunch_spacing

Elementary charge [C]: 1.60E-19

		I_mean_batch [mA]	Bunch spacing [ns] 25	50	75	150	300
# charges/bunch	Pb min	5.60E+08	3.59	1.79	1.20	0.60	0.30
	Pb max	5.60E+09	35.88	17.94	11.96	5.98	2.99
	p nominal	1.15E+11	736.92	368.46	245.64	122.82	61.41
	p ultimate	1.67E+11	1070.14	535.07	356.71	178.36	89.18

Fig 6: Tests performed in the laboratory for different filling patterns. Green box means successfully tested, i.e. no issues observed. Pink box means still to be tested as our current set-up is not powerful enough to simulate such patterns.

In addition, during the second half of the year, it is planned to test a new 24 bit ADC acquisition board to cover the entire dynamic range without gain switching to improve our resolution for high intensity beams in 2012.

Finally, we will continue to work in collaboration with PH on the reduction of the BCT DC scale factor uncertainty.

Our Plans for the Fast BCTs

The situation with the fast BCTs is less favourable since the main source of errors comes from the monitor itself. Several ideas are currently under investigation to overcome this issue without replacing the monitor itself but their efficiency is still to be determined. We will therefore again have to rely on cross-calibration with the BCT DC to optimize precision during the Van de Meer scans.

In addition, a good estimation of the parasitic population (ghost, satellite, unbunched beam) will be important and BI will commission two new instruments (the Longitudinal Density Monitor and the Wall Current Monitor) for this purpose.

The New Players

The Longitudinal Density Monitor (LDM)

The LHC LDM uses the light from the Beam Synchrotron Radiation Telescopes to produce a high-dynamic-range longitudinal profile. An avalanche photo-diode operated in Geiger mode detects the arrival of single photons and a time-to-digital converter is used to make a histogram of their arrival times.

Correction algorithms need to be applied to these systems (to cancel afterpulsing and adjust for the effects of the detector's deadtime) but first measurements look promising and we plan to achieve a dynamic range better than 10^4 with an integration time of 5-10 minutes (see Fig 5). This would be sufficient for the characterization of unbunched beam and satellite and ghost bunches. A measurement with lower dynamic range showing the length, shape and relative current of all 'main' bunches around the ring could be made in a few seconds.

Both rings will be equipped in 2011 (only beam 2 was equipped at the end of last year) and efforts are ongoing to incorporate the LDMs into our standard control system (via a FESA server) and have relevant data logged for offline studies.

The Wall Current Monitor (WCM)

The WCMs are acquired via fast oscilloscopes controlled by a standard FESA server. The instrument is already linked to the LHC database and should be able to provide relative population of the main bunches at 0.1 Hz whilst also providing other parameters such as bunch length.

Neither the LDM or WCM can be directly calibrated and hence both will also rely on cross-calibration via the DC BCT. It is also not clear what additional systematics and non linearities these methods introduce. We have some studies ahead of us there but the first results look promising.

Outlook for 2011

In 2011 the DC BCT will remain our main source of absolute calibration. We will push its performance as much as we can with the current hardware and can reasonably think to reduce the absolute scale factor uncertainty below 1% in all 2011/12 physics beam conditions.

We saw during the October Van de Meer scans that we can achieve a 1% relative uncertainty between bunches with the fast BCTs but we will have to ensure this is still the case if we mix pilot and nominal bunches during the future scans.

In addition to this, the final fast BCT absolute accuracy will depend on:

- The LHC injectors' ability to deliver satellite free bunches
- A proper estimation of the ghost and unbunched beam population contributions to fast and DC measurements
- The stability of the bunch length and bunch position at the monitor

Even if all these conditions are met it will be difficult to guarantee an absolute accuracy of the fast BCT scale factor below 1% at all times. However, it should be able to achieve it on request for dedicated luminosity calibration measurements.

Finally, we will commission and assess the LDM and WCM in 2011. These instruments may play a key role in the evaluation of ghost, satellite and unbunched beam populations or even eventually become good alternatives to the fast BCT for precise bunch population measurements (albeit with much longer integration times).

CONCLUSIONS

To conclude, we would like to take the opportunity of this workshop to thank the experiments for:

- Their unreasonable accuracy requirements and constant pressure, which significantly speeded up our progress in fully understanding our instruments.
- Their trust in our capacity to solve our issues
- Their patience
- Their help in analysing the results from our instruments. Special thanks go to the BCNWG members and in particular Carolina Gabaldon Ruiz, Gabriel Anders, Thilo Pauli and Colin Barschel for their extremely valuable analysis of our data.

Despite all the issues encountered, we are satisfied to see that the results of these luminosity calibration measurements look amazingly precise and coherent for a first year of physics and we will keep working hard to achieve even better results in 2011..

REFERENCES

[1] "On the Measurements of the Beam Current, Lifetime and Decay Rate in the LHC Rings." (https://edms.cern.ch/file/359172/1.0/LHC-BCT-ES-0001-10-00.pdf)

[2] "LHC Bunch Current Normalisation for the April-May 2010 Luminosity Calibration Measurements" (http://cdsweb.cern.ch/record/1325370?ln=en).

[3] "LHC Bunch Current Normalisation for the October 2010 Luminosity Calibration Measurements" CERN-ATS-Note to come.

Other instruments, ghost/satellite bunch monitoring, halo, emittance, new developments*

E. Bravin, CERN, Geneva, Switzerland

Abstract

In order to estimate in absolute terms the luminosity of LHC certain beam parameters have to be measured very accurately. In particular the total beam current and the relative distribution of the charges around the ring, the transverse size of the beams at the interaction points and the relative position of the beams at the interaction point. The experiments can themselves measure several of these parameters very accurately thanks to the versatility of their detectors, other parameters need however to be measured using the monitors installed on the machine. The beam instrumentation is usually built for the purpose of aiding the operation team in setting up and optimizing the beams, often this only requires precise relative measurements and therefore the absolute scale is usually not very precisely calibrated. The luminosity calibration requires several machine-side instruments to be pushed beyond their initial scope.

COLLIDING AND NON COLLIDING CHARGES

In general in colliders the particles circulating in opposite directions are kept separated and only allowed to encounter each other at the designated interaction points. This is even more true for the LHC where the particles travel in different vacuum tubes for most of the accelerator length. Particles colliding outside of the experiments would provide no useful information and would only contribute to the background and reduce the lifetime of the beams. In order to estimate the luminosity it is therefore important to quantify the number of particles that can potentially collide in a given interaction point more than just the total current stored in the machine. The distribution of particles around the ring can be rather complicated. In theory there should be only a well known number of equal bunches spaced by well known amounts of time and in this situation it would be easy to calculate the colliding charges from the total current. In reality the bunches have all different currents and there can be charges also outside of these bunches. In the LHC the radio frequency (RF) system has a frequency of 400.8 MHz and only every 10th bucket at most is filled. This means that there are plenty of *wrong* RF buckets that can store particles in a stable way. It can happen that capture problems (also upstream in the injectors) create unwanted small intensity bunches near by the main ones. These, named satellite bunches, have typically intensities of up to 1% of the main bunch and are only a few RF buckets away from the main bunch (usually a multiple of the RF period of one of the preceding accelerators). Other effects can lead to particles escaping from the main buckets and becoming un-captured, these particles are no longer synchronous and will just diffuse around the ring where they can remain for very long time. In case some RF gymnastic is performed (like inserting dips in the accelerating voltage in order to improve injection efficiency) it can happen that some un-captured beam is recaptured forming a very large number of very faint bunches. These are called ghost bunches and have typically currents below the permill of the main bunches. In the LHC ghost bunches have been observed, in particular during the heavy ions run due to the special RF tricks used at injection when injecting ions. It is worth mentioning that un-captured particles will be lost if the energy of the machine is changed (e.g. during the ramp) due to the fact that they can not be properly accelerated by not being synchronous with the RF.

MEASURING THE COLLIDING CHARGE

Usually fast current transformers should be sufficient to measure the relative current variations from bunch to bunch. The dynamic range and speed of these detectors are however not sufficient to detect the satellites and the ghost bunches. Moreover in the LHC the fast current transformers integrate the beam current over 25 ns (10 RF buckets) bins and it is not possible to know if and which satellites are included in the integration. Detectors with better time resolution and higher dynamic range are required. Candidates are:

- Wall current monitor
- Strip line pick-up
- Fast light detector sampling the synchrotron light vs. time
- Precise time stamping and counting of synchrotron light

Wall current monitor

The wall current monitors can probably be used to estimate the satellites. This requires however averaging over many turns and correcting for quirks in the frequency response of the detector and the cables. It is in particular important to verify that reflection/noise or other effects are not limiting the potential of the averaging. For the moment the amount of charge in satellites is calculated by studying the frequency spectra of the acquired signals, as satellites are out of the nominal bunching pattern it is possible to compare the expected spectra with the measured one ad estimate the amount of charge producing the distortion. One

* This contribution is presented by the author on behalf of the BE-BI group

complication to this process arises from the fact that the bunches are not necessarily Gaussian and their shape is not precisely known. It is however difficult to get sufficient accuracy in order to take care of the ghosts. At the moment a continuous analysis of the spectrum of the wall current monitor is performed by the front-end software and provides an estimate of the amount of charge outside of the correct buckets which is stored in the database. Figure 1 shows the signal from a wall current monitor acquired with a 10 GSample scope. A long tail after the bunch can be observed, this arises from the frequency response of the detector and is corrected for in the analysis.

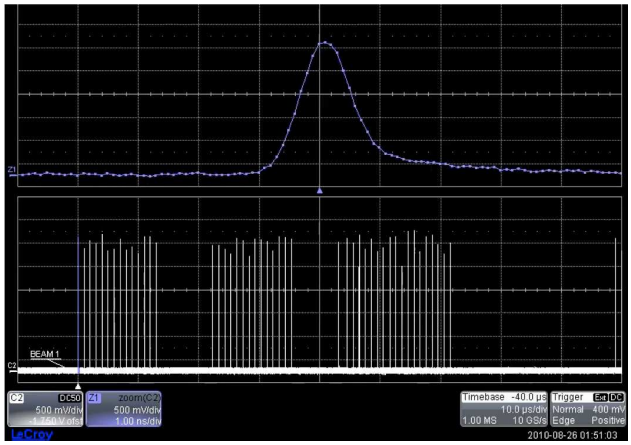

Figure 1: Signal from a wall current monitor. The top graph shows a zoom into a single bunch while the bottom graph shows the entire ring.

Strip line pick-ups

The strip line pick-ups provide signals comparable to the ones of the wall current monitor with the drawback of a perfectly reflected pulse shortly after the main pulse with a delay that depends on the strip length, 30 cm for the devices installed in the LHC, intrinsic to the principle of the device (see Fig. 2). This reflection complicates the treatment of the signal resulting in the impossibility of using this instrument for the identification of ghosts and satellites.

Synchrotron light detection

There are two possibilities for using the synchrotron light for longitudinal measurements. One consists in simply using a fast optical detector connected to a fast sampler and record the intensity of synchrotron light as function of time. The principle is simple and photo-diodes in the order of 50 GHz are commercially available, there are however a few difficulties associated with this technique. As for the WCM the transport of the high frequency signals is not simple and the cables response will modify the pulses requiring frequency domain corrections. Another problem is introduced by the need of fast digitizers implying a reduced dynamic range (typically 8 bits only), noise

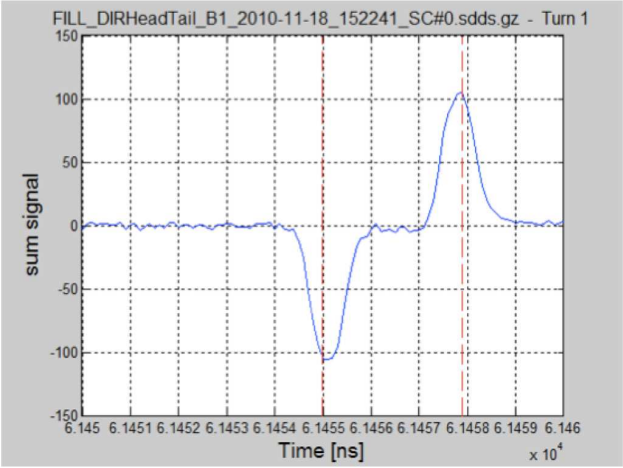

Figure 2: Signal from a strip line pick-up.

etc. On the other end the response of the detector itself should be much more linear than the one of the WCM and can in principle extend down to DC. It is surely worth trying this possibility however it will be very difficult to be able to measure the ghost bunches in this way. The other alternative is to count single SR photons with precise time stamping of the arrival time. Detectors suitable for the task exists (avalanche photo diodes, APD) and time to digital converters with resolutions of a few tens of ps also exists. The only draw back of this technique is that the counting rate is limited and the light has to be attenuated such that the probability of detecting a photon during a bunch passage should be less than 60%. Such a detector has been operated during the last part of the 2010 run (mainly during the ions period) and has given very promising results, it is known as the longitudinal density monitor or LDM (see Fig. 3.)

Longitudinal density monitor LDM

The LDM is based on avalanche photodiodes from either id-Quantique or Micro Photon Devices connected to a fast TDC from Agilent (former Acquiris). The detector can resolve single photons with a time resolution of the order of 50 ps, the TDC has a resolution of 50 ps as well. At the moment the temporal resolution of the system is limited to about 75 ps (300 ps pk-pk) due to the reference timing used (turn clock from the BST receiver, BOBR), in the future this limitation will be removed by using a dedicated RF timing signal [1]. The avalanche photo diodes present a short dead-time used to quench the avalanche (tens of ns) and there is also a small probability that at the end of this dead-time trapped electrons or holes will trigger a new avalanche (the probability of this type of events is of the order of 3%.) These effects, together with the dark count rate, although small, must be corrected for, a rather simple statistical algorithms is sufficient. The probability of SL photon triggering an avalanche per bunch-crossing must be maintained below a certain level (60-70%) otherwise the error

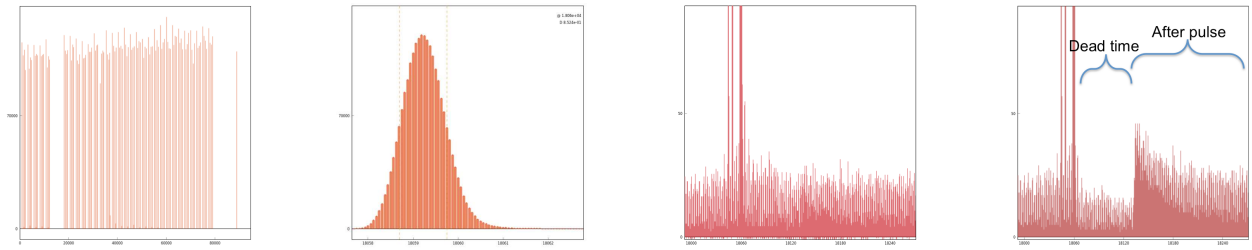

a) b) c) d)

Figure 3: Longitudinal profiles measured with the LDM. Distribution of particles around the whole ring (a), zoom on a single bunch (b), zoom at the base of a bunch showing the main bunch (thick line), satellites (thinner lines next to the main bunch) and ghost bunches ("noise" lines around the baseline) (c). Same zoom as (c), but before correction (d).

on these corrections becomes too large. This has an impact on the maximum counting rate and thus on the integration time required for acquiring a profile with sufficient resolution. In fact the integration time required depends on what is being observed; if the aim is just to measure the so called core parameters of a bunch (mainly the bunch length) a few seconds are sufficient, on the other hand if the population of ghosts and satellites has to be measured an integration of several minutes may be required. The dynamic range observed in 2010 was of the order of 10^6 with an integration time of 500 s. The LDMs consist of an extension to the already complex synchrotron light telescope, this means that there may be interferences between the optimization of the LDM and the other detectors present on the optical table (fast and slow cameras and abort gap monitor.) In 2011 the LDM should become operational for both beams.

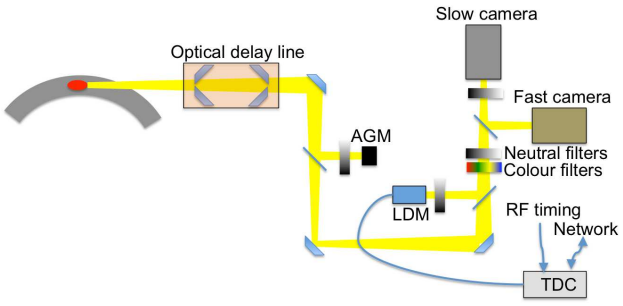

Figure 4: Schematics of the BSRT optical system.

BUNCH LENGTH

At the moment bunch lengths is LHC are typically of the order of 0.8 ns FWHM, the nominal value is 250 ps one sigma. In order to measure this parameter a detector with high bandwidth is required (several GHz) however even a limited dynamic range would be sufficient. The list of candidates for this measurement is similar to the one presented before for the measurement of the satellites/ghost bunches

- Wall current monitor
- Strip line pick-up
- Fast light detector sampling the synchrotron light vs. time
- LDM

Wall current monitor

This device measures the image current flowing on the beam pipe. The WCMs installed on LHC have an upper cut-off frequency of about 3 GHz and the signals are sampled using a scope with 10 GSample/s. These characteristics are sufficient for the measurement of the bunch length, however the non flat transfer function of the detectors introduce tails at the end of the bunch. By analyzing the signals in frequency domain these artifacts can be removed, Fig. 1 shows the signal directly on the scope display before processing.

Strip line pick-up

The main function of this device is to measure the position of the beam with high temporal accuracy, in particular it allows to study the head-tail oscillations of the beam which provide hindsights on the stability of the beams and also a way to measure the chromaticity (variation of the betatron tune vs. the error in momentum of the particle). The device is composed of 4 electrodes, 30 cm long, mounted at 90°. The amplitude of the signal on each electrode depends on the instantaneous beam current as well of the distance between the bunch and the electrode. By summing the signals on opposite electrodes one obtains a signal only proportional to the beam current while subtracting the signals from opposite electrodes and dividing by the sum one obtains a signal proportional to the position only. The bandwidth is similar to the one of the WCM, mainly limited by the characteristics of the feed-through and resonances in the electrodes. The acquisition is in fact performed with the same type of scope used for the WCM. The advantage of the strip line is that the transfer function is almost flat. Another characteristic of the strip line detectors has been already mentioned and consists of a second pulse, inverted in polarity, after the first one, the distance between the two being determined by the length of the electrodes (to be precise twice the length of the line divided by the speed of

light) see Fig. 2. Of course both the WCM and the strip line can provide single passage measurements as well as averaged measurements.

LDM

As seen before the LDM allows the sampling of the whole LHC ring with high time accuracy, with the present system 50 ps resolution is possible. The 50 ps temporal resolution is enough to measure the bunch length, provided the beam is stable over the integration time needed to acquire a profile, typically a few seconds. It has already been mentioned that the intensity of the synchrotron light could be acquired directly by a photon detector instead of performing single photon counting. This technique has however not yet been used in LHC as it would carry all the problematics of the strip-line pick-ups for example (cables transfer functions, fast sampling) without adding substantial advantages.

TRANSVERSE EMITTANCE

Another important factor in the determination of the luminosity from the machine parameters is the transverse emittance. Several instruments have been installed in the LHC for this purpose. In particular the instrument used to measure accurately the beam size and thus the beam emittance is the wire scanner. This instruments however only produces measurements on demand and can not be used when the total beam intensity is above 2 10^{13} protons. In order to cope with the limitations of the wire scanner two different monitors capable of continuous monitoring have been installed, the synchrotron light telescope (BSRT) and the rest gas ionization monitor (BGI.) All these devices only measure the transverse beam sizes, in order to calculate the emittance the knowledge of the optics of the machine at the location of the devices is needed, in particular the betatron function. Thanks to the accurate modeling and precise measurements the beta functions are known with an error between 5 and 10% all around the machine.

Wire scanner

This is the reference device for emittance measurement, since the systematic errors of this technique can be controlled well. The principle is rather simple and consists of scanning a 30 μm diameter carbon wire across the beam at about 1 m/s. The interaction of the particles in the beam with the nuclei in the wire produce high energetic secondary particles that are detected by a scintillator-photomultiplier assembly some 10 m downstream of the scanner. The beam profile is inferred by the amplitude of the PMT signal as function of the wire position. Because the wire scanner needs to intercept the beam in order to make a measurement the range of beam intensity were it can be used is limited. There are two situations that need to be avoided: overheating the wire up to the point were it breaks or inducing secondary particles and beam losses of intensity sufficient to induce a quench in the neighboring superconducting magnets. At injection energy the first effect dominates while at top energy it is the second. The intensities of these two limits are rather close and for this reason only one value (the smaller) is used imposing an upper limit of 2 10^{13} particles per beam (about 200 nominal bunches) [2]. The accuracy of the wire scanner in the LHC has not yet been studied, however a detailed study on similar devices has been carried out in the SPS a few years ago leading to an error of the order of 1% in the beam emittance for beams of $\sigma = 1$ mm transverse size [3]. At the end of 2010 the bunch-by-bunch acquisition mode was also commissioning, the wire scanners can thus be used now either to measure the average over all bunches or the profile of individual bunches.

BSRT

The two synchrotron light telescopes are installed at point 4 and take advantage of the D3 dipoles used to separate the beam around the RF cavities. Since at injection energy the spectra from these dipoles is in the far infrared two undulators have been developed and installed at the entrance of the D3. These special magnets provide sufficient radiation in the visible range up to about 1 TeV where the radiation from the dipole magnet takes over, Fig. 4 shows a simplified sketch of the BSRT setup. The imaging requires a complex mirror-based optical telescope and since it can not be accessed when there is beam present many components have to be adjusted remotely. The image acquisition is performed by an intensified camera which image intensifier can be gated to a single bunch allowing single bunch single turn acquisition. By scanning the gate delay all the bunches can be scanned in turn, this process is however long since the acquisition system is limited to one image per second. This type of bunch scan was performed regularly at the end of the 2010 run. Another camera, the fast camera, allows the single bunch single turn measurement, but in this case images can be acquired at over 11 kHz allowing the acquisition of the full ring in a fraction of second. The fast camera was not installed in 2010, but will be made operational during 2011. Due to the complexity of the optical system and the many constrains the optical resolution of the telescope is intrinsically limited to a few hundred microns [4], this limit has not yet been achieved yet and the reasons are not entirely understood [5]. The point spread function of the BSRTs have been calculated by comparing the sizes measured by the BSRT and the wire scanners, this PSFs are then de-convoluted from the measured values

$$\sigma_{beam} = \sqrt{\sigma^2_{meas} - PSF^2} \qquad (1)$$

Presently the PSF values are different for the two beams and for the two planes, but are all around 500 μm.

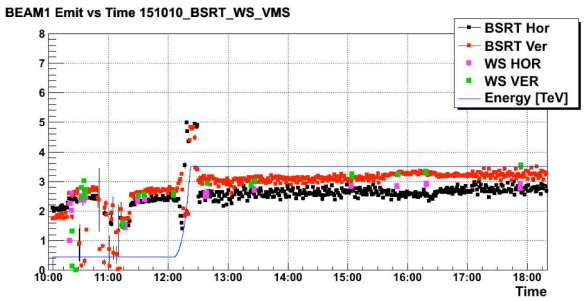

Figure 5: Evolution of the B1 beam emittance during a fill as measured by the BSRT and the wire scanner

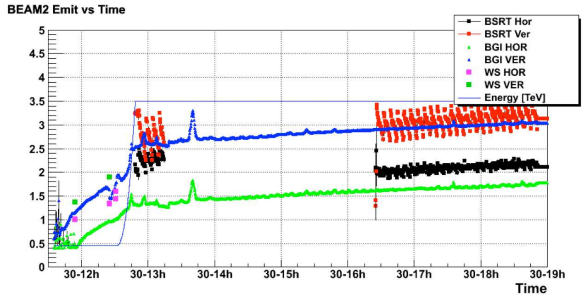

Figure 6: Evolution of the B2 beam emittance during a fill as measured by the BGI, BSRT and the wire scanner. The vertical BGI follows the BSRT and the WS while the horizontal one is quite off.

Rest gas ionization monitor

The BGI allows the measurement of the transverse projection of the beam in one direction (horizontal or vertical). The particles in the beam leave behind an ionized column where the ions (free-electrons) density reproduces the density of the beam. An electric field drifts the electrons toward a multi channel plate while a magnetic field, parallel to the electric one, guides the electrons and avoids smearing due to the thermal velocity and beam space charge effects. The MCP multiplies the impinging electrons which are imaged on a phosphor screen from where it can be acquired using an intensified camera [6]. This device is very sensitive to many effects, beam space charge, electron cloud, stray fields and fields non homogeneity, but if all parameters are well controlled the accuracy can be elevated. The problem with the BGI is that in order to obtain sufficient signal either a large number of particles in the beam is needed or a local pressure bump must be created. A local pressure bump will also increase beam losses locally imposing a stringent control and limits. Due to these constraints the four BGIs installed in LHC (1 per beam and per plane) could not be fully commissioned. The results obtained so far show that for some device the agreement between BGI, BSRT and WS is good while for the others it is quite off. The reasons for this discrepancies will be investigated in 2011.

BEAM HALO AND TAILS

In the BSRT design it is foreseen to install an optical mask in order to cut the core of the beam and allow the observation of the tails, a technique known in astronomy as a ”corona” monitor used in sun observations. At the moment the required hardware is not installed as this functionality is not considered a high priority, but if really needed this could be developed in a reasonable amount of time. The overall performance of this halo monitor is in the end limited by the amount os scattered light in the optical components and in general inside the telescope hatch.

BEAM POSITION AT THE IP

In order to monitor the beam position at the IP dedicated beam position monitors are installed just outside of the experiments and before the triplets. Around all the four interaction regions strip line pick-ups are installed, the choice for this type of devices is dictated by the fact that in multi bunch mode an incoming and an outgoing bunch can pass trough the detector with very small time difference making impossible to disentangle the signals from one or the other beam. The strip line devices have the advantage that although each strip has an upstream and a downstream port, the beam induces a pulse only in the upstream port, so the signals of the two beams can be read out independently from the two ports. The disadvantage of this method is that the electronic chains used to acquire the signals are different from one beam and the other, adding the possibility of an unknown electronic offset and making the overlap of the two beams more difficult. For this reason around IP1 and IP5 additional button pick-ups have been installed, these devices have the advantage that the readout chain is the same for the incoming and the outgoing beam so that any electronics offset cancels out. The disadvantage is that the bunch spacing must be larger than 150 ns. In order to calculate the overlap one can use a simple ballistic model, the experiments have however strong magnetic fields which can complicate the situation, especially for LHC-b and ALICE where spectrometer magnets exist. The orbit mode resolution for the strip line detectors is of the order of 1 μm and for the buttons it is slightly worse, but the electronic offset can be substantially larger than this value.

CONCLUSIONS

In order to compute the luminosity of the LHC beams several parameters must be measured accurately. In particular the distribution of charges around the machine needs to be precisely known in order to calculate the fraction of colliding charges. The wall current monitor and the longitudinal density monitors are both able to provide this information, with the LDM probably able to give better accuracy, also because it can measure the DC component as well while the WCM is limited to AC. The other important parameter to measure and monitor is the transverse emittance and for this purpose the wire scanners and the BSRT

are providing the required information.

REFERENCES

[1] A. Jeff et al., “Design for a Longitudinal Density Monitor for the LHC”, Proceeding of the IPAC Conference, Kyoto, Japan, (2010), MOPE055, and CERN-ATS-2010-110

[2] M. Sapinski, Tom Kroyer, “Operational limits of wire scanners on LHC beam”, Proceeding of the Beam Instrumentation Workshop, Lake Tahoe, California, (2008), pp383

[3] F. Roncarolo, B. Dehning, C. Fischer and J.Koopmann, “Accuracy of the SPS transverse emittance measurements”, CERN-AB-2005-081

[4] A.S. Fisher, “Expected Performance of the LHC Synchrotron-Light Telescope (BSRT) and Abort-Gap Monitor (BSRA)”, LHC- Performance-Note-014

[5] T. Lefevre et al.,“First Beam Measurements with the LHC Synchrotron Light Monitors”, Proceeding of the IPAC Conference, Kyoto, Japan, (2010), pp.1104 and CERN-ATS-2010-108

[6] J. Koopman et al., “Design and Tests of a New Rest Gas Ionisation Profile Monitor Installed in the SPS as a Prototype for the LHC”, AIP Conf. Proc. 732 (2004) pp.133- 140.

IP Positions and Angles, Knowledge and Correction

Jörg Wenninger
CERN, Switzerland.

A paper was not submitted to the proceedings. However, the slides presented are available in electronic form at http://indico.cern.ch/conferenceOtherViews.py?view=standard&confId=109784. The cover slide from this talk is given as reference.

IP positions and angles, knowledge and correction

J. Wenninger
BE-OP-LHC

LHC Lumi days - J. Wenninger

14/1/2011

Acknowledgments: W. White, E. Calvo

1

HIGH-BETA OPTICS

H. Burkhardt, CERN, Geneva, Switzerland

Abstract

High-beta optics are essential for the LHC forward physics program which includes the total proton-proton cross-section measurement, and which can be expected to ultimately allow for the most precise absolute luminosity calibration at the LHC. The strategy to commission the intermediate 90 m optics is discussed, as well as a possible running scenario for this year and requirements of the knowledge of beam parameters.

INTRODUCTION

Special high-β optics and dedicated running time are required for the forward physics program of TOTEM and ATLAS-ALFA [1, 2]. The status and prospects of these experiments have been discussed earlier in this workshop [3, 4].

We will concentrate here on the optics and commissioning aspects of this part of the LHC physics program.

The LHC interactions regions have been designed with low-β^* insertions to allow squeezing the beams to small beam sizes ($\sigma = \sqrt{\beta^* \epsilon}$, where ϵ is the beam emittance) at the interaction points (IPs) for maximum luminosity and interaction rates.

High-β^* optics are required to minimize the beam-divergence $\sqrt{\epsilon/\beta^*}$ at the interaction point for measurements at small scattering angles. Challenges of high-β^* optics include

- large tune changes compared to the normal optics implying global optics changes
- additional constraints between the IPs and roman-pots
- aperture limitations at very high-β^*
- need for precision and stability of optics parameters
- operation of some insertion quadrupoles and power converters at their limits

The effect on the tunes of the squeeze and un-squeeze can be understood by general optics considerations. The betatron phase advance is

$$\mu(s) = \int_0^s \frac{1}{\beta(s')}\,\mathrm{d}s'. \qquad (1)$$

We recall that the phase advance μ and tune are directly related by $Q = \mu(C)/\,2\pi$, (where C stands for the circumference).

The β-function in a drift space where s_0 is the position of the interaction point is given by

$$\beta(s) = \beta^* + \frac{(s-s_0)^2}{\beta^*}\,. \qquad (2)$$

The phase advance and tune contribution from the insertion can be obtained analytically by integration from -ℓ to +ℓ. The result is

$$\mu = 2\,\arctan\left(\frac{\ell}{\beta^*}\right)\,. \qquad (3)$$

This agrees well with the phase advanced obtained from MAD-X for $\ell = 26.15\,\mathrm{m}$, which is the distance between the IP and the centre of the first quadrupoles (Q1). A low-β insertion with $\beta^* \ll \ell$ contributes with a phase advance of π and tune of 0.5. For very high $\beta^* \gg \ell$ instead, the phase advance and tune contribution drops to zero.

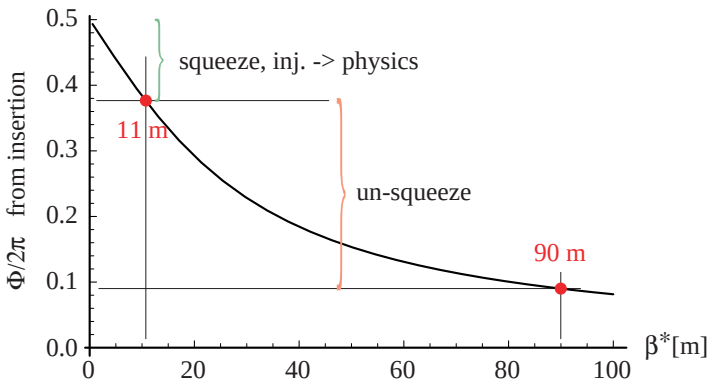

Figure 1: Tune contribution from the insertion $\pm 26\,\mathrm{m}$ from the IP as relevant for the LHC.

This is illustrated in Fig.1. We see that the local tune change from the IR for the squeeze from 11 m to 0.55 m is approximately +0.1 and about -0.3 for the un-squeeze from 11 m to 90 m. The tune changes in the un-squeeze are too large to be fully compensated internally.

The 90 m optics for TOTEM is shown in Fig. 2. It provides a phase advance between the IP and the roman pot at 220 m of π in the horizontal and of $\pi/2$ in the vertical plane.

A similar optics for ATLAS-ALFA is currently being prepared together with S. Cavalier for a phase advance of $\pi/2$ in the vertical plan to the roman pots, which in the case of ATLAS-ALFA are located at 240 m downstream from the IP.

The aperture for the 90 m optics is not critical, see Fig. 3.

STRATEGY

The top priority for LHC operation in 2011 is to maximize the total integrated luminosity.

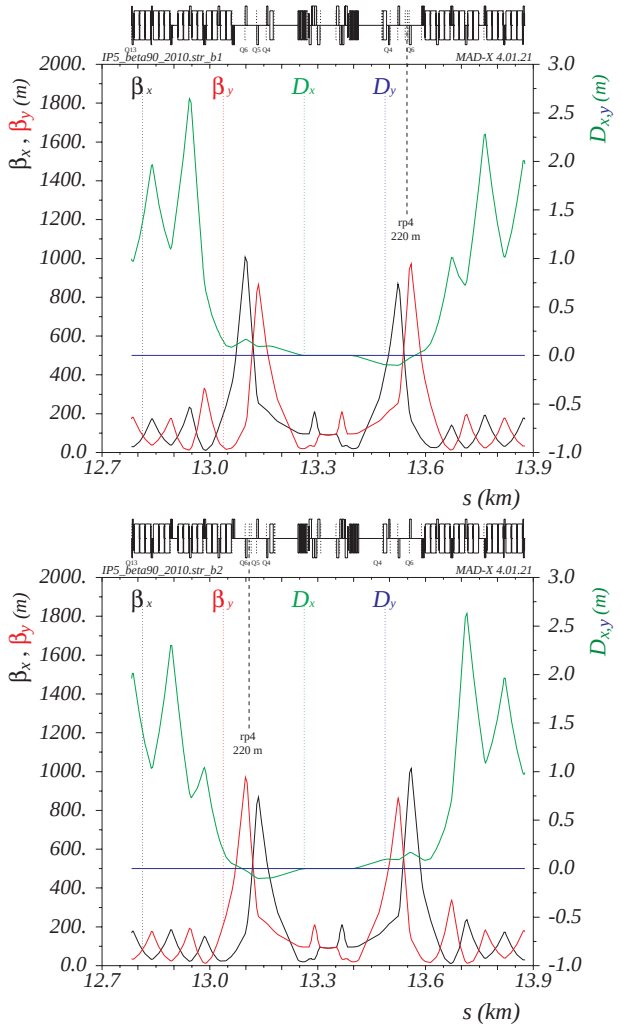

Figure 2: 90 m TOTEM optics, compatible with all known constraints of the nominal LHC. Up for Beam 1 and down for Beam 2.

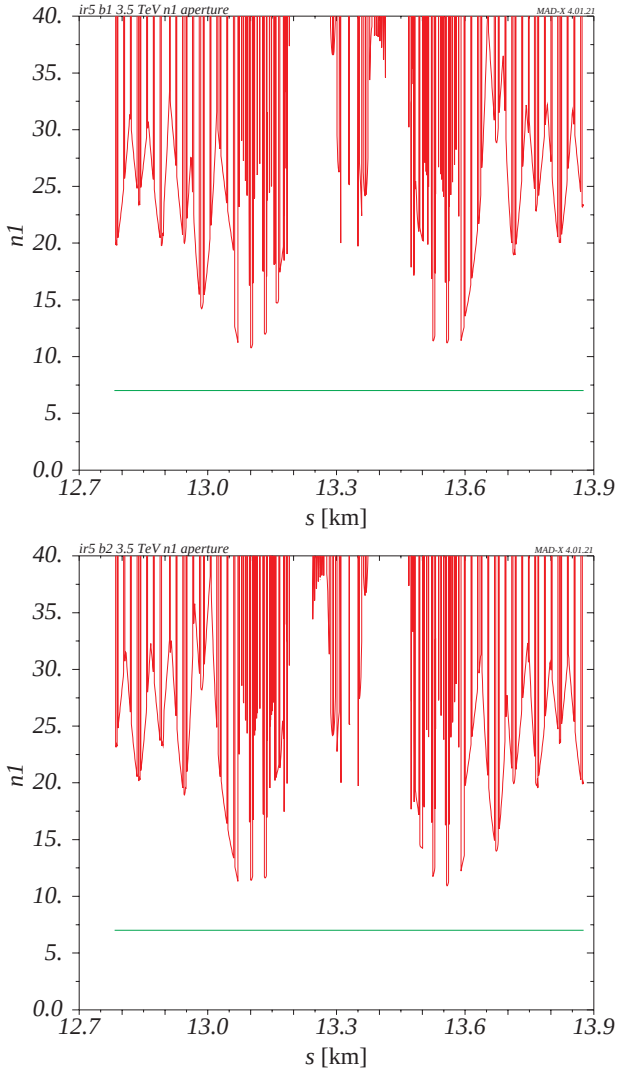

Figure 3: Aperture in terms of n1 at 90 m with vertical separation of ± 2 mm at 3.5 TeV, for $\epsilon_N = 3.75\,\mu$m. Up for Beam 1, down for Beam 2.

Here we will argue, that it will be very important to nevertheless spend some shifts in 2011 to commission the 90 m optics for IP1&5 and to allow for some days of physics operation in 2011. In addition to physics arguments, this will provide essential input for the "real" high-β optics, which can only be realized later. Further delaying high-β operation may interfere with LHC upgrade plans and the reduction of the beam-pipe radii at the IPs.

As discussed in [5], the very high-β^* ($\gg$90 m) optics were designed for the full LHC beam energy of 7 TeV and a reduced emittance of $\epsilon_N = 1\,\mu$m.

The $\beta^* = 1535$ m TOTEM optics requires additional cables to be installed [6].

The $\beta^* = 2625$ m ATLAS-ALFA optics was designed for an inverted Q4 polarity (the hardware to allow the switching is installed) and requires dedicated injection at $\beta^* = 200$ m and a dedicated ramp and un-squeeze.

Experience with the 90 m optics will be important to determine which cables should be added for TOTEM, and to develop a realistic and effective strategy to get to very high-β^* in later years : using un-squeeze starting from the standard ramp or by dedicated injection, ramp and squeeze.

STUDIES AND COMMISSIONING PROPOSED FOR 2011

The first step proposed for a machine development shift, is to study the feasibility of an un-squeeze to 90 m with external tune compensation. It is planned to use the standard injection and ramp optics with ($\beta = 11$ m at IP 1 and 5) for this purpose. The crossing angles in IP1&5 have to be off for the un-squeeze and at 90 m. Seventeen intermediate optics files have been prepared to allow for a very smooth un-squeeze from 11 to 90 m. The files have been matched with knobs to allow for a constant ± 2 mm parallel separation through the un-squeeze.

The main difference compared to the squeeze to low-β

is the need for a significant external tune compensation of 0.22 in the horizontal and 0.05 in the vertical plane. Details are described in [5].

Three alternatives have been considered for the external tune compensation

- use another IP like IP4 (with consequences on instrumentation and the damper); limited to changes of 0.2 in tune [7]
- use the trim quadrupoles, implies some β-beating (8.5% in x and 4.5% in y)
- use the main arc quadrupoles, implies small β-beating (4.5% in x and 1.5% in y)

To save time, we will try to test and commission the 90 m TOTEM and ATLAS-ALFA optics simultaneously. This doubles the need for external tune compensation. For the large tune compensation required, the most attractive alternative is to ramp up the arc quadrupoles during the unsqueeze for tune compensation. An initial eight hours shift to study this will be requested for the first machine development period in 2011.

PHYSICS OPERATION AND REQUIRED ACCURACY

Depending on the progress in the initial machine study, further machine development studies or commissioning time will be needed to get the 90 m optics ready for physics operation in the second part of 2011.

A good knowledge and stability of the beam parameters is important for physics operation at high β^*. Following discussions with H. Niewiadomski et al. from TOTEM for the required accuracy at 90 m, we should aim for a 1% precision in the knowledge of β-functions and phase advances between the IP and the roman pots and also for a knowledge of the dispersion at the roman pots to the 1% level. Following discussions with R. Tomas, high-β^* should be easier to measure than low-β^* and a precision around 1% may become feasible with dedicated measurements at $\beta^* = 90\,\mathrm{m}$.

It is very likely that several iterations will be required to reach a good precision.

For the physics operation at 90 m in 2011, we are talking about few days or fills : TOTEM requests four fills of each eight hours [3]. The schedule should allow for some days between 90 m physics fills for checks, validation and optimization.

ACKNOWLEDGMENT

I would like to thank all colleagues who contributed with ideas, work or constructive critics and discussions to the work and ideas presented in this contribution.

From the machine side, I would like to thank in particular M. Giovannozzi, W. Herr, O. Brüning and S. White for input on optics and R. Tomas for discussions on measurements and correction of β-functions. For input on the on-line and commissioning parts I would like to acknowledge S. Redaelli, M. Lamont and G. Müller.

For ATLAS-ALFA I would like to thank in particular P. Grafstrom, P. Puzo and S. Cavalier, and for TOTEM V. Avati, M. Deile, K. Eggert and H. Niewiadomski.

REFERENCES

[1] **TOTEM** Collaboration, G. Anelli *et al.*, "The TOTEM experiment at the CERN Large Hadron Collider", *JINST* 3 (2008) S08007,

[2] ATLAS collaboration, "ATLAS Dectectors for Measurement of Elastic Scattering and Luminosity", CERN-LHCC-2008-004, 2008

[3] M. Deile, "TOTEM: Prospects for Total Cross-Section and Luminosity Measurements", Contribution to this workshop.

[4] K. Hiller, "Status and prospects of ALFA", Contribution to this workshop.

[5] H. Burkhardt and S. White, "High-beta Optics for the LHC", LHC Project Note 431

[6] H. Burkhardt, presentation at the LMC#32, CERN, 14 October 2009

[7] M. Aiba et al., "Optics Flexibility in the LHC at Top Energy", LHC-PROJECT-Report-1106

Luminosity Scans at the LHC

S. M. White, CERN, Geneva, Switzerland

Abstract

INTRODUCTION

For particle colliders, the most important performance parameters are the beam energy and the luminosity. High energies allow the particle physics experiments to study and observe new effects and the luminosity is used as a measure of the number of collisions. It is defined as the proportionality factor between the event rate, measured by the experiments, and the cross section of the process observed.

The **L**arge **H**adron **C**ollider (LHC) is designed to produce proton proton collisions at a center of mass energy of 14 TeV. This energy will be the highest ever reached in a particle accelerator. The knowledge and understanding of particle physics at such high energy is based on simulations and theoretical predictions. As opposed to e^+e^- colliders, for which the Bhabba scattering cross section can be accurately calculated and used for luminosity calibration, there are no processes with well known cross sections and sufficiently high production rate to be directly used for the purpose of luminosity calibration in the early operation of the LHC.

The luminosity for colliding beams can be directly obtained from geometry and numbers of particles flowing per time unit, as pioneered by S. Van Der Meer at the ISR [1]. For the LHC, it was proposed to use this method to provide a first luminosity calibration based on machine parameters for the physics experiments [2, 3].

Later, dedicated operation of the LHC using special special high-β^* optics should allow to independently obtain an accurate cross section and luminosity calibration close to the 1% level, by measurements of the very forward proton proton scattering with the TOTEM and ATLAS experiments [4, 5].

THE VAN DER MEER METHOD

We consider two bunches of N_1 and N_2 particles colliding in an interaction region as shown in Figure 1. For bunches crossing head-on at a frequency f (revolution frequency in the case of a circular collider) the luminosity is expressed as:

$$\mathcal{L}_0 = \frac{N_1\, N_2\, f}{A_{\text{eff}}}, \tag{1}$$

where A_{eff} is the effective transverse area in which the collisions take place. The revolution frequency in a collider is accurately known and the number of particles or beam intensity is continuously measured with beam current transformers which should reach an accuracy of 1 % for LHC nominal beam parameters [6]. The only unknown parameter that needs to be measured is the effective transverse area which depends on the density distribution ρ_1 and ρ_2 of the two beams.

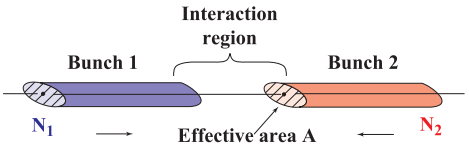

Figure 1: Luminosity from particles flux and geometry.

It was shown by S. Van Der Meer in [1], that if the density distributions in the horizontal and the vertical plane are uncorrelated and stable, the effective transverse beam size can be measured by performing scans in separation and integrating the resulting curve of the interaction rate versus the separation δu (where u stands for x or y). Independently of the beam shape, the effective area is then given by:

$$A_{\text{eff}} = \frac{\int R_x(\delta x)\, d\delta x}{R_x(0)} \frac{\int R_y(\delta y)\, d\delta y}{R_y(0)}, \tag{2}$$

where $R(\delta x, \delta y) = R_x(\delta x)\, R_y(\delta y)$ if the horizontal and vertical density distributions are uncorrelated, describes the evolution of the interaction rate as a function of the transverse offsets δx and δy measured during the separation scans.

For Gaussian distributions, the luminosity $\mathcal{L}$ as a function of the transverse offsets is also a Gaussian

$$\mathcal{L} = \mathcal{L}_0\, \exp\left[-\frac{\delta x^2}{2\,(\sigma_{1x}^2 + \sigma_{2x}^2)} - \frac{\delta y^2}{2\,(\sigma_{1y}^2 + \sigma_{2y}^2)} \right], \tag{3}$$

where σ_{1u} and σ_{2u} are the individual r.m.s. beam widths. Applying Equation 2 to compute the effective area we get:

$$A_{\text{eff}} = 2\,\pi \sqrt{\sigma_{1x}^2 + \sigma_{2x}^2}\, \sqrt{\sigma_{1y}^2 + \sigma_{2y}^2}, \tag{4}$$

and

$$\mathcal{L}_0 = \frac{N_1\, N_2\, f\, N_b}{2\,\pi \sqrt{\sigma_{1x}^2 + \sigma_{2x}^2}\, \sqrt{\sigma_{1y}^2 + \sigma_{2y}^2}}, \tag{5}$$

which is the standard formulae of the luminosity for elliptical beams colliding head-on [7]. To be noted that the

functions R_u reach a maximum for zero separation. Separation scans can therefore also be used to optimize the collision rate.

For completeness other potential systematic effects in the absolute luminosity determination from beam parameters are discussed, and it will be shown that they are very small for the relevant LHC beam conditions.

CROSSING ANGLE

The LHC beams share the same beam chamber from the interaction point up to the first separation dipole 60 m from the IP which deflects them into two separate rings. For high luminosity operation, the LHC is filled with many bunches and a crossing angle introduced to avoid extra collisions in the common beam pipe section.

A crossing angle between the two beams ϕ_u in one plane $u = x, y$, decreases the luminosity as follows:

$$\mathcal{L} = \mathcal{L}_0 \cdot S_u = \mathcal{L}_0 \frac{1}{\sqrt{1 + \frac{\sigma_{1s}^2+\sigma_{2s}^2}{\sigma_{1u}^2+\sigma_{2u}^2}\left(\tan\frac{\phi_u}{2}\right)^2}}. \quad (6)$$

where $\mathcal{L}_0$ is the luminosity without crossing angle defined in Equation 5. $\sigma_{1,2\,s}$ are the bunch lengths of the beams. ϕ_u is the full crossing angle between the beams. The decrease in luminosity is equivalent to an increase of the effective beam size in the crossing plane.

The extension of Eq. 6 to describe the luminosity reduction by the combination of vertical and horizontal crossing angles is:

$$\mathcal{L} = \mathcal{L}_0 \cdot S \quad (7)$$

where

$$S = \frac{1}{\sqrt{1 + \frac{\sigma_{1s}^2+\sigma_{2s}^2}{\sigma_{1y}^2+\sigma_{2y}^2}\left(\tan\frac{\phi_y}{2}\right)^2 + \frac{\sigma_{1s}^2+\sigma_{2s}^2}{\sigma_{1x}^2+\sigma_{2x}^2}\left(\tan\frac{\phi_x}{2}\right)^2}}, \quad (8)$$

where ϕ_x and ϕ_y are the projections of the crossing angle in the transverse planes.

The luminosity in the presence of transverse offsets and crossing angles can be factorized as follows:

$$\mathcal{L} = \mathcal{L}_0 \cdot S \cdot T \cdot U, \quad (9)$$

where S is the reduction factor from the crossing angles at zero separation given in Eq. 8, T the reduction factor from transverse offsets in the luminosity scans from Eq. 3, and U a cross term that can be written as:

$$U = \exp\left[S^2 \frac{\sigma_{1s}^2+\sigma_{2s}^2}{2}\left(\frac{\delta x \tan\frac{\phi_x}{2}}{\sigma_{1x}^2+\sigma_{2x}^2} - \frac{\delta y \tan\frac{\phi_y}{2}}{\sigma_{1y}^2+\sigma_{2y}^2}\right)^2\right]. \quad (10)$$

Applying Equation 2 to compute the effective area we get:

$$A_{\text{eff}} = 2\,\pi \frac{\sqrt{\sigma_{1x}^2+\sigma_{2x}^2}\sqrt{\sigma_{1y}^2+\sigma_{2y}^2}}{S}\frac{S_x\,S_y}{S} \quad (11)$$

where

$$S_u = \frac{1}{\sqrt{1 + \frac{\sigma_{1s}^2+\sigma_{2s}^2}{\sigma_{1u}^2+\sigma_{2u}^2}\left(\tan\frac{\phi}{2}\right)^2}}. \quad (12)$$

Compared to Eq. 7 we have the extra factor

$$X_{\text{corr}} = \frac{S_x\,S_y}{S}. \quad (13)$$

For scans performed exactly in the crossing plane ($\phi_x = 0$, $S_x = 1$ and $S = S_y$ or $\phi_y = 0$, $S_y = 1$ and $S = S_x$), the Van Der Meer scan method directly measures the correct effective beam-size including the effect of the crossing angle ($X_{\text{corr}} = 1$).

This remains approximately true also in case of a crossing angle in both planes. The correction factor X_{corr} is shown in Figure 2 for the 2010 LHC beam parameters and the nominal 7 TeV beam parameters and remains very close to 1 in all practical cases for the LHC.

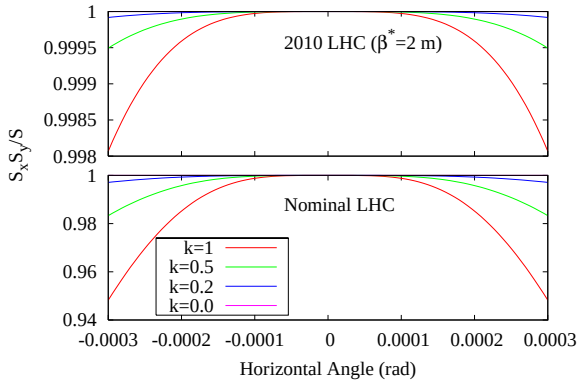

Figure 2: Ratio $S_x\,S_y/S$ for 7 TeV nominal LHC (bottom) and the 2010 LHC parameters (top) with ($E = 3.5$ TeV, $\beta^* = 2$ m). k represents the ratio between the projected angles, in this case ϕ_y/ϕ_x. The error becomes significant for the nominal LHC beam parameters when the angles are of equivalent amplitudes of several 100 μrad, which represents a very unlikely situation for the LHC.

HOURGLASS EFFECT

The β-function in a drift space varies with the distance to the minimum like:

$$\beta(s) = \beta^*\left(1 + \frac{s^2}{\beta^{*2}}\right), \quad (14)$$

and therefore the beam size $\sigma = \sqrt{\beta(s)\,\varepsilon}$

$$\sigma(s) = \sigma^*\sqrt{1 + \frac{s^2}{\beta^{*2}}}. \quad (15)$$

The β-function around the interaction point has the shape of a parabola. When the ratio β^*/σ_s, where σ_s is

the rms bunch length becomes ≤ 1, a correction factor is required. The factor can be calculated according to [8]

$$H(t) = \frac{1}{\sqrt{\pi}} \int_{-\infty}^{+\infty} \frac{e^{-t^2}}{\sqrt{(1+t^2/t_x^2)(1+t^2/t_y^2)}}\, dt, \quad (16)$$

where

$$t_u^2 = \frac{2\,(\sigma_{1u}^{*2} + \sigma_{2u}^{*2})}{(\sigma_{1s}^2 + \sigma_{2s}^2)(\sigma_{1u}^{*2}/\beta_{1u}^{*2} + \sigma_{2u}^{*2}/\beta_{2u}^{*2})}, \quad (17)$$

where $u = x, y$. For round beams we have

$$t_x^2 = t_y^2 = t_r^2 = \frac{2\,\beta^{*2}}{\sigma_{1s}^2 + \sigma_{2s}^2}, \quad (18)$$

and

$$H(t_r) = \sqrt{\pi}\, t_r\, e^{t_r^2}\, \mathrm{erfc(t_r)}, \quad (19)$$

Table 1: Hourglass luminosity reduction factor as function of β^* calculated with $\sigma_s = 0.0755$ m for round beams.

β^*	t_r	$H(t_r)$
2.0	26.5	0.9992
1.0	13.2	0.9972
0.55	7.3	0.9908

Table 1 shows, that the luminosity reduction due to the hourglass effect reaches a level of 1 % for the nominal $\beta^* = 0.55\,\mathrm{m}$ and becomes negligible for larger values like $\beta^* = 2\,\mathrm{m}$ as relevant for the first years of LHC operation. The effect is more significant in the case of the RHIC collider. A description of the analysis of separation scans in presence of a non-negligible hourglass effect can be found in [9, 10].

BEAM-BEAM EFFECTS

Beam-beam effects are relevant at high intensities. Ideally all the calibration scans should be performed at low intensity to minimize this effect. However, the LHC will be running at high intensities and it could be interesting to perform scans in these beam conditions. In this case, the beam-beam force will introduce a non-linear behavior as a function of the separation which can affect the orbit or emittance and will couple the transverse distributions. The emittance growth due to the beam-beam interactions in the presence of transverse offsets was estimated in [11] and proved to be very small. The beam-beam effect will perturb the lattice as a function of the separation resulting in a dynamic change of the tunes and β-functions [13] and therefore beam size. The β-function relates to a tune shift ΔQ as follows:

$$\frac{\beta^*}{\beta_0^*} = \frac{\sin(2\pi Q)}{\sin(2\pi Q + 2\pi\Delta Q)}, \quad (20)$$

where Q is the unperturbed tune of the machine and β^* and β_0^* are the perturbed and unperturbed β-functions at the IP. The tune shift introduced by the head-on beam-beam interaction is largest for the central particles and reaches a value (for round beams) of

$$\xi = \frac{N\, r_0}{4\,\pi\,\varepsilon_N}, \quad (21)$$

which is referred to as the beam-beam parameter; r_0 is the classical particle radius and ε_N is the normalized emittance. The variation of β^* as a function of the separation was estimated to be of the order of 1 % in the case of nominal LHC beam parameters.

Table 2: Linear beam-beam parameter without crossing angle and β^* maximum variations for nominal LHC tunes (64.31, 59.32).

N [p/bunch]	ξ	$\Delta\beta/\beta$
5×10^9	0.0002	0.0005
4×10^{10}	0.0013	0.0040
1.15×10^{11}	0.0037	0.0097

Table 2 shows the amplitude of the β^* variations as a function of intensity for the nominal LHC tunes. We see that this effect can be reduced to a negligible level by reducing the bunch intensity. For a finite beam separation, the beam-beam interaction will also result in a change of the closed orbit. As illustrated in Figure 3, the orbit offset introduced by collisions at finite separation at the interaction points of the LHC is also very small. When the LHC is filled with many closely spaced bunches, we have to add to this the long-range beam-beam kicks from several bunch passages left and right of each IP and get effects of up to $0.3\,\sigma$ for the nominal LHC filling scheme. Luminosity calibration measurements in the LHC are best performed with a limited number of bunches (≤ 156) to avoid any complication by long range beam-beam interactions.

LINEAR COUPLING

By design, the betatron oscillation in the transverse x, y planes of the LHC are fully decoupled. In practice, there will be a small residual coupling which corresponds to a tilt of the beam ellipse by an angle ϕ. In addition, this effect can be slightly different for both beams present in the LHC. As shown in [14], the luminosity in the presence of asymmetric coupling can be written as:

$$\mathcal{L} = \mathcal{L}_0 \frac{1}{\sqrt{1 + \frac{(\sigma_{1\xi}^2 - \sigma_{1\eta}^2)(\sigma_{2\xi}^2 - \sigma_{2\eta}^2)}{(\sigma_{1\xi}^2 + \sigma_{2\xi}^2)(\sigma_{1\eta}^2 + \sigma_{2\eta}^2)} \sin^2(\phi_2 - \phi_1)}}. \quad (22)$$

where $\sigma_{i\eta}$, $\sigma_{i\xi}$ and ϕ_i $(i = 1, 2)$ are the beam sizes along the ellipse main axes and the tilt angles of the two beams.

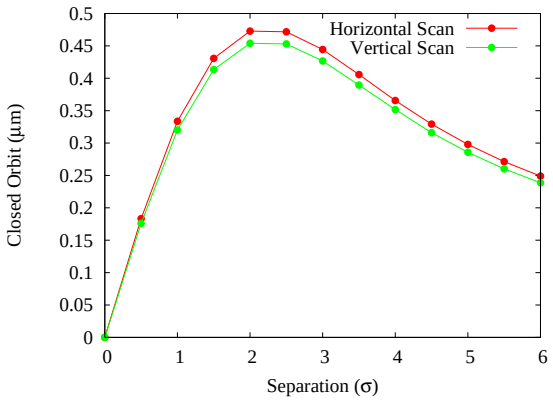

Figure 3: Self-consistent closed orbit as a function of the separation simulated with TRAIN[12] for $\xi = 0.003$ and LHC nominal tunes (64.31, 59.32).

In the case of round beams, coupling has no effect on luminosity and separation scans along the horizontal and vertical axes, and the x, y coordinates shown in Figure 4 provide the correct measurement of the effective area. In the case of elliptical beams, the coupling will result in a luminosity reduction and produce a tilt of the overlap region [14]. The effective area is then determined by the product of the effective beam sizes along the main axes of the overlap ellipse, noted as ξ and η in Figure 4. Scanning in the horizontal and vertical planes would introduce a bias. The correct result for the effective area could still be obtained using a raster scan along several parallel horizontal and vertical lines.

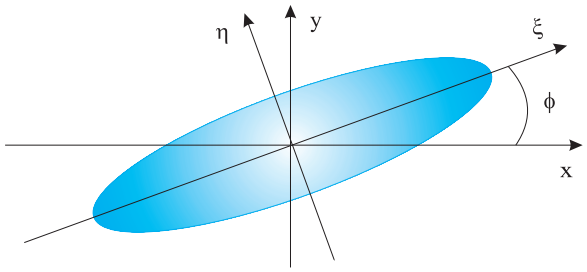

Figure 4: Tilted beam ellipse.

The bias can be computed from the **C**–matrix, β^* and emittance measurements [15]. An estimate of this effect is shown in Figure 5 based on optics and coupling measurements done at the LHC in 2010 at IP8 [16, 17]. For these measurements, an uncertainty of 1 % is reached at a ratio of four between the horizontal and vertical emittances. In the LHC the beams are round by design. In practice, there will be some differences between the horizontal and vertical emittances but it is straightforward to keep these well below a factor two, such that the uncertainty becomes negligible.

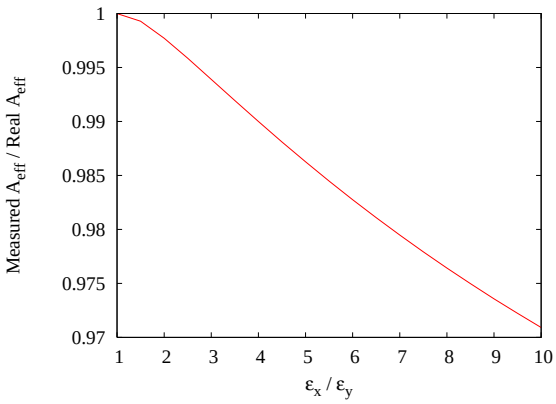

Figure 5: Effect of coupling on the measurement of the effective area derived from optics measurements performed at IP8.

OPTIMAL CONDITION FOR CALIBRATION MEASUREMENTS

Table 3: Optimal beam parameters for calibration scans. Luminosity and events per bunch crossing are calculated for an energy of 3.5 TeV.

β^* [m]	>1.0
Intensity [10^{10} p/bunch]	<4.0
Number of bunch crossing	156
Emittance [μm]	3.75
Crossing angle [μrad]	0.0
Beam-Beam Parameter	0.0013
$\mathcal{L}$ per bunch [$10^{28}\mathrm{cm}^{-2}\mathrm{s}^{-1}$]	3.52
Events per bunch crossing	0.226
Event Rate [Hz]	2541

Table 3 lists a possible set of beam parameter which would minimize the non-linear effects (beam-beam, pile-up, hourglass) as well as the uncertainty on the beam current measurement, and allow to reach a statistical accuracy of the order of 1 % within a few seconds. In addition it is desirable to have beams as round as possible to keep the uncertainty from linear coupling negligible. Another advantage of this proposal is that the setup time is minimized as it uses all the default LHC parameters, especially optics, and would not cost too much in terms of integrated luminosity.

MACHINE PROTECTION

The beams are displaced at the IP via a closed orbit bump that consists of four magnets and allows to control the beams independently.

One can see in Figure 6 that a four magnet separation bump extends over a large fraction of the straight section around the IP. More specifically, displacing the beams at

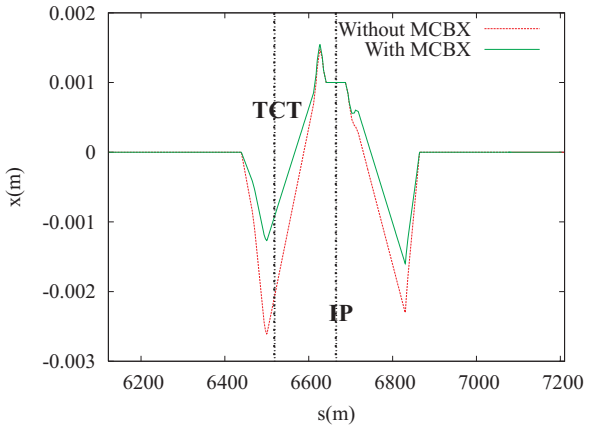

Figure 6: Example of closed orbit bumps using different orbit correctors at IP5. Displacing the beam at the IP also changes the orbit at the tertiary collimator location.

the IP will result in a change of orbit at the tertiary collimators (TCT). Given the non-negligible offset at the TCT introduced by the bumps, one has to ensure that while performing a separation scan the beams remain far enough from the aperture set by the collimators and that the displacement does not compromise the machine protection. In 2010, the displacement at the TCT was minimized by splitting the amplitude of the corrections required to find the optimum collision point between the two beams. In addition a re-qualification of the collimation system was done with the TCTs closed by 2σ with respect to their nominal settings to ensure that the margins were sufficient to safely perform the full scan.

In 2011, it was decided to move the TCTs together with the beam [18] in order to provide more flexibility and operation efficiency and ensure that the aperture margin between the dump protection and the TCTs remains large enough. It does not guarantee, that the safety margin between the TCTs and the triplet magnets is always respected. A complete assessment of the aperture reduction due the scans, especially in the crossing angle plane, should therefore be performed in order to ensure safe operation.

SUMMARY

Calibration scans were performed in the four LHC interaction points [19]. The experiments first published results and latest offline analysis can be found in [20, 21], [22], [24, 23] and [26, 25]. Two sets of measurements were performed. The first measurements, in spring 2010, were performed early in the commissioning phase of the LHC and the beam conditions and instrumentation were not optimal. The final uncertainty on the measurement was found to be of 11% from which 10% came from the preliminary determination of the beam intensity [27]. A more detailed offline analysis of the beam current data improved the overall uncertainty to about 6 %. The earlier measurements also suffered from a larger emittance blow-up due related to instrumental noise picked-up by the beam [28]. The second set of measurements was performed in October 2010. Significant progress in the calibration of the LHC instrumentation and better beams conditions and stability helped reducing the overall systematic uncertainty to about 5% for these measurements.

The precision obtained during the first year of operation of a machine as complex as the LHC represents a significant achievement and could be improved based on the arguments presented above.

Table 4: Uncertainties on the absolute luminosity for optimal beam conditions.

Beam-beam effects	negligible
Hourglass effect	negligible
Fit Model	1%
Emittance blow-up	$<$1%
Beam current	1-2 %
Beam displacement	1-2%
Total	3-4%

Table 4 lists the known uncertainties for optimal beam parameters. The contributions from coupling and hysteresis are considered to be negligible. A total 3–4 % systematic uncertainty seems to be within reach with the current equipment and procedures. This assumes perfectly stable beam conditions, low background and well working and calibrated instruments. The dominant uncertainty in these conditions originates in intensity measurement and the determination of the beam displacement.

REFERENCES

[1] S. Van Der Meer, ISR-PO/68-31, KEK68-64.

[2] H. Burkhardt and P. Grafström, "Absolute Luminosity from Machine Parameters", LHC Project Report 1019, 2007.

[3] S. M. White et al., "Luminosity Optimization and Calibration in the LHC", PAC Proceedings, 2009.

[4] TOTEM Collaboration, G. Anelli et al., "The TOTEM experiment at the CERN Large Hadron Collider", JINST 3 S08007, 2008.

[5] ATLAS Collaboration, "ATLAS Dectectors for Measurement of Elastic Scattering and Luminosity",CERN-LHCC-2008-004, 2008.

[6] C. Fischer and R. Schmidt, On the Measurements of the Beam Current, Lifetime and Decay Rate in the LHC Rings, LHC-BCT-ES001, 2005.

[7] W.Herr and B.Muratori, Concept of Luminosity, Yellow Report CERN 2006-002, 2006.

[8] M. A. Furman, "Hourglass Effects for Asymmetric Colliders", PAC 1991 Proceedings, 1991.

[9] A. Drees et al., "Results from Vernier Scans During the RHIC During 2008 PP run", PAC Proceedings, 2009.

[10] A. Drees and S. M. White, "Vernier Scan Results from the First RHIC Polarized Proton Run at 250 GeV", IPAC Proceedings, 2010.

[11] T. Pieloni, W. Herr and Ji Qiang, "Emittance Growth due to Beam-Beam Effects with a Static Offset in Collision in the LHC", PAC Proceedings, 2009.

[12] H. Grote and W. Herr, CERN-LHC-PROJECT-REPORT-502.

[13] A. Chao, "Beam-Beam Instability", AIP Conf. Proceedings, 1983.

[14] Y. Cai,"Luminosity of Asymmetric e+e- Collider with Coupling Lattices", EPAC Proceedings, 2000.

[15] Y. Luo, "Transverse Beam sizes and Quasi Emittances for Linearly Coupled Optics", NIM, A562, 2006.

[16] R. Tomás et al., "CERN Large Hadron Collider Optics Model, Measurements and Corrections, Phys. Rev. ST Accel. Beams 13, 121004, 2010.

[17] M. Aiba et al., "Coupling and Vertical Dispersion Correction Studies for the LHC Using Skew Quadrupoles and Vertical Orbit Bumps, IPAC Proceedings, 2010.

[18] R. Bruce, "How low can we go? Getting below 3.5 m β^*, LHC Beam Commissioning Workshop, Evian, 2010.

[19] S. M. White, R. Alemany-Fernandez and H. Burkhardt, "First Luminosity Scans in the LHC", IPAC Proceedings, 2010.

[20] The ATLAS Collaboration, "Luminosity Determination Using the ATLAS Detector", ATL-ATLAS-CONF-2010-060, 2010.

[21] M. Huhtinen,"ATLAS 2010 Luminosity Determination", this workshop.

[22] K. Oyama,"ALICE 2010 Luminosity Determination", this workshop.

[23] The CMS Collaboration, "Measurement of CMS Luminosity", CMS PAS EWK-10-004, 2010.

[24] M. Zanetti, "Luminosity Normalization Measurements Based on Van Der Meer Scans at CMS", this workshop.

[25] The LHCb Collaboration, R. Aaij et al, "Measurement of sigma(pp $\rightarrow$ b anti-b X) at $\sqrt{s} = 7$ TeV in the forward region, Submitted to Phys. Lett. B., 2010.

[26] V. Balagura,"LHCb 2010 Luminosity Determination with Van Der Meer Scans", this workshop.

[27] G. Anders et al. " LHC Bunch Current Normalization for the April-May 2010 Luminosity Calibration Measurements", CERN-ATS-Note-2011-004 PERF, 2011.

[28] G. Arduini, "The hump: how did it impact the luminosity performance?", Evian Beam Commissioning Workshop Proceedings, 2010.

Direct Luminosity Measurements at the LHC – summary

Jaap Panman
CERN, Geneva, Switzerland

March 15, 2011

Abstract

A summary of the present status of direct measurements of the luminosity at the LHC is given. Two methods were used, the van der Meer scan method and the beam-gas imaging method, which are briefly explained. Requirements and ideas for improved measurements in 2011 are presented.

1 Introduction

Measurements of luminosity on an absolute scale are of general interest for colliding-beam experiments at storage rings. These measurements are needed to determine the absolute cross sections of reaction processes and to quantify the performance of the machine. The required accuracy on the absolute value of the cross section depends on the process of interest and depends on the theoretical precision of the predictions. Arguments for precision targets in the range of 1–2% have been given at this workshop for the production of vector bosons and the elastic production of muon pairs [1, 2, 3].

The present status of direct luminosity measurements have been presented at this workshop by all experiments [4, 5]. The present precision is of the order of 5% using the most recent information on the calibration of the beam intensities [6, 7]. Based on the results of the measurements done in 2010, more knowledge has been gathered on systematic limitations of these measurements. Here, some of these ideas will be presented with the aim to achieve higher precision in forthcoming runs. The optimal solution may be different for each experiment, due to differences in their capabilities. However, an attempt will be made to reconcile the requirements for the different experiments.

In a circular collider the average instantaneous luminosity can be expressed for one pair of colliding bunches as [8, 9]:

$$L = n_1 n_2 \, f \sqrt{(\vec{v}_1 - \vec{v}_2)^2 - \frac{(\vec{v}_1 \times \vec{v}_2)^2}{c^2}} \int \rho_1(x,y,z,t) \rho_2(x,y,z,t) \; \mathrm{d}x \, \mathrm{d}y \, \mathrm{d}z \, \mathrm{d}t \; , \qquad (1)$$

where we have introduced the revolution frequency f (11245 Hz), the numbers of protons in the bunches n_1 and n_2 in both beams, the velocities $\vec{v}_1$ and $\vec{v}_2$, the half crossing-angle θ, and the normalized time and position dependent bunch densities $\rho_j(x,y,z,t)$. The bunch particle densities $\rho_j(x,y,z,t)$ are normalized such that their individual integrals over full space are unity.

For highly relativistic beams colliding with a very small half crossing-angle θ the Møller factor (the square root factor in the equation) reduces to $2c\cos^2\theta \simeq 2c$. The integral in Eq. 1 is known as the beam overlap integral.

At the LHC a series of experiments were carried out to perform luminosity calibration measurements at each Interaction Point (IP). Two methods were used: the "van der Meer scan" method (VDM) and the "beam-gas imaging" method (BGI).

1.1 The "van der Meer scan" method

Van der Meer proposed a beam position scanning method for the ISR which provides a direct measurement of an effective cross section σ by measuring the corresponding counting rate as a function of relative offset of the positions of two colliding beams [10]. At the ISR, only vertical displacements where needed owing to the crossing angle between the beams in the horizontal plane and owing to the fact that the beams where not bunched.

For the LHC the beams have to be scanned in both transverse planes [11]. The cross section σ can be measured using the equation

$$\sigma = \frac{\int R(\Delta(x), \Delta(y_0))d\Delta(x) \times \int R(\Delta(x_0), \Delta(y))d\Delta(y)}{n_1 n_2 \, f \, R(\Delta(x_0), \Delta(y_0))} \, . \tag{2}$$

$R(\Delta(x),\Delta(y))$ are rates corresponding to the process with cross section σ. These rates are measured at offsets $\Delta(x)$ and $\Delta(y)$ with respect to the nominal "working point" (x_0, y_0). The scans consist in creating offsets $\Delta(x)$ and $\Delta(y)$ such that practically the full shape of the beams are explored. When integrated over the displacements, the measured rate gives the cross section.

The main assumption is that the density distributions can be factorized. In that case two scans are sufficient to obtain the cross section: one along a constant y-displacement $\Delta(y_0)$ and one along a constant x-displacement $\Delta(x_0)$. It can be shown that this equation holds in the presence of a non-zero crossing angle θ [12]. It is also assumed that effects due to bunch evolution during the scans (shape distortions or transverse kicks due to beam-beam effects, emittance growth, bunch current decay), effects due to the transverse bunch distribution tails and effects of the absolute length scale calibration against magnet current trims either are negligible or can be corrected for.

Experiments have shown that the VDM scans of 2010 can already give ≈5% precision.

1.2 The beam-gas imaging method

The beam-gas imaging method is based on the detection of interaction vertices of the beam particles with the residual gas in the machine. The position of the beam-gas interactions can be used to measure the beam angles, profiles and relative positions. The transverse shapes of the bunches are then used to calculate the overlap integral. As is also the case for the VDM method the bunch intensities have to be known in addition.

The beam–gas imaging method [13] uses equation (1) directly and neglecting the crossing angle and beam positioning offsets reads:

$$L \approx \frac{n_1 n_2 \, f}{4\pi \sqrt{\left(\sigma_1^{x\,2} + \sigma_2^{x\,2}\right)\left(\sigma_1^{y\,2} + \sigma_2^{y\,2}\right)}} \, , \tag{3}$$

in terms of the Gaussian beam widths $\sigma_{1/2}^{x/y}$.

The reconstruction of beam-gas vertices allows one to obtain an image of the transverse bunch profile along the beam trajectory. The beam overlap-integral is then calculated from the two individual bunch profiles. The simultaneous reconstruction of the luminous region with the vertex detector can also be used to further constrain the beam parameters.

For this method a vertex resolution is needed that is comparable or smaller than the transverse beam sizes. Compared to the VDM method, the disadvantage of a small rate is balanced by the advantages that the method is non-disruptive, the beams do not move and, at least in principle, the method can be applied while taking physics data. The rate can be increased by a limited, controlled increase of the residual vacuum pressure in the vertex detector without danger to the experiment.

It is advantageous to perform the BGI measurement in the same fill as the VDM scans. This would allow a very strict comparison to be performed between the two measurements, and makes it possible to do a large number of cross-checks. Here, emphasis will be given to the van der Meer method.

2 Measurements performed

Measurements were carried out at the beam energy of 3.5 TeV ($\sqrt{s} = 7$ TeV) with the BGI method by LHCb [5] and the VDM method at all IPs [4]. The first measurements were performed in April–May 2010 at a $\beta^* = 2$ m, corresponding to an individual beam size of about 45 μm. Due to the presence of a spectrometer dipole, a net crossing angle of 280 (540) μrad in the vertical (horizontal) plane was present at IP2 (IP8). No external crossing angle was applied. The VDM scans were done for CMS (IP5) in LHC fills 1058 and 1089 for ATLAS (IP1) in fills 1059 and 1089, for LHCb (IP8) in fill 1059 and for ALICE (IP2) in fill 1090, with either two (1058) or one (1059, 1089, 1090) colliding bunch pair. The bunch population was $\sim 1\,10^{10}$ protons (fills 1058, 1059) or $\sim 2\,10^{10}$ protons (fills 1089, 1090).

A second set of measurements was done in October at the same beam energy with a $\beta^* = 3.5$ m. Scans where performed for ATLAS and CMS in fill 1386, and in fill 1422 for ALICE, ATLAS, and LHCb. In each case at least one scan was performed in both the x and y direction moving both beams symmetrically in opposite direction. ALICE, CMS and LHCb also performed scans where only one beam moved while the other was kept at fixed position. The scans extended up to ~ 6 nominal beam σ separation between the two beams.

A measurement of the bunch population product $n_1\, n_2$ (see Eq. 1) is essential to obtain a measurement of the luminosity. Two beam current transformers were installed on the vacuum chamber of each circulating beam [14]. For each beam one DC transformer (DCCT) measures the total circulating current and one fast transformer (FBCT) the current observed per 25 ns time slot (i.e. per bunch). The FBCT was cross-checked using the ATLAS BPTX system [15].

The procedure to obtain the number of protons per bunch was defined in Ref. [7]. The DCCT was used to constrain the total intensity while the FBCT defines the intensity ratios per bunch. The "ghost charge", or charge outside the wanted bunches was determined by a combination of counting beam-gas interactions in LHCb and analysis of satellite bunches in ATLAS and CMS. The largest uncertainty is introduced by the current product measured with the DCCT and is 2.7%. This error will improve in 2011.

For the VDM method it is important to check the correspondence of the nominal beam displacement and the actual length scale. The check is done by several methods, each essentially moving both beams in the same direction and measuring the position of the luminous region with the vertex detectors.

The overall uncertainty in the VDM method was estimated by the experiments to be of the order of 4–5%. Error sources in addition to the beam intensity uncertainty are the reproducibility, length scale calibration, beam stability (emittance growth) and event counting systematics.

3 Requirements for 2011

During VDM scans a number of operational parameters may be chosen to optimize the result of the measurements. These parameters include the LHC filling pattern, individual bunch intensities and emittance, optics parameters such as the β^* and crossing angles. We will take the parameters one-by-one and try to find an optimum making use of the 2010 experience.

In some cases a change may need new machine development and qualification procedures, thus only essential parameters should be modified.

3.1 LHC filling scheme

The experiments favour to perform the measurements with a limited number of isolated bunches in the machine. The usage of bunch-trains is dis-favoured since it introduces more satellite current (*i.e.* protons outside the intended RF buckets) and aggravates the effects of "afterglow" in the detectors (*i.e.* activity in bunches directly following collisions).

Due to unavoidable differences among the bunches in the machine, the analyses are performed on a bunch-by-bunch basis. When the number of bunches is limited, more statistics *per bunch* can be obtained within the capabilities of the DAQ systems of the experiments. It is also better to create *private* bunch-pairs, *i.e.* pairs colliding in 1 and 5 only, or in 2 and 8 separately. This limits the influence of beam-beam effects.

Taking these considerations into account, ATLAS prefers about 6 colliding bunches and CMS up to 12. ALICE prefers one bunch at a time while for LHCb 12 colliding bunches are optimal. These limitations are not absolute: if more than six bunch pairs collide in ATLAS the surplus bunches can be masked in the DAQ.

Thus, a filling scheme with up to 25 bunches in the machine looks optimal.

3.2 Choice of μ

Another important parameter is the number of visible interactions per bunch crossing, μ. The values quoted here are the ones for head-on beams. A too low value would stretch the time spent in VDM scan unnecessarily, while a too high value would create too much pile-up in the detectors.

ATLAS, CMS and LHCb favour $\mu \approx 1$ or a bit higher (up to ≈ 2). This optimizes the rate while keeping the pile-up under control. ALICE favours a lower value $\mu \approx 0.1$ or a bit higher (up to $\mu \approx 0.5$ can be tolerated).

The optimization of the rate per crossing pair sets constraints on combination of ϵ, β^*, and bunch intensities. These different "knobs" act differently on other parameters, so that a reasonable optimum set must be defined.

3.3 Choice of β^*

The value of β^* is an optics parameter and therefore constant for all bunches. It can, however, be chosen per interaction point.

One should use preferentially existing optics to reduce time spent in specific MD for the scans. Although, for instance the value used at injection is already available, it may need safety qualification for use in collision. At a fixed emittance and beam intensity, a variation of the β^* does not influence beam-beam effects contrary to a variation in emittance.

Some systematic difference between different VDM scans have been observed in 2010. These may be due to effects of hysteresis in the corrector magnets. It is possible that higher values of β^* reduce these effects. Thus it is interesting to perform at least some measurements with relatively high values.

ATLAS and CMS prefer a value of β^* in the range 3.5–11 m. Depending on the intensity of the colliding bunches 10–11 m may give a too low rate for some of the intensity monitors of ATLAS. ALICE has no specific request for β^*. Their requirement is to limit the rate, so that they may need to work at about 10 m. LHCb prefers to combine the measurements based on the VDM scan with a BGI measurement within the same fill. In that case the 10 m optics is better to fully profit from the vertex resolution in the beam-gas imaging method. It should be studied whether the beam displacements required for the VDM method can be reached for this value of β^*.

3.4 Choice of ϵ

In 2010 the emittance was increased in the SPS for physics fills. With the aim to increase the luminosity this may no longer be the case in the physics fills of 2011. For the luminosity calibration fills it is probably better to work with an increased emittance as was done in 2010; a too low values enhances beam–beam effects. To avoid additional systematic errors in the BGI method it is optimal to make the emittance of colliding bunch-pairs symmetric between beam1 and beam2.

If it is possible to blow up the emittance for selected bunches in the LHC, interesting studies of systematic effects can be performed.

3.5 Choice of bunch intensities

A lower bound on the current in the machine is given by beam instrumentation and the required counting rate in the experiments. Too high values introduce beam–beam effects and pile-up corrections in the experiments. The latter are experiment dependent. The preferred values are approximate and depend on the β^* and ϵ values. ATLAS, CMS and LHCb prefer values in the range $0.8 - 1.0\,10^{11}$, while ALICE prefers lower values. The need for precise orbit measurements constrains these values to be above $0.6\,10^{11}$.

Together with the requested number of bunches, these intensities make offset corrections in the BCTs negligible. The beam intensity measurements put another constraint: it is better to avoid "Range 4" of the DCCT, and with a small number of bunches in the machine the best results can be obtained if the total intensity corresponds to the higher end of "Range 3".

3.6 Combination of β^*, ϵ and intensities

A combination of the number of bunches, bunch populations, β^* and ϵ values should be chosen to reconcile requests of each of the experiments. The development of new optics for the machine should be avoided.

The filling scheme should be chosen to maximally decouple the different IPs. This is not possible for ATLAS and CMS which share colliding bunch pairs. As ball-park numbers, ATLAS and CMS prefer to use 6–12 colliding pairs, with an intensity of $\approx 0.8\,10^{11}$ and $\beta^* = 3.5$ m. The value of ϵ should then be chosen to produce a maximum μ between 1 and 2. ATLAS is also studying the option of using a larger β^*, such as the value of 10 m used at injection.

ALICE wants to work at lower rates, and to use one colliding pair at the same time. Thus an intensity of $\approx 0.6\,10^{11}$ and a $\beta^* = 10$ m looks optimal with a fairly large emittance.

LHCb wants to combine the VDM and BGI methods in one fill. The optimization of the BGI method requires larger beam widths, so that $\beta^* = 10$ m and fairly large emittances are required. The detector can work optimally with 12 colliding pairs and bunch intensities around $\approx 1.2\,10^{11}$. This provides approximately equal count rates as in the scans of October 2010. To achieve sufficient statistics with the BGI method, a pressure bump should be applied in the vertex detector during these measurements.

A spread of values of the intensities, and possibly ϵ from bunch to bunch would allow the study of systematic effects to be performed.

3.7 Choice of crossing angle

In physics fills with bunch-trains the LHC beams collide with an external crossing angle. This angle is applied in order to avoid parasitic collisions outside the IPs. Since the VDM scans will be performed with small numbers of individual bunches in the machine, in principle no crossing angle is needed. One should keep in mind that ALICE and LHCb have an internal crossing angle due to the field of their dipole spectrometer magnet.

ATLAS and CMS can run without crossing angle. A non-zero crossing angle does not introduce corrections to the VDM method but has to be taken into account for the BGI method.

Other considerations can influence the decision on crossing angles. At zero angle the measurement of satellite interactions allows the experiments to reveal the presence of protons in RF-buckets near the main buckets. However, a new device, the Longitudinal Density Monitor (LDM) which is being commissioned by the BI-group, once operational, can provide the measurement of charges outside the main buckets with high precision.

Therefore there is no compelling reason to have a zero angle in ATLAS and CMS and to profit from existing machine optics settings, the setting for physics fills can be used.

For LHCb the situation is different when the VDM and BGI methods are combined in one fill. LHCb prefers a finite angle (≈ 0.4 mrad) to eliminate parasitic collisions which make

it impossible to apply the beam-gas method. At the VDM scans in October 2010 satellite collisions were observed at ± 75 cm from the IP at large beam displacements. It is better to avoid these collisions during the VDM scan by applying an sufficiently large crossing angle.

3.8 Scanning procedures

For the VDM scan several strategies are possible to achieve the required beam displacements. Separations of up to 6 sigma seem optimal. One has to be careful to sweep the magnet currents in one direction during a scan to avoid hysteresis effects. The most straightforward way to achieve this is by starting the two beams positioned at an opposite extreme and then sweep symmetrically in opposite directions. The scan is first done in one coordinate (e.g. x) and then in the other orthogonal coordinate. Although the VDM method does not require it, ATLAS preferred to re-centre the scan in the second coordinate on the maximum of the first one.

Another straightforward strategy is to keep one beam at fixed position and move the other beam across. Aperture considerations can limit the maximum excursion in this case. A system of co-moving TCTs may be needed to achieve sufficient beam separation.

A third method was used consisting in starting with the two beams at opposite extreme positions, keeping one beam fixed while moving the other until the beams hit approximately head-on, and then continue by moving the first beam and keeping the second beam fixed.

Differences observed in the final results obtained with these methods have been used as a measure of systematic errors, although the causes are not precisely known. It is therefore important to explore these differences further. Thus one should plan for at least two VDM scans per IP using different scanning strategies. In addition, to understand hysteresis effects, beam movements and measurements which would be expected to maximize these should be envisaged.

It is important to have fully automated procedures. This reduces the time spent and allows the experiments to follow the measurements on-line. For flexibility of the operations it may be needed to make these "file-driven", i.e. going through a list of pre-defined settings. As an example, the ATLAS length scale calibration had to be performed "by hand", and required a few hours of beam time.

3.9 Supporting measurement procedures

A number of supporting measurements are needed to complete the VDM scans.

3.9.1 Study of x–y coupling

The VDM scan is performed by a "crossed" scan in two coordinates. The basic underlying assumption is the factorization of the bunch shapes in these two coordinates. There are some indications (population of the luminous region) that this assumption does not hold perfectly. Thus a dedicated set of measurements to check the x–y coupling will be needed. One idea is to perform scans in the $x + y$ and $x - y$ coordinates, but this may be time-consuming and may not be trivial to set up.

3.9.2 Study of length scale

The evaluation of the integral in Eq. (2) needs the knowledge of the length scale. The uncertainty introduced in the present measurements is of the order of 1%.

ATLAS used a method whereby the position of each beam was calibrated separately against the vertex detector by measuring the centre of the luminous region scanning each time the other beam across to find the head-on situation. This procedure turned out to be quite lengthy, although some time reduction can be achieved by automation.

LHCb and CMS used a method whereby first the two beams were separated by $\sqrt{2}\,\sigma$ and then both moved in the same direction by the same nominal amount. By measuring at the

same time the position of the luminous region and the rate, both the average and differential movements can be controlled. This method can be applied in a much shorter period, but is a bit more difficult to interpret.

It may be possible to combine the two methods into a kind of "leap-frog" movement where each position of beam1 is measured against three positions of beam2 and vice-versa by moving the beams in turn in only one direction. One would measure rate and position for each setting.

Some discussions are still needed to decide on the optimal procedure.

Longitudinal scans have beean performed in 2010. They may have to be repeated to understand geometrical effects.

3.9.3 Hysteresis

There are some indications that hysteresis effects limit the precisions of the VDM scans. A definitive test has not yet been devised, and good ideas are needed to get more knowledge.

One possibility is to perform scans in inverted directions. Other short tests can be designed e.g. by separating the beams by moving one at a separation of 1.5 σ and back while measuring the rate at each point.

3.10 Beam instrumentation

The experiments rely on the excellent performance of the beam instrumentation.

The knowledge of the absolute scale of the beam intensity is essential. Thus one needs the best possible performance of the DCCTs, and calibration strategies optimized for the fills where the VDM/BGI measurements are done.

The bunch-by-bunch populations have been measured using the FBCTs. These remain important for this measurement. A new measurement system, the longitudinal density monitor (LDM) is being commissioned which has the potential to also provide the relative intensities of the bunches. This monitor is expected to make a significant improvement in the uncertainty due to ghost charge.

The measurement of ghost charge outside the wanted buckets has been provided by the experiments. However, the data from the LDM look very promising to provide this measurement with high precision.

Other supporting measurements are helpful: wire-scans and emittance measurements using synchrotron light monitors. The synchrotron light monitors provide valuable information on the emittance growth of the beam. The wire scans provide rough cross-checks but do not enter directly into the measurements.

3.11 Combination of VDM and beam-gas imaging method

Important systematics checks can be made by performing the VDM and BGI in the same fill at the same IP, such as at LHCb. The beam intensity systematics drop out so checks of absolute scale of the two methods can be more precise. Beam shape measurements can be compared. The VDM scan can be used to determine a precise beam centring and determine the ratio of the sizes of the two beams. These constraints can reduce the systematic errors in the BGI method.

The BGI method needs a few hours of stable beam conditions. (Assuming that the amount of gas can be increased by passively applying a vacuum bump at the vertex detector.) An optimization of the BGI result requires beam sizes much larger than the resolution of the vertex detector. For LHCb this requirement would favour large values of β^* such as 10 m. Such a β^* would also be acceptable for the VDM method.

3.12 Additional ideas

The question arises whether we can do the scans simultaneously for different experiments. This would bring an obvious gain in time. However, one is not sure that the induced beam movements are sufficiently controlled.

The performance of more frequent VDM scans at end of fills under physics conditions can be investigated. While this is useful for width measurements of the beams it remains to be understood whether competing luminosity measurements can be achieved.

LHCb is planning to run BGI measurements and VDM scans at $\beta^* = 10$ m during TOTEM-CMS/ALPHA runs.

4 Summary

A precise measurement of the luminosity have a clear physics justification down to the few % level. For the first year of operation the precision reached is already better than 5% and expectations are that this can be improved significantly. Such a performance was only possible thanks to close collaboration of machine experts and the experiments.

Although the requirements of the experiments are quite diverse, they may still be accommodated by the machine.

5 Acknowledgements

I would like to thank the ALICE, ATLAS, CMS and LHCb speakers for their valuable input and for making available their talks ahead of time, the theorists for providing guidance and inspiration, the machine experts for their clear presentation of the capabilities of the LHC and its instrumentation and Massi Ferro-Luzzi for valuable discussions and for recording the comments after this presentation.

References

[1] *"Motivations and precision targets for luminosity"*, M. Mangano, *Talk presented at this workshop*, (2011).

[2] *"Indirect luminosity measurements: theoretical assessment"*, V. Khoze, *Talk presented at this workshop*, (2011).

[3] *"Indirect luminosity measurement"*, J. Anderson, *Talk presented at this workshop*, (2011).

[4] *"ALICE 2010 luminosity determination"*, K. Oyama, *Talk presented at this workshop*, (2011); *"LHCb 2010 luminosity determination"*, V. Balagura, *Talk presented at this workshop*, (2011); *"CMS 2010 luminosity determination"*, M. Zanetti, *Talk presented at this workshop*, (2011); *"ATLAS 2010 luminosity determination"*, M. Huhtinen, *Talk presented at this workshop*, (2011).

[5] *"LHCb beam-gas imaging results"*, P. Hopchev, *Talk presented at this workshop*, (2011).

[6] *"BCTs and BPTX analysis results"*, T. Pauly, *Talk presented at this workshop*, (2011).

[7] *"LHC Bunch Current Normalisation for the April-May 2010 Luminosity Calibration Measurements"*, G. Anders *et al.*, CERN-ATS-Note-2011-004 (2011).

[8] C. Møller, K. Danske Vidensk. Selsk. Mat.-Fys. Medd. **23**, 1 (1945).

[9] see e.g. O. Napoly, *Particle Acc.*, **40**, 181 (1993); W. Herr, B. Muratory, "Concept of Luminosity", Proceedings of CERN Accelerator School, 361 (2003).

[10] *"Calibration of the effective beam height in the ISR"*, S. van der Meer, ISR-PO/68-31, 1968 (CERN).

[11] *"Absolute Luminosity from Machine Parameters"*, H. Burkhardt, P. Grafström, LHC-PROJECT- -Report-1019 ; CERN-LHC-PROJECT-Report-1019.

[12] V. Balagura, arXiv:1103.1129 [physics.ins-det], 2011; *"Luminosity measurements in the first LHCb data"*, V. Balagura, in proc. of the 2010 Rencontres de Moriond (QCD), La Thuile, 2010.

[13] *"Proposal for an absolute luminosity determination in colliding beam experiments using vertex detection of beam-gas interactions"*, M. Ferro-Luzzi, Nucl. Instrum. Methods **A 553**, 388 (2005).

[14] *"The 2010 LHC DC BCT measurement system [...]"*, P. Odier, J.-J. Gras, M. Ludwig, S. Thoulet, LHC-Project-Note-432, and *"The 2010 LHC ring Fast BCT measurement system [...]"*, D. Belohrad, J.-J. Gras, M. Ludwig, LHC-Project-Note-433.

[15] *"The ATLAS beam pick-up based timing system"*, C. Ohm, T. Pauly, Nucl. Instrum. Methods **A 623**, 558 (2010).

SUMMARY AS VIEWED BY THE MACHINE

P. Collier, M. Ferro-Luzzi CERN, Geneva, Switzerland

Abstract

The last session included a discussion of the issues concerning the machine. These covered three areas; hardware, beam studies and dedicated beam time requests. During the discussion requirements in each case as well as the necessary resources were identified. The summary of these discussions is presented here.

HARDWARE AND SOFTWARE

A number of areas where effort is needed on the machine hardware and software were addressed.

DC Current Transformers

Two issues were addressed, namely the bunch pattern dependence of the DCCT readings and the stability of the DCCT scale factor. The first issue is a hardware problem that was identified during the 2010 running period. Investigations are underway and it is hoped to have a working solution before the start-up. The stability of the DCCT scale factors will be studied carefully in 2011 based on regular precise calibration campaign results. It was agreed that an upgrade of the current calibration quick check allowing automated and online precise calibrations would be extremely useful in this context and BI will investigate the feasibility of such an improvement in 2011.

Fast Beam Current Transformers

The FBCT's can measure the bunch population of the individual bunches in the machine and have generally worked very well during the 2010 run. There are two issues to be addressed. The first concerns the observed bunch length and position dependence of the FBCT reading, the second concerns improving our understanding of the offset and linearity of these devices.

The first problem is being actively worked on by the team. It is coming from the transformer itself and it is not clear yet that it can be fixed entirely with the current monitors. Fortunately, the bunch length and positions are reasonably controlled during physics and we should be able to control the error introduced in these conditions. The understanding of the offset and linearity requires a more long-term effort essentially based on comparison with the other instruments that will be commissioned this year, i.e. the Longitudinal Density Monitors and the Wall Current Monitors.

An FBCT calibration independent of the DCCT, if achievable with precision comparable to that of the DCCT, would be useful.

Longitudinal Density Monitor

The LDM is a very promising device to measure the population in satellite bunches. Initial tests and measurements indicate a high degree of precision should be possible from this device. The work here during the coming run will concentrate on the commissioning and performance assessment of this system. It was also noted that the linearity of the device needs in particular to be checked.

BPMWF

These pickups sit close to the experiments and need to be commissioned and calibrated in time for the high-β operation.

Lumi Scan Application

This application allows scanning of the beam collisions in each IP. This functionality covers mini-scans used during routine operation as well as the large range Van de Meer scans. A number of cosmetic and functional improvements to the application were discussed and agreed. Other items require more study before an implementation can be envisaged. A suggestion was made to drive the scan using a generic, file-driven sequence. This would easily allow different scan types to be performed and would cover the needs for VdM as well as length scale scans. However, machine protection issues mean that quality checks on the contents of the file would have to be made before such a file could be driven into the machine. Complete freedom to scan cannot be given. Having the TCT collimators move during the scan could ease the restrictions here. The work to prepare for the TCT's to move during the scan is already done, but requires testing and qualification before it can be used routinely.

Transverse Emittance Measurement

The cross-calibration of the various emittance measuring devices was discussed at length as well as the absolute calibration of each. Studies and work in BI will continue on these issues. An additional request to allow selection of bunches for the wirescanner application was agreed and will be implemented.

BEAM STUDIES

A number of machine studies will be needed for the calibration of the luminosity and other matters within the scope of the workshop. Requests will have to be prepared and proposed for consideration following the procedure now set-up by the LMC. The prioritization of these requests will then be considered in relation to all other requests for machine development time.

The list or machine studies topics that was discussed included

- Parallel scans (simultaneously in more than one IP) and systematic effects due to cross-talk between IPs,

- Position reproducibility effects coming from hysteresis in the correctors,
- Synchronized movement of the TCT's with the scan in order to keep the beam centered and the protection optimized throughout the scan,
- Minimizing (and measuring) the amount of beam outside the nominal RF buckets,
- Bunch-by-bunch emittance control (to equalize emittances between beams and bunches),
- VdM scan reproducibility tests.

DEDICATED BEAM TIME REQUESTS

There are a number of areas where "parasitic" (or end-of-fill) studies not sufficient to achieve the requested goals and dedicated machine time will have to be requested and granted. The following is a list of the requests that are of direct relevance to the workshop:

- The commissioning and optics measurements of the 90m β optics as well as the qualification of the protection systems to allow physics operation with this. Approximately 5 shifts will be needed for this,
- Following this there will need to be about 4 special physics fills with the 90m β optics in IP1 and 5,
- There will need to be a few (2?) dedicated fills during 2011 for VdM scans,
- Precise calibrations of the β* are also requested and would require dedicated time. Here it was noted that the β* should be measured (and if necessary corrected) during the machine commissioning. However, it is not clear if the precision will be high enough for the calibration measurements.

SPECIFICATION OF THE REQUIRED ACCURACIES FOR THE LUMINOSITY CALIBRATION

The workshop showed that the total luminosity uncertainty is already at the level of 5%, with a dozen systematic effects contributing to this uncertainty. Most individual contributions are already below 1%. The dominant uncertainty may remain for some time the bunch population product normalization. If we assume this will improve down to the specified accuracy (1-2% on the population product), we should aim at having all other contributions at the level of <0.5%. Clearly, such a requirement may evolve depending on the evolution of the actual uncertainties that will be found during the course of 2011. But it is a reasonable target.

Individually, these are the requirements (all given in terms of 68% confidence levels):

- DCCT: as just said, this is the main contribution. It is used to set the scale of the total proton population in each ring and goes directly into the luminosity (for each beam). The LHC Design Report quotes a design goal of 1% per beam. We take this as a 2011 milestone and a reference for the other systematic uncertainties.
- FBCT: used for determining the relative size of the bunch populations, i.e. offset and linearity errors contribute. These enter in the product of the beam1 and beam2 populations. Therefore, an uncertainty of $dN/N<0.3\%$ for the relative bunch population is desirable. It is important to remind that the experiments care about the bunch population in the nominal 2.5ns RF bucket, while the FBCT integrates over 25ns (including satellites), with some possibly varying efficiency across the 25ns slot. This may contribute to the uncertainty.
- LDM: complements the BCTs to determine the relevant populations from the total beam populations and the 25ns FBCT relative populations. The requirement is therefore linked to the two above. It should be accurate enough to allow the LDM-corrected FBCT relative populations to meet their required accuracy. This includes determination of the ghost charge and of the satellite charge around a nominally filled RF bucket. Most important will be the linearity (error on the extracted satellite/main bunch population ratio).
- WCM (wall current monitor): complements FBCT measurements.
- Position reproducibility: this is important for the VdM scans, including length scale calibrations. Applying the same trims in one plane should bring each beam individually back to the same position, ideally within an accuracy such that the luminosity change is <0.3% (assume all other parameters don't change). This error enters twice, once per plane. Ideally, a position reproducibility of $dD/\sigma_{beam} <1\%$ is desirable (dD is the position error or non-reproducibility) [1].
- Emittance measurement: this does not enter directly the luminosity determination (neither in the VdM nor in the beam-gas method). However,
  a. in the VdM method the emittance measurement is used to monitor and possibly correct for the change in emittance during the scans. The absolute scale is not important, though the relative scale between the devices (especially ring 1 and ring 2) may play a role. It is mainly the relative change $d\varepsilon/\varepsilon$ of a given emittance over time (~1hour) that is needed. It would be useful to have this measured with an accuracy of $d\varepsilon/\varepsilon< \sim 1\%$.
  b. For the beam-gas method, the emittance of the beams plays a role. Beam-gas imaging is used mainly to measure the beam offsets and the ratio of bunch sizes within a colliding bunch pair. The pp collision (much more copious) are used to constrain the other parameters. In this exercise, the more equal the emittances of the colliding bunches (in the same plane), the smaller the resulting error. Therefore, a precise ring1/ring2 relative bunch-by-bunch measurement is required to possibly allow one equalizing the

emittances bunch-by-bunch. An accuracy of <5% is desirable.

c. The BSRT provides a measurement of more than just two orthogonal RMS values. The complete fit results (RMS, orientation of the principal axes, amplitudes, ...) can be useful and the experiments would like to profit from this information (could the date be stored to the logging database ?).

- BPMWF: TOTEM/ALFA will require measurements of the β* and dispersion at the 1% level.

[1] The luminosity depends on the separation D by $r = e^{-(\frac{D}{2\sigma_{beam}})^2}$. Around $D = 0$, a small D error (dD) causes a relative drop $\frac{dr}{r} = -(\frac{dD}{2\sigma_{beam}})^2$. However, around $D = \sqrt{2}\,\sigma_{beam}$ (which is used in some calibration scans), this causes a larger relative drop $\frac{dr}{r} = -\frac{dD}{\sqrt{2}\sigma_{beam}}$.